

This item was submitted to Loughborough's Institutional Repository (<https://dspace.lboro.ac.uk/>) by the author and is made available under the following Creative Commons Licence conditions.



CC creative commons
COMMONS DEED

Attribution-NonCommercial-NoDerivs 2.5

You are free:

- to copy, distribute, display, and perform the work

Under the following conditions:

BY: **Attribution.** You must attribute the work in the manner specified by the author or licensor.

Noncommercial. You may not use this work for commercial purposes.

No Derivative Works. You may not alter, transform, or build upon this work.

- For any reuse or distribution, you must make clear to others the license terms of this work.
- Any of these conditions can be waived if you get permission from the copyright holder.

Your fair use and other rights are in no way affected by the above.

This is a human-readable summary of the [Legal Code \(the full license\)](#).

[Disclaimer](#) 

For the full text of this licence, please go to:
<http://creativecommons.org/licenses/by-nc-nd/2.5/>



**MECHANICAL BEHAVIOUR OF THERMALLY
BONDED BICOMPONENT FIBRE NONWOVENS:
EXPERIMENTAL ANALYSIS AND NUMERICAL
MODELLING**

by

Emrah Demirci

A Doctoral Thesis

Submitted in partial fulfilment of the requirements for the award of
Doctor of Philosophy of Loughborough University

February 2011

© 2011 Emrah Demirci

Research Student Office, Academic Registry
Loughborough University Leicestershire LE11 3TU UK
Switchboard: +44 (0)1509 263171 Fax: +44 (0)1509 223938



CERTIFICATE OF ORIGINALITY

This is to certify that I am responsible for the work submitted in this thesis, that the original work is my own except as specified in acknowledgments or in footnotes, and that neither the thesis nor the original work contained therein has been submitted to this or any other institution for a degree.

11.03.2011 (Signed)

Emrah Demirci (Date)

ABSTRACT

In contrast to composites and woven fabrics, nonwoven materials have a unique web structure, which is composed of randomly oriented fibres bonded in a pattern by mechanical, thermal or chemical techniques. The type of nonwovens studied in this research is a thermally bonded one with polymer-based bicomponent fibres. Such fibres have a core/sheath structure with outer layer (sheath) having a lower melting temperature than that of the core. In thermal bonding of such fibres, as the hot calender with an engraved pattern contacts the fibrous web, bond points are formed thanks to melting of the sheath material. Molten sheath material acts as an adhesive while core parts of the fibres remain fully intact in the bond points. On the other hand, web regions, which are not in contact with the hot engraved pattern, remain unaffected and form the fibre matrix that acts as a link between bond points. With two distinct regions, namely, bond points and fibre matrix, with different structures, nonwovens exhibit a unique deformation behaviour. This research aims to analyse the complex mechanical behaviour of thermally bonded bicomponent fibre nonwoven materials using a combination of experimental and numerical methods.

A novel approach is introduced in the thesis to predict the complex mechanical behaviour of thermally bonded bicomponent fibre nonwovens under various three-dimensional time-dependent loading conditions. Development of the approach starts with experimental studies on thermally bonded bicomponent fibre nonwovens to achieve a better understating of their complex deformation characteristics. Mechanical performance of single bicomponent fibres is investigated with tensile and relaxation tests since they are the basic constituents of nonwoven fabrics. The fabric microstructure, which is one of the most important factors affecting its mechanical behaviour, is examined with scanning electron microscopy and X-ray micro computed tomography techniques. At the final part of experimental studies,

mechanical response of thermally bonded bicomponent fibre nonwovens is characterised with several mechanical tests.

Numerical studies begin with the assessment of mechanical properties of regions of bond points and fibre matrix of nonwovens considering mechanical anisotropy in their microstructure due to randomly oriented fibres. In order to accomplish this assessment, firstly, mechanical anisotropy of nonwovens is analysed. A digital image processing algorithm is developed to compute an orientation distribution function of fibres in the material and assess its anisotropy. Furthermore, the effect of deformation on mechanical anisotropy of nonwoven fabrics is studied. Secondly, assessment of anisotropic viscoelastic-plastic mechanical properties of bond points and a fibre matrix is performed. A second algorithm, based on a single-fibre behaviour and manufacturing parameters of fabric, is developed for this assessment.

After developing two new algorithms to analyse mechanical anisotropy and orthotropic viscoelastic-plastic mechanical properties of regions of bond points and fibre matrix of nonwovens, thermally bonded bicomponent fibre nonwovens are modelled in the finite element software with shell elements having thicknesses identical to those of the bond points and fibre matrix. Unlike the existing numerical models in the literature, the model developed in the thesis is capable of simulating 3D loading conditions of thermally bonded nonwovens as well as their time-dependent anisotropic behaviour. Finally, finite element simulations of several nonwovens are compared with respective experimental results to evaluate the efficiency of the proposed numerical modelling approach.

Keywords: Thermally bonded nonwoven; Bicomponent fibre; Orientation distribution function; Mechanical anisotropy; Digital image processing; Finite element; Viscoelastic-plastic properties

To my home city, TRABZON,

ACKNOWLEDGEMENTS

I would like to express my gratefulness and appreciation to Prof. Vadim V. Silberschmidt for guidance and insight in supervising the research, his invaluable help, and kindness. His knowledge, patience and understanding made possible the successful completion of the thesis.

I would like to express my deepest gratitude and appreciation to my supervisor Prof. Memiş Acar, who inspired, encouraged and supported me for this study. He helped me improve my communication and presentation skills.

I would like thank my supervisor, Prof. Behnam Pourdeyhimi, for consistent guidance, encouragement and support at all levels from the other side of the Atlantic.

Many thanks to the members of Mechanics of Advanced Materials Research Group at Loughborough University for their great support and invaluable friendship. Special thanks to the most skilled technician, Mr. Andy Sandaver, for his unique friendship and assistance in experiments.

Support of Nonwovens Cooperative Research Center of North Carolina State University, USA is appreciated. I would like to thank my industrial advisors, Mr. Carl Wust from Fibervisions Corp. and Mr. Ray Volpe from Ahlstrom Corp., for their support and feedbacks during the research.

My best wishes to Loughborough and Leicester Turkish communities for their strong fellowship and enthusiasm.

Finally, I would like to appreciate my parents, Hasan Fahri & Aynur Demirci, for their patience, love, encouragement and unique support during my studies. To my brother, Erman, for his patience and endless support. You are loved deeply. I would like to thank my wife, Fatma, for her precious support, kindness, and being in my life with her endless love.

PUBLICATIONS & AWARDS

Journals

Demirci, E., Acar, M., Pourdeyhimi, B., Silberschmidt, V.V. (2011), “Finite element modelling of thermally bonded bicomponent fibre nonwovens: Tensile behaviour”, *Computational Materials Science*, **50** (4), 1286-1291.

Demirci, E., Acar, M., Pourdeyhimi, B., Silberschmidt, V.V., “Computation of mechanical anisotropy in thermally bonded bicomponent fibre nonwovens”, *Computational Materials Science* (2011),
<http://dx.doi.org/10.1016/j.commatsci.2011.01.033>

Conferences

Demirci, E., Acar, M., Pourdeyhimi, B., Silberschmidt, V.V., “Modeling the Mechanical Behavior of Thermally Bonded Bicomponent Fiber Nonwoven Materials”, *Semiannual International Advisory Board Meetings*, Nonwovens Cooperative Research Center, NC State University, Raleigh, NC State, USA, 2007-2010.

Demirci, E., Acar, M., Pourdeyhimi, B., Silberschmidt, V.V., “Numerical Modelling of Thermally Bonded Bicomponent Fibre Nonwovens”, *8th World Congress on Computational Mechanics (WCCM8)*, Venice, ITALY, 30 June - 5 July 2008. [ISBN: 978-84-96736-55-9]

Demirci, E., Acar, M., Pourdeyhimi, B., Silberschmidt, V.V., “Finite Element Modelling of Thermally Bonded Bicomponent Fibre Nonwovens for Elastic-Plastic Response”, *19th International Workshop on Computational Mechanics of Materials*

(*IWCMM19*), Constanta, ROMANIA, 1-4 September 2009. [ISBN: 978-973-614-503-2]

Demirci, E., Acar, M., Pourdeyhimi, B., Silberschmidt, V.V., “Anisotropic Elastic-Plastic Mechanical Properties of Thermally Bonded Bicomponent Fibre Nonwovens”, *ASME 2010 10th Biennial Conference on Engineering Systems Design and Analysis (ESDA 2010)*, Istanbul, TURKEY, 12-14 July 2010. [ISBN: 978-0-7918-4918-7] doi: 10.1115/ESDA2010-24664

Demirci, E., Acar, M., Pourdeyhimi, B., Silberschmidt, V.V., “Finite Element Modelling of Thermally Bonded Bicomponent Fibre Nonwovens: Viscoelastic Behaviour”, *20th International Workshop on Computational Mechanics of Materials (IWCMM20)*, Loughborough, UNITED KINGDOM, 8-10 September 2010.

Demirci, E., Acar, M., Pourdeyhimi, B., Silberschmidt, V.V., “Assessment of Anisotropic Viscoelastic-Plastic Mechanical Properties of Thermally Bonded Bicomponent Fibre Nonwovens”, *Innovative Nonwovens Conference 2010 (2010 NET INC.)*, Raleigh, North Carolina, USA, 10-12 November 2010.

Awards

- East Midlands Engineering and Science Professionals (EMESP), Masters Prize Winner (2009), Loughborough University, UK.
- Nonwovens Cooperative Research Center (NCRC), Industrial Advisors Board, Best Paper Award (November, 2009), North Carolina State University, USA.

CONTENTS

| | |
|---|------------|
| ABSTRACT | I |
| ACKNOWLEDGEMENTS..... | IV |
| PUBLICATIONS & AWARDS | V |
| CONTENTS..... | VII |
| LIST OF FIGURES | XII |
| LIST OF TABLES | XXI |
| 1. INTRODUCTION | 1 |
| 1.1. Motivation | 3 |
| 1.2. Aims and Objectives | 5 |
| 1.3. Methodology | 6 |
| 1.4. Outline | 8 |
| 2. INTRODUCTION TO NONWOVEN MATERIALS..... | 10 |
| 2.1. Application Areas | 11 |
| 2.2. Production Stages of Nonwoven Fabrics | 13 |
| 2.2.1. Web Forming | 14 |
| 2.2.2. Web Manipulation..... | 15 |
| 2.2.3. Bonding..... | 15 |
| 2.2.4. Finishing..... | 16 |
| 2.3. Raw Materials..... | 18 |
| 2.4. Properties of Nonwovens | 19 |
| 2.4.1. Geometrical properties | 19 |

| | | |
|-----------|---|-----------|
| 2.4.2. | Mechanical properties | 20 |
| 2.5. | Thermally Bonded Bicomponent Fibre Nonwoven Materials | 21 |
| 2.6. | Summary | 28 |
| 3. | MECHANICS OF NONWOVEN FABRICS | 29 |
| 3.1. | Characterisation of Nonwoven Fabrics | 30 |
| 3.1.1. | Mechanical Properties of Fibres..... | 31 |
| 3.1.2. | Orientation Distribution of Fibres..... | 32 |
| 3.1.3. | Physical Properties of Nonwoven Fabrics | 37 |
| 3.2. | Mechanical Behaviour of Nonwovens | 38 |
| 3.3. | Summary | 43 |
| 4. | MODELLING OF MECHANICAL BEHAVIOUR OF MATERIALS | 44 |
| 4.1. | Basics of Mechanical Properties | 45 |
| 4.1.1. | Material Symmetry and Corresponding Tensor Structures..... | 45 |
| 4.1.2. | Scale Concept in Mechanics | 49 |
| 4.2. | Modelling of Plastic Behaviour..... | 51 |
| 4.2.1. | Yield Criterion | 51 |
| 4.2.2. | Flow Rule..... | 55 |
| 4.2.3. | Strain Hardening | 57 |
| 4.2.4. | Extensions to Anisotropy | 58 |
| 4.3. | Modelling of Viscous Behaviour..... | 62 |
| 4.4. | Review of Finite Element Method | 66 |
| 4.4.1. | Basic Procedure of FEM in Solid Mechanics | 66 |
| 4.4.2. | Finite Element Approach for Large Plastic Deformation | 67 |
| 4.4.3. | Types of Formulation Regarding the Coordinate Frame | 68 |
| 4.4.4. | Solution Methods | 72 |

| | | |
|-----------|---|------------|
| 4.4.5. | Convergence Controls..... | 74 |
| 4.5. | Existing Finite Element Models for Nonwoven Materials..... | 76 |
| 4.6. | Summary | 81 |
| 5. | MECHANICAL BEHAVIOUR OF THERMALLY BONDED BICOMPONENT FIBRE NONWOVENS: EXPERIMENTAL STUDIES | 83 |
| 5.1. | Mechanical Behaviour of Bicomponent Fibres..... | 84 |
| 5.1.1. | Simple Tension Tests | 88 |
| 5.1.2. | Cyclic Loading Tests..... | 92 |
| 5.1.3. | Relaxation Tests..... | 95 |
| 5.2. | Microstructure of Thermally Bonded Bicomponent Fibre Nonwovens..... | 97 |
| 5.2.1. | Examination with Scanning Electron Microscopy..... | 98 |
| 5.2.2. | Examination with X-Ray Micro Computed Tomography | 101 |
| 5.3. | Mechanical Behaviour of Thermally Bonded Bicomponent Fibre Nonwovens..... | 104 |
| 5.3.1. | Simple Tension Tests | 105 |
| 5.3.2. | Compression Tests in Thickness Direction..... | 110 |
| 5.3.3. | Cyclic Loading Tests..... | 112 |
| 5.4. | Effect of Calendering Temperature on Mechanical Performance of Nonwovens..... | 114 |
| 5.5. | Conclusions | 118 |
| 6. | ASSESSMENT OF MECHANICAL PROPERTIES OF THERMALLY BONDED NONWOVENS..... | 119 |
| 6.1. | Analysis of Anisotropy in Thermally Bonded Nonwoven Fabrics | 120 |
| 6.1.1. | Orientation Distribution Function | 121 |
| 6.1.2. | Anisotropic Parameters | 128 |
| 6.2. | Analysis of Orthotropic Mechanical Properties | 132 |

| | | |
|-----------|---|------------|
| 6.2.1. | Elastic Properties..... | 135 |
| 6.2.2. | Plastic Properties..... | 138 |
| 6.2.3. | Viscous Properties..... | 140 |
| 6.3. | Conclusions | 143 |
| 7. | FINITE ELEMENT SIMULATIONS OF THERMALLY BONDED BICOMPONENT FIBRE NONWOVENS | 144 |
| 7.1. | Models | 145 |
| 7.1.1. | Models A and B | 147 |
| 7.1.2. | Model C..... | 149 |
| 7.1.3. | Model D | 151 |
| 7.2. | Microstructure and Manufacturing Parameters | 154 |
| 7.2.1. | Models A and D | 155 |
| 7.2.2. | Model B..... | 158 |
| 7.2.3. | Model C..... | 160 |
| 7.3. | Assessment of Mechanical Properties | 162 |
| 7.3.1. | Models A and D | 163 |
| 7.3.2. | Model B..... | 165 |
| 7.3.3. | Model C..... | 167 |
| 7.4. | Boundary Conditions..... | 169 |
| 7.4.1. | Models A, B and C..... | 169 |
| 7.4.2. | Model D | 170 |
| 7.5. | Results and Experimental Verification..... | 172 |
| 7.5.1. | Model A | 172 |
| 7.5.2. | Model B..... | 175 |
| 7.5.3. | Model C..... | 177 |

| | |
|-----------------------------|------------|
| 7.5.4. Model D | 180 |
| 7.6. Conclusions | 183 |
| 8. CONCLUSIONS | 186 |
| 8.1. Outcomes | 188 |
| 8.2. Future Work | 189 |
| REFERENCES | 192 |

LIST OF FIGURES

| | |
|--|----|
| Figure 1.1. SEM image of thermally bonded mono-component fibre nonwoven..... | 2 |
| Figure 1.2. Magnified SEM image of bond point in Figure 1.1 | 3 |
| Figure 1.3. Research methodology for developing 3D finite element model of thermally bonded bicomponent fibre nonwovens (Red and black boxes designate numerical and experimental studies, respectively.) | 8 |
| Figure 2.1. Nonwoven parts in the design of an automobile (Fibertex A/S, 2008) .. | 13 |
| Figure 2.2. Nonwoven production facility (Hietel, 2006)..... | 14 |
| Figure 2.3. Simulation of web formation from individual fibres (Hietel, 2006)..... | 14 |
| Figure 2.4. SEM image of polypropylene fibres before bonding (Wei <i>et al.</i> , 2007) | 15 |
| Figure 2.5. Bond pattern of thermally bonded nonwoven material | 16 |
| Figure 2.6. Schematic diagram of nonwoven production (spunbond) (Fedorova, 2006) | 18 |
| Figure 2.7. Load-extension graphs for unstabilised and stabilised polyester (Albrecht <i>et al.</i> , 2003) | 20 |
| Figure 2.8. (a) Deformed fibres at the edge of a mechanical bond point. (b) Deformed single fibre in a mechanical bond point (Chidambaram <i>et al.</i> , 2000)..... | 22 |
| Figure 2.9. Several types of bicomponent fibre cross-sections (different colours represent different materials) | 22 |
| Figure 2.10. Cross-section of core/sheath bicomponent fibre..... | 23 |
| Figure 2.11. Bond points of bicomponent fibre nonwoven (a) and mono-component fibre nonwoven (b)..... | 23 |
| Figure 2.12. Schematic diagram of bicomponent spunbond process with belt collector (Fedorova, 2006)..... | 24 |
| Figure 2.13. Hot calendering process of thermally bonded nonwovens | 25 |
| Figure 2.14. Schematic of through-air bonding process (Gao and Huang, 2004)..... | 26 |

| | |
|---|----|
| Figure 2.15. Effect of bonding temperature on stress-strain behaviour of nonwoven fabrics (Kim <i>et al.</i> , 2002)..... | 27 |
| Figure 2.16. Effect of heat treatment time on shrinkage of PET and PP/PET webs at different temperatures (Zhao <i>et al.</i> , 2003) | 27 |
| Figure 3.1. Bond points and fibre group distribution (Limem and Warner, 2005)... | 32 |
| Figure 3.2. Typical ODF of nonwoven fabric (Kim <i>et al.</i> , 2000)..... | 33 |
| Figure 3.3. Device for characterizing structural changes in nonwoven materials during tensile tests (Kim <i>et al.</i> , 2000)..... | 33 |
| Figure 3.4. SEM image of web matrix of thermally bonded nonwoven fabric which can be used for ODF detection..... | 34 |
| Figure 3.5. SEM image of nonwoven (a) and FFT spectrum of this image (b) (Ghassemieh <i>et al.</i> , 2002a)..... | 35 |
| Figure 3.6. Binarized image of nonwoven fabric (a) and Hough space of this image (b) (Ghassemieh <i>et al.</i> , 2002a)..... | 37 |
| Figure 3.7. MD and CD with respect to bond pattern and geometry (Kim, 2004b) . | 38 |
| Figure 3.8. Angular mechanical properties and failure behaviours of thermally bonded nonwovens; 0° and 90° represent MD and CD, respectively (Michielsen <i>et al.</i> , 2006) | 39 |
| Figure 3.9. Secant modulus of nonwovens with 15% and 40% bond area ratio for varying loading directions; 0° and 90° represent MD and CD, respectively (Kim, 2004b) | 40 |
| Figure 3.10. Images and deformation mechanisms of nonwoven fabric after 50% elongation in CD (a) and MD (b) (Kim <i>et al.</i> , 2000)..... | 41 |
| Figure 3.11. Schematics of variation in fibre curl in typical fibrous web (Rawal, 2006) | 42 |
| Figure 3.12. Rupture images of nonwovens for various tensile directions (Kim, 2004b) | 43 |
| Figure 4.1. Principal directions in orthotropic material model | 47 |
| Figure 4.2. Mechanical behaviour of a material..... | 52 |
| Figure 4.3. Comparison of Tresca and von Mises yield criteria in plane stress condition..... | 55 |

| | |
|---|----|
| Figure 4.4. Demonstration of normality rule in plane-stress conditions for von Mises yield function | 57 |
| Figure 4.5. Axes of anisotropy in a cold-rolled sheet | 59 |
| Figure 4.6. Comparison of normalized yield loci of isotropic (von Mises) and anisotropic (Hill) yield functions | 61 |
| Figure 4.7. Stress-strain curves of purely elastic (a) and viscoelastic (b) materials (The red area represents the amount of energy lost in a loading-unloading cycle.) .. | 62 |
| Figure 4.8. Creep strain (ϵ_c) vs. time (uniaxial test at constant stress and temperature) | 63 |
| Figure 4.9. Relaxation curve (uniaxial test at constant strain and temperature) | 63 |
| Figure 4.10. Perfectly elastic (a) and viscous (b) elements (E-modulus of elasticity, η –Viscosity of the dashpot) | 63 |
| Figure 4.11. Maxwell model | 64 |
| Figure 4.12. Kelvin-Voigt model | 65 |
| Figure 4.13. Generalized Maxwell model (Kaliske <i>et al.</i> , 2005) | 65 |
| Figure 4.14. Convergence of Newton-Raphson method (Tekkaya, 2003) | 74 |
| Figure 4.15. FE model of adhesively point-bonded spunbond nonwovens (Limem and Warner, 2005) | 76 |
| Figure 4.16. Equivalent stress-strain behavior of PP filaments in tension/compression (Limem and Warner, 2005) | 77 |
| Figure 4.17. Base cell with bonding points and boundary (Mueller and Kochmann, 2004) | 78 |
| Figure 4.18. FE model of thermobonded nonwoven with square bond points (Mueller and Kochmann, 2004) | 79 |
| Figure 4.19. Models containing 50 lines (a) and 150 lines (b) (Kim and Pourdeyhimi, 2001) | 80 |
| Figure 4.20. Model and experimental unloading behaviour of paper in CD (Ramasubramanian and Wang, 2007) | 81 |
| Figure 5.1. Structure of bicomponent fibre | 84 |
| Figure 5.2. Unbonded region of thermally bonded nonwoven fabric | 86 |

| | |
|---|-----|
| Figure 5.3. Tensile test rigs for bicomponent fibre experiments: Textechno Favimat (a) and Instron Micro Tester 5848 (b)..... | 86 |
| Figure 5.4. Instron 2530-436 load cell (± 5 N) used for single fibre testing..... | 87 |
| Figure 5.5. Gripping system for single fibre testing | 88 |
| Figure 5.6. Simple tension test results for five specimens of PP/PE fibres (strain rate: 0.01 s^{-1}) | 89 |
| Figure 5.7. Variations in fibre diameter (all units in μm ; fibre: PP/PE, planar density: 50 g/m^2)..... | 90 |
| Figure 5.8. Mechanical behaviour of PP/PE (a), PA6/PE (b) and PET/PE (c) fibres for three deformation rates (scatter: $\pm 6\%$) | 91 |
| Figure 5.9. Cyclic loading test results for PP/PE fibre (b) and corresponding loading-unloading control graph (a)..... | 93 |
| Figure 5.10. PET/PE fibre undergoing a load cycle with a hysteresis loop | 94 |
| Figure 5.11. Relaxation behaviour of PP/PE fibre for various applied strains (scatter: $\pm 6\%$)..... | 95 |
| Figure 5.12. Relaxation rate curves of PP/PE fibre for various applied strains (scatter: $\pm 6\%$)..... | 96 |
| Figure 5.13. SEM image of thermally bonded nonwoven fabric composed of bond points and fibre matrix (fibre: PA6/PE, planar density: 150 g/m^2)..... | 98 |
| Figure 5.14. Fibre matrix region of thermally bonded nonwoven fabric (fibre: PA6/PE, planar density: 50 g/m^2) | 99 |
| Figure 5.15. Fibre matrix region of thermally bonded nonwoven fabric (fibre: PA6/PE, planar density: 150 g/m^2) | 99 |
| Figure 5.16. Bond point of thermally bonded nonwoven fabric with the illustration of principal directions (fibre: PA6/PE, planar density: 150 g/m^2)..... | 100 |
| Figure 5.17. X-ray micro computed tomography device, Loughborough University, UK..... | 101 |
| Figure 5.18. 3D micro CT model of thermally bonded nonwoven fabric (fibre: PP/PE, planar density: 150 g/m^2)..... | 102 |
| Figure 5.19. Through-thickness image of thermally bonded nonwoven fabric obtained with X-ray micro CT (fibre: PP/PE, planar density: 150 g/m^2) | 103 |

| | |
|---|-----|
| Figure 5.20. Hounsfield Benchtop Tester with pneumatic grips | 105 |
| Figure 5.21. Bond pattern of nonwoven fabrics given in Table 5.5 (fibre: PA6/PE, planar density: 150 g/m ²) | 106 |
| Figure 5.22. Simple tension test results for nonwoven fabric tested in MD (a) and in CD (b) for three deformation rates (fibre: PP/PE, planar density: 50 g/m ² , specimen dimensions: 30 mm x 15 mm, scatter: ±10%)..... | 107 |
| Figure 5.23. Nonwoven fabric under tension (fibre: PA6/PE, planar density: 100 g/m ² , initial specimen dimensions: 30 mm x 15 mm)..... | 108 |
| Figure 5.24. Graphical definition of tangential modulus (E_t)..... | 109 |
| Figure 5.25. Tangential modulus curves of nonwoven fabric in MD and CD (fibre: PA6/PE, planar density: 150 g/m ²) | 109 |
| Figure 5.26. Mechanical behaviour of thermally bonded nonwoven fabric in MD and CD and TD (fibre: PA6/PE, planar density: 150 g/m ² , strain rate: 0.01 s ⁻¹ , scatter: ±10%) (Absolute magnitude of true strain is used for TD) | 111 |
| Figure 5.27. X-ray micro CT image of through-thickness cross section of thermally bonded nonwoven (fibre: PA6/PE, planar density: 150 g/m ²)..... | 111 |
| Figure 5.28. Cyclic loading of nonwoven fabric in MD (strain range: 0-1) (fibre: PA6/PE, planar density: 100 g/m ²) (b) and corresponding loading-unloading control graph (a) | 112 |
| Figure 5.29. Cyclic loading of nonwoven fabric in MD (strain range: 0-0.1) (fibre: PA6/PE, planar density: 100 g/m ²) | 113 |
| Figure 5.30. Mechanical behaviour of hot and cold calendered nonwoven fabrics in MD (a) and CD (b) (fibre: PA6/PE, planar density: 150 g/m ² , strain rate: 0.01 s ⁻¹ , scatter: ±10%) | 114 |
| Figure 5.31. Damage behaviour of nonwoven fabrics manufactured with hot calendering (a) and cold calendering (b) (fibre: PA6/PE, planar density: 150 g/m ²) | 115 |
| Figure 5.32. Mechanical behaviour of nonwovens manufactured with various calendering temperatures in MD (a) and CD (b) (fibre: PP/PE, planar density: 50 g/m ² , scatter: ±10%)..... | 116 |

| | |
|---|-----|
| Figure 5.33. Normalized flow stress graph of the flow curves in Figure 5.32 (fibre: PP/PE, planar density: 50 g/m ²)..... | 117 |
| Figure 6.1. GUI of Nonwovens Anisotropy V1 for computing ODF and mechanical anisotropy of fibrous materials | 121 |
| Figure 6.2. Image processing steps followed in Nonwovens Anisotropy V1 algorithm | 122 |
| Figure 6.3. Binary image containing randomly oriented twelve lines (a) and their ODF computed with Nonwovens Anisotropy V1 (b) | 123 |
| Figure 6.4. SEM image of nonwoven fabric (a) and its ODF computed with Nonwovens Anisotropy V1 (b)..... | 124 |
| Figure 6.5. SEM image of nonwoven fabric (a) and its ODF computed with Nonwovens Anisotropy V1 (b)..... | 125 |
| Figure 6.6. X-ray micro CT image of nonwoven fibre matrix region (fibre: PP/PE, planar density: 50 g/m ²)..... | 126 |
| Figure 6.7. Subdomains of fibre matrix image (Figure 6.6) processed with Nonwovens Anisotropy V1..... | 127 |
| Figure 6.8. ODF of each subdomain in Figure 6.7..... | 128 |
| Figure 6.9. Resultant ODF obtained from subdomain ODFs in Figure 6.8..... | 129 |
| Figure 6.10. Experimental orthotropic ratio of nonwoven fabric (fibre: PP/PE, planar density: 50 g/m ²)..... | 131 |
| Figure 6.11. GUI of Nonwovens V4 for analysing orthotropic viscoelastic-plastic mechanical properties of thermally bonded bicomponent fibre nonwoven materials | 133 |
| Figure 6.12. Truss elements oriented along principal directions (b) representing orthotropic behaviour of randomly oriented ones (a) | 135 |
| Figure 6.13. Assessment of flow curves of bond points and fibre matrix of PP/PE 50 g/m ² nonwoven | 139 |
| Figure 6.14. Tensile (a) and shear (b) relaxation moduli curves of bond points and fibre matrix of PP/PE 50 g/m ² nonwoven..... | 142 |
| Figure 7.1. Form of shell element used in FE modelling of nonwovens (MSC.Marc [®] , 2008r1)..... | 147 |

| | |
|--|-----|
| Figure 7.2. Nonwoven tensile test sample (a) and corresponding FE model (Models A and B) (b) | 148 |
| Figure 7.3. SEM image of thermally bonded bicomponent fibre nonwoven (a) and corresponding FE model (Models A and B) (b) | 149 |
| Figure 7.4. FE model of nonwoven tensile test sample (Model C)..... | 150 |
| Figure 7.5. SEM image of 35 g/m ² PP/PE 50/50 thermally bonded nonwoven (a) and corresponding FE model (Model C) (b)..... | 151 |
| Figure 7.6. Test setup of Model D (a) and corresponding FE model (b)..... | 152 |
| Figure 7.7. X-ray micro CT image of fibre matrix region of 50 g/m ² PP/PE 75/25 thermally bonded nonwoven simulated with Models A and D..... | 154 |
| Figure 7.8. Experimental flow (strain rate: 0.01 s ⁻¹) (a) and relaxation (constant strain: 0.1) (b) curves of PP/PE 75/25 fibre | 156 |
| Figure 7.9. SEM image of fibre matrix region of 150 g/m ² PA6/PE 75/25 thermally bonded nonwoven simulated with Model B..... | 157 |
| Figure 7.10. Experimental flow (strain rate: 0.01 s ⁻¹) (a) and relaxation (constant strain: 0.1) (b) curves of PA6/PE 75/25 fibre | 159 |
| Figure 7.11. SEM image of fibre matrix region of 35 g/m ² PP/PE 50/50 thermally bonded nonwoven simulated with Model C..... | 160 |
| Figure 7.12. Experimental flow (strain rate: 0.01 s ⁻¹) (a) and relaxation (constant strain: 0.1) (b) curves of PP/PE 50/50 fibre | 162 |
| Figure 7.13. Flow curves of 50 g/m ² PP/PE 75/25 nonwoven regions used in Models A and D | 164 |
| Figure 7.14. Orthotropic tensile (a) and shear (b) relaxation moduli of 50 g/m ² PP/PE 75/25 nonwoven regions used in Models A and D..... | 164 |
| Figure 7.15. Flow curves of 150 g/m ² PA6/PE 75/25 nonwoven regions used in Model B..... | 166 |
| Figure 7.16. Orthotropic tensile (a) and shear (b) relaxation moduli of 150 g/m ² PA6/PE 75/25 nonwoven regions used in Model B..... | 166 |
| Figure 7.17. Flow curves of 35 g/m ² PP/PE 50/50 nonwoven regions used in Model C..... | 168 |

| | |
|--|-----|
| Figure 7.18. Orthotropic tensile (a) and shear (b) relaxation moduli of 35 g/m ² PP/PE 50/50 nonwoven regions used in Model C | 168 |
| Figure 7.19. FE model of tensile-test specimen with boundary conditions | 170 |
| Figure 7.20. Components of Model D with boundary conditions..... | 171 |
| Figure 7.21. FE results for deformed nonwoven in Model A after 60% extension in MD: (a) regions in deformed model; (b) equivalent von Mises stresses (MPa) | 173 |
| Figure 7.22. FE results for deformed nonwoven in Model A after 60% extension in CD: (a) regions in deformed model; (b) equivalent von Mises stresses (MPa)..... | 173 |
| Figure 7.23. Force-extension curves from tensile tests and FE simulations in MD and CD for 50 g/m ² PP/PE 75/25 thermally bonded bicomponent fibre nonwovens | 174 |
| Figure 7.24. FE results for deformed nonwoven in Model B after 70% extension in MD: (a) regions in deformed model; (b) equivalent von Mises stresses (MPa) | 175 |
| Figure 7.25. FE results for deformed nonwoven in Model B after 70% extension in CD: (a) regions in deformed model; (b) equivalent von Mises stresses (MPa)..... | 176 |
| Figure 7.26. Force-extension curves from tensile tests and FE simulations in MD and CD for 150 g/m ² PA6/PE 75/25 thermally bonded bicomponent fibre nonwovens | 177 |
| Figure 7.27. FE results for deformed nonwoven in Model C after 25% extension in MD: (a) regions in deformed model; (b) equivalent von Mises stresses (MPa) | 178 |
| Figure 7.28. Force-extension curves from tensile tests and FE simulations in MD and CD for 35 g/m ² PP/PE 50/50 thermally bonded bicomponent fibre nonwovens | 179 |
| Figure 7.29. Equivalent von Mises stress distribution (MPa) of deformed nonwoven in Model D at first (a), second (b), third (c) and fourth (d) impacts | 180 |
| Figure 7.30. Metal sphere at initial height (h_0) (a), and its maximum heights at first (b), second (c), third (d) and fourth (e) bounces (h_i : height of the sphere at i^{th} bounce) | 181 |
| Figure 7.31. Height of sphere in experiment and FE simulations performed with Model D | 182 |

| | |
|---|-----|
| Figure 7.32. Procedure of FE simulation of thermally bonded bicomponent fibre nonwovens in the research | 185 |
| Figure 8.1. FE model of thermally bonded nonwovens with interface region for simulating damage behaviour | 190 |

LIST OF TABLES

| | |
|---|-----|
| Table 2.1. European-produced nonwoven deliveries by end use (Russell, 2007)..... | 12 |
| Table 2.2. Overview of nonwoven manufacturing technologies (Russell, 2007) | 17 |
| Table 4.1. Modulus of elasticity values of some metals in macro-scale | 50 |
| Table 4.2. Modulus of elasticity values for several metals at various crystallographic orientations at micro-scale (Callister, 2003) | 50 |
| Table 5.1. Properties of polymer materials used for bicomponent fibre production (Brinson and Brinson, 2008) | 85 |
| Table 5.2. Specifications of bicomponent fibre specimens | 88 |
| Table 5.3. Yield strain values of bicomponent fibres (Ward and Sweeney, 2004)... | 94 |
| Table 5.4. Average fibre matrix thickness of nonwoven fabrics used in this research | 102 |
| Table 5.5. Physical properties of thermally bonded nonwoven fabrics used in this research. | 106 |
| Table 6.1. Experimental and theoretical orthotropic ratios of several nonwoven fabrics | 132 |
| Table 6.2. Input parameters for Nonwovens V4 | 134 |
| Table 6.3. Elastic properties of PP/PE 50 g/m ² nonwoven regions analysed with Nonwovens V4..... | 137 |
| Table 7.1. Distinctive features of four models developed in this research..... | 146 |
| Table 7.2. Manufacturing parameters of 50 g/m ² PP/PE 75/25 thermally boned nonwoven simulated with Models A and D..... | 155 |
| Table 7.3. Properties of core and sheath materials for manufacturing 50 g/m ² PP/PE 75/25 thermally boned nonwoven simulated with Models A and D..... | 156 |
| Table 7.4. Manufacturing parameters of 150 g/m ² PA6/PE 75/25 thermally boned nonwoven simulated with Model B | 158 |

| | |
|---|-----|
| Table 7.5. Properties of core and sheath materials for manufacturing 150 g/m ² PA6/PE 75/25 thermally boned nonwoven simulated with Model B | 159 |
| Table 7.6. Manufacturing parameters of 35 g/m ² PP/PE 50/50 thermally boned nonwoven simulated with Model C | 161 |
| Table 7.7. Properties of core and sheath materials for manufacturing 35 g/m ² PP/PE 50/50 thermally boned nonwoven simulated with Model C | 161 |
| Table 7.8. Orthotropic elastic properties of 50 g/m ² PP/PE 75/25 nonwoven regions used in Models A and D..... | 163 |
| Table 7.9. Orthotropic elastic properties of 150 g/m ² PA6/PE 75/25 nonwoven regions used in Model B | 165 |
| Table 7.10. Orthotropic elastic properties of 35 g/m ² PP/PE 50/50 nonwoven regions used in Model C | 167 |

CHAPTER I

1. INTRODUCTION

A nonwoven material could be defined as a manufactured sheet, web or batch of directionally or randomly orientated fibres, bonded by mechanical, thermal or chemical techniques, excluding paper and products that are woven, knitted or tufted (EDANA, 2009a). Nonwoven materials are engineered fabrics, which could be disposable or durable. The properties of these materials such as softness, flame retardency, absorbency, strength, stretch etc. could be designed according to their specific purposes (hygiene, filtering etc.). Thermal bonding of fibres is one of the most popular manufacturing processes of nonwoven materials, resulting in a good combination of their properties (Dharmadhikary *et al.*, 1995). Hot calendaring is the most frequently used method for thermal bonding of nonwovens in the industry. In this method, a raised pattern on a calender roll with controlled temperature is transferred under pressure onto the preformed web of polymer fibres, passing thorough the calender. This process is responsible for forming a more ordered,

macroscopically periodic structure of nonwovens (Figure 1.1) from the loosely connected web of fibres. While providing the requested bonding, hot calendering changes the state of fibres within bonded areas, as a magnified image of a bond point in Figure 1.2 vividly demonstrates. These changes result in deterioration of mechanical properties of fibres and, subsequently, of thermally bonded nonwoven materials.

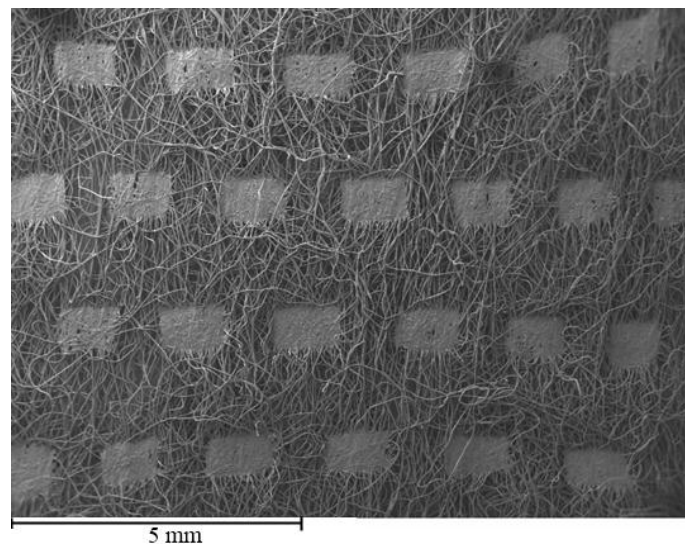


Figure 1.1. SEM image of thermally bonded mono-component fibre nonwoven

The mechanisms underlying thermal bonding have been studied by various methods (Bhat *et al.*, 2004; Chidambaram *et al.*, 2000), but quantification of their effect on mechanical properties of nonwovens is not fully implemented. Still, even without such an implementation there is an obvious way to improve the thermal bonding process by transition to fibres that will be less affected by the process. One of the possible ways is to use core/sheath bicomponent fibres with the sheath material having a lower melting temperature than that of the core. Such a transition will undoubtedly change the character of bond points and their mechanical behaviour thus affecting properties and performance of nonwoven materials made of such fibres.

This research into mechanical properties of thermally bonded bicomponent fibre nonwovens aims at a detailed analysis of both bond points and representative

elements of nonwoven fabrics obtained by thermal bonding with various process parameters and with various bicomponent fibres.

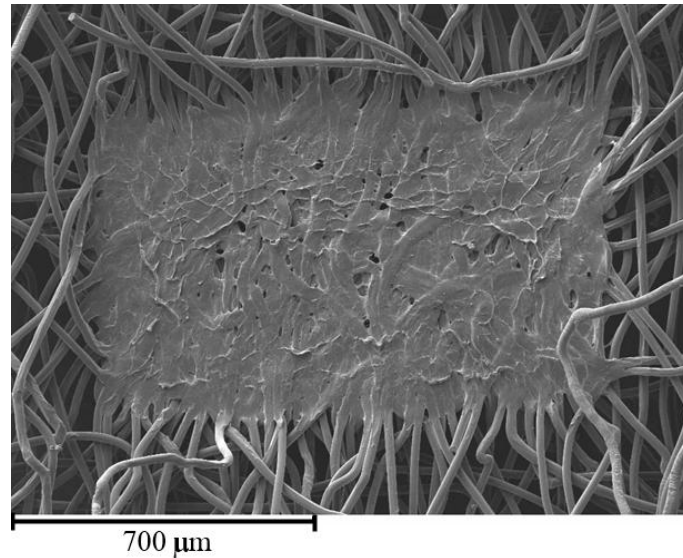


Figure 1.2. Magnified SEM image of bond point in Figure 1.1

1.1. Motivation

The issues motivating this research are mainly originating from industry, related to design and manufacturing of nonwoven textiles. Manufacturing of nonwovens is one of the fastest growing textile sectors with diverse applications. The total amount of nonwovens manufactured in the world in 2007 is 5.75 million tonnes, which corresponds to \$2 billion (EDANA, 2010). Since nonwovens are lightweight polymer-based materials, the annual production rate indicates a large market volume of nonwovens. Hygiene is the largest field in nonwoven usage, followed by civil engineering, construction and building materials (Russell, 2007). According to statistics, a significant part of the nonwoven market's share serves to mechanical or structural purposes, which require knowledge on mechanical properties of these materials. Therefore, one of the main requirements of the nonwovens industry is good understanding of mechanical properties of these materials as well as mechanisms of their deformation at both microscopic and macroscopic levels. Additionally, due to numerous trials taking place during product development and

optimization stages, design of nonwovens is an expensive and time-consuming process. In order to reduce the design cost of nonwovens linked to expensive product development and time-consuming product optimization stages, numerical tools could be introduced to predict their mechanical properties determined by manufacturing parameters.

The automotive industry has a low portion of the nonwoven consumption compared to other fields. Increasing fuel prices and the resulting demand for more economical vehicles make weight reduction one of the key factors for the automotive industry today. Therefore, usage of these materials in the automotive industry is growing every year (Smith, 2004). At this point, optimization of weight with regard to mechanical performance becomes a major topic for lightweight production. Such optimization requires a parametric numerical model of nonwoven materials for efficient lightweight design.

Structural design of a product containing a nonwoven part (armband, lab cloth, etc.), that is loaded during service conditions, requires mechanical properties of the used nonwoven material. Moreover, if the design procedure requires numerical simulation of that product, parameters defining the mechanical behaviour of the nonwoven part should be known to the designer. Mechanical testing is a costly and time-consuming process and, usually, mechanical properties of nonwovens depend on their manufacturing parameters. A numerical tool, which can adequately reproduce the mechanical behaviour of these materials, is necessary to designers dealing with nonwoven parts, which will deform in service.

Very few studies can be found in the literature concerning numerical modelling of nonwovens (Limem and Warner, 2005; Mueller and Kochmann, 2004; Kim and Pourdeyhimi, 2001). These studies offer only partial solutions for the prediction of a complex mechanical response of these materials to loading in 2D. Introducing a complete parametric 3D numerical model of nonwovens, which can represent their complicated mechanical behaviour, would be a novel contribution to scientific knowledge.

Finally, this research is performed within the framework of collaboration with the North Carolina State University Nonwovens Cooperative Research Center, which is a consortium of industry-leading companies. The progression of the research was tracked and evaluated semi-annually by the industrial advisors from well-known nonwoven manufacturing companies, such as P&G, DuPont, 3M, Ahlstrom, etc. The outcome of this research will help these companies to develop and optimize their nonwoven products with regard to the manufacturing parameters using numerical simulations rather than a trial-and-error method.

1.2. Aims and Objectives

With randomly distributed polymer-based fibres and being composed of two discrete regions – bond points and a fibre matrix – nonwovens have a unique mechanical behaviour, partially similar to, but distinct from, that of solid polymers and woven fabrics. Nonwovens studied in this research have a high planar density ($>50 \text{ g/m}^2$); they are manufactured with bicomponent fibres and bonded with thermal techniques. This research aims to analyse the complex mechanical behaviour of thermally bonded bicomponent fibre nonwoven materials with experimental and numerical methods. Numerical methods developed to study the unique mechanical behaviour of nonwovens accounting for their microstructure and manufacturing parameters will be a novel contribution to the academia and industry. To achieve the aim of the project, its major objectives are formulated in the following way:

1. To investigate the mechanical behaviour of bicomponent fibres by means of various mechanical experiments and to establish a link between the mechanical behaviour of the nonwoven fabric and that of its bicomponent fibres;
2. To examine the microstructure of nonwoven fabrics with various imaging techniques and to study its effects on their mechanical properties;
3. To investigate the mechanical behaviour of thermally bonded bicomponent fibre nonwovens using several types of mechanical tests and to analyse their main deformation mechanisms;

4. To develop a relation between the microstructure and mechanical anisotropy of thermally bonded high-planar-density nonwoven materials;
5. To analyse the anisotropic viscoelastic-plastic mechanical properties of bond points and the fibre matrix, constituting the nonwoven fabric;
6. To develop a parametric 3D finite element model of thermally bonded bicomponent fibre nonwoven materials to simulate their time-dependent mechanical response;
7. To analyse the efficiency of the introduced numerical model using experimental verification for several case studies.

1.3. Methodology

This research employs a novel approach to simulate a real-life deformation behaviour of high planar density ($>50 \text{ g/m}^2$) thermally bonded bicomponent fibre nonwoven materials utilizing mechanical properties of bicomponent fibres and manufacturing parameters such as planar density, core/sheath ratio, fibre diameter etc. In order to accomplish the project, several experimental and computational procedures described below should be followed.

Initially, the mechanical behaviour of bicomponent fibres will be acquired using tensile and relaxation tests. Since bicomponent fibres are the basic constituent of nonwoven materials used in this research, a mechanical behaviour of nonwovens will be analysed based on that of the fibres. Not only the mechanical behaviour of fibres but also their orientations play an important role in anisotropic mechanical performance of nonwovens. Each fibre acts as a truss member in tension between two bond points and mechanical response of each one depends on the direction of applied force with respect to its orientation. Direction dependent response of individual fibres leads to an overall mechanical anisotropy in the fabric. Therefore, several imaging techniques will be used to examine the microstructure of nonwovens composed of bond points and a fibre matrix. The last part of experimental stage aims to analyse mechanical performance of thermally bonded nonwovens, since it will be simulated with the developed 3D finite element model at the final stage of this study.

The numerical part will start with developing a relationship between a random microstructure of nonwoven materials and their mechanical anisotropy, which refers to their direction-dependent mechanical response. Randomness in the microstructure will be introduced in terms of an orientation distribution function of fibres determined from images of microstructure of the fibre matrix using digital image processing techniques. This novel approach will be performed using a specifically developed parametric algorithm for analysing mechanical anisotropy of the material. After dealing with anisotropy, assessment of anisotropic mechanical properties of thermally bonded bicomponent fibre nonwovens will be performed. The nonwoven fabric will be treated as an assembly of two regions having distinct mechanical properties: fibre matrix and bond points. The fibre matrix is composed of randomly oriented core/sheath type fibres acting as load-transfer links between bond points. On the other hand, bond points will be treated as a deformable bicomponent composite material composed of the sheath material as its matrix and the core material having random orientations as reinforcement. An original algorithm will be developed to assess anisotropic viscoelastic-plastic material properties of these regions based on properties of fibres and manufacturing parameters such as the planar density, core/sheath ratio, fibre diameter etc.

With anisotropic mechanical properties analysed for two regions, the fabric will be modelled in finite element software with 3D shell elements with thicknesses identical to those of bond points and the fibre matrix. In this final stage, simulations of several nonwovens with various manufacturing parameters and bicomponent fibres will be simulated using the proposed numerical modelling approach and results of these simulations will be verified with several experiments. The methodology for developing a 3D finite element model of thermally bonded bicomponent fibre nonwovens is also described in a block diagram in Figure 1.3.

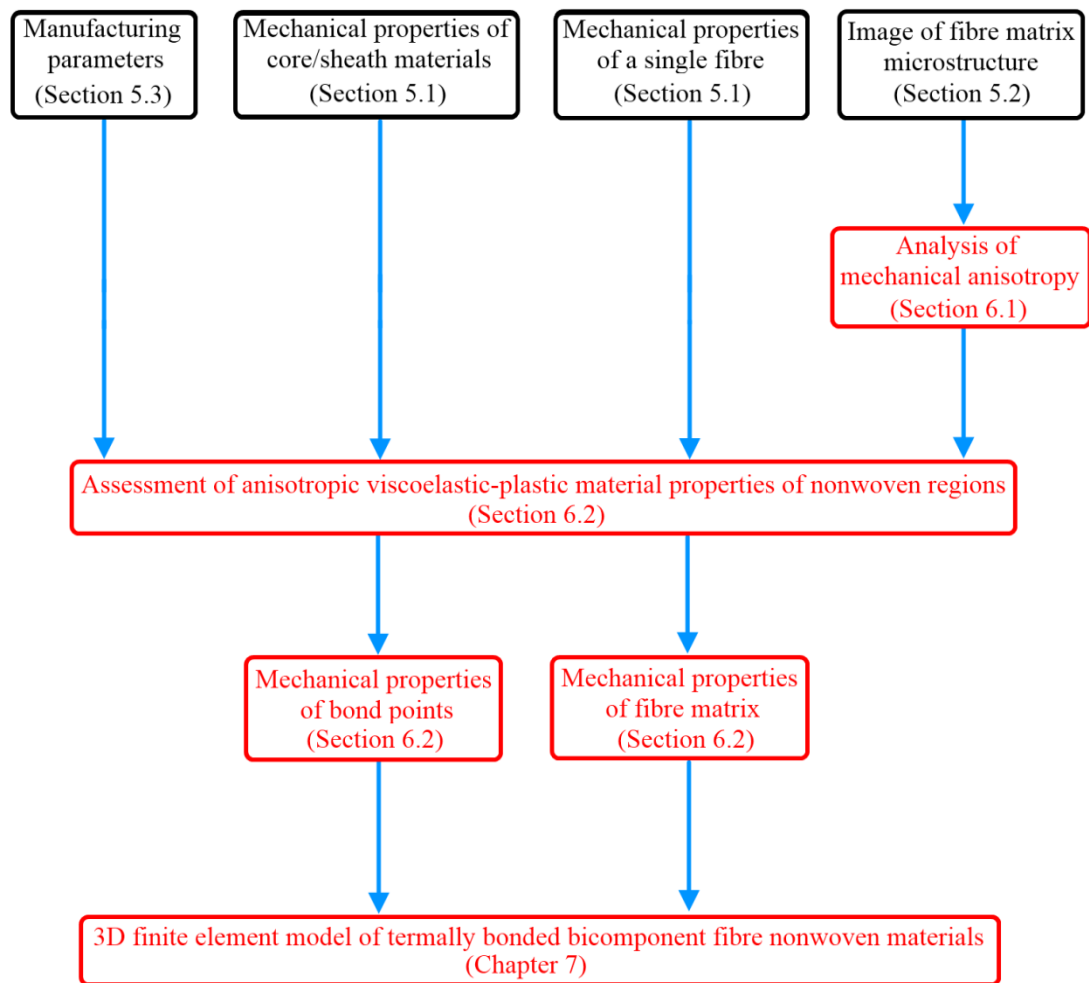


Figure 1.3. Research methodology for developing 3D finite element model of thermally bonded bicomponent fibre nonwovens (Red and black boxes designate numerical and experimental studies, respectively.)

1.4. Outline

The present work incorporates seven other chapters, the summary of which is the following:

Chapter 2 provides general background information on nonwovens related to their application areas, manufacturing methods and general properties. Detailed information about thermally bonded bicomponent fibre nonwovens is presented in this chapter as well.

Chapter 3 explains microstructural and physical features and underlying mechanisms characterizing the deformation behaviour of nonwoven materials.

Chapter 4 provides a review of the finite element method and equations used to model several mechanical behaviour types in this method. Existing numerical models developed to simulate mechanical performance of nonwovens are also presented in this chapter.

Chapter 5 presents experimental studies focussing on mechanical performance of thermally bonded nonwovens and their bicomponent fibres. Microstructure of nonwoven materials studied in this research is examined using several micro-scale imaging techniques.

Chapter 6 explains the assessment of complex mechanical properties of bond points and the fibre matrix using manufacturing parameters of the nonwoven material and mechanical behaviour of its bicomponent fibres. This chapter also explains a numerical method to assess mechanical anisotropy of nonwoven materials using their random microstructure.

Chapter 7 deals with a 3D finite element model developed to simulate a mechanical response of thermally bonded bicomponent fibre nonwoven materials. Several experiments are simulated with the introduced finite element model in order to compare experimental results with the numerical ones.

Chapter 8 summarizes the outcomes of the research and its contribution to academia and industry. This chapter also suggests future studies based on the results of this research.

CHAPTER II

2. INTRODUCTION TO NONWOVEN MATERIALS

According to EDANA (The European Disposables and Nonwovens Association), which is one of the main authorities in nonwovens in the world, a nonwoven is defined as "a manufactured sheet, web or batch of directionally or randomly orientated fibres, bonded by friction, and/or cohesion and/or adhesion, excluding paper and products which are woven, knitted, tufted, stitch-bonded incorporating binding yarns or filaments, or felted by wet-milling, whether or not additionally needled" (EDANA, 2009a). Nonwoven fabrics are engineered fabrics, which could be disposable or durable. The properties of these materials such as softness, flame retardancy, absorbency, strength, stretch, etc. could be designed according to their specific purposes (hygiene, filtering, etc.) (INDA, 2009).

In this chapter, basic information about nonwoven textiles will be given in terms of application areas, production techniques, raw materials, properties and thermally bonded bicomponent fibre type nonwoven materials.

2.1. Application Areas

Nonwoven fabrics are designed to serve specific purpose-defined functions. For this reason, nonwovens provide a large spectrum of products with diverse chemical and physical properties. This is reflected in the large variety of industrial, engineering, consumer and healthcare products. The most common products made with nonwovens according to EDANA (2009b) are:

- disposable diapers,
- sanitary napkins and tampons,
- sterile wraps, caps, gowns, masks and draping used in the medical field,
- household and personal wipes,
- laundry aids (fabric dryer-sheets),
- apparel interlining,
- carpeting and upholstery fabrics, padding and backing,
- wall coverings,
- agricultural coverings and seed strips,
- automotive headliners and upholstery,
- filters,
- envelopes,
- tags,
- labels,
- insulation,
- house wraps,
- roofing products,
- civil engineering fabrics/geotextiles.

The structure of the end-use market for nonwoven textiles is shown in Table 2.1 in terms of percentage for each purpose.

| Classification | % of total |
|----------------------------------|------------|
| Hygiene | 33.1 |
| Building/roofing | 12.5 |
| Wipes, personal care | 8.1 |
| Upholstery/table linen/household | 6.8 |
| Wipes, other | 6.7 |
| Civil Engineering/underground | 5.4 |
| Automotive | 3.9 |
| Liquid filtration | 3.7 |
| Medical/surgical | 2.6 |
| Coating substrates | 2.4 |
| Air/gas filtration | 2.4 |
| Floorcovering | 2.3 |
| Interlinings | 2.1 |
| Shoe leathergoods | 1.9 |
| Garments | 0.8 |
| Others/unidentified | 5.3 |

Table 2.1. European-produced nonwoven deliveries by end use (Russell, 2007)

Hygiene is the largest field in nonwoven usage, followed by civil engineering, construction and building materials. Therefore, it is clear that a considerable part of nonwovens are used for mechanical or structural purposes, which require knowledge of mechanical properties of these materials. Although automotive industry has a low percentage on the nonwoven consumption as compared to other fields, the use of these materials in the automotive industry is steadily growing every year (Smith, 2004). Increasing fuel prices and the resulting demand for more economical vehicles make weight reduction one of the key success factors for the automotive industry today (Fibertex A/S, 2008). Nonwovens play an important role in the lightweight

design of some automotive parts. As an example, nonwoven materials, which are used in different parts of an AUDI A2, are shown in Figure 2.1.

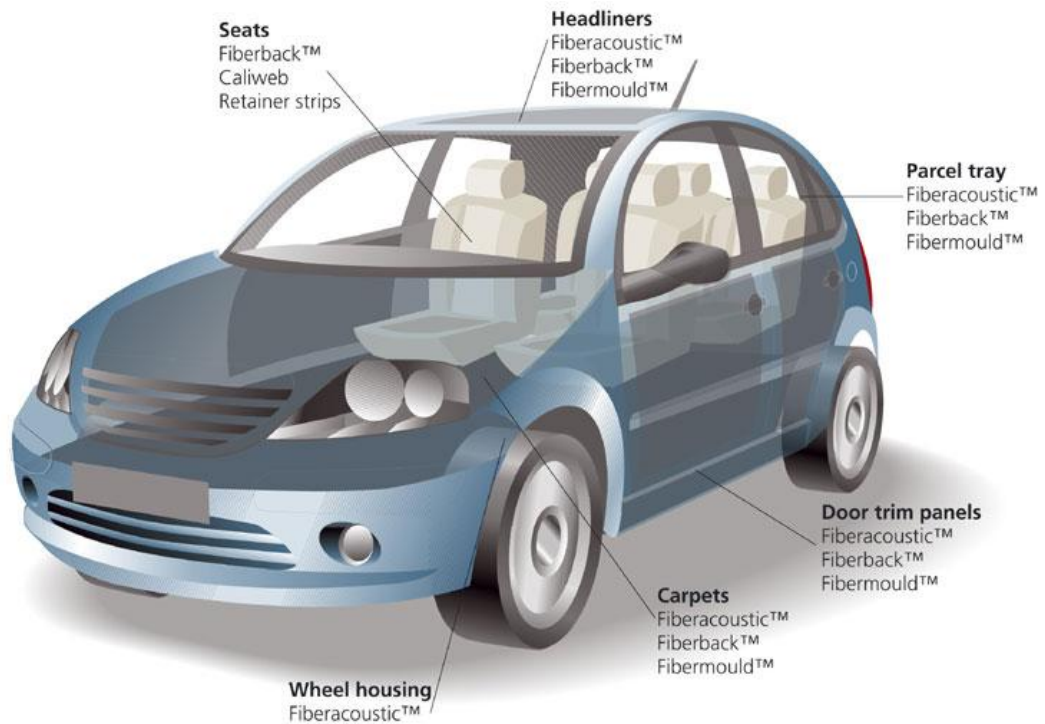


Figure 2.1. Nonwoven parts in the design of an automobile (Fibertex A/S, 2008)

2.2. Production Stages of Nonwoven Fabrics

Knowledge of the manufacturing processes of nonwoven fabrics is necessary in order to have a better understanding of the mechanical behaviour of these textile materials. Nonwoven fabrics are mainly manufactured with polymer materials. The mechanical properties of polymers can change depending on process conditions such as production speed, which affects the cooling rate of the polymer. A typical production process of nonwoven materials could be subdivided into four main parts: web forming, web manipulation, bonding and finishing (Table 2.2). The machine assembly, which performs these four manufacturing operations, is shown in Figure 2.2; their details are discussed below.



Figure 2.2. Nonwoven production facility (Hietel, 2006)

2.2.1. Web Forming

At this stage the fibres are produced from the molten raw material(s) and deposited onto a surface to form the web. The conditions of the fibres at this stage could be dry-laid, wet-laid or polymer-laid (Purdy, 1983). The orientation distribution of the fibres determining the anisotropy in the material is formed at this stage. A typical web formation formed of free-falling fibres on the surface of conveyor is illustrated in Figure 2.3.

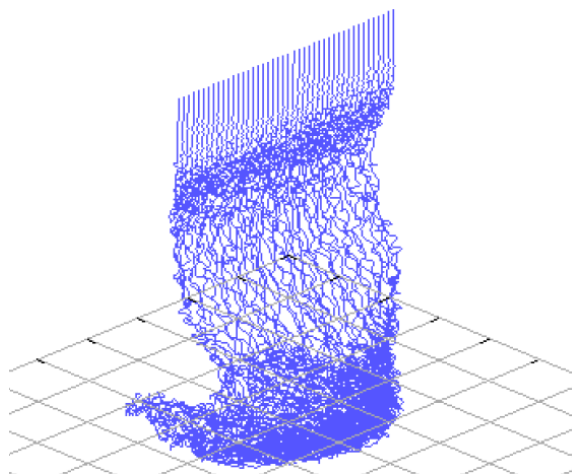


Figure 2.3. Simulation of web formation from individual fibres (Hietel, 2006)

2.2.2. Web Manipulation

At this stage, the distribution of the web structure is determined to satisfy the geometric requirements of the final product. The web is spread, scrambled, etc. to obtain the required geometrical properties for the nonwoven fabric.

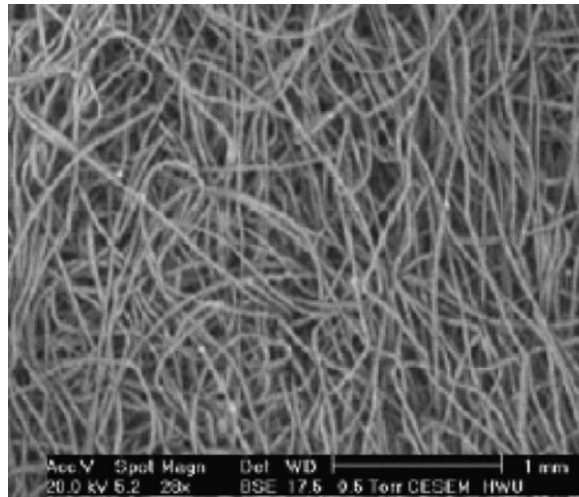


Figure 2.4. SEM image of polypropylene fibres before bonding (Wei *et al.*, 2007)

2.2.3. Bonding

During the web bonding process fibres are consolidated in order to attain the necessary performance parameters. The degree of web bonding depends on fibre characteristics, such as fibre geometry, tenacity and shape as well as the density of the web to be bonded (Albrecht *et al.*, 2003).

The fibre web could be bonded using three main processes: mechanical, thermal or chemical (Batra, 1998). More than one bonding process could be used in some fabric constructions. Mechanical bonding methods include needle punching, stitch bonding and hydroentangling. Chemical bonding processes involve applying adhesive materials to the web by spraying, printing, foaming techniques. In thermally bonding, heat is used together with pressure to soften or melt fibres in order to weld each other as shown in Figure 2.5. Generally, heat is applied to the web employing a

hot calendar with an engraved pattern or hot air blown through the web. Thermal bonding techniques will be explained further in Section 2.5.

Bonding is the major factor determining the mechanical properties of a nonwoven material (Chidambaram *et al.*, 2000). The shape, type and pattern of bond points as well as bonding temperature change the mechanical behaviour of the material dramatically (Bhat *et al.*, 2004).

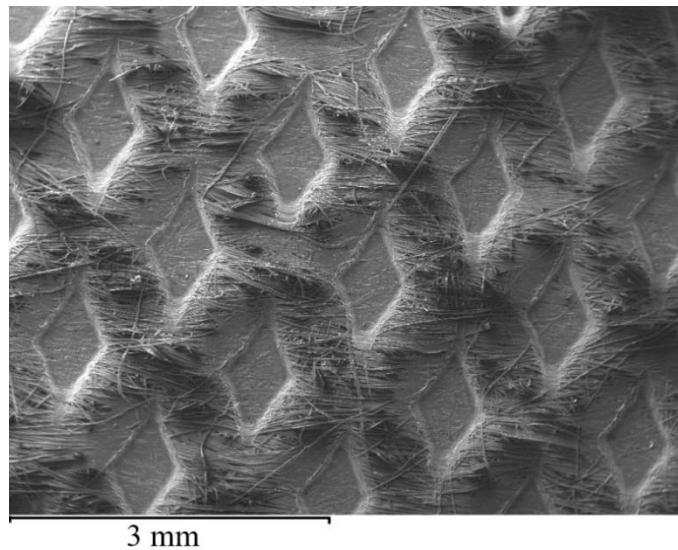


Figure 2.5. Bond pattern of thermally bonded nonwoven material

2.2.4. Finishing

Finishing is an additional procedure used to functionalise nonwoven fabrics. There is no standard finishing routine for nonwovens. Traditionally, finishing is classified as wet finishing (washing, dyeing, coating, etc.) and dry finishing (embossing, calendaring, etc.). Due to service conditions, nonwovens could be coated for specific purposes such as changing electrical properties (Weia *et al.*, 2008).

Each manufacturing stage explained above is performed by a dedicated section of the machine assembly designed for nonwoven production. A simple sketch describing the production of nonwoven fabrics is given in Figure 2.6. The raw polymer material is molten and extruded to produce fibres. Then fibres are accumulated on the conveyor to obtain the web assembly. Finally, the web assembly is manipulated to have a sheet form in a compaction roll and then bonded with a calender.

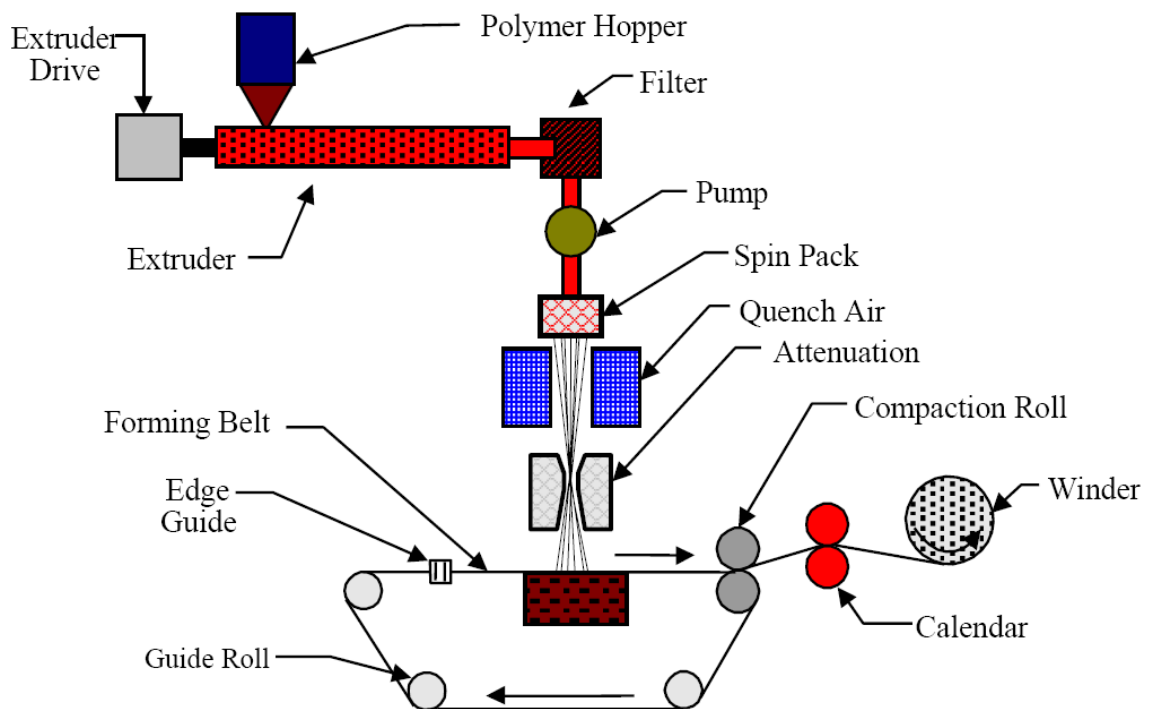


Figure 2.6. Schematic diagram of nonwoven production (spunbond) (Fedorova, 2006)

2.3. Raw Materials

Most of the fibres for nonwoven materials are produced from natural polymers, synthetic polymers or inorganic materials (Krcma, 1962). According to (Russell, 2007), the world usage of raw materials for the production of nonwoven fibres is:

- Polypropylene - 63%,
- Polyester - 23%,

- Viscose rayon - 8%,
- Acrylic - 2%,
- Polyamide - 1.5%,
- Other speciality fibres - 3%.

Polypropylene is the most frequently used material for the nonwovens due to its low density, low glass transition and melting temperatures, chemical stability, good mechanical strength and abrasion resistance.

2.4. Properties of Nonwovens

According to (Krcma, 1962) the main parameters of nonwoven fabrics, which affect the material properties and manufacturing processes, are:

- a) Geometrical properties,
- b) Mechanical properties of fibres,
- c) Physico-chemical properties,
- d) Chemical properties,
- e) Physiological properties.

Geometrical and mechanical properties of fibres are the essential factors that determine mechanical properties of nonwovens.

2.4.1. Geometrical properties

To some extent, the structure of the nonwoven determines its mechanical properties.

The core factors of nonwovens are:

- Fibre length and cross-section,
- Distribution of fibres,
- Surface characteristics,
- Bond points (shape, type, pattern and bonding temperature).

2.4.2. Mechanical properties

Deformation mechanisms of nonwovens are important factors with regard to the end-use properties of final products. Many researches (Adanur and Liao, 1999; Kim, 2004; Rawal, 2006; Michielsen *et al.*, 2006) have been done to study five basic aspects of a mechanical behaviour:

- Deformation characteristics,
- Tensile strength,
- Break length,
- Elongation properties,
- Elasticity.

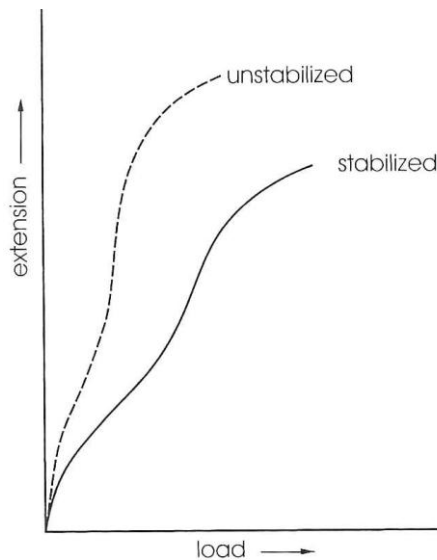


Figure 2.7. Load-extension graphs for unstabilised and stabilised polyester
(Albrecht *et al.*, 2003)

The mechanical properties of polymer materials change during the production stages, especially at the web-forming stage (Datla, 2002). Because the mechanical properties of the polymers depend on the temperature variation with respect to time, the mechanical properties of the raw material are different from those of the material in the nonwoven fabric. For instance, during stretching at the web-forming stage, the molecules of a fibre are aligned parallel to one another causing tension in the fibres.

Because of this tension, the fibres can shrink when heated, if they are not held tight at both ends. The stretched, unfixed fibres are called unstabilised fibres. If the molecules of the fibre are parallel to one another with an optimum alignment, the fibres will not shrink in subsequent processing. Such fibres are referred as stabilised fibres. Figure 2.7 demonstrates the difference between the mechanical behaviour of stabilised and unstabilised polyester fibres. During the hot calendaring process unstabilised fibres will shrink and their mechanical properties will change (Albrecht *et al.*, 2003).

2.5. Thermally Bonded Bicomponent Fibre Nonwoven Materials

The aim of this research is to model the mechanical performance of thermally bonded nonwoven fabrics. These types of nonwovens have outstanding properties, which we focus on. This section gives brief information about these nonwovens and the features specific to them as compared to other nonwovens. Due to such properties thermally bonded bicomponent fibre nonwovens are among the most common manufactured types of nonwovens in the industry and usually demonstrate higher strength properties than other nonwoven types.

As explained above, nonwoven fabrics are engineered materials to serve specific purposes. For structural or mechanical applications such as geotextiles, the mechanical properties of the fabric should be superior with respect to the fabrics for disposable usage. Especially, bond points play a very important role in determining the mechanical behaviour of the material. As explained in Section 2.2.3, one of the methods for bonding fibres is mechanical bonding. In the case of mechanical bonding, fibres can be damaged (Figure 2.8) at the boundaries of the bond points due to punching (Chidambaram *et al.*, 2000).

In order to overcome the strength loss due to mechanical bonding, thermal bonding could be an alternative. In thermal bonding, bond formation is succeeded with melting of fibres at bond points, resulting in discontinuous fibres (Datla, 2002).

With this respect, bicomponent fibres retaining their continuity in the fabric demonstrate superior properties due to increase in strength of nonwovens (Wang *et al.*, 2006).

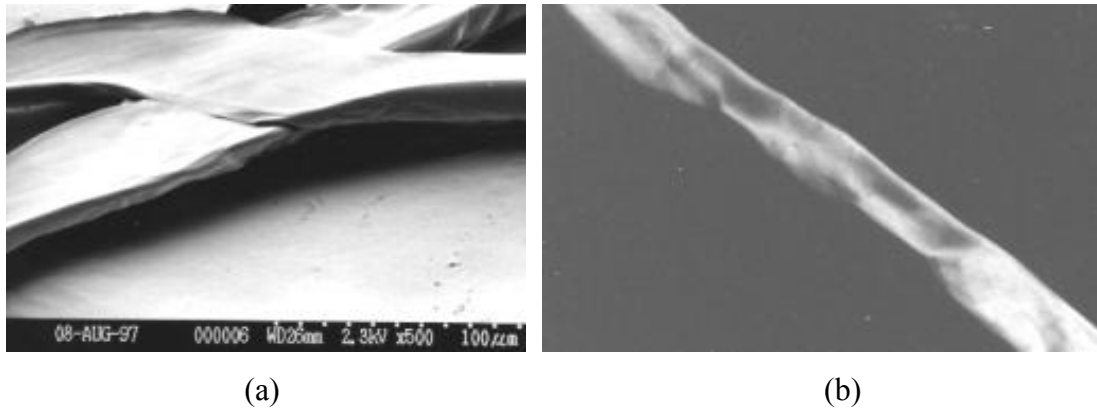


Figure 2.8. (a) Deformed fibres at the edge of a mechanical bond point. (b) Deformed single fibre in a mechanical bond point (Chidambaram *et al.*, 2000).

The increase in strength of nonwovens is linked to specific microstructure of bicomponent fibres. They have domains of two distinct materials, one of which has a lower melting point. When the bicomponent fibres are exposed to a temperature between the melting temperatures of two constituent materials, the one with the lower melting point melts. With the pressure applied, molten parts of the neighbouring fibres combine and then solidify when cooled. In this way, the fibres are bonded together with continuous un-melted parts. Different types of bicomponent fibres could be seen in Figure 2.9.



Figure 2.9. Several types of bicomponent fibre cross-sections (different colours represent different materials)

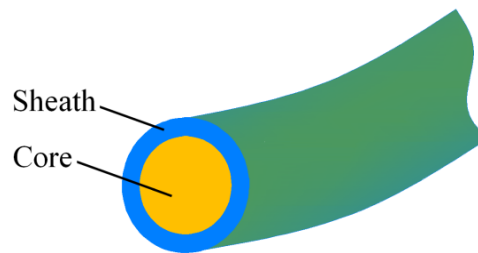


Figure 2.10. Cross-section of core/sheath bicomponent fibre

The most frequently used bicomponent fibre type is the core/sheath type (Figure 2.10), which has the core material surrounded by the sheath material with a lower melting point (Xina *et al.*, 2008). Compared to mono-component fibre type nonwovens, bicomponent fibre nonwovens have superior mechanical properties due to continuous and undamaged shape of the core material after the bonding process. The images of the bond points of nonwovens formed by mono-component and bicomponent fibres are shown in Figure 2.11.

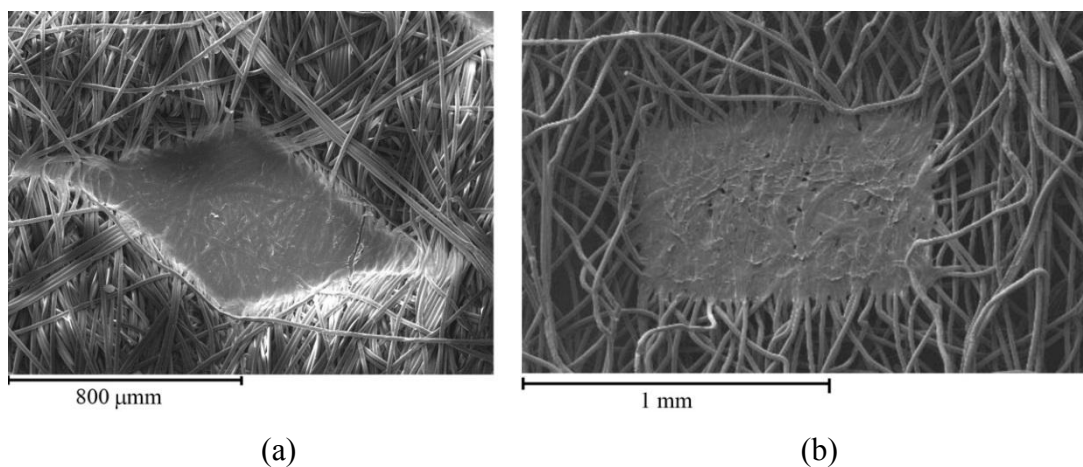


Figure 2.11. Bond points of bicomponent fibre nonwoven (a) and mono-component fibre nonwoven (b)

One of the most common processes to manufacture bicomponent fibre nonwovens is the spunbonding process. Spunbonding involves direct conversion of a polymer into continuous filaments, integrated with the conversion of filaments into a random-laid, bonded nonwoven (Bhat *et al.*, 2002). During the production of

bicomponent fibre nonwovens in spunbonding process, five operations take place: filament extrusion, drawing, quenching, lay down and bonding (Fedorova, 2006). The facility, which performs these operations, consists of the following elements (Figure 2.12): a polymer feed, an extruder, a metering pump, a die assembly, a filament spinning, a drawing and deposition system, a collecting belt, a bonding zone and a winding unit. Each operation affects the structural parameters of a nonwoven such as fibre density, fibre diameter, orientation distribution, porosity, etc. For instance, to minimize the pore size in a bicomponent fibre nonwoven filter, thermal bonding temperature, air velocity and dwell time should be optimized (Wang and Gong, 2006).

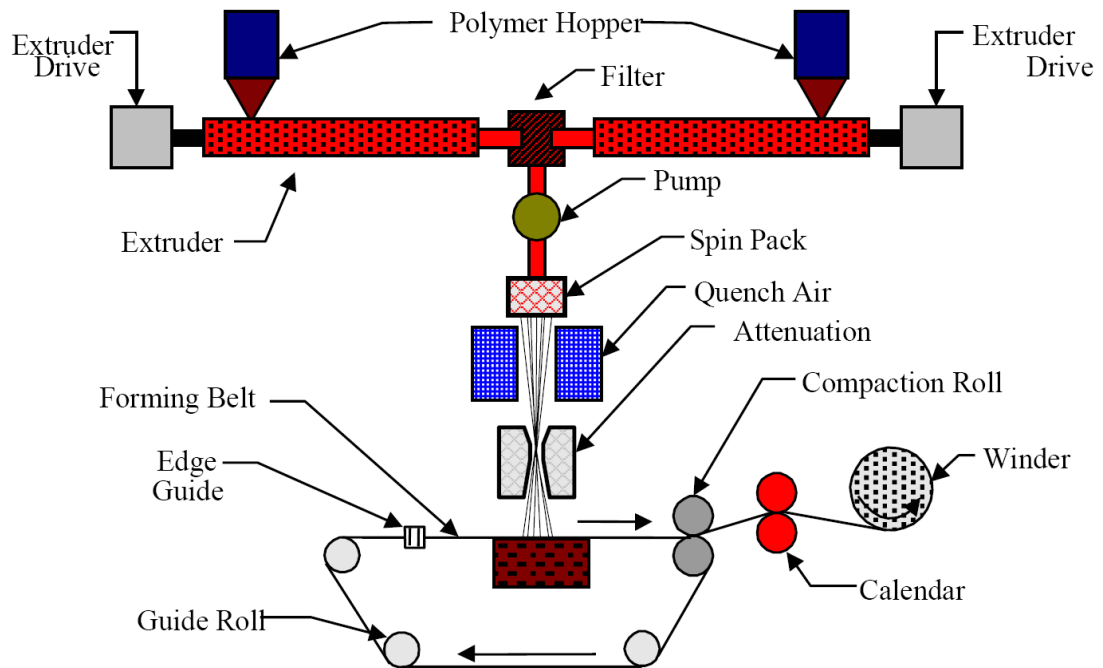


Figure 2.12. Schematic diagram of bicomponent spunbond process with belt collector (Fedorova, 2006)

There are several techniques to perform thermal bonding of bicomponent fibre nonwoven fabrics. Hot calendaring is the most frequently used method for thermal bonding in the industry. Thermal bonding is performed on the nonwoven web with a temperature-controlled calender using a combined action of heat and pressure. As a

result of this, the sheath material melts and fibres are pressed, forming a bond when the sheath material solidifies (Figure 2.13).

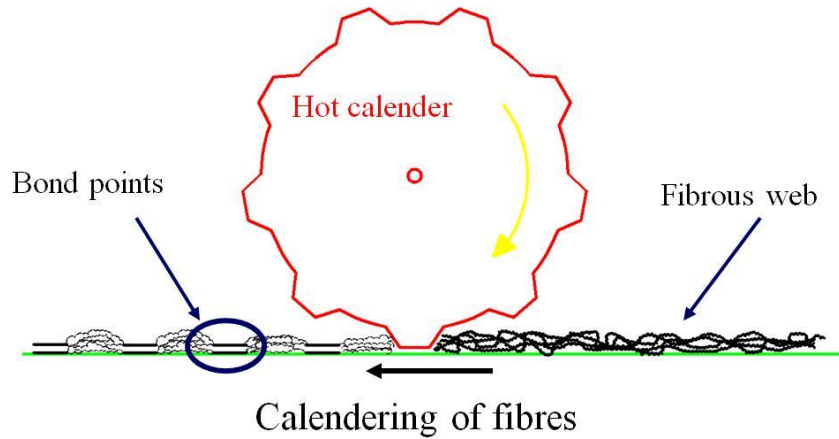


Figure 2.13. Hot calendaring process of thermally bonded nonwovens

Compared with other types of bonding, thermal bonding brings significant advantages (Albrecht *et al.*, 2003):

- It has high economic efficiency compared to chemical bonding, since thermal bonding process uses less binder agents and need less energy.
- Generally, the used manufacturing systems are cheaper than those for other process.
- The process can be used for a thick web, and the bonding effect is controllable.
- The material is recyclable, which is good for environment, since it is possible to use pure-polymer fibres in the process.
- The fibre properties are controllable, so there are opportunities to produce nonwovens with different functions (e.g. flame-retardancy, high bulk and resilience, heat-insulation, etc.).

Another way of thermal bonding is through-air bonding. This process produces bulkier products by the overall bonding of a web containing low-melting-temperature fibres. The hot air flows through holes in a plenum positioned just above the nonwoven. A negative pressure or suction pulls the air through the open conveyor

apron that supports the nonwoven as it passes through the oven (Figure 2.14). Binders such as crystalline binder fibres, bicomponent binder fibres, and powders are necessary to help the bonding. When using crystalline binder fibres or powders, the binder melts entirely and forms molten droplets throughout the nonwoven's cross-section. Bonding occurs at these points upon cooling. In the case of core/sheath binder fibres, the sheath is the binder and the core is the carrier fibre (Gao and Huang, 2004; Hoyle, 1990).

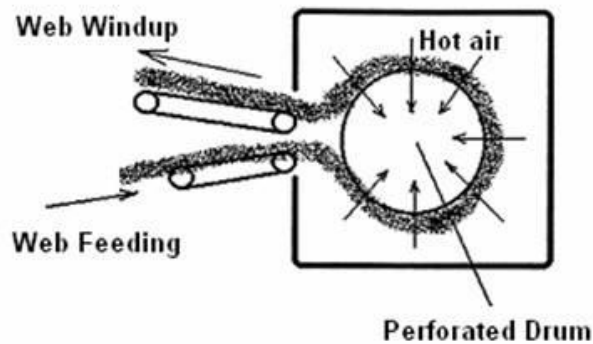


Figure 2.14. Schematic of through-air bonding process (Gao and Huang, 2004)

Ultrasonic bonding is another method used to bond bicomponent fibres thermally. When ultrasonic vibration is applied to the material, these mechanical excitations are converted into thermal energy via friction and melt the sheath material. Upon removal from the source of ultrasonic vibration, the softened fibres cool, solidifying the bond points (Gao and Huang, 2004).

The type and parameters of the thermal bonding process are very important for mechanical properties of nonwovens due to the effect of temperature on the polymer structure. The most important parameter in the thermal bonding is the bonding temperature. Although the temperature window is relatively narrow between the melting points of the two polymers, the tensile behaviour of the nonwoven is affected significantly (Figure 2.15) by any change in the bonding temperature (Michielsen *et al.*, 2006). In addition to bonding stage, heat could be applied during finishing process as well.

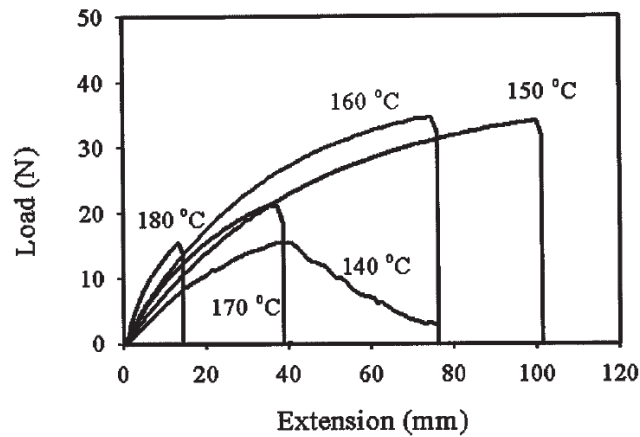


Figure 2.15. Effect of bonding temperature on stress-strain behaviour of nonwoven fabrics (Kim *et al.*, 2002)

Finishing process could be applied to nonwoven fabrics to serve specific purposes. One of them is to improve the dimensional stability of polypropylene/polyester (PP/PET) fibres by increasing the crystallization rate of PET by heat treatment. Due to the heat treatment, fibres shrink (Figure 2.16) and their mechanical properties change (Zhao *et al.*, 2003). According to Figure 2.16, inclusion of 25% PP to fibres significantly stabilizes the heat shrinkage to approximately 5% under conditions of 150° for 9 min. This is due to the fact that the crystallization of PP develops faster than that of PET. The shrinkage increases with the treatment time and becomes stable after 7 min.

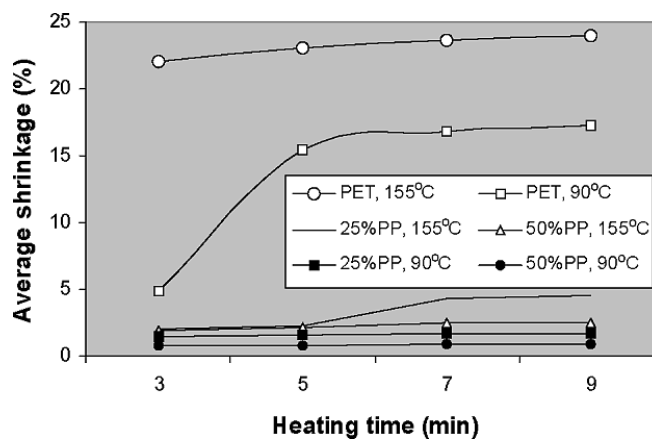


Figure 2.16. Effect of heat treatment time on shrinkage of PET and PP/PET webs at different temperatures (Zhao *et al.*, 2003)

2.6. Summary

Brief information about application areas, manufacturing techniques, raw materials and general properties of nonwoven fabrics is given in this chapter. Having unique properties and significant usage and manufacturing advantages, such as cost-effectiveness and fast production rate, compared to other types of fabrics, nonwovens have wide range of applications. Since nonwovens are engineered materials, mechanical properties of these fabrics could be modified depending on the application areas. This research focuses on modelling the mechanical performance of nonwoven fabrics. The study is closely related to their mechanical and structural properties, which will be explained in the next chapter.

CHAPTER III

3. MECHANICS OF NONWOVEN FABRICS

The research field of mechanics of fabrics mainly focuses on mechanics of woven fabrics rather than mechanics of nonwovens. The reason is that, due to their higher strength properties and recoverability, woven materials are preferred as reinforcement in composites and in military applications which are the main fields using textiles for mechanical purposes (Backer and Petterson, 1960). Therefore, few researches have been done on the mechanics of nonwoven materials.

The increasing usage of nonwoven textiles (Russell, 2007) requires a better understanding on mechanics of these materials. As explained in the previous chapter, nonwoven fabrics are frequently used in the civil engineering applications such as geotextiles for structural purposes. In order to use nonwoven fabrics in engineering design, knowledge on mechanics of these materials is necessary.

Based on a through literature survey, this chapter aims to explain mechanics of nonwovens with regard to two aspects: characterisation of nonwovens and their mechanical behaviour.

3.1. Characterisation of Nonwoven Fabrics

Mechanical, physical and chemical properties of nonwoven fabrics, which define their suitability for specific applications, depend on the properties of the fibre composition and the fabric structure. The fibre composition refers to the materials forming fibres and the mechanical behaviour that they exhibit. The fabric structure is linked to the bond pattern and geometry, orientation distribution and planar density of the fibre web.

A nonwoven structure is different from other textile structures due to the following features (Russell, 2007):

- Nonwovens are composed of individual fibres or layers of fibrous webs rather than yarns.
- The material is anisotropic in terms of structure and properties because of the fibre orientation distribution and bond pattern.
- Nonwoven materials are non-uniform structures in terms of both weight and thickness distributions.
- The material is highly porous and permeable.

Additionally, both physical and mechanical properties of nonwovens are affected by the web formation, bonding and fabric finishing processes. Although chemical properties of the nonwoven materials are important from the manufacturing point of view, only physical and mechanical properties of the nonwovens, which are related to their deformational behaviour, are going to be utilized for the characterisation of nonwoven materials in this study.

3.1.1. Mechanical Properties of Fibres

A thermally bonded nonwoven fabric is composed of two regions: bond points and the fibre matrix. Bond points are composed of fibres joined via mechanical, thermal or chemical methods. On the other hand, the matrix is the web of fibres connecting bond points together. In order to understand the mechanical behaviour of the matrix, mechanical properties of the fibres forming the web assembly should be known.

There are important parameters defining the mechanical behaviour of a fibre: the breaking force, tenacity, initial modulus, chord modulus (secant modulus) at break, and elongation at break (Gusick *et al.*, 1963). The breaking force is the maximum force applied to a fibre to cause its rupture. The elongation is the ratio of the extension of a fibre to its length prior to stretching. The tenacity is the breaking force divided by the linear density of the fibre. The initial modulus is a measure of the resistance of the fibres to extension under an applied force below the fibre yield point and defined as the maximum slope of the tangent line to the stress-strain curve at the initial stage of deformation. The chord modulus is the ratio of stress to strain at any point on the stress-strain curve (Saville, 1999).

The mechanical properties of a fibre are determined with the use of tensile testing. On the other hand, the dimensional stability of polymer fibres could be established by determining the molecular orientation of the material. The latter can be measured by using an interference microscope equipped with a polarizing filter (Barakat, 1971; Hamza *et al.*, 1986).

Due to the nature of polymer materials, mechanical properties of the nonwoven fibres at the raw form, hot calendered and heat treated form are different due to the effect of temperature playing an important role on their molecular structure and dimensional stability (Michielsen *et al.*, 2006; Zhao *et al.*, 2003). This will be considered in determining the mechanical properties of nonwoven fibres in Section 5.1.

3.1.2. Orientation Distribution of Fibres

The distribution of fibres in a nonwoven media is a major concern of researchers dealing with their randomness. This factor affects the relation between a given bond and the bonds within its neighbourhood (Figure 3.1).

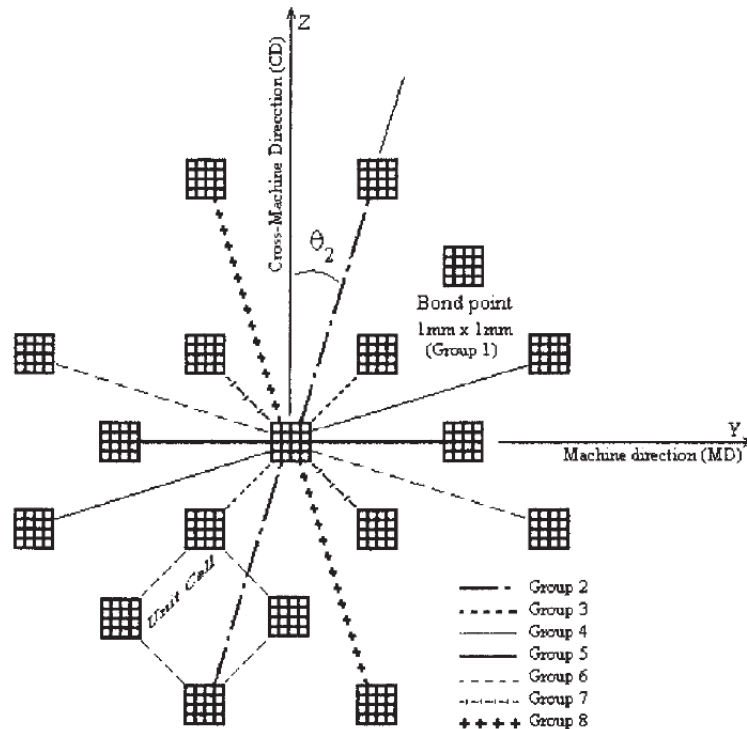


Figure 3.1. Bond points and fibre group distribution (Limem and Warner, 2005)

The fibre distribution is inherited from the web formation and bonding processes. Orientations of fibre segments can be controlled partially at these production stages. Due to shrinkage, fibres tend to curl during any stage requiring thermal or chemical processing (Hearle and Ozsanlav, 1979).

In order to represent randomness of the fibre distribution in a fibrous media mathematically, a concept of “distribution function” was introduced in 1952 (Cox, 1952). Then determination of the orientation distribution function (ODF) became a major interest in the field of textiles.

An ODF is a histogram defining the angle of fibres with respect to a reference direction (Figure 3.2). Detection of the ODF is necessary not only for nonwovens but also for woven textiles to detect the weave pattern and identify the structure (Wood, 1990; Xu, 1996). Nonwoven materials have two principal directions: machine direction (MD) and cross direction (CD). MD is the flow direction of the web assembly on the conveyor during manufacturing. CD is perpendicular to MD on the plane of conveyor, where the web assembly forms the sheet geometry.

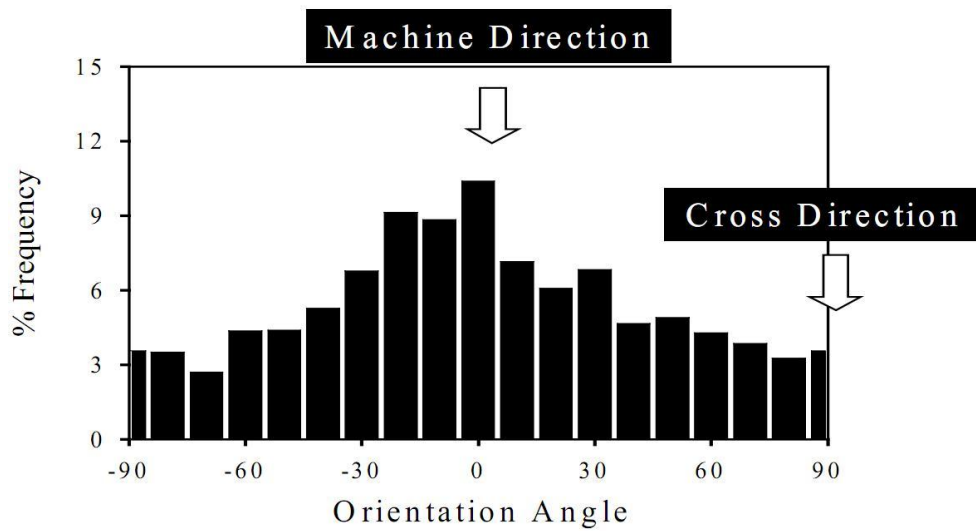


Figure 3.2. Typical ODF of nonwoven fabric (Kim *et al.*, 2000)

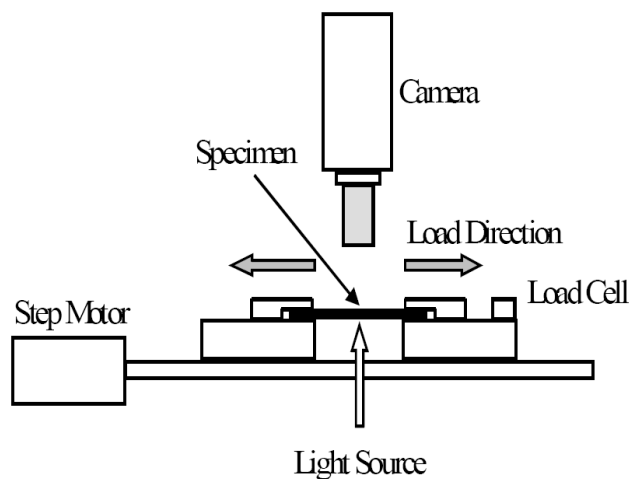


Figure 3.3. Device for characterizing structural changes in nonwoven materials during tensile tests (Kim *et al.*, 2000)

The ODF is detected via optical methods combined with image processing techniques. The apparatus in Figure 3.3 uses a CCD camera to detect the ODF under deformation. Not only camera images, but also SEM images (Figure 3.4) are used to compute the ODF (Ghassemieh *et al.*, 2001).

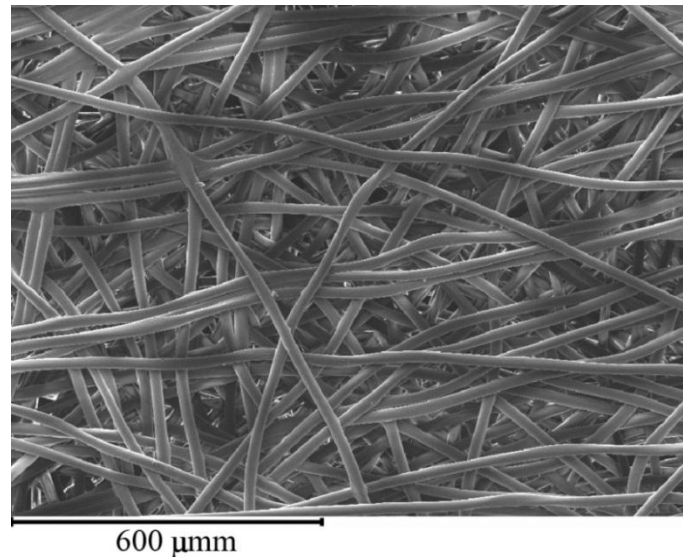


Figure 3.4. SEM image of web matrix of thermally bonded nonwoven fabric which can be used for ODF detection

The initial work for computing the ODF of nonwoven materials was performed for adhesively bonded nonwoven fabrics by expressing the ODF in powers of the cosine function (Hearle and Ozsanlav, 1979). Today there are two main methods for computing the ODF from the textile images: Fast Fourier Transform (FFT) and Hough Transform (HT).

3.1.2.1. Fast Fourier Transform

The FFT has been used as an efficient computational tool in a wide range of applications. In the field of image processing, it is one of the most useful techniques used for image enhancement and measurement (Xu and Ting, 1995). An image, a 2D function in a spatial domain, often contains periodic structures, non-periodic elements, noise and background. It is, sometimes, difficult or even impossible to separate and analyse these image components in the spatial domain since they are

often embedded and entangled together. A 2D FFT decomposes an image from its spatial domain of intensities into spatial frequency domain (Figure 3.5). The spatial frequency domain is important because it highlights periodic relationships in the spatial domain and some image processing is more efficient in the frequency domain (Ghassemieh *et al.*, 2001). A higher rate of change in the greyscale intensity is reflected in higher amplitudes. A function $f(x, y)$ in the spatial domain could be defined in the frequency domain as;

$$F(u, v) = \int \int_{-\infty-\infty}^{\infty \infty} f(x, y) e^{-2\pi i(xu+ yv)} dx dy , \quad (3.1)$$

where $F(u, v)$ is the Fourier transform of the function, u and v are the variables in the frequency domain. As observed, $F(u, v)$ is a complex function with phase and magnitude.

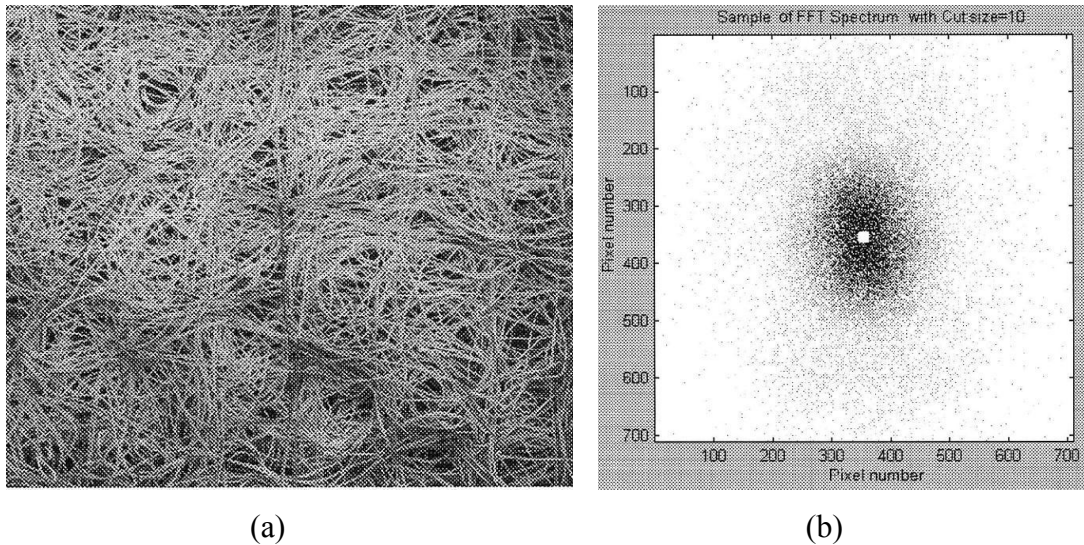


Figure 3.5. SEM image of nonwoven (a) and FFT spectrum of this image (b)
(Ghassemieh *et al.*, 2002a)

When the FFT method is used to process nonwoven images, the frequency of fibre orientations could be calculated. Commercial software based on the FFT method for ODF detection was introduced to the industry (Pourdeyhimi *et al.*, 1997;

Pourdeyhimi *et al.*, 1999; Pourdeyhimi and Ramanathan, 1997; Pourdeyhimi *et al.*, 1996a; Pourdeyhimi *et al.*, 1996b).

The use of this method in ODF detection has several disadvantages. Lighting conditions (brightness) and scope of the nonwoven area affect the results. The scope of the nonwoven image should be representative for the whole fabric. Since the FFT algorithm uses grey scale images, binarized or skeletonized images of fibres can give different ODF outcomes (Ghassemieh *et al.*, 2002a). Finally, in the denser structures, as the number of cross-over points increases, the efficiency of the FFT method decreases (Xu, 1996).

3.1.2.2. Hough Transform

The Hough transform is one of the most effective methods for object detection in an image. The HT requires the desired features to be specified in a parametric form, such as line, circle, and ellipse. In most of the cases, it is necessary to know the type of geometry that is to be fitted to the data. To determine ODFs of nonwovens, straight-line segments of fibres are detected via HT (Xu and Yu, 1997).

A straight line passing through the origin could be defined with two parameters in polar coordinates as

$$r = x \cos(\theta) + y \sin(\theta), \quad (3.2)$$

where r is the distance of a second point to the origin and θ is the angle of the line with respect to the x -axis. In the binarized image, after the edge detection is performed on the objects, collinear points (x_i, y_i) with $i = 1, \dots, N$ are transformed into sinusoidal curves $r = x_i \cos \theta + y_i \sin \theta$ in the Hough plane, which intersect at the point (r, θ) . For a certain range of parameters r and θ , each (x_i, y_i) is mapped onto the Hough space and the points that map onto the locations (r_m, θ_m) are accumulated in a 2D histogram (Figure 3.6). Local maxima of the intensity in the Hough space identify straight line segments in the original image (Ghassemieh *et al.*, 2002a).

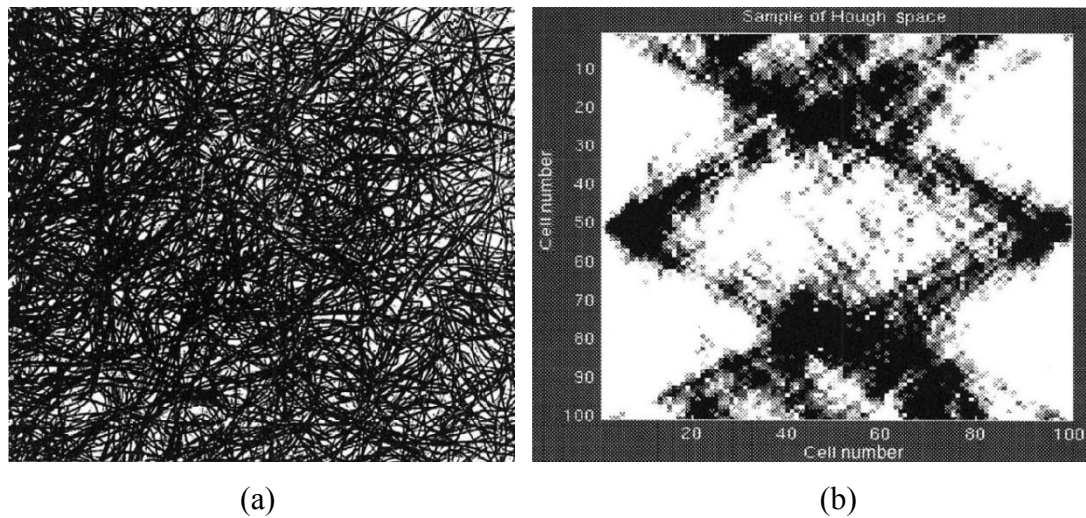


Figure 3.6. Binarized image of nonwoven fabric (a) and Hough space of this image (b)
(Ghassemieh *et al.*, 2002a)

Application of the HT technique to determine ODF is more recent than that of the FFT method. These methods were used to obtain the ODF of hydroentangled nonwoven fabrics, and the results of HT were closer to the experimental results than those of the FFT (Ghassemieh *et al.*, 2002b). Each method has several advantages depending on the noise, lighting conditions and web structure (Pourdeyhimi and Kim, 2002). Main advantages of the HT method are that it is tolerant to gaps at object edges and relatively unaffected by the image noise (Ghassemieh *et al.*, 2002b).

3.1.3. Physical Properties of Nonwoven Fabrics

Basis weight is the most important parameter for defining a nonwoven textile and represents the mass per area unit. Many properties including strength, thickness, porosity, tearing strength, etc. are influenced by changes in the basis weight of the fabric (Rawal *et al.*, 2008).

The thickness of fabrics is determined as the distance between the upper and the lower surfaces of the material, measured under a specified pressure (Fedorova, 2006). The bulk density of the samples is determined by dividing the fabric basis weight on its thickness.

Finally, the fibre diameter is measured with SEM. In order to consider shrinkage of polymers due to thermal effects, the fibre diameter is measured after the web-finishing process. 50 to 100 fibres are measured to account for fluctuations in their diameter.

3.2. Mechanical Behaviour of Nonwovens

Nonwoven fabrics have a unique mechanical behaviour, which has not been defined completely in the literature. The deformational behaviour of nonwoven fabrics resemble to some extent the behaviour of different materials; e.g. they are anisotropic similar to woven textiles and exhibit viscoelasticity similar to polymers. In fact, the mechanical response of a nonwoven fabric is a mixture of the behaviours of bond points and the fibre matrix, which exhibit distinct mechanical performances.

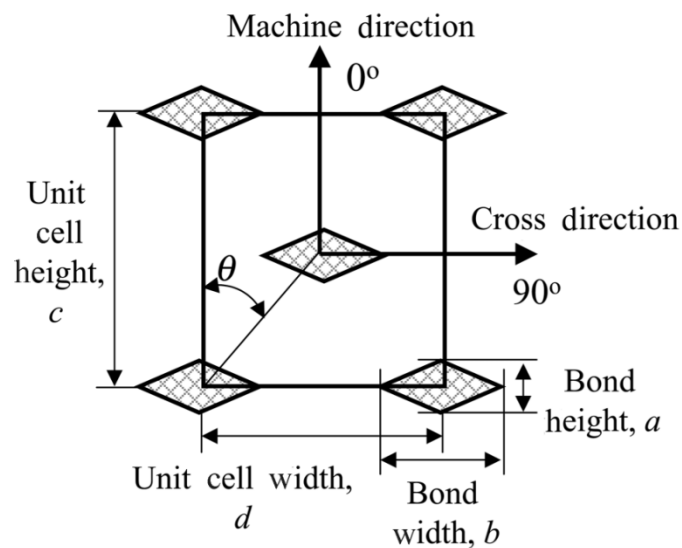


Figure 3.7. MD and CD with respect to bond pattern and geometry (Kim, 2004b)

There are many aspects of the mechanical behaviour of nonwoven fabrics, but one of them – anisotropy – is the most prominent one. Nonwoven fabrics exhibit an anisotropic mechanical behaviour due to a random distribution of fibres and a pattern of bond points. The deformation characteristics of these materials depend on the direction of loading. Two principle directions having different mechanical properties

in woven fabrics, namely, warp and weft, enable them to be modelled as orthotropic (Price *et al.*, 2006). In the case of nonwovens, due to the random distribution of fibres characterised by the ODF, the level of anisotropy is higher than in the woven fabrics. In order to simplify the anisotropy of the nonwovens, two principle directions - MD and CD - are used (Figure 3.7).

The microstructural randomness of the fabric and the pattern of bond points yield a dependence of a stress-strain curve on the loading direction. The effect of loading direction on the mechanical performance of a nonwoven material could be observed in Figure 3.8.

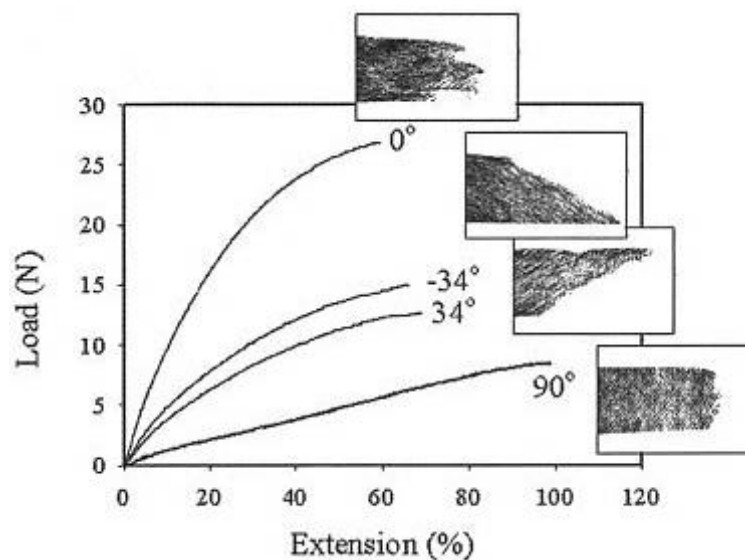


Figure 3.8. Angular mechanical properties and failure behaviours of thermally bonded nonwovens; 0° and 90° represent MD and CD, respectively (Michielsen *et al.*, 2006)

The geometry and pattern of bond points contribute to the level of anisotropy in addition to the distribution of fibres (Lin *et al.*, 1973). For instance, the ratio of the area of bond points to that of fibre matrix is a major concern in the mechanical performance due to their distinct microstructure (Figure 3.9).

Obviously, the strength along MD is more than that along CD according to Figures 3.8 and 3.9. In a typical ODF curve the density of orientation of fibres is concentrated near the MD due to the fact that in the web-forming process fibres are

laid along the conveyor direction. Due to this fact the deformation behaviour of nonwovens along MD and CD differs. Deformation of the web and bond points under loading along MD and CD is presented in Figure 3.10. Obviously, the nonwovens possess higher mechanical properties for MD than for CD.

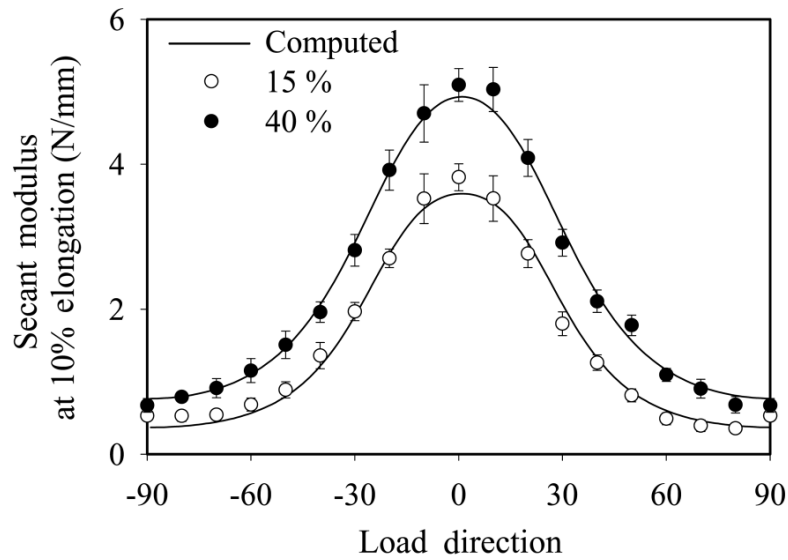


Figure 3.9. Secant modulus of nonwovens with 15% and 40% bond area ratio for varying loading directions; 0° and 90° represent MD and CD, respectively (Kim, 2004b)

Although the type of anisotropy differs from orthotropy, some simplified models based on orthotropy are introduced for prediction of the mechanical behaviour of these materials (Kim, 2004a). Despite some interesting assumptions such as a Poisson's ratio larger than 0.5, the model is consistent with the experiments. Although a main source of anisotropy is the random orientation of fibres, there are other sources contributing to this phenomenon.

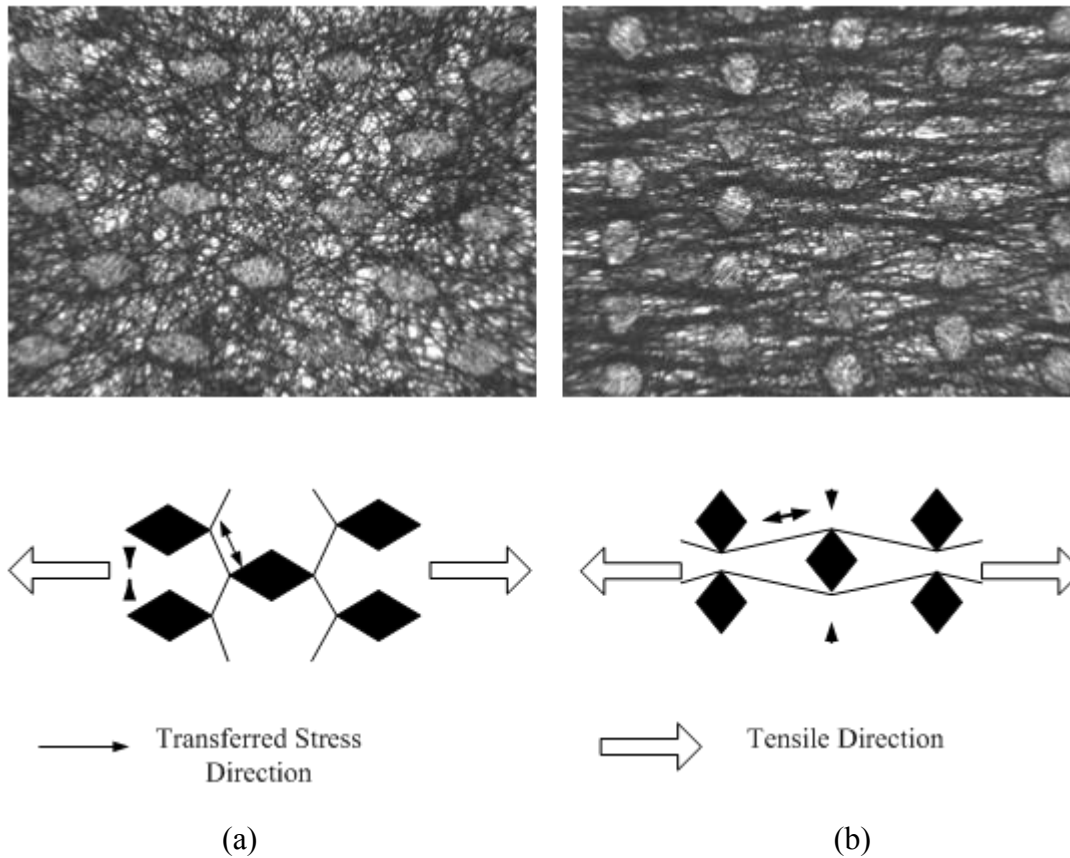


Figure 3.10. Images and deformation mechanisms of nonwoven fabric after 50% elongation in CD (a) and MD (b) (Kim *et al.*, 2000)

In addition to random orientation of fibres and bond pattern properties, crimp of fibres contributes to an anisotropic behaviour of nonwoven fabrics. Due to the curly character of fibres, not all the fibres are loaded at the initial stage of loading. This phenomenon was deeply investigated and the curl factor was introduced to calculate the mechanical properties of nonwoven fabrics (Adanur and Liao, 1999). A micromechanical model for prediction of the tensile behaviour of nonwoven materials was developed based on modification of the model introduced by Adanur and Liao (1999). In that model due to curliness of fibres, a fibre curl factor was introduced to improve the understanding of the loading behaviour of a single fibre (Rawal, 2006). The fibre curl factor (C_i) is defined as the extent of curvature:

$$C_i(\%) = \frac{L_c - L_s}{L_s} \times 100, \quad (3.3)$$

where L_c and L_s are the curve and straight lengths defined between two points. In a fibrous web, curl factor varies widely; the curl factor of a fibre similar to segment A (Figure 3.11) is higher than that of other segments. As seen in Figure 3.11, the curl factor in fibre segment E is zero.

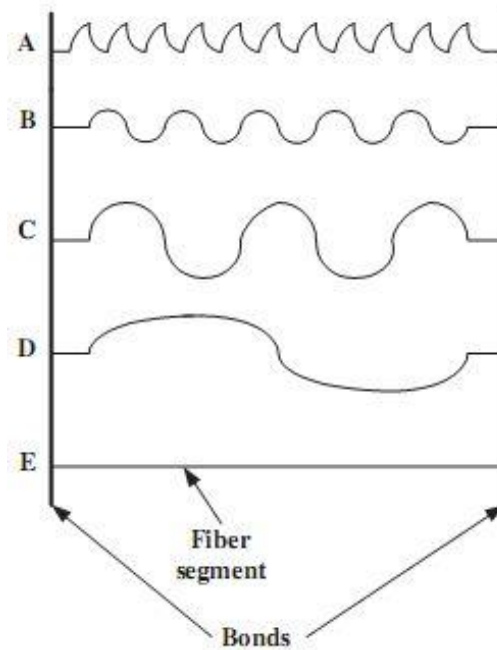


Figure 3.11. Schematics of variation in fibre curl in typical fibrous web (Rawal, 2006)

The final issue related to anisotropy of nonwovens fabrics is the failure mechanism. Due to randomness in the structure, nonwovens exhibit complex damage behaviour. As shown in Figure 3.12, damage characteristics of nonwoven fabrics differ depending on the direction of load with respect to MD. A few studies were made on the failure mechanism of nonwovens. A damage criterion based on fibre failure and bond rupture was introduced to predict damage in nonwoven fabrics (Britton *et al.*, 1983). The failure model was implemented in a numerical simulation (Britton *et al.*, 1984a; Britton *et al.*, 1984b).

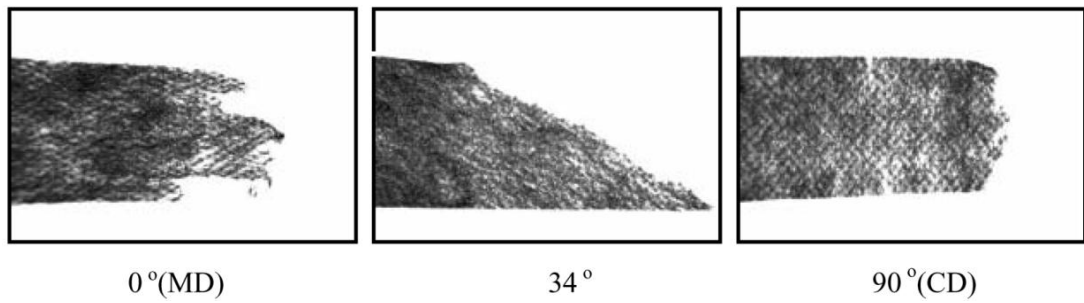


Figure 3.12. Rupture images of nonwovens for various tensile directions (Kim, 2004b)

3.3. Summary

To sum up, from the established point of view of computational mechanics, a material model based on mechanical and physical properties of nonwoven materials has not been developed yet. Most of the research performed up to now on the mechanical behaviour of nonwovens aims to explain a partial phenomenon with respect to the textile engineering point of view. For instance, only a few studies in the literature consider plastic deformation of nonwoven materials (Mishakov *et al.*, 2006). Therefore, a thorough investigation of the mechanical behaviour of these materials from the computational mechanics point of view should be implemented.

Basic characteristics and mechanical behaviours of nonwovens are explained in this chapter. These materials are different from woven fabrics and composites in terms of microstructure and mechanical performance. Their mechanical behaviour is complicated due to their microstructure and polymer-based constituent materials leading to anisotropic nonlinear viscoelastic-plastic deformation. This complex behaviour should be investigated and incorporated in models used to analyse the performance of thermally bonded bicomponent fibre nonwoven fabrics, which are the main topic of this study. Despite the complex behaviour, there are some simplified numerical models of these materials in the literature, which will be explained in the next chapter.

CHAPTER IV

4. MODELLING OF MECHANICAL BEHAVIOUR OF MATERIALS

A need to improve properties and performance of nonwovens leads companies to use simulations in order to design and manufacture products faster and cost-effectively. A realistic simulation requires a material model, which represents the deformation characteristics of the material in real-life applications such as sports and automotive industry (Smith, 2004). The most prominent deformation characteristics of nonwovens to be accounted in models are anisotropy in their mechanical properties and a viscoelastic-plastic mechanical behaviour.

Anisotropy is the dependence of the mechanical response of material on the direction of applied load. As explained in Section 3.2, nonwoven fabrics possess anisotropic mechanical properties due to randomly oriented fibres and manufacturing-induced pattern of bond points. In order to implement direction

dependence of mechanical properties in numerical modelling, brief information about anisotropy and related topics will be given in this chapter.

Additionally, nonwovens made of polymer-based fibres possess viscoelastic-plastic behaviour. Due to viscous effects, mechanical properties of nonwovens depend on time. On the other hand, they can exhibit plasticity, i.e. which means irreversible deformation. In order to introduce a complete mechanical model, these behaviours should be considered. This chapter provides mathematical characterisation of these behaviours, which could be utilized in numerical modelling.

Finite element (FE) is one of the most suitable computational tools to simulate the deformational behaviour of nonwovens under service loadings since it is commonly available as commercial software packages. In this chapter, a brief review of nonlinear finite element analysis and the existing finite element models of nonwovens in the literature will be given.

4.1. Basics of Mechanical Properties

Mechanical properties of a solid material can be represented in mathematical terms illustrating the behaviour of that material in a specific direction. These properties may change with varying scales and microstructure. This section discusses material symmetry and a scale concept, which affect the mechanical properties used in numerical modelling.

4.1.1. Material Symmetry and Corresponding Tensor Structures

Material symmetry is related to substructure of a material. The basic concept to describe the substructure is to define its motif where a motif is the periodically repeated arrangement of substructure elements in space to generate the pattern (Newham, 2005). The periodic spatial arrangement of the motif is mathematically described by a space lattice. There are symmetry planes in these motives where mechanical properties do not change such as infinite numbers of symmetry planes exist in the materials which are assumed as isotropic.

Material symmetry can be defined at a single material particle and/or within a region of material and can change from particle-to-particle and/or region-to-region. Any symmetry in material structure will be reflected by symmetry in mechanical properties. An inhomogeneous mechanical behaviour is characterized by changing symmetry and/or properties throughout the material. The change in mechanical properties due to material symmetry is introduced in three material models: anisotropic, orthotropic and isotropic material models (Ting, 1996).

4.1.1.1. Anisotropic Material

An anisotropic material lacks any material symmetry. Its 4th order elasticity tensor (or tensor of elastic constants) C_{ijkl} , that relates the stress tensor to the strain tensor, is fully populated and contains $3^4=81$ terms. C_{ijkl} is found according to (Asaro and Lubarda, 2006)

$$C_{ijkl} = \frac{\partial^2 \psi^e}{\partial \varepsilon_{ij}^e \partial \varepsilon_{kl}^e} \quad (4.1)$$

where ψ^e is the elastic potential and ε^e are the elastic strains from strain tensor.

However, due to symmetry of the stress and strain tensors and due to the existence of the strain energy function, the number of independent elastic constants is reduced to 21 for the fully anisotropic material (Newham, 2005). Therefore the fourth order indices, $ijkl$, are mapped to their matrix counterparts as follows

$$[11,22,33,12,13,23] \rightarrow [1,2,3,4,5,6] \quad (4.2)$$

(for instance, C_{1123} reduces to C_{16}) and the elastic constants reduce to the form

$$[C]_{\text{anisotropic}} = \begin{bmatrix} C_{11} & C_{12} & C_{13} & C_{14} & C_{15} & C_{16} \\ C_{21} & C_{22} & C_{23} & C_{24} & C_{25} & C_{26} \\ C_{31} & C_{32} & C_{33} & C_{34} & C_{35} & C_{36} \\ C_{41} & C_{42} & C_{43} & C_{44} & C_{45} & C_{46} \\ C_{51} & C_{52} & C_{53} & C_{54} & C_{55} & C_{56} \\ C_{61} & C_{62} & C_{63} & C_{64} & C_{65} & C_{66} \end{bmatrix}. \quad (4.3)$$

Let also note that $C_{ij} = C_{ji}$.

4.1.1.2. Orthotropic Material

An orthotropic material has three principal directions as shown in Figure 4.1. Properties of the material are symmetric with respect to three orthogonal planes defined by these directions.

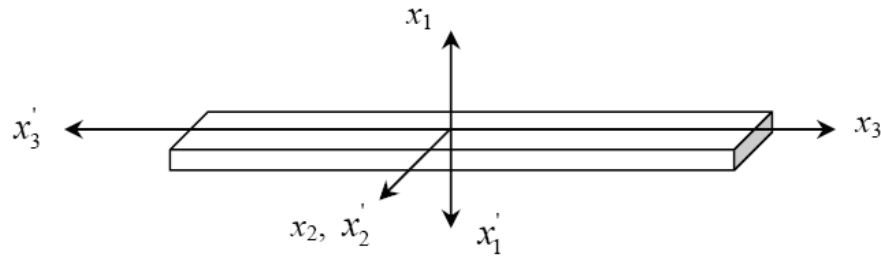


Figure 4.1. Principal directions in orthotropic material model

$$[C]_{\text{orthotropic}} = \begin{bmatrix} C_{11} & C_{12} & C_{13} & 0 & 0 & 0 \\ C_{21} & C_{22} & C_{23} & 0 & 0 & 0 \\ C_{31} & C_{32} & C_{33} & 0 & 0 & 0 \\ 0 & 0 & 0 & C_{44} & 0 & 0 \\ 0 & 0 & 0 & 0 & C_{55} & 0 \\ 0 & 0 & 0 & 0 & 0 & C_{66} \end{bmatrix} \quad (4.4)$$

Due to symmetry conditions, orthotropic elasticity tensor (Equation 4.4) is symmetric with respect its diagonal. Therefore, elasticity tensor has 9 independent constants in orthotropy. These constants could be stated in terms of Young's

modulus (E_i), Poisson's ratio (ν_{ij}) and shear modulus (G_{ij}) with respect to three principal directions as follows (Roesler *et al.*, 2007):

$$\begin{aligned} C_{11} &= 1/E_1 & C_{12} &= -\nu_{12}/E_2 & C_{44} &= 1/G_{23}, \\ C_{22} &= 1/E_2 & C_{13} &= -\nu_{13}/E_3 & C_{44} &= 1/G_{13}, \\ C_{33} &= 1/E_3 & C_{23} &= -\nu_{23}/E_3 & C_{44} &= 1/G_{12}. \end{aligned} \quad (4.5)$$

4.1.1.3. Isotropic Material

An isotropic material has the same mechanical properties in all spatial directions. Therefore, the elasticity tensor must remain unchanged by arbitrary rotations of the material or the coordinate system. The elastic constants must be invariant with respect to rotations. As a result of infinite number of symmetry planes the number of independent elastic constants in isotropic elasticity tensor reduces to 2:

$$[C]_{\text{isotropic}} = \begin{bmatrix} C_{11} & C_{12} & C_{12} & 0 & 0 & 0 \\ C_{12} & C_{11} & C_{12} & 0 & 0 & 0 \\ C_{12} & C_{12} & C_{11} & 0 & 0 & 0 \\ 0 & 0 & 0 & \frac{C_{11} - C_{12}}{2} & 0 & 0 \\ 0 & 0 & 0 & 0 & \frac{C_{11} - C_{12}}{2} & 0 \\ 0 & 0 & 0 & 0 & 0 & \frac{C_{11} - C_{12}}{2} \end{bmatrix}. \quad (4.6)$$

The relations between isotropic elastic constants (C_{11} and C_{12}) and Young's modulus (E), Poisson's ratio (ν) and shear modulus (G) are

$$\begin{aligned} C_{11} &= \frac{E(1-\nu)}{(1+\nu)(1-2\nu)}, \\ C_{12} &= \frac{E\nu}{(1+\nu)(1-2\nu)}. \end{aligned} \quad (4.7)$$

Three material models described in this section represent direction dependent mechanical properties for three levels of material symmetry. As explained, material symmetry, which can change from particle-to-particle and/or region-to-region, is

affected by the substructure of the material. This effect is related to the scale of substructure in a way that inhomogeneity in mechanical properties increases with substructure size.

4.1.2. Scale Concept in Mechanics

4.1.2.1. Representative Volume Element Concept

Representative Volume Element (RVE) is a model of the material that can be used to determine the corresponding effective properties for the homogenized macroscopic model. RVE is the minimal material volume, which contains statistically enough mechanisms of deformation processes. The increase of this volume should not lead to changes in parameters of evolution equations for field values, describing these mechanisms. For instance, RVE is a unit cell for a periodic microstructure and volume containing a very large set of grains, possessing statistically homogeneous properties (Gitman *et al.*, 2007).

The micro-scale is characterized by a statistically representative volume, which contains micro-structural information such as crystallographic texture in metals (Miehe *et al.*, 1999). RVE should be large enough to contain sufficient information about the microstructure in order to be representative; however, it should be much smaller than the macroscopic body because it is the smallest possible volume that reflects its macroscopic properties. For instance, RVE for metals is highly dependent on the grain size. If the metal part is fine grained, the material may be assumed as homogeneous and isotropic material properties could be used for RVE. On the other hand, if the metal part is coarse grained, it may be assumed as inhomogeneous and anisotropic material properties could be used for RVE.

4.1.2.2. Homogenization and Its Use in Meso-Modelling

The mechanical behaviour of materials within structures under mechanical load is the result of mechanisms active at a micro-scale within their constituents and at their interfaces, and of the spatial distribution of these constituents. The prediction of the macroscopic behaviour, based on these data, requires complex scale-transition

operations representing the interaction phenomena between the constituents. Instead, some mathematical constituents in the form of mechanical properties such as modulus of elasticity and in the form of field variables such as stress and strain are introduced to illustrate the mechanical behaviour. This approach is called *homogenization*. Homogenization intrinsically includes volume averaging of micro-scalar properties to represent them in the macro-scale (Miehe *et al.*, 1999).

For an isotropic material, RVE is a very large set of constituents. As a result of homogenization, elastic behaviour of a very large set of constituents, e.g. grains for metals, is represented by a single modulus of elasticity value. Homogenized moduli of elasticity values for several metals are shown in Table 4.1.

| Metal | Modulus of Elasticity (GPa) |
|--------------|------------------------------------|
| Aluminium | 68.0 |
| Copper | 200.0 |
| Iron | 110.0 |

Table 4.1. Modulus of elasticity values of some metals in macro-scale

As the scale gets smaller, the data starts to scatter with respect to the crystallographic texture in these metals (Table 4.2). Therefore a single modulus of elasticity term loses its validity for representing the elastic behaviour in the micro-scale.

| Metal | Modulus of Elasticity (GPa) | | |
|--------------|------------------------------------|--------------|--------------|
| | [100] | [110] | [111] |
| Aluminium | 63.7 | 72.6 | 76.1 |
| Copper | 66.7 | 130.3 | 191.1 |
| Iron | 125.0 | 210.5 | 272.7 |

Table 4.2. Modulus of elasticity values for several metals at various crystallographic orientations at micro-scale (Callister, 2003)

The effect of material size with respect to its constituent elements on the mechanical properties is explained using an example of metals (Tables 4.1 & 4.2). This phenomenon is similar in nonwovens in a way that homogenized mechanical

properties could be assigned to the fabric's size significantly larger than its constituents' (bond points & fibres) size. Basically, these macro-scale properties will be results of homogenization of mechanical properties of bicomponent fibres constituting fibre matrix and polymer composite bond points. Homogenized properties will scatter with decreasing material size; on the other hand, numerical model becomes more complicated when it is built with sub-models of the material's negligibly small substructures.

Plastic deformation in macro-scale is a result of dislocation movement in the grains of a metal or reorientation of molecular chains in a polymer in micro-scale. Instead of grain-by-grain or molecule-by-molecule modelling plastic behaviour in macro scale, homogenization approach is facilitated to avoid vast computational power requirements. As a result of this approach, several equations are developed to model characteristics of this behaviour. Next section explains these equations, which are used to model plastic behaviour of a material.

4.2. Modelling of Plastic Behaviour

Plasticity, which refers to irreversible deformation, plays an important role in the mechanical behaviour of polymer-based materials. This behaviour should be included in the numerical modelling of nonwoven materials. This section gives background information about theory of plasticity, which explains the relationship between stress and strain in plastically deformed solids. Four main aspects are covered briefly: yield criterion, flow rule, strain hardening and extensions to anisotropy.

4.2.1. Yield Criterion

Yield strength or yield point (Figure 4.2) is the stress at which a material starts to deform plastically. Prior to the yield point the material will deform elastically and will return to its original shape when the applied stress is removed. Once the yield point is passed some fraction of the deformation will be permanent and irreversible.

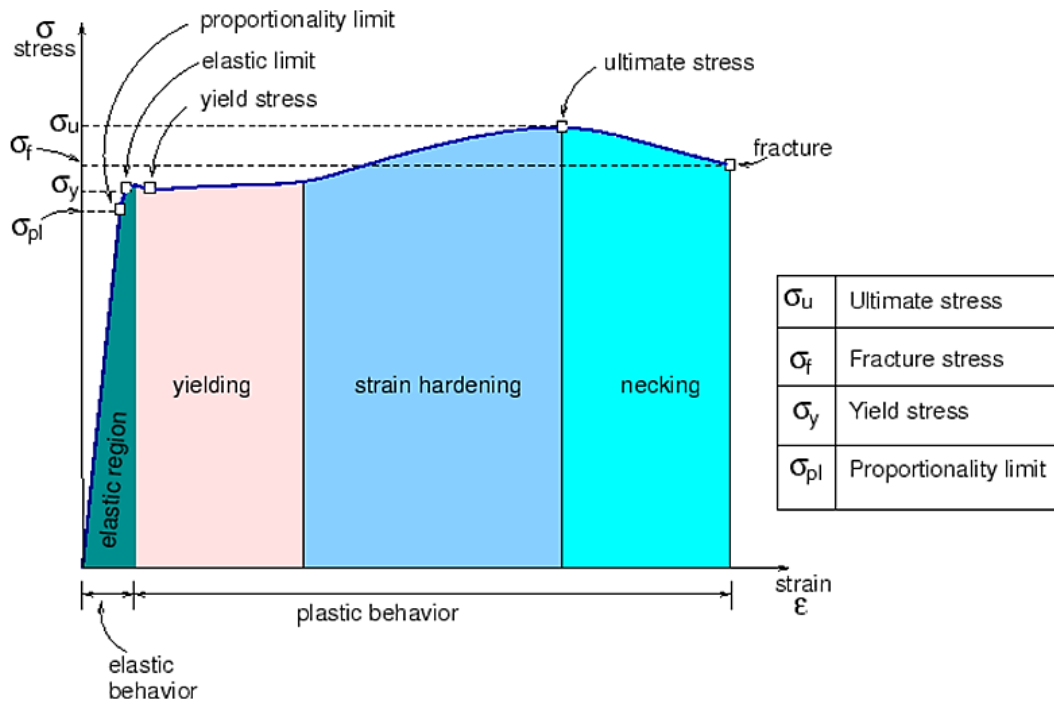


Figure 4.2. Mechanical behaviour of a material

A relation defining the limit of elasticity under any possible combination of stresses is known as a yield criterion (Hill, 1950). The first step of plastic flow analysis is to determine a yield criterion. When the material is supposed to be isotropic, plastic yielding depends only on the magnitudes of the principal applied stresses, not on their directions. Any yield criterion is expressible in the form (Hosford, 2005)

$$f(I_1, I_2, I_3) = C, \quad (4.8)$$

where I_1, I_2, I_3 are the first three invariants of the stress tensor σ_{ij} and C is a constant (Hill, 1950). The invariants are defined in terms of the principal components of stress (σ_1, σ_2 and σ_3) by relations;

$$I_1 = \sigma_1 + \sigma_2 + \sigma_3, \quad (4.9)$$

$$I_2 = -(\sigma_1\sigma_2 + \sigma_2\sigma_3 + \sigma_1\sigma_3), \quad (4.10)$$

$$I_3 = \sigma_1 \sigma_2 \sigma_3. \quad (4.11)$$

The principal stresses are the roots of the characteristic equation of the eigenvalue problem:

$$\lambda^3 - I_1 \lambda^2 - I_2 \lambda - I_3 = 0. \quad (4.12)$$

Apparently, any function of the invariants can be expressed in terms of the principal stresses.

A simplification of Equation 4.8 is possible using a fact that the yielding of an ideal plastic body is unaffected by hydrostatic stress. Therefore, yielding depends only on the deviatoric principal stress components $(\sigma'_1, \sigma'_2, \sigma'_3)$ which are derived as

$$\sigma'_{ij} = \sigma_{ij} - \sigma_h \delta_{ij}, \quad (4.13)$$

$$\sigma_h = \frac{\sigma_{xx} + \sigma_{yy} + \sigma_{zz}}{3}, \quad (4.14)$$

where σ_h is the hydrostatic component of the stress and δ_{ij} is Kronecker's function. Since $\sigma'_1 + \sigma'_2 + \sigma'_3 = 0$, the yield criterion in Equation 4.8 reduces to the form

$$f(J_2, J_3) = C, \quad (4.15)$$

where

$$J_2 = -(\sigma'_1 \sigma'_2 + \sigma'_2 \sigma'_3 + \sigma'_1 \sigma'_3), \quad (4.16)$$

$$J_3 = \sigma'_1 \sigma'_2 \sigma'_3. \quad (4.17)$$

Numerous criteria have been proposed for yielding; two of them – Tresca and von Mises – are going to be explained briefly.

4.2.1.1. Tresca Yield Criterion

This criterion was proposed by Henri Edouard Tresca (1864). According to the criterion yielding occurs when the maximum shear stress reaches a certain value; it could be given in the form:

$$\sigma_{\max} - \sigma_{\min} = \sigma_y = 2k, \quad (4.18)$$

where k is the yield stress in shear, σ_y is the yield stress in tension and σ_{\max} and σ_{\min} are the maximum and minimum principal stresses. According to Tresca, yield stress in pure shear is half of the yield stress in simple tension (Mendelson, 1968).

4.2.1.2. Von Mises Yield Criterion

This criterion was proposed by Richard von Mises (1913). According to the criterion, yielding occurs when J_2 reaches a critical value;

$$2J_2 = (\sigma'_1)^2 + (\sigma'_2)^2 + (\sigma'_3)^2 = 2k^2 \quad (4.19)$$

or

$$(\sigma_1 - \sigma_2)^2 + (\sigma_2 - \sigma_3)^2 + (\sigma_1 - \sigma_3)^2 = 6k^2. \quad (4.20)$$

A physical interpretation of von Mises criterion is: yielding begins when the elastic energy of distortion reaches a critical value. Thus, a hydrostatic pressure does not cause yielding since it produces only elastic energy of dilatation. According to von Mises, yield stress in pure shear is $1/\sqrt{3}$ times the yield stress in simple tension (Mendelson, 1968).

Comparison of Tresca and von Mises criteria is shown in Figure 4.3. Apparently, Tresca criterion is more conservative than von Mises criterion, but the normal of the Tresca's yield locus is discontinuous at the corners (each having two normal directions) leading to instability in numerical calculations of flow direction.

Due to this fact, von Mises yield criterion is mostly preferred in numerical simulation tools.

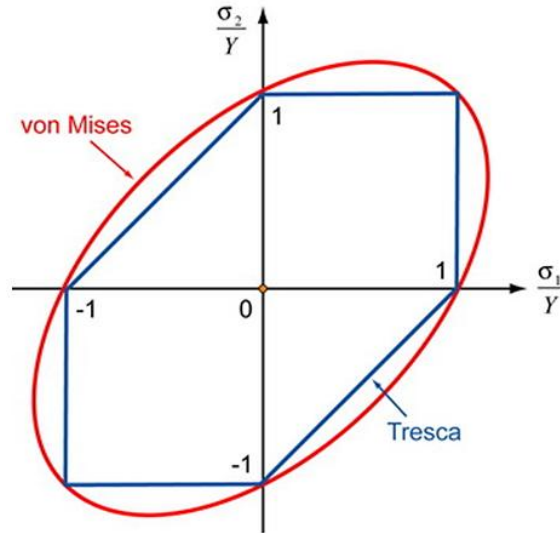


Figure 4.3. Comparison of Tresca and von Mises yield criteria in plane stress condition

Material starts to deform plastically after the yield point determined by either of the two criteria explained in this part. Due to irreversible nature of plastic deformation, stress-strain relations for modelling this behaviour are quite different than the ones for modelling elastic behaviour. These relations will be explained in the next part.

4.2.2. Flow Rule

A material-dependent relationship between stress and strain in plasticity is termed as *flow rule* (Tekkaya, 2002). A general relationship between the ratios of components of the strain increment and the stress ratios was suggested by Levy (1871) and von Mises (1913). The Levy-Mises equations are expressed in the form

$$\frac{d\varepsilon_1}{\sigma'_1} = \frac{d\varepsilon_2}{\sigma'_2} = \frac{d\varepsilon_3}{\sigma'_3} = d\lambda \quad (4.21)$$

or

$$d\varepsilon_{ij}^p = \sigma'_{ij} d\lambda, \quad (4.22)$$

where $d\varepsilon_{ij}^p$ is the plastic true strain increment, $d\lambda$ is a non-negative real number and σ'_{ij} is the deviatoric true stress. According to the Levy-Mises flow rule, the material is assumed to be rigid plastic (Chakrabarty, 2006). Hence, the first invariant of the strain increment tensor is zero. After derivations, Levy-Mises rule for non-hardening (perfect plastic) case can be rewritten as

$$d\varepsilon_{ij}^p = \sigma'_{ij} \left(\frac{3 d\bar{\varepsilon}^p}{2 \sigma_f} \right), \quad (4.23)$$

where σ_f is the flow stress and $d\bar{\varepsilon}^p$ is the equivalent plastic strain increment which can be formulated as

$$d\bar{\varepsilon}^p = \sqrt{\frac{2}{3} (d\varepsilon_{ij}^p d\varepsilon_{ij}^p)}. \quad (4.24)$$

The Levy-Mises rule can be considered as an application of the plastic potential theory in the form

$$d\varepsilon_{ij}^p = d\lambda \frac{\partial f(\sigma_{ij})}{\sigma_{ij}}, \quad (4.25)$$

where $f(\sigma_{ij})$ is the plastic potential, corresponding to the yield function in plasticity. Equation 4.25 indicates that the strain increment vector is normal to the yield function in the stress space (Figure 4.4); this is termed as *normality rule*.

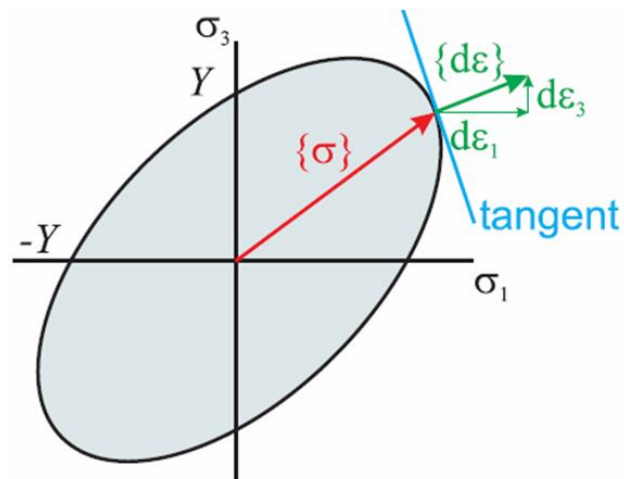


Figure 4.4. Demonstration of normality rule in plane-stress conditions for von Mises yield function

For materials with strengthening, the yield locus enlarges with their plastic deformation according to the normality rule. The yield surface must be convex in order to attain a stable material flow. As explained, the Tresca yield surface has instabilities at the corner points since each corner point has more than one normal vector. In order to use the Tresca yield criterion with normality rule, corners must be smoothed.

4.2.3. Strain Hardening

Evolution of the yield surface with plastic deformation is named as hardening. Plastic deformation leads to the hardening of a material and the increase of its elastic limit (in the direction of the deformation). The evolution of the yield surface is governed by one scalar variable, either the dissipated plastic work, or the accumulated plastic strain. If the evolution of the yield surface is correlated with dissipated plastic work, the hardening is termed as *work hardening*. The dependence of the yield surface on the plastic strain history called *strain hardening* (Kachanov, 1971).

A flow curve (plastic strain vs. true stress) of a material could be found with a simple tension or compression test. In the cold plastic deformation case, the governing scalar variable on the hardening behaviour is the plastic strain. Therefore,

the flow stress (σ_f) could be presented as a function of equivalent plastic strain ($\overline{\varepsilon^p}$) in many forms such as

$$\sigma_f = K \left(\overline{\varepsilon^p} \right)^n \quad (\text{Ludwik expression}), \quad (4.26)$$

or

$$\sigma_f = A \left(\varepsilon_0 + \overline{\varepsilon^p} \right)^n \quad (\text{power law}), \quad (4.27)$$

where n is the strain-hardening exponent, K and A are constants. For a hardening material, according to the flow curve $\sigma_f(\overline{\varepsilon^p})$, the local slope H (hardening slope) is defined as

$$H = \frac{d\sigma_f}{d\varepsilon^p}. \quad (4.28)$$

Inserting Equation 4.28 in to the Levy-Mises rule for the perfect plastic case in Equation 4.23 gives

$$d\varepsilon_{ij}^p = \sigma'_{ij} \left(\frac{3 d\sigma_f}{2 H \sigma_f} \right). \quad (4.29)$$

According to Equations 4.24 and 4.29, a definite contribution to the hardening is made by every plastic distortion because equivalent plastic strain increment is always positive (Hill, 1950).

4.2.4. Extensions to Anisotropy

This part is a brief explanation of the Hill's anisotropic flow theory based on (Hill, 1950), which offers a numerical solution for the anisotropic plastic deformation problem of nonwoven materials. This theory considers states of anisotropy that possess three mutually orthogonal planes of symmetry at every point; the

intersections of these planes are known as the principal axes of anisotropy. These axes may vary in direction throughout the specimen. For instance, a strip cut from the centre of a cold-rolled sheet provides an example of uniformly directed anisotropy with the principal axes coinciding with the rolling direction, transversely in the plane of the sheet, and normal to this plane (Figure 4.5). The principal axes in a given element can also vary relative to the element itself during continued deformation such as in the case of simple shear test.

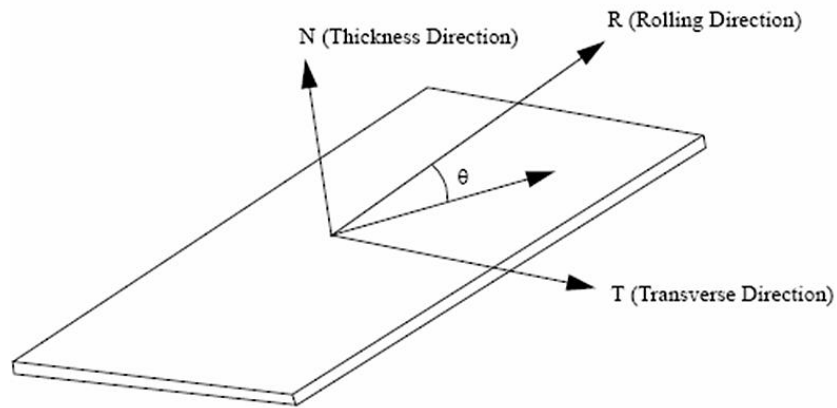


Figure 4.5. Axes of anisotropy in a cold-rolled sheet

Here it is assumed that the principal axes of a material are set as Cartesian axes of reference. The criterion describing the yielding of isotropic material is that of von Mises. The simplest yield criterion for anisotropic material is the one, which reduces to von Mises' law when the anisotropy disappears. According to this, the yield criterion can be given in the form

$$2f(\sigma_{ij}) \equiv F(\sigma_y - \sigma_z)^2 + G(\sigma_z - \sigma_x)^2 + H(\sigma_x - \sigma_y)^2 + 2L\tau_{yz}^2 + 2M\tau_{zx}^2 + 2N\tau_{xy}^2 = 1, \quad (4.30)$$

where F, G, H, L, M, N are characteristic parameters of the current state of anisotropy. The yield criterion has this form when the principal axes of anisotropy are the axes of reference; otherwise the form changes in a way that can be found by transforming the stress components.

If X, Y, Z are the tensile yield stresses in the principal directions of anisotropy, it could be shown that (Hill, 1950)

$$\frac{1}{X^2} = G + H, \quad 2F = \frac{1}{Y^2} + \frac{1}{Z^2} - \frac{1}{X^2}, \quad (4.31)$$

$$\frac{1}{Y^2} = F + H, \quad 2G = \frac{1}{X^2} + \frac{1}{Z^2} - \frac{1}{Y^2}, \quad (4.32)$$

$$\frac{1}{Z^2} = G + F, \quad 2H = \frac{1}{Y^2} + \frac{1}{X^2} - \frac{1}{Z^2}. \quad (4.33)$$

If R, S, T are shear yield stresses with respect to the principal axes of anisotropy, then (Hill, 1950)

$$2L = \frac{1}{R^2}, \quad 2M = \frac{1}{S^2}, \quad 2N = \frac{1}{T^2}. \quad (4.34)$$

If there is rotational symmetry of anisotropy in an element about the z -axis, the form of Equation 4.30 remains invariant for arbitrary x and y axes for reference. The rotational symmetry about z -axis changes the Equation 4.30 to the form

$$\begin{aligned} & \left[(G + H)\sigma_x^2 - 2H\sigma_x\sigma_y + (F + H)\sigma_y^2 + 2N\tau_{xy}^2 \right] \\ & - 2(G\sigma_x + F\sigma_y)\sigma_z + 2(L\tau_{yz}^2 + M\tau_{zx}^2) + (F + G)\sigma_z^2 = 1. \end{aligned} \quad (4.35)$$

If there is a complete spherical symmetry, or isotropy, $F = G = H = 3L = 3M = 3N$ and Equation 4.30 reduces to von Mises criterion when $2F$ is equated to $1/Y^2$.

To describe fully the state of anisotropy in an element, the orientations of the principal axes and the values of the six independent yield stresses X, Y, Z, R, S, T must be known. These values could be determined via tensile and torsion tests.

The strain increment relations, referred to the principal axes of anisotropy are

$$d\varepsilon_x = d\lambda[H(\sigma_x - \sigma_y) + G(\sigma_x - \sigma_z)], \quad d\gamma_{yz} = L\tau_{yz}d\lambda, \quad (4.36)$$

$$d\varepsilon_y = d\lambda[F(\sigma_y - \sigma_z) + H(\sigma_y - \sigma_x)], \quad d\gamma_{zx} = M\tau_{zx}d\lambda, \quad (4.37)$$

$$d\varepsilon_z = d\lambda[G(\sigma_z - \sigma_x) + F(\sigma_z - \sigma_y)], \quad d\gamma_{xy} = N\tau_{xy}d\lambda. \quad (4.38)$$

It should be noticed that $d\varepsilon_x + d\varepsilon_y + d\varepsilon_z = 0$ identically. If the principal axes of stress coincide with the axes of anisotropy, so do the principal axes of strain increment. As seen in Figure 4.6, the elastic region of the Hill's yield function differs from the one of von Mises' function due to imposed anisotropic parameters.

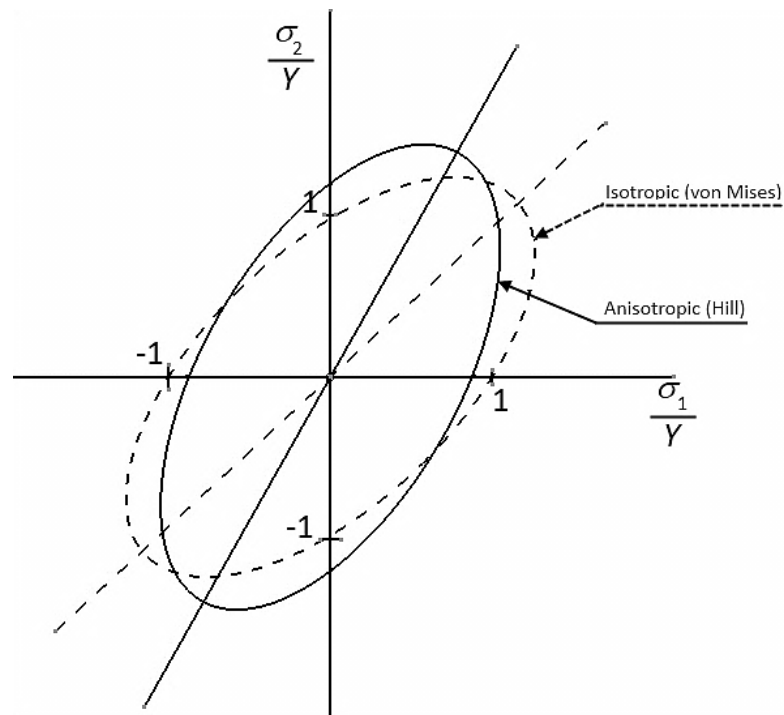


Figure 4.6. Comparison of normalized yield loci of isotropic (von Mises) and anisotropic (Hill) yield functions

4.3. Modelling of Viscous Behaviour

Fundamental deformation of materials can be classified into three main types: elastic, plastic and viscous. Polymer-based materials show time-dependent properties even at room temperature due to their low melting points (Ferry, 1980). As explained in Section 2.3, polymer fibres are mainly used for the manufacturing of nonwoven fabrics. Due to the nature of polymer materials, nonwovens exhibit a viscous behaviour, which should be considered in their numerical models.

The relationship between stresses and strains in viscoelastic materials depends on time. Normally, viscoelasticity is observed in many structural materials (steel, aluminium, etc.), but the deviation of the elastic portion of stress-strain curves from straight lines is usually neglected. However, in polymers, this effect is very important. The rate of loading affects the deformation behaviour dramatically and energy is dissipated during spring back (Figure 4.7).

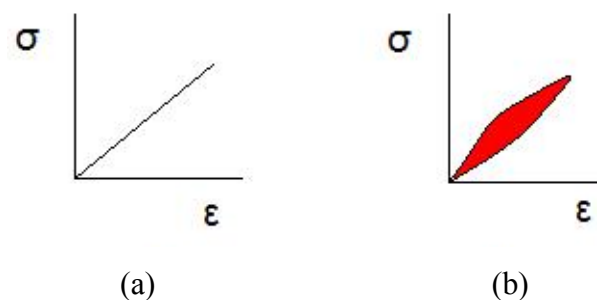


Figure 4.7. Stress-strain curves of purely elastic (a) and viscoelastic (b) materials (The red area represents the amount of energy lost in a loading-unloading cycle.)

There are some phenomena, which are attributed to viscoelasticity, such as creep and relaxation. Creep is the increase of strain with time at constant stress (Figure 4.8); on the other hand, relaxation is the decrease in stress with time when strain is held constant (Figure 4.9) (Shaw and MacKnight, 2005).

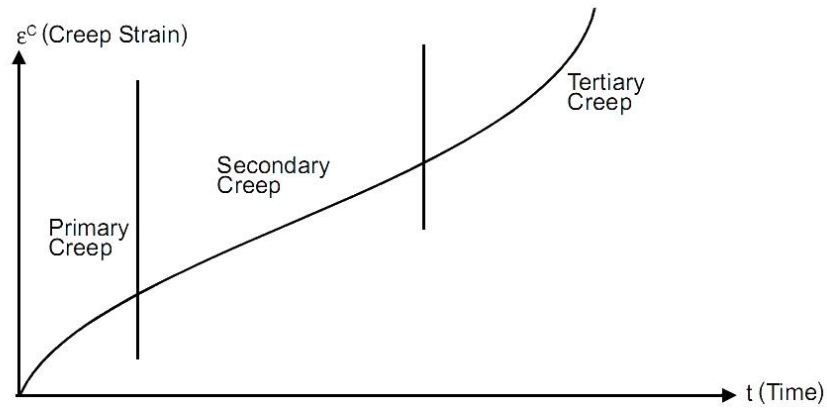


Figure 4.8. Creep strain (ϵ^c) vs. time (uniaxial test at constant stress and temperature)

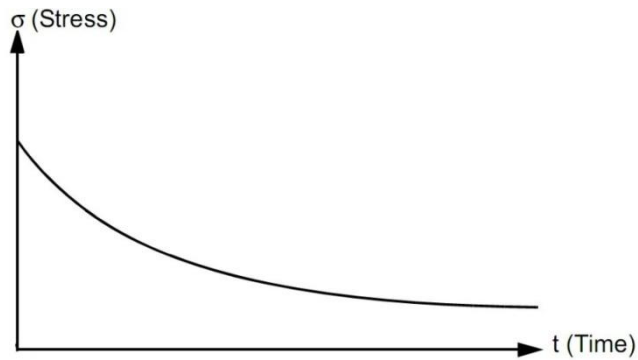


Figure 4.9. Relaxation curve (uniaxial test at constant strain and temperature)

Purely elastic materials can be modelled with springs, whereas the time-dependency of the stress-strain curve requires an additional element such as a dashpot in structural mechanical models. Spring and dashpot elements shown in Figure 4.10 are used to represent elastic and viscous deformation, respectively, in the numerical models of viscoelasticity.

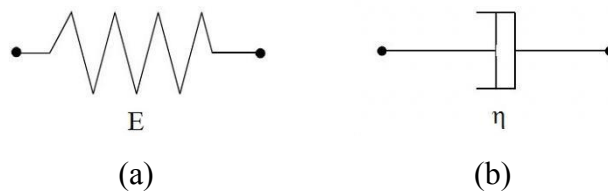


Figure 4.10. Perfectly elastic (a) and viscous (b) elements (E -modulus of elasticity, η -Viscosity of the dashpot)

The constitutive equations between stress (σ) and strain (ε) of the spring and dashpot elements are, respectively, as follows:

$$\sigma = E\varepsilon \quad \text{and} \quad \sigma = \eta \frac{d\varepsilon}{dt}, \quad (4.39)$$

where E and η are the modulus of elasticity of the spring and viscosity of the dashpot, respectively. Stress of a spring element is linearly related with its strain. On the other hand, stress of a dashpot element is related with a strain rate making the constitutive relation time-dependent. Linear viscoelastic deformation can be described by the constitutive equations describing combinations of spring and dashpot elements. Two simplest models that are commonly used to relate stress and strain are the Maxwell and Kelvin-Voigt models (Ikegami, 2001).

The Maxwell model introduces viscoelasticity by combining a spring and a dashpot in series (Figure 4.11). The constitutive equation of this series model is

$$\sigma = \eta \frac{d\varepsilon}{dt} - \frac{\eta}{E} \frac{d\sigma}{dt}. \quad (4.40)$$

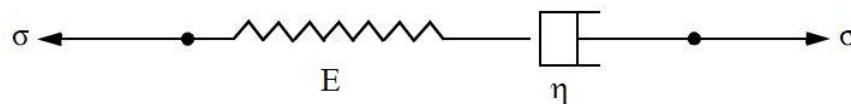


Figure 4.11. Maxwell model

The Kelvin-Voigt model uses a spring and a dashpot in parallel to represent the viscoelastic behaviour of a material (Figure 4.12). The constitutive equation of the parallel model of a spring and a dashpot element is

$$\sigma = E\varepsilon + \eta \frac{d\varepsilon}{dt}. \quad (4.41)$$

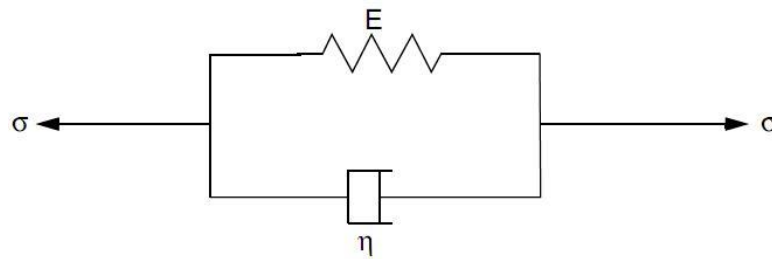


Figure 4.12. Kelvin-Voigt model

There are some deficiencies of Kelvin-Voigt and Maxwell models (Ikegami, 2001), e.g. an instantaneous strain cannot be imposed on the Kelvin-Voigt model. Due to this reason, many variations of spring and dashpot configurations are available in the literature to model viscoelastic deformation of various materials such as the Generalized Maxwell model, which combines a spring and a finite number of Maxwell elements in parallel (Figure 4.13). In order to avoid disadvantages of Kelvin-Voigt and Maxwell models, this model could be used to model viscous behaviour of nonwoven materials.

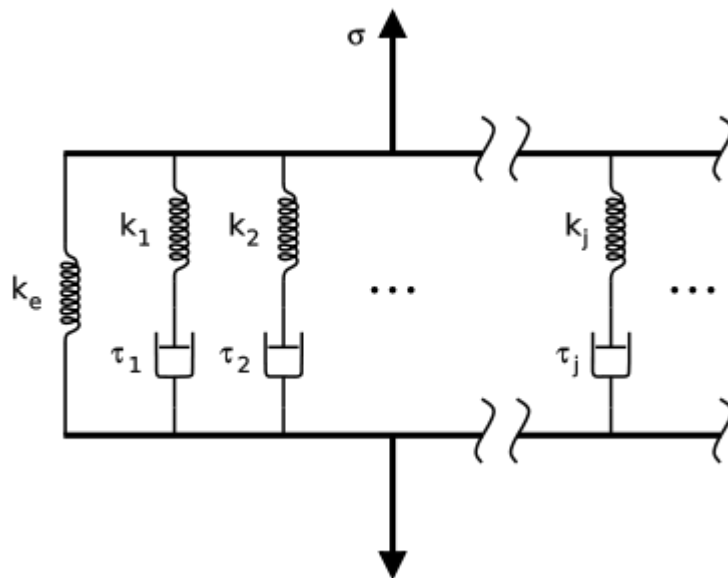


Figure 4.13. Generalized Maxwell model (Kaliske *et al.*, 2005)

4.4. Review of Finite Element Method

In solution of complex engineering problems, application of the conventional analytical methods may be impossible or impractical. The engineering approach in these cases is to approximate the solution of the problem by replacing the continuum with an appropriate model with finite degrees of freedom (DOF). This is the main aim of the finite element method (FEM). With this method, the exact solution can be approximated with an acceptable degree of inaccuracy in a reasonable time. This section explains FEM briefly in five parts.

4.4.1. Basic Procedure of FEM in Solid Mechanics

The analysis procedure should start with a detailed identification of physics of the problem, i.e. determination of constraints. The general procedure is composed of seven main steps (Tekkaya, 2002):

Idealization: The continuum is divided into a finite number of elements, which can be described as the parts of the actual structure, capable to reproduce a local response of the system to an excitation.

Discretization: The infinite number of unknowns (DOF) is reduced to a finite number in this step.

Determination of the Stiffness: In this step, the response of the elements to an excitation is determined. In solid mechanics, the relationship between unknown displacements and the known loads is established and it is indicated by

$$\{f\} = [k]\{u\}, \quad (4.42)$$

where $\{f\}$ is the load vector, $\{u\}$ is the displacement vector and $[k]$ is the element's stiffness matrix.

Assembly of the Element Stiffness to Discretize the Whole Continuum: The assembly process is realized by formulation of the conditions of compatibility. The first

condition is equality of nodal displacements of the coinciding nodes. It is a necessary condition to satisfy the continuity within a solid body. The second condition is the equilibrium of nodal forces that act at a single node. Application of these two conditions to the system nodes ends up with a set of equations for the whole system, which is expressed as

$$[K]\{u\} = \{F\}, \quad (4.43)$$

where $[K]$ is the overall, or global, stiffness matrix of the system and $\{F\}$ is the global load vector including all the forces applied on the system.

Introducing Boundary Conditions: In this step, the known constraints on the nodes are introduced. External forces and displacements are inserted to Equation 4.43.

Solution of the System Equations: The unknown quantities (displacements in Equation 4.43) are determined by using standard methods such as Gauss elimination, etc.

Computation of the Dependent Variables: The quantities defined for the problem are solved. In solid mechanics, they are the stresses and strains.

4.4.2. Finite Element Approach for Large Plastic Deformation

In solid mechanics, the nonlinearity in finite element analysis can simply be defined as the dependence of the stiffness matrix on displacement and/or force. There may be three main reasons of nonlinearity.

Geometric nonlinearity may be observed in various situations. Large rotations and displacements in the system with small strains cause geometric nonlinearity. The distribution or magnitude of the applied forces may also be altered as a result of shape changes. Nonlinearity may also be observed in case of relatively small displacements, with displacements exceeding the dimension of the deforming body as in the case of thin-sheet metals (Cook, 1995).

Material Nonlinearity is described as a nonlinear relationship between strains and stresses. Among many possible cases, it is observed in metal forming applications when the material starts to flow plastically under the applied loads. Some hyperelastic materials, such as rubber, exhibit nonlinear behaviour in the elastic region.

Contact Nonlinearity is observed when the portions of a deforming body come gradually in contact with other bodies during the deformation process. Also, friction may be a cause of contact nonlinearity.

Two main approaches are available for the solution of nonlinear problems, namely, the elastic-plastic and the rigid-plastic procedures (MSC.Marc[®], 2008r1). In the elastic-plastic approach, the elastic deformation of the material is included in the solution. In the rigid-plastic approach, the effects of elasticity are not included. The latter is widely used for applications, in which plastic deformation significantly exceeds the elastic strains. In this case, the computation time decreases since the formulation does not require consideration of elastic strains. Furthermore, numerical implementation is simple and the solution procedure is robust and reliable. Besides the advantages, the rigid-plastic formulation has some disadvantages. A physical behaviour that depends on elasticity, such as spring back or residual stresses, cannot be obtained in the solution. The exact final shape and characteristics of the specimen may not fulfil the accuracy requirements. Furthermore, the regions that deform within the elastic range are regarded as rigid and this may lead to incorrect results. On the other hand, both approaches could be utilized to model a time-dependent behaviour, such as viscous behaviour. The elastic strain range of polymers may extend to more than 5%. In order to reflect the characteristics of the deformation accurately, the elastic-plastic approach is preferred for polymer-based materials.

4.4.3. Types of Formulation Regarding the Coordinate Frame

There are two main types of formulations to define kinematics of deformation, namely, the Eulerian and Lagrangian approaches. In the Eulerian approach, the coordinate frame is fixed in space, and the material flows through this fixed mesh. It

is suitable in cases, where the process is steady-state. In Lagrangian approach, the mesh is considered to be attached to the body and displaces in space with the material (Cook, 1995). The Lagrangian formulation is more appropriate for this study.

The Lagrangian formulations can be divided into two types, namely, the total Lagrangian and the updated Lagrangian methods. In the total Lagrangian approach the initial state of the body serves as a reference state, whereas in the updated Lagrangian approach the reference state is altered considering the current configuration. The updated Lagrange procedure is applicable to problems of plastic deformation with large strains such as deformation of nonwoven materials. Due to this fact, updated Lagrange formulation is will be explained.

The Lagrangian approach is used in applications, in which the initial coordinate frame has a little physical significance due to the nature of the problem because the reference frame is redefined in each iteration of an increment (MSC.Marc[®], 2008r1).

In the updated Lagrangian approach, the principle of virtual work is used to define the equilibrium condition:

$$\int_{V_0} S_{ij} \delta E_{ij} dV = \int_{V_0} b_i^0 \delta \eta_i dV + \int_{A_0} t_i^0 \delta \eta_i dA, \quad (4.44)$$

where S_{ij} is the second Piola-Kirchhoff stress tensor, E_{ij} is the Green-Lagrange strain tensor, b_i^0 is the body force in the reference configuration, t_i^0 is the traction vector in the reference configuration and η_i refers to virtual displacements.

The second Piola-Kirchhoff stress tensor is expressed by the relation (Belytschko *et al.*, 2000)

$$\mathbf{S} = J \mathbf{F}^{-1} \boldsymbol{\sigma} \mathbf{F}^{-T}, \quad (4.45)$$

where \mathbf{F} is the deformation gradient and $\boldsymbol{\sigma}$ is the Cauchy stress tensor. J denotes the Jacobian of the deformation gradient and defined by

$$J = \det(\mathbf{F}). \quad (4.46)$$

The Green-Lagrange strain tensor is defined as (Cook, 1995)

$$E_{ij} = \frac{1}{2} \left(\frac{\partial u_i}{\partial X_j} + \frac{\partial u_j}{\partial X_i} + \frac{\partial u_k}{\partial X_i} \frac{\partial u_k}{\partial X_j} \right), \quad (4.47)$$

where u_i is the displacement and X_i refers to position in a reference configuration.

The Cauchy stress tensor (σ_{ij}) is formulated as

$$\sigma_{ij} = \frac{1}{J} F_{im} S_{mn} F_{jn}, \quad (4.48)$$

which is an important parameter used in characterisation of deformation. The deformation gradient is the Jacobian matrix of the motion described by $\Phi(\mathbf{X},t)$ (Belytschko *et al.* 2000). It is expressed as

$$F_{ij} = \frac{\partial \Phi_i}{\partial X_j} \equiv \frac{\partial x_i}{\partial X_j}, \quad (4.49)$$

where x_i is the position of a point in the deformed current configuration.

The deformation gradient is used to describe an infinitesimal line segment $d\mathbf{x}$ in the current configuration that corresponds to a line segment in $d\mathbf{X}$ in the reference configuration. This is expressed as

$$dx_i = F_{ij} dX_j, \quad (4.50)$$

In the updated Lagrangian approach, the direct linearization of the left-hand side of Equation 4.44 yields

$$\int_{V_0} dS_{ij} \delta E_{ij} dV = \int_{V_{n+1}} \nabla^S \eta_{ij} L_{ijkl} \nabla^S (\Delta u_{kl}) dV. \quad (4.51)$$

where n refers to the increment number.

In this approach, the reference state is the current state; therefore, the following set of equations is valid:

$$F_{ij} = \delta_{ij}, \quad \delta E_{ij} = \delta d_{ij}, \quad \frac{\partial}{\partial X_i} = \frac{\partial}{\partial x_i}, \quad S_{ij} = \sigma_{ij}, \quad (4.52)$$

where \mathbf{F} is the deformation tensor and \mathbf{d} is the rate of deformation. Hence,

$$\int_{V_{n+1}} \left[\sigma_{ij}^{\nabla T} \delta d_{ij} + \sigma_{ij} \frac{\partial v_k}{\partial x_i} \frac{\partial \delta \eta_k}{\partial x_j} \right] dV = \int_{V_{n+1}} b_i \delta \eta_i dV + \int_{A_{n+1}} t_i \delta \eta_i dA, \quad (4.53)$$

where b_i represents the body force and t_i represents the surface traction in the current configuration. The Truesdell stress rate ($\sigma_{ij}^{\nabla T}$) that appears in Equation 4.53 is defined as (Belytschko *et al.*, 2000)

$$\sigma_{ij}^{\nabla T} = \frac{D\sigma_{ij}}{Dt} - \frac{\partial v_i}{\partial x_k} \sigma_{kj} - \sigma_{ik} \frac{\partial v_j}{\partial x_k} + \sigma_{ij} \frac{\partial v_k}{\partial x_k}, \quad (4.54)$$

where $\frac{D\sigma_{ij}}{Dt}$ is the material rate for the Cauchy stress tensor.

If a rigid-body rotation is applied to the body, the usual material rate does not vanish but the Truesdell rate vanishes. Therefore, it has a crucial importance in solution of problems, in which large rotations are present. The constitutive equations can be written in terms of the Truesdell rate of Cauchy stress as

$$\sigma_{ij}^{\nabla T} = L_{ijkl} D_{kl}, \quad (4.55)$$

where L_{ijkl} is the tensor of material's moduli in the current configuration in terms of material moduli tensor in the reference configuration. On the other hand, in the

small-strain problems, the classical elastic-plastic modulus is used. It is used to describe the Jaumann rate of Cauchy stress tensor by

$$\sigma^{\nabla J} = L_{ijkl}^{ep} D_{kl}. \quad (4.56)$$

The Jaumann rate of the Cauchy stress tensor is defined as

$$\sigma_{ij}^{\nabla J} = \frac{D\sigma_{ij}}{Dt} - W_{ik}\sigma_{kj} - \sigma_{ik}W_{kj}^T, \quad (4.57)$$

where \mathbf{W} is the spin tensor given by

$$W_{ij} = \frac{1}{2} \left(\frac{\partial v_i}{\partial x_j} - \frac{\partial v_j}{\partial x_i} \right). \quad (4.58)$$

Using Equations 4.56, 4.57 and 4.58, the Truesdell rate of Cauchy stress tensor is written in term of the Jaumann rate by

$$\sigma_{ij}^{\nabla T} = \sigma_{ij}^{\nabla J} - D_{ik}\sigma_{kj} - \sigma_{ik}D_{kj} + \sigma_{ij}D_{kk}. \quad (4.59)$$

Thus the relation between the large-strain moduli and the classical elastic-plastic moduli is

$$L_{ijkl} = L_{ijkl}^{ep} - \delta_{il}\sigma_{kj} - \sigma_{il}\delta_{kj} + \delta_{ij}\sigma_{kl}. \quad (4.60)$$

4.4.4. Solution Methods

Analyses of large-strain applications require solution of nonlinear equations. There are various solution techniques, such as the Euler method, self-correcting Euler method, direct iteration method, Newton-Raphson method and modified Newton-Raphson method (Tekkaya, 2003). The Newton-Raphson method is used in the study.

The Newton-Raphson method is an iterative procedure - the displacement value is recalculated until a certain amount of accuracy is reached. For the nonlinear equation

$$[k(\{u\})]\{u\} = \{f\}, \quad (4.61)$$

$\{u^{i-1}\}$ is calculated, which in turn yields a residual force $\{R\}$ defined by (Tekkaya, 2003)

$$\{R(\{u^{i-1}\})\} = \{f\} - [k(\{u^{i-1}\})]\{u^{i-1}\}. \quad (4.62)$$

The aim of the procedure is to minimize the value of residual at the end of a number of iterations. The residual force at the i^{th} iteration can be approximated at $\{u^{i-1}\}$ by means of the Taylor series expansion:

$$\{R(\{u^{i-1} + \Delta u^i\})\} = (R(\{u^{i-1}\})) + \left[\frac{\partial \{R(\{u\})\}}{\partial \{u\}} \right]_{\{u^{i-1}\}} \{\Delta u^i\} + \dots \quad (4.63)$$

In the last iteration the residual force should approach zero, therefore Equation 4.63 can be rewritten as

$$-\left[\frac{\partial \{R(\{u\})\}}{\partial \{u\}} \right]_{\{u^{i-1}\}} \{\Delta u^i\} = (R(\{u^{i-1}\})). \quad (4.64)$$

Defining the tangent stiffness matrix (k_t), Equation 4.64 is rewritten as follows

$$[k_t(\{u^{i-1}\})]\{\Delta u^i\} = (R(\{u^{i-1}\})). \quad (4.65)$$

The solution method is presented in Figure 4.14. The stability of the process depends on the initial state. It has quadratic convergence properties; in other words,

the error decreases quadratically in each subsequent iteration. In the nonlinear problems, the Newton-Raphson method is useful; however it may require high computational efforts in three-dimensional problems (Cook, 1995).

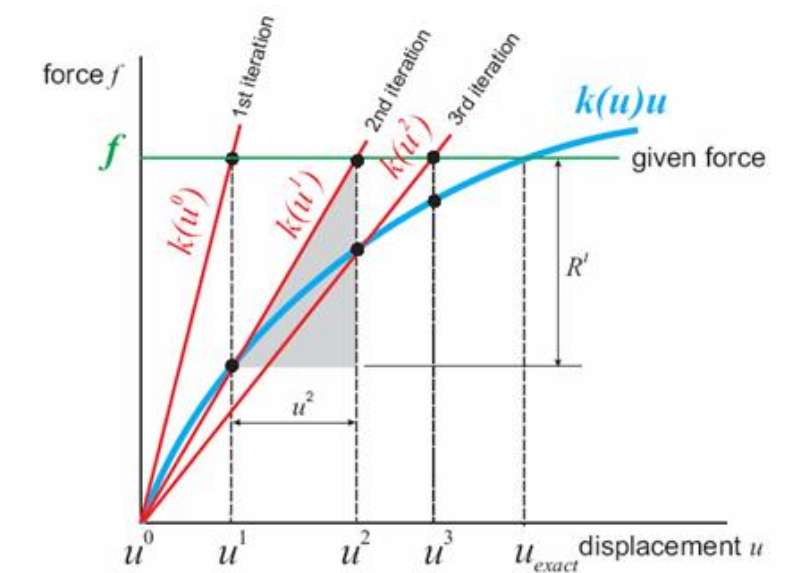


Figure 4.14. Convergence of Newton-Raphson method (Tekkaya, 2003)

4.4.5. Convergence Controls

The convergence criteria are assigned in the calculations in order to conclude the iterations when a desired value of accuracy is reached. In the commercial FE software, the convergence criteria are based on a relative and/or an absolute value of residual forces and/or displacements.

Using residual forces as a convergence criterion depends on minimization of the residual forces. Either the absolute value of residuals or the ratio of the maximum residual load to the maximum reaction force is selected as the convergence criterion. The convergence is defined by the following equations (Cook, 1995):

$$\frac{\|F_{residual}\|_{\infty}}{\|F_{reaction}\|_{\infty}} < Tolerance \quad (4.66)$$

and

$$\|F_{residual}\|_{\infty} < Tolerance, \quad (4.67)$$

where $\|F\|_{\infty}$ denotes the force with the highest absolute value. The displacements may constitute a criterion for checking the convergence of the solution. The convergence is described by the following equations:

$$\frac{\|\delta u\|_{\infty}}{\|\Delta u\|_{\infty}} < Tolerance \quad (4.68)$$

and

$$\|\delta u\|_{\infty} < Tolerance, \quad (4.69)$$

in which Δu denotes the displacement increment vector, δu denotes the correction to the incremental displacement vector. In this method, convergence is satisfied if the maximum of the last iteration within an increment is small compared to the displacement change in the increment.

One or more of the convergence criteria described above can be used in the solution. If the tolerance intervals decrease the solution becomes more accurate, however, the calculation time increases. There is a compromise between the accuracy of the solution and the time; therefore, the convergence criteria should be arranged carefully to obtain the sufficient accuracy in the least possible amount of time.

Due to sufficient accuracy in a reasonable time, FEM could be an appropriate approach for modelling the mechanical response of nonwoven fabrics. Several attempts were made to model nonwovens with FEM. Next section will give brief information about the existing FE models of nonwoven materials.

4.5. Existing Finite Element Models for Nonwoven Materials

Because of strength concerns, woven fabrics are modelled for various loading conditions, e.g. in impact simulations for ballistic purposes (Barauskas and Abraitene, 2007). Very few studies could be found concerning FE modelling of nonwoven textiles. In this section, a brief overview of researches based on FE modelling of nonwoven textiles in the literature will be given.

A first FE model deals with simulations of adhesively point-bonded spunbond nonwovens (Limem and Warner, 2005). This model treats the nonwoven media as a structure composed of fibres acting as truss links between bond points (Figure 4.15).

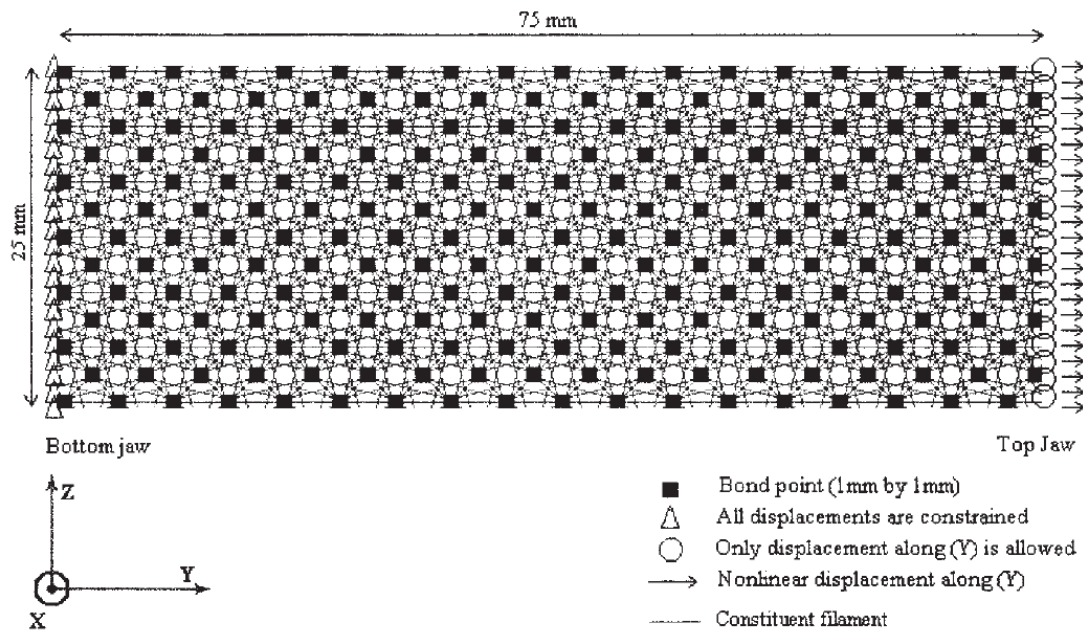


Figure 4.15. FE model of adhesively point-bonded spunbond nonwovens
(Limem and Warner, 2005)

The fibres simulated in this model are polypropylene, which is the most frequently used polymer in the nonwovens industry (Russell, 2007). In the truss-based model, all fibres are straight between consecutive bond points, have a

cylindrical shape, and demonstrate the same stress-strain behaviour, similar to that shown in Figure 4.16. All bond points in the model are identical, square-shaped isotropic with an elastic behaviour. The distribution of adhesive weight is uniform. Fabric failure is mainly due to fibre breakage. Fibres located in the fabric cross-machine direction have a negligible effect on the tensile behaviour of spunbond fabrics in the machine direction. Every fibre is bonded at least to its third neighbour, if not to a closer one. Engineering strain is used in all models.

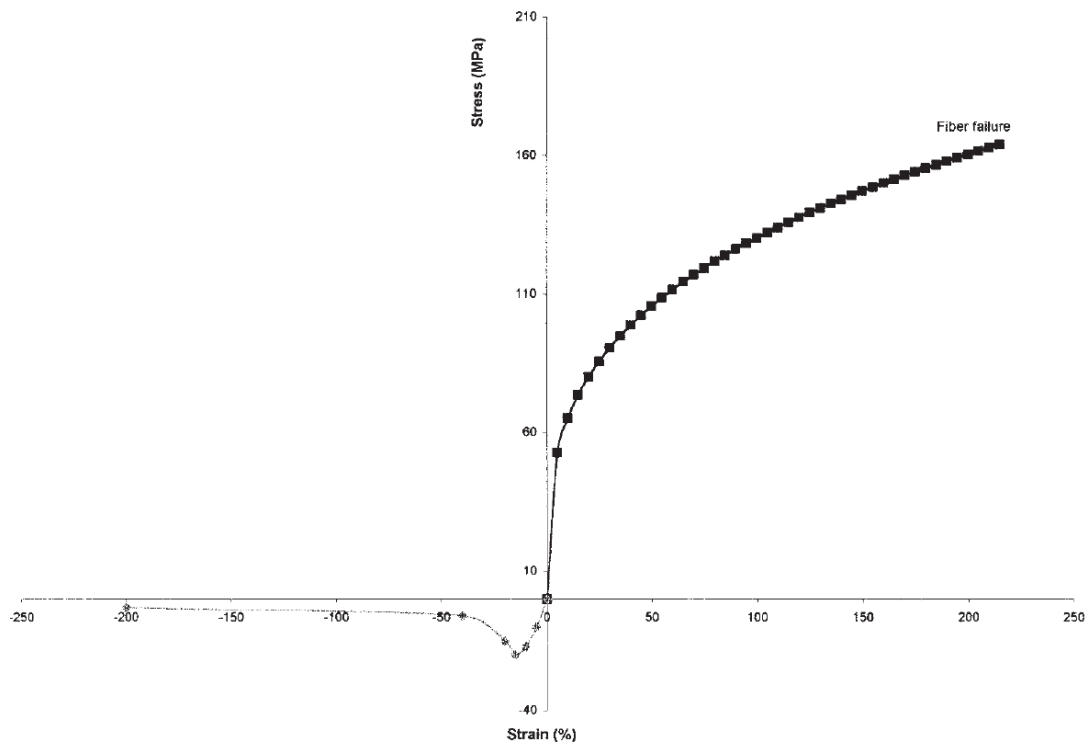


Figure 4.16. Equivalent stress-strain behavior of PP filaments in tension/compression (Limem and Warner, 2005)

The main disadvantage of this model is that the fibres in this model are linear elastic which represent a very small portion of deformation. For most of the polymers, the elastic region is nonlinear. Moreover, time dependency of the mechanical behaviour (viscoelasticity) is not mentioned. In addition to these deficiencies, this model is developed for 2D applications being far from real-life ones.

The second model is a FE model for thermobonded nonwovens by Mueller and Kochmann (2004). The used approach is based on the modelling of single fibres as trusses. The representation of a fibre by a single element allows a significant reduction in computational efforts. The behaviour of a number of single fibres is combined and mapped onto elements representing fibre bundles. These bundles are used to model the nonwoven. The bond points are composed of two regions: bond core and boundary zone (Figure 4.17). The boundary zone of the bond points represents the deformed fibres and partly-bonded regions (Mueller and Kochmann, 2004). The area of the nonwoven, which lies outside the bond points, is mapped onto the model using sets of fibre bundles. The elements connect the boundary of neighbouring bond points within a base cell (Figure 4.17).

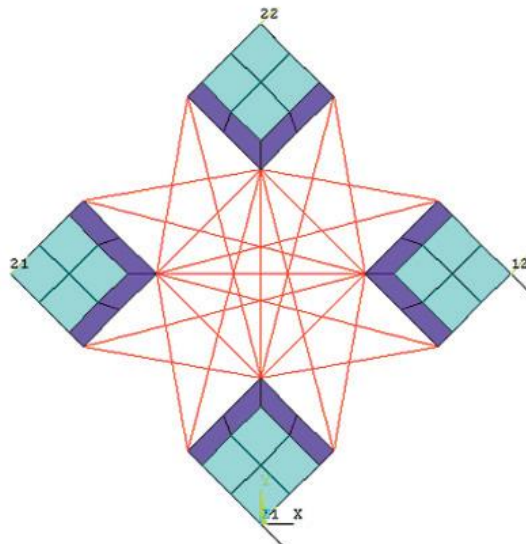


Figure 4.17. Base cell with bonding points and boundary (Mueller and Kochmann, 2004)

Different shapes of bond points are investigated in that study and the effect of bond geometry on the mechanical response of the nonwoven fabric is simulated with the model (Figure 4.18). However, implementation of ODF of fibres is very difficult in this approach because the unit cell is symmetric and the number of nodes on one bond point is limited. Moreover, similar to the previous model (Limem and Warner, 2005), this one is only applicable to 2D problems as well.

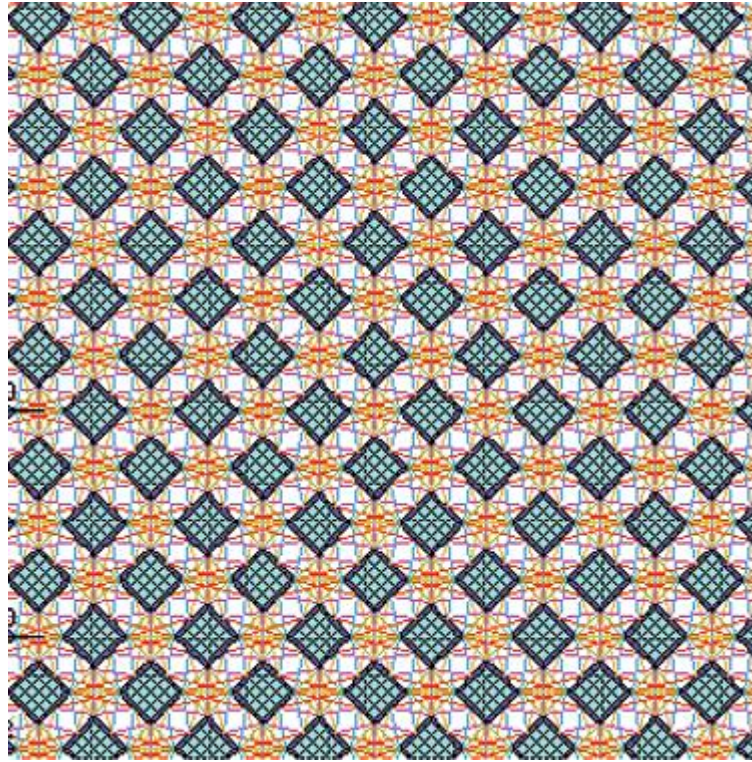


Figure 4.18. FE model of thermobonded nonwoven with square bond points
(Mueller and Kochmann, 2004)

The third approach is not a FE model, but was developed to predict the mechanical performance of thermally point-bonded nonwovens (Kim and Pourdeyhimi, 2001). This model is based on the calculation of deformation of fibre individuals incrementally. Each fibre is treated as a truss element, which is straight and continuous throughout the model (Figure 4.19).

The elements are oriented following the ODF measured for real nonwoven materials. The implementation of the ODF in the model is perfect. In terms of modelling the micromechanical behaviour and illustrating the anisotropy of the structure, the model is very successful. However, the dimensional range of the model is limited and the representation of the bond points is poor.

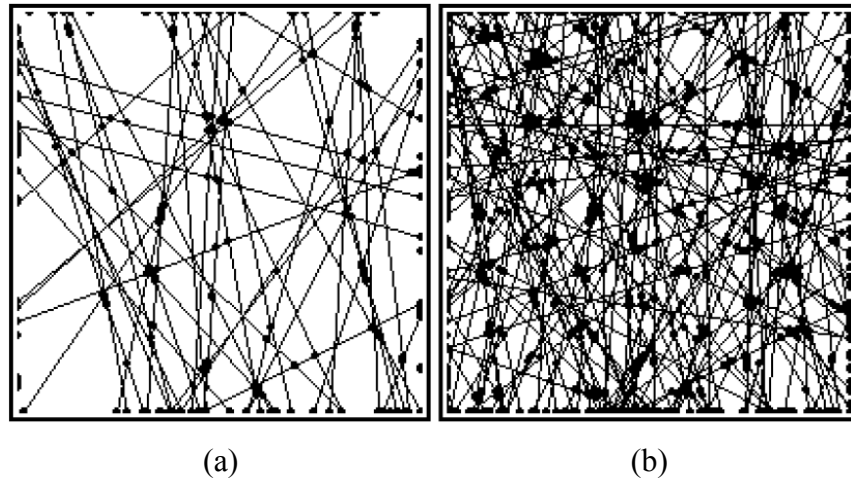


Figure 4.19. Models containing 50 lines (a) and 150 lines (b) (Kim and Pourdeyhimi, 2001)

The final model to review is a FE approach modelling paper, which is basically a nonwoven material (Ramasubramanian and Wang, 2007). A material subroutine is generated to reproduce the elastic-plastic behaviour of papers. The unloading behaviour of paper is investigated using the material-specific subroutine in that research. Introduced FE model is effective in modelling the deformation performance of paper including unloading (Figure 4.20). However, due to its dense structure, the mechanical behaviour of paper does not resemble that of nonwovens. Although papers do not exhibit viscoelasticity and large-strain deformation due to its dense structure, their anisotropic behaviour resembles nonwovens.

In conclusion, four models explained above are successful in representing some practical features of the complex mechanical behaviour of nonwoven materials. They are not suitable for modelling large-scale materials, since the number of elements can become prohibitive due to unreasonable computation time when the specimen size gets larger. Furthermore, 3D deformation conditions, such as out-of-fabric-plane loading, are difficult – if not impossible – with these models due to contact problems induced by truss elements. A ballistic fabric simulation might be an example where the fabric's model should be capable of handling 3D out-of-plane loads.

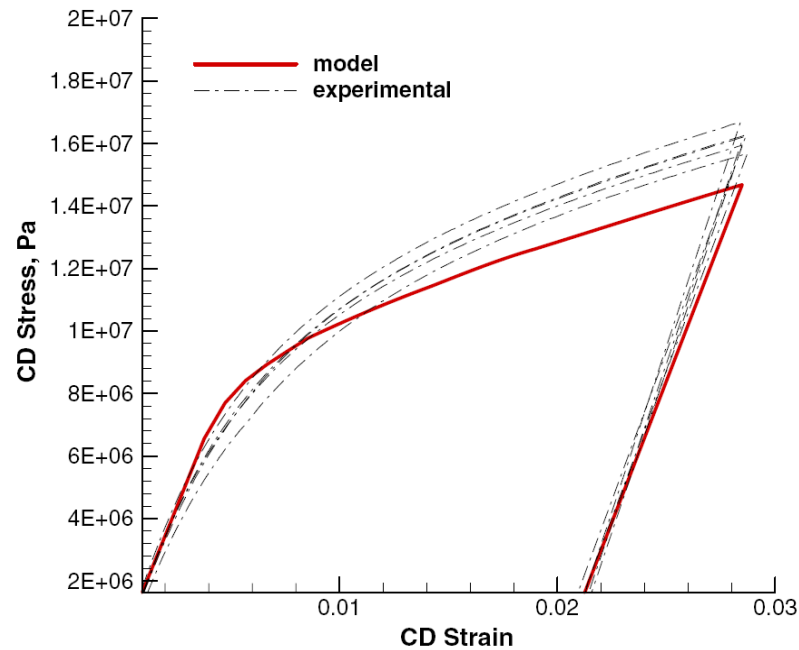


Figure 4.20. Model and experimental unloading behaviour of paper in CD
(Ramasubramanian and Wang, 2007)

4.6. Summary

Due to the nature of this research, with an aim to model the mechanical behaviour of nonwoven fabrics in the FE environment, background information about numerical modelling of the mechanical behaviour of materials is given in this chapter. Mathematical formulations, helping to model various deformation characteristics of the material, are explained. These formulations are vital for defining the deformation characteristics of material in a numerical environment.

The concept of anisotropy is discussed to demonstrate representation of the direction-dependant performance of nonwoven materials. Additionally, formulations for plastic and viscous behaviours are explained, since these studied materials possess them and none of the FE models in the literature consider these behaviours. A brief review of nonlinear finite element analysis is given to have a better understanding on the most frequently used numerical tool for simulating real-life

problems. The basic information given in this chapter plays an important role on the modelling approach followed in Chapters 6 and 7.

In order to assess closeness of the developed numerical model to a material's behaviour, necessary mechanical tests should be performed. Basic mechanical tests, which are necessary to clarify the time-dependent mechanical behaviour of a material, are tensile and creep/relaxation tests. The next chapter is dedicated to experimental studies on thermally bonded nonwoven fabrics and their bicomponent fibres to identify their deformational characteristics.

CHAPTER V

5. MECHANICAL BEHAVIOUR OF THERMALLY BONDED BICOMPONENT FIBRE NONWOVENS: EXPERIMENTAL STUDIES

As described in Chapter 2, having randomly distributed polymer-based fibres and being composed of two discrete regions – bond points and matrix – nonwovens have a unique mechanical behaviour that is partially similar, but still differs from that of composites, polymers and woven fabrics. Nonwovens focussed in this thesis are manufactured with bicomponent fibres and bonded using thermal techniques. Due to a core/sheath structure of fibre, during the thermal bonding process a sheath material

melts and acts as an adhesive for the core part of the fibres, which remain fully intact throughout the fabric. The continuity of the core regions throughout the nonwoven fabrics having bicomponent fibres increases the strength of the material when compared with the ones having monocomponent fibres (Albrecht *et al.*, 2003). Therefore, it is advantageous to use bicomponent fibres in nonwoven materials to improve their strength.

The major aim of this study is to simulate the real-life deformation performance of thermally bonded bicomponent fibre nonwoven textiles in the finite element (FE) environment. A deep understanding of the mechanical behaviour of these fabrics is necessary to develop a realistic FE model. As a starting point, mechanical performance of single bicomponent fibres will be investigated since they are the basic constituents of nonwoven fabrics. Secondly, the fabric microstructure, which is one of the most important factors affecting its mechanical behaviour, will be examined. Finally, mechanical characterisation of thermally bonded bicomponent fibre nonwovens will be performed applying several mechanical tests.

5.1. Mechanical Behaviour of Bicomponent Fibres

Fibres are the basic constituents of nonwoven fabrics and play an important role in determination of their mechanical properties. In our case, the type of fibres is a core/sheath bicomponent one, i.e. they are composed of a sheath material having a lower melting temperature with respect to core material (Figure 5.1).

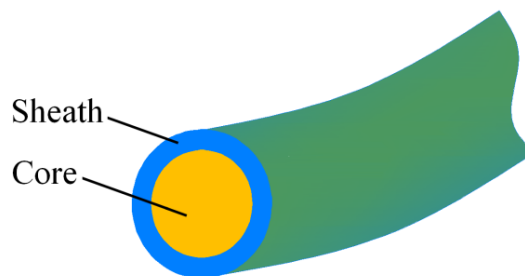


Figure 5.1. Structure of bicomponent fibre

As explained in Chapter 2, polymers are the raw materials for manufacturing nonwoven fibres. For bicomponent fibres, polyethylene (PE) is frequently used as sheath material, whereas polypropylene (PP), polyamide 6 (PA6) and polyester (PET) are the most commonly used polymers as core material (Russell, 2007). Polymers are graded with respect to their usage such as moulding, extrusion, etc., and their mechanical properties change accordingly. The type of polymers used for the manufacturing of fibres is called the fibre grade referring to their manufacturing purpose. Basic mechanical properties at room temperature of the polymers used to manufacture the bicomponent fibres for this research are given in Table 5.1. The polymers used for core region have higher values for the modulus of elasticity and melting point than the ones used for sheath region (Table 5.1), and the cross-sectional area of core is usually larger than or equal to that of sheath.

| Material | PE | PA6 | PP | PET |
|------------------------------------|-----------|------------|-----------|------------|
| Density (g/cm³) | 0.955 | 1.13 | 0.89 | 1.3 |
| Modulus of Elasticity (MPa) | 250 | 3000 | 1450 | 3500 |
| Shear Modulus (MPa) | 110 | 760 | 680 | 1400 |
| Poisson's Ratio | 0.42 | 0.42 | 0.42 | 0.25 |
| Yield Strain | 0.02 | 0.013 | 0.06 | 0.014 |
| Melting Point (°C) | 131 | 220 | 165 | 265 |

Table 5.1. Properties of polymer materials used for bicomponent fibre production (Brinson and Brinson, 2008)

In order to have a better understanding of the mechanical behaviour of thermally bonded nonwovens, constituent fibre behaviour should be examined first. Bicomponent fibres extracted from the free edges of nonwoven fabrics are tested to determine their mechanical behaviour. Figure 5.2 shows an unbonded free edge of a thermally bonded nonwoven fabric, which is used for fibre extraction. Extracted fibres are subjected to several mechanical tests such as tensile, ramp loading and relaxation for various test parameters. Each fibre is tested several times to examine variability of test results. Initial tensile tests were performed at the facilities of Nonwovens Cooperative Research Center (NCRC) in North Carolina State

University (Figure 5.3a) and all the remaining ones at Loughborough University (Figure 5.3b).

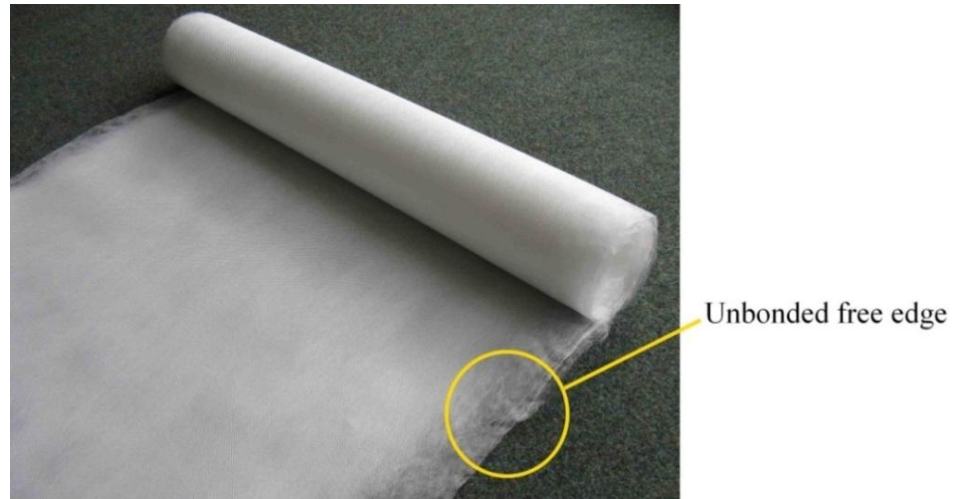


Figure 5.2. Unbonded region of thermally bonded nonwoven fabric



(a)



(b)

Figure 5.3. Tensile test rigs for bicomponent fibre experiments: Textechno Favimat (a) and Instron Micro Tester 5848 (b)

Textechno Favimat (Figure 5.3a) is specifically designed for polymer fibre testing. This machine has a 2.10 N capacity high-precision load cell and a 0.1 μm resolution linear encoder to measure force and displacement during tensile testing. Due to limitations of its software, only simple tension test with a prescribed loading speed could be performed. On the other hand, Instron Micro Tester 5848 (Figure 5.3b) is a high-precision electromechanical universal tester for miniature components and specimens. It is equipped with an Instron 2530-439 high-precision load cell having ± 5 N capacity (Figure 5.4) and an incremental encoder with a displacement resolution of 0.02 μm . Due to the capabilities of its software, Bluehill[®], not only simple tension but also cyclic loading and relaxations tests can be performed with Instron Micro Tester 5848.



Figure 5.4. Instron 2530-436 load cell (± 5 N) used for single fibre testing

Mechanical testing of single fibres is a cumbersome process due to handling issues related to size and softness of the specimens. In order to ensure that the polymer-based single fibre is not damaged by the grips and do not slip or dislocate during the tests, sticky colour-coding labels with a diameter of 6.35 mm are used at each grip region of a fibre specimen (Figure 5.5). A label is stuck and folded at each end of a fibre, and then the labels are placed between the grips of testing rig (Figure 5.5). Peg type grips with sticky rubber contact surfaces are used to enhance the

handling and gripping efficiency. This method is commonly used by Nonwovens Cooperative Research Center and its industrial members for mechanical testing of polymer-based single fibres.

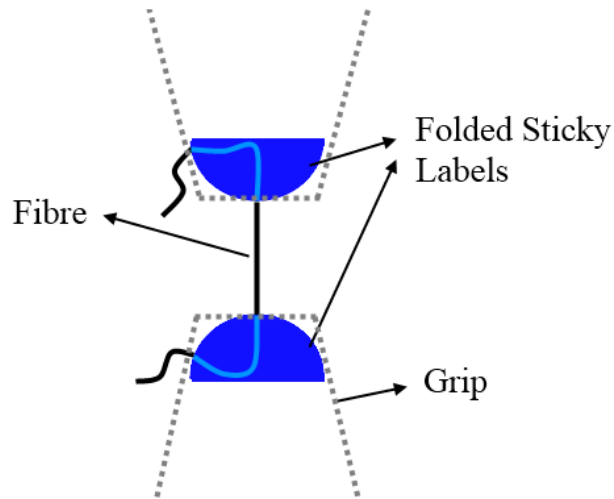


Figure 5.5. Gripping system for single fibre testing

5.1.1. Simple Tension Tests

As a starting point for testing the bicomponent fibres, a tension test is performed since it is the basic mechanical test to characterize the material's behaviour. Three types of bicomponent fibres (Table 5.2) having different core materials are tested for various deformation rates in this stage.

| Material (Core/Sheath) | Bicomponent Fibre | | |
|--|-------------------|--------|--------|
| | PP/PE | PA6/PE | PET/PE |
| Cross-Section Fraction (%) (Core/Sheath) | 75/25 | 75/25 | 75/25 |
| Mean Fibre Diameter (μm) | 20 | 18 | 16 |
| Gauge Length (mm) | 14 | 14 | 14 |

Table 5.2. Specifications of bicomponent fibre specimens

Each fibre is tested several times (>10) under the same test. Fibres are loaded up to true strain of 1 which corresponds to 172% extension during the tests. This extension value is adequate since damage strains of the nonwoven fabrics studied in

the research are less than it. Due to large strain values (strain $\gg 10\%$), true stress vs. true strain data based on current length and cross-sectional area of test specimen is utilized. Tensile test results for PP/PE fibres for deformation rate of 0.01 s^{-1} are given in Figure 5.6.

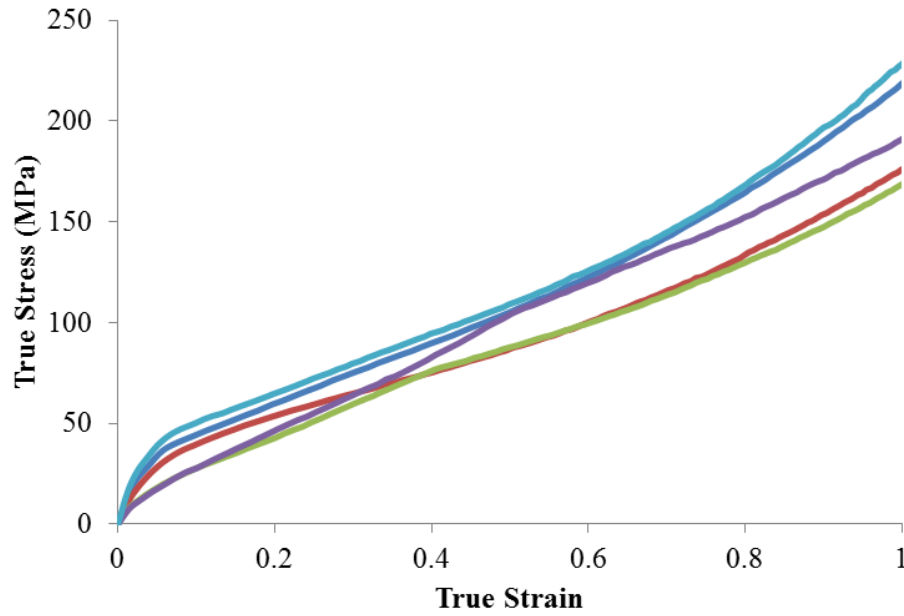


Figure 5.6. Simple tension test results for five specimens of PP/PE fibres (strain rate: 0.01 s^{-1})

According to Figure 5.6, the mechanical behaviour of bicomponent fibres do scatter significantly. This phenomenon could be a result of some local shape irregularities of the fibres due to the effect of heat or physical contact during web forming or hot calendering stages. In addition to shape irregularities, a fibre diameter is not constant along its length (Figure 5.7). Furthermore, diameters of various fibres are not the same (Figure 5.7) but vary for several reasons such as slight variations in cooling conditions or shrinkage behaviour. Diameters of the fibres are measured with scanning electron microscopy (SEM) as shown in Figure 5.7.

A representative stress-strain curve of bicomponent fibre is necessary for computation of mechanical properties of nonwoven fabrics, which will be explained in Chapter 6. To do that, a mean curve of each tensile test is utilized. On the other

hand, a representative diameter of each fibre is determined based on the average value of SEM image measurements (Figure 5.7). According to these statements, stress-strain diagram of PA6/PE, PP/PE, PET/PE bicomponent fibres with the specifications shown in Table 5.2 are given in Figure 5.8 for various strain rates.

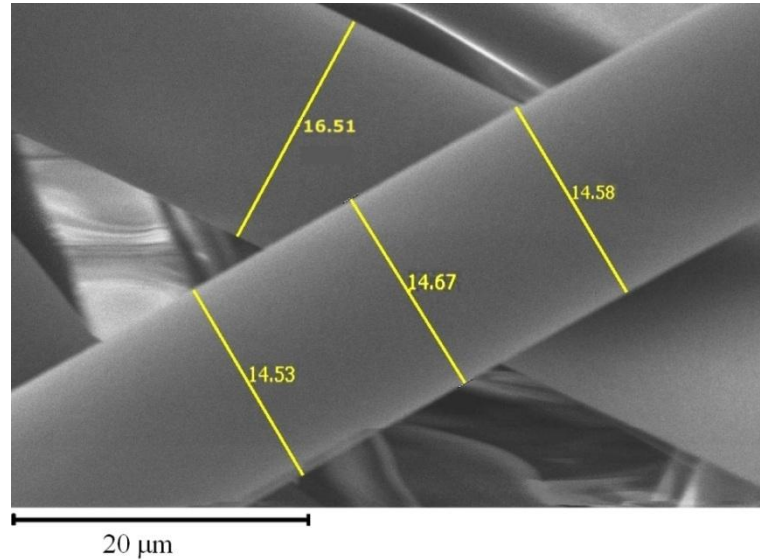


Figure 5.7. Variations in fibre diameter (all units in μm ; fibre: PP/PE, planar density: 50 g/m^2)

Figure 5.8 shows that the bicomponent fibres tested at different strain rates exhibit a typical polymer behaviour characterised by a high level of strain and nonlinearity. The difference between the curves (Figure 5.8) is due to strain-rate sensitivity linked to viscous effects in the material that will be explained in Section 5.1.3. Moreover, the stress-strain curves indicate that hardening, i.e. material's strengthening with plastic deformation, occurs throughout the whole deformation range. Due to superior strength of PA6 and PET compared to PP (Table 5.1), bicomponent fibres with PA6 and PET cores can demonstrate larger stress values than those with PP core. Finally, as indicated before fibres are extended up to 172% of their original length during tensile testing. These curves will be used to assess the mechanical performance of nonwovens having rupture strain less than the maximum strain implemented in the tensile tests of their fibres in Figure 5.8.

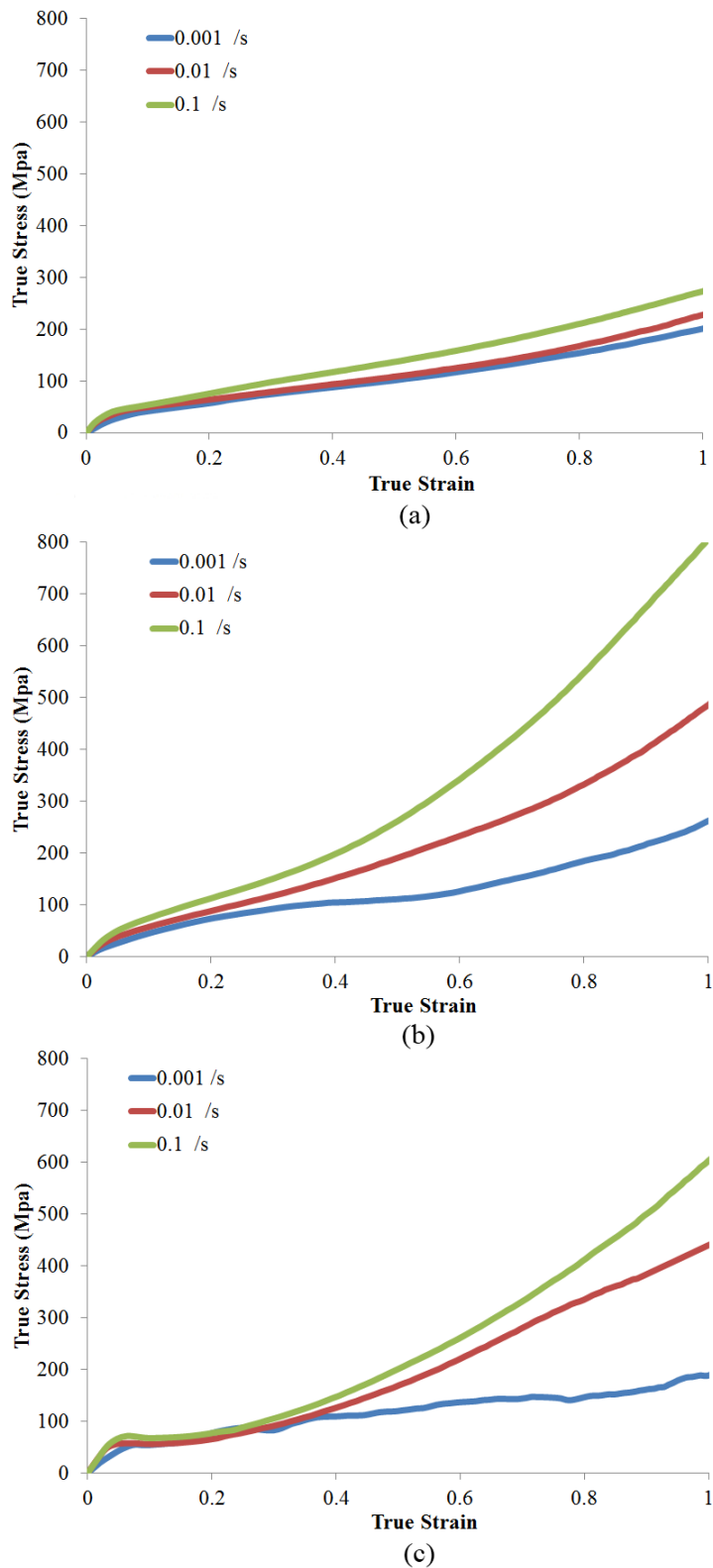


Figure 5.8. Mechanical behaviour of PP/PE (a), PA6/PE (b) and PET/PE (c) fibres for three deformation rates (scatter: $\pm 6\%$)

A simple tension test is inadequate to figure out the elastic behaviour of bicomponent polymer fibres. In order to have an idea about the elastic behaviour of these fibres, cyclic loading-unloading tests at small strain levels should be carried out.

5.1.2. Cyclic Loading Tests

Cyclic loading test is the repetitive application of consecutive loading and unloading with increasing tensile displacement or force in each cycle. This test can reveal the elastic behaviour of bicomponent fibres, i.e. large-strain or small-strain, linear or nonlinear. An identified elastic behaviour of fibres as a result of cyclic loading tests will play an important role in modelling strategy for thermally bonded nonwoven fabrics in this research. Bicomponent fibres with specifications indicated in Table 5.2 are exposed to this test to identify their elastic behaviour. Fibres are loaded and unloaded repetitively with an increasing tensile extension at each loading stage up to a total strain value of 0.04. Typical cyclic loading test results for a bicomponent fibre are given in Figure 5.9.

A practical way to decide on the elastic behaviour of fibres according to their cyclic loading data is to interpret unloading stages. As the load is removed from the specimen, recovery of the elastic portion of deformation, which is defined as spring back, takes place and a pure elastic behaviour is observed. As seen from unloading portions in Figure 5.9, bicomponent fibres possess a nonlinear elastic behaviour. On the other hand, due to this nonlinear behaviour, it is hard to determine their yield point. The difficulty of determining the yield strain of fibres arises from the fact that an infinite number of loading and unloading cycles without scatter in the experimental data is required to identify a sharp strain point to separate elastic region from the plastic one. Due to this fact, yield strain of a bicomponent fibre is assumed as that of its constituent polymer with smaller yield strain, e.g. yield strain of PA6/PE fibre is 0.013 which is the yield strain of PA6 (Table 5.1). According to this assumption, yield strains of bicomponent fibres used in this study are listed in Table 5.3.

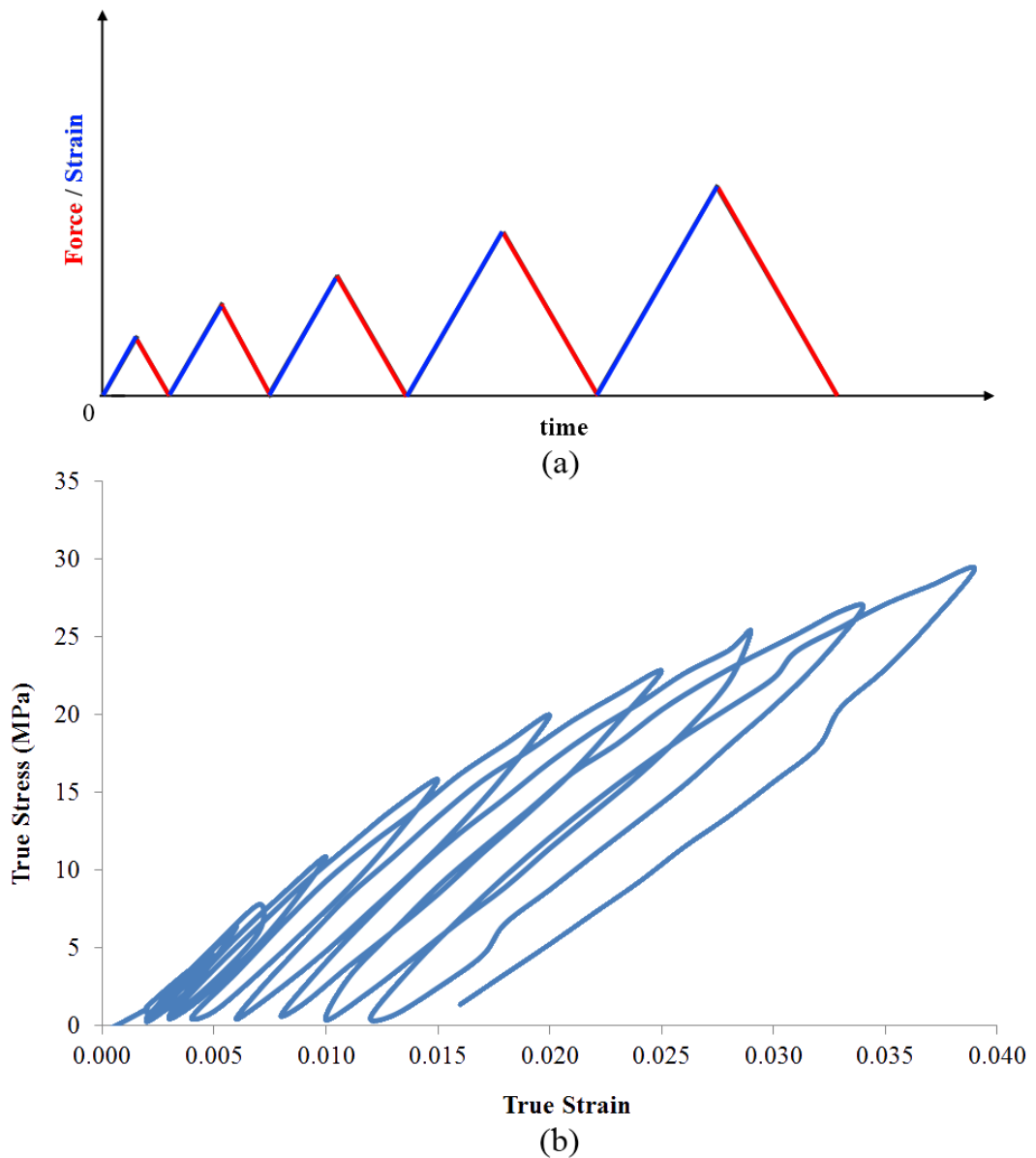


Figure 5.9. Cyclic loading test results for PP/PE fibre (b) and corresponding loading-unloading control graph (a)

A plastic behaviour of bicomponent fibres is distinguished after examining their elastic behaviour. When their yield strain (0.013 - 0.02) is compared to their rupture strain (>1.2), it is obvious that the governing deformation type is plastic during a large-strain deformation, i.e. the portion of irreversible deformation is more than that of reversible one. Plastic behaviour is nonlinear similar to elastic one.

| Fibre (Core/Sheath) | PA6/PE | PP/PE | PET/PE |
|---------------------|--------|-------|--------|
| Yield Strain | 0.013 | 0.02 | 0.014 |

Table 5.3. Yield strain values of bicomponent fibres (Ward and Sweeney, 2004)

As mentioned in Section 5.1.1, mechanical performance of polymer fibres are influenced by viscous effects. Deformation behaviour of these fibres is time-dependent due to these affects. Furthermore, nonlinear behaviour in the elastic region originates from these viscous effects. Elasticity combined with viscous effects is termed *viscoelasticity*. One typical symptom of viscoelasticity is a hysteresis loop on stress-strain curves, which is a deviation of unloading path from a loading path during spring back as seen in Figure 5.10. Each hysteresis loop is an indication of energy dissipation during unloading. Next section deals with a relaxation behaviour, which is another symptom of viscoelasticity and used to determine viscoelastic properties of a material.

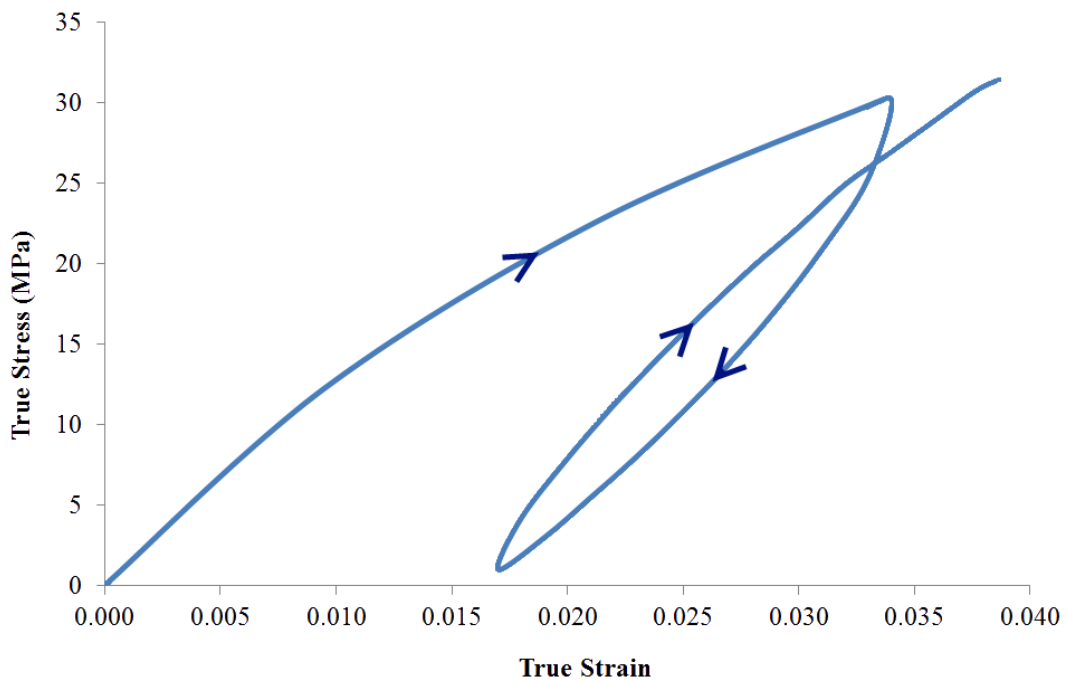


Figure 5.10. PET/PE fibre undergoing a load cycle with a hysteresis loop

5.1.3. Relaxation Tests

Viscoelasticity is a typical deformation behaviour of polymers, and it should be included in numerical modelling of these materials. Viscoelastic parameters of time-dependent viscoelastic material model should be obtained experimentally. There are two types of tests – creep and relaxation – used to characterize viscoelastic properties of a material. As explained in Section 4.3, the creep test records strain *vs.* time while a specimen is kept at constant stress; on the other hand, relaxation test records stress *vs.* time for a specimen at constant strain. In this study, a relaxation test is preferred to identify viscoelastic properties of bicomponent fibres.

PP/PE, PA6/PE and PET/PE fibres with specifications shown in Table 5.2 are exposed to relaxation tests performed at various constant strain levels: 0.05, 0.1, 0.2, 0.4 and 0.8. The test duration is 20000 s (5.5 h). A typical relaxation behaviour of these fibres is illustrated in Figure 5.11 for first 60 s in which major portion of the stress is dissipated. The graph is plotted for normalized stress for better comparison since we are interested in a character of stress decay rather than in stress values which vary with fibre material.

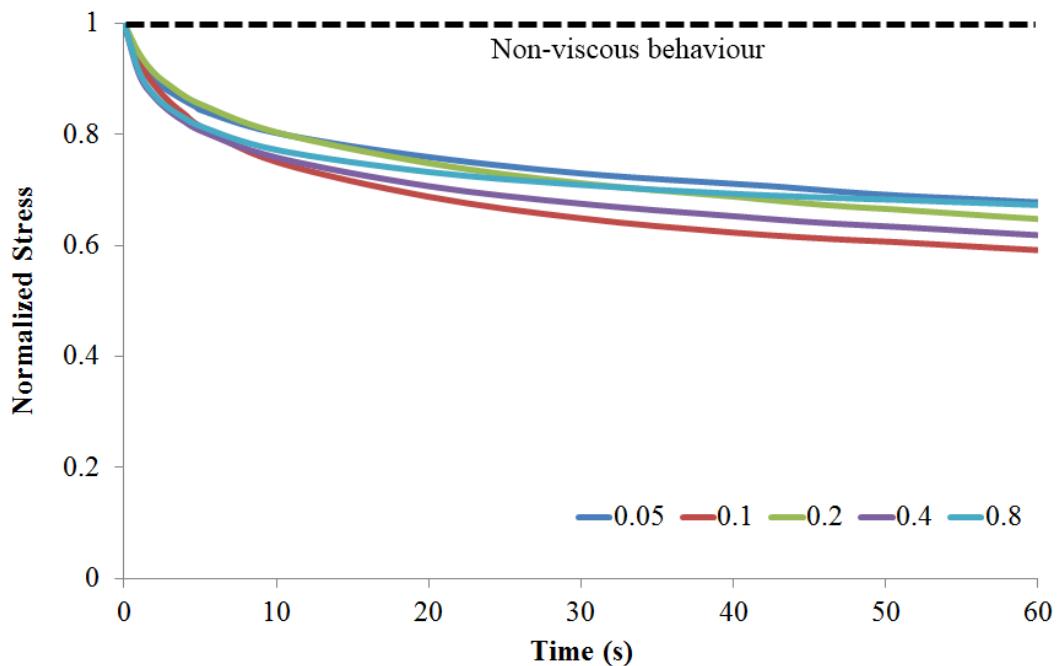


Figure 5.11. Relaxation behaviour of PP/PE fibre for various applied strains (scatter: $\pm 6\%$)

Relaxation curves in Figure 5.11 prove that polymer-based bicomponent fibres exhibit viscous behaviour since stress level decreases with time. Normalized stress value for a non-viscous material should remain 1 because the stress level does not change with time (Figure 5.11). Deviation of relaxation curves from the non-viscous value indicates that deformation performance of these materials is time-dependent. According to Figure 5.11, which shows the relaxation behaviour of the PP/PE fibre for 60 s period, approximately 35% of the stress is attenuated by the material in this period. Such a large amount of stress dissipation in a short time should be considered in numerical modelling of fabrics made of these fibres.

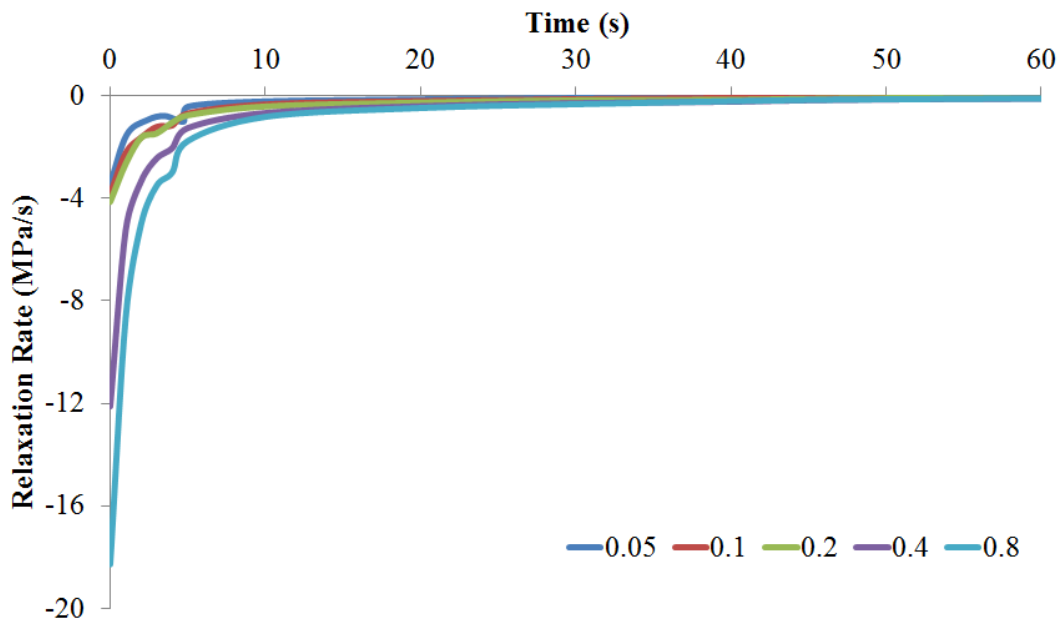


Figure 5.12. Relaxation rate curves of PP/PE fibre for various applied strains (scatter: $\pm 6\%$)

Another interesting point in the relaxation behaviour of bicomponent fibres is that their viscous behaviour depends on the applied strain level. Relaxation performance is affected by the level of applied strain regardless of polymer material type. In the relaxation rate graph (Figure 5.12), based on the time differentiation of relaxation curves, the effect of applied strain on stress is more apparent. According to Figure 5.12, as the applied strain increases, the magnitude of initial relaxation rate of the material increases. Additionally, the relaxation rate at the initial stages of tests is significantly large. Especially for the applied initial strain of 0.8, the relaxation rate

starts with -18 MPa/s, which is a very high value. In 15 s, the magnitude of relaxation rate of fibres falls below 1 MPa/s and in 60 s it becomes less than 0.1 MPa/s. As a result, time is an unavoidable parameter for determining the mechanical behaviour and performance of bicomponent fibres.

To sum up, polymer-based bicomponent fibres used for manufacturing nonwoven fabrics have a complicated mechanical behaviour, which could be described as nonlinear large-strain viscoelastic-plastic. Deformation of such fibres is mainly governed by the non-elastic stage because their yield strain is negligibly small when compared to their rupture strain. Another complexity regarding to their performance is its scatter. Due to several imperfections related to the manufacturing process explained in Section 5.1.1, the experimental results scatter significantly. Therefore, the representative mean curve is facilitated in each experiment type to characterize the fibre behaviour. Numerical parameters, obtained for these representative curves, will be used as input data for numerical modelling of nonwoven fabrics made of such fibres. This topic will be discussed further in Chapter 7.

As the basic element of nonwovens, bicomponent fibres play an important role in determining their deformation behaviour. In addition to fibres, microstructure of thermally bonded nonwovens is a prominent factor influencing their deformation performance. Microstructure of these fabrics should be examined to better understand their mechanical behaviour and to develop accurate numerical models.

5.2. Microstructure of Thermally Bonded Bicomponent Fibre Nonwovens

Characterisation of thermally bonded bicomponent fibre nonwovens requires a detailed study of their microstructure since it is the key to understanding the dependence of material's mechanical response on the direction of applied force as well as their damage behaviour. Hence, their microstructure should be examined to understand specific features of unique mechanical behaviour of these materials. In

order to observe the microstructure of these materials, scanning electron microscopy (SEM) and X-ray micro computed tomography (micro CT) facilities of Loughborough University are used. SEM is used to obtain 2D surface images whereas a micro CT system is utilized to acquire detailed 3D images of nonwoven materials. Each technique is used to examine the structure of nonwoven fabrics to reveal a particular feature.

5.2.1. Examination with Scanning Electron Microscopy

SEM technique enables us to examine surface images of nonwoven fabrics. Dimensions of structural entities observed on a planar surface could be measured with it. A thermally bonded nonwoven fabric shown in Figure 5.13 has a planar density of 150 g/m^2 and manufactured with bicomponent fibres. The fibres in this case are composed of PE as sheath and PA6 as core material. The fabric is composed of two regions, namely, bond points and the fibre matrix. Bond points are composed of core (PA6) fibres surrounded by molten sheath (PE) while the matrix is composed of distinct PA6/PE bicomponent fibres connecting bond points together as shown in Figure 5.13.

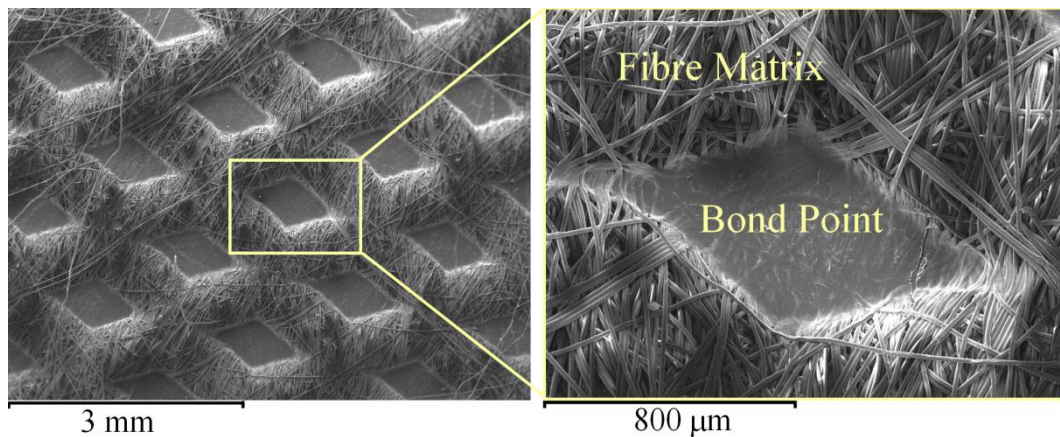


Figure 5.13. SEM image of thermally bonded nonwoven fabric composed of bond points and fibre matrix (fibre: PA6/PE, planar density: 150 g/m^2)

A typical fibre matrix structure of a thermally bonded nonwoven fabric is shown in Figure 5.14. The matrix region is composed of randomly oriented

bicomponent fibres acting as links between bond points. Most of them are straight meaning that they carry load whenever the fabric is exposed to deformation acting along their axes, whereas a small portion of them are slightly curly and can only contribute to the strength of fabric after being straightened which requires deformation of the fabric. Due to the core/sheath structure, the core part of fibres is continuous throughout the fabric, contributing to its mechanical strength.

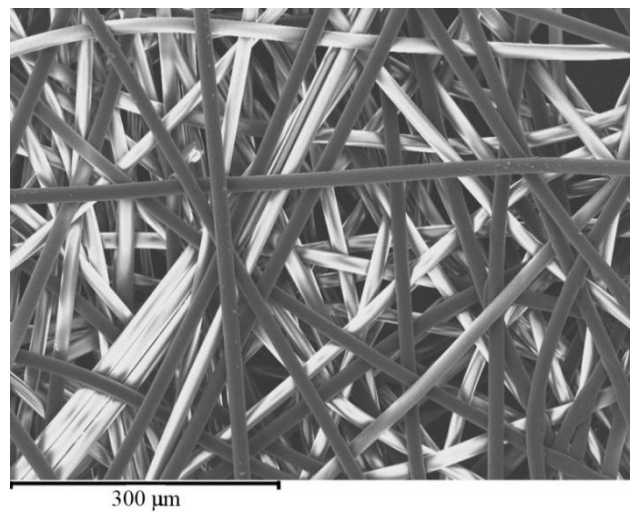


Figure 5.14. Fibre matrix region of thermally bonded nonwoven fabric (fibre: PA6/PE, planar density: 50 g/m²)

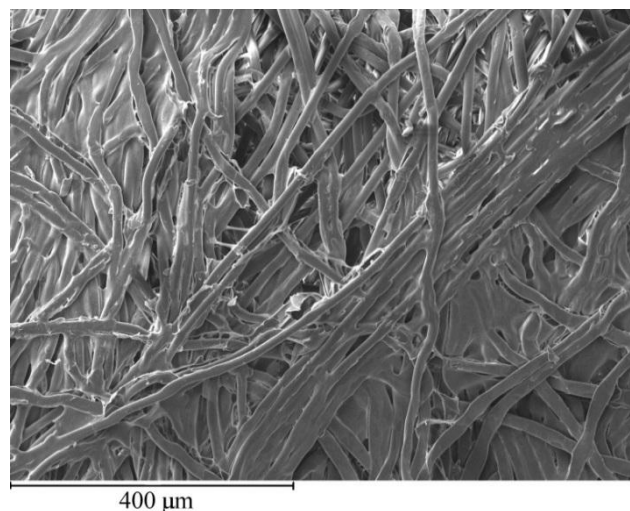


Figure 5.15. Fibre matrix region of thermally bonded nonwoven fabric (fibre: PA6/PE, planar density: 150 g/m²)

Unlike the distinct fibres shown in Figure 5.14, a significant amount of surface regions of matrix have fibres stuck to each other due to the effect of heat used to form bond points during the hot calendering stage (Figure 5.15). As a result, a portion of the matrix region shown in Figure 5.15 contains the molten sheath material. These molten parts in the fibre matrix surface increases the bending stiffness of the fabric.

Bond points are continuous regions, and their structure is similar to that of fibre-reinforced composites composed of sheath material as matrix and core material as fibres. When a hot calender with a pattern contacts and compresses the fibre matrix, the sheath part of bicomponent fibres melts and acts as an adhesive for the core parts of fibres, forming bond points. Unlike the fibre matrix, bond points are solid, continuous and thinner. Their bending stiffness is more than that of the fibre matrix. The shape and pattern of bond points vary according to the application area. A typical bond point shape of a thermally bonded nonwoven is shown in Figure 5.16. As explained in Section 3.1.2, nonwovens have two principal directions, namely, the cross direction (CD) and the machine direction (MD). These principal directions are shown in Figure 5.16 with respect to the orientation of the bond point.

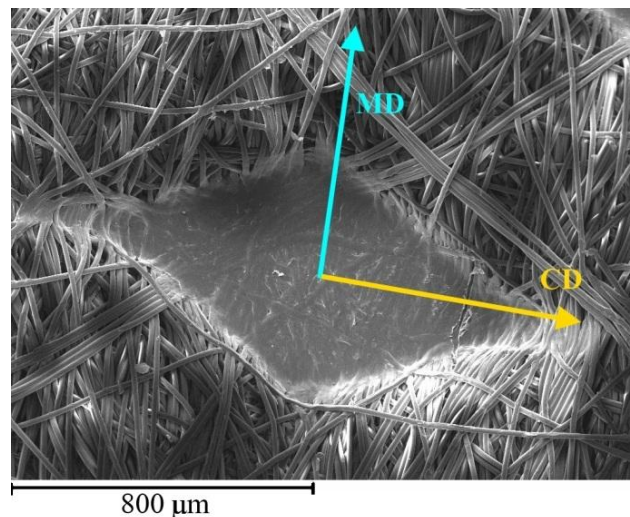


Figure 5.16. Bond point of thermally bonded nonwoven fabric with the illustration of principal directions (fibre: PA6/PE, planar density: 150 g/m²)

5.2.2. Examination with X-Ray Micro Computed Tomography

X-ray micro CT scanning of nonwoven fabrics is performed using the facilities of Loughborough University with XTEK XT-H 160Xi device (Figure 5.17) capable of submicron scanning resolution. Unlike SEM, micro CT is capable of obtaining 3D models, which can supply structural information about the material's inner volume. Since this method is completely non-destructive, it is possible to use analysed specimens in further tests.



Figure 5.17. X-ray micro computed tomography device, Loughborough University, UK

A 3D model of a thermally bonded nonwoven fabric obtained with X-ray micro CT technique is shown in Figure 5.18. Due to the periodic bond pattern generated by engraved hot calender, surface topology is in the form of consecutive hills and valleys. Random orientation of fibres acting as links between bond points is identifiable in 3D space. Thickness decreases significantly at bond point regions due to pressure and heat applied during calendering stage, therefore near-surface fibres linking two neighbour bond points are stretched. As explained in the previous section, curly fibres do not contribute to strength of fabric at initial stage of deformation before they are stretched. This is one of the main reasons for a different

mechanical behaviour of low-density nonwovens (Hou, 2010) compared to that of high-density ones.

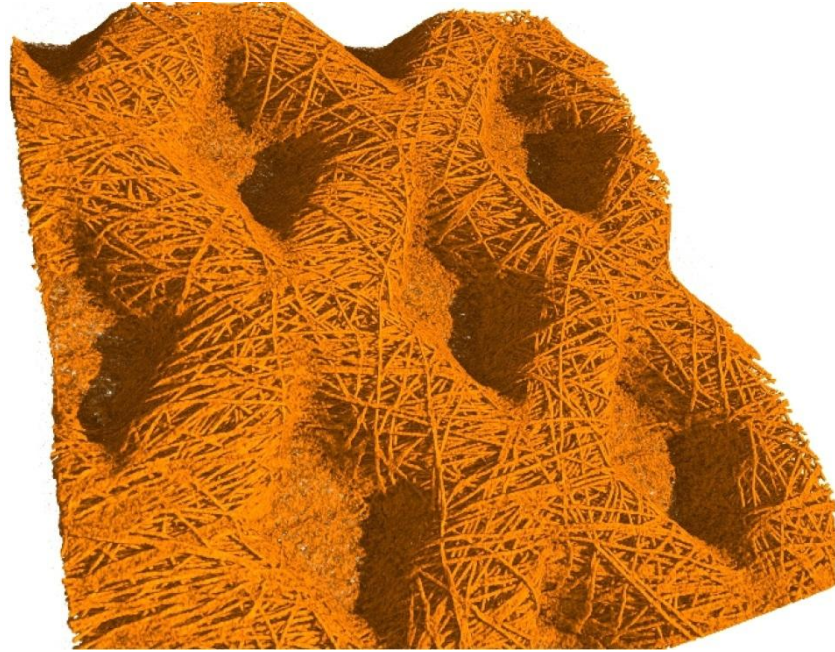


Figure 5.18. 3D micro CT model of thermally bonded nonwoven fabric (fibre: PP/PE, planar density: 150 g/m²)

In this study, the micro CT device is also used to obtain a very important parameter necessary for a numerical model and computation of mechanical properties of nonwoven fabrics. Average thickness of fibre matrix regions is measured with the X-ray micro CT system using images of through-thickness sections crossing the centre of bond points (Figure 5.19). Average thickness values for fibre matrix of various nonwoven fabrics shown in Table 5.4 will be used to compute their mechanical performance in Chapter 6.

| Fibre (Core/Sheath) | Planar Density (g/m ²) | | |
|---------------------|------------------------------------|---------|---------|
| | 50 | 100 | 150 |
| PP/PE | 0.35 mm | 0.47 mm | 0.55 mm |
| PA6/PE | 0.3 mm | 0.42 mm | 0.50 mm |
| PET/PE | 0.28 mm | 0.40 mm | 0.45 mm |

Table 5.4. Average fibre matrix thickness of nonwoven fabrics used in this research

Due to compressible structure of fibre matrix, micro CT technique is very suitable for obtaining through-thickness images without deforming nonwoven specimens. The difference between the porosity of matrix and that of bond points could be seen in Figure 5.19. During the bonding stage, as a result of pressure and melting of sheath part of fibres, bond points are formed as solid and continuous. Due to this difference, fibre matrix region is highly compressible compared to bond points. This is the main reason for differences between the mechanical characteristics of bond points and the fibre matrix. Mechanical performance of a porous and a nonporous structure will be definitely different, at least their compressive behaviour.

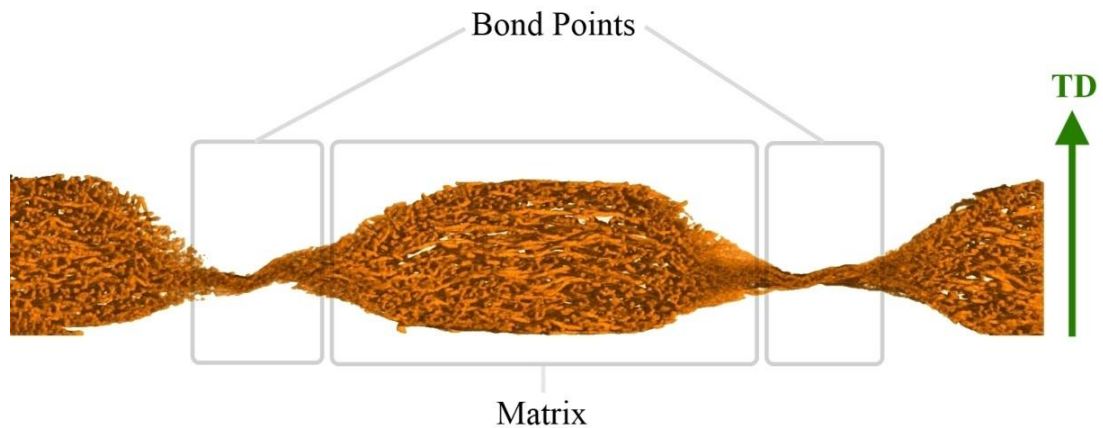


Figure 5.19. Through-thickness image of thermally bonded nonwoven fabric obtained with X-ray micro CT (fibre: PP/PE, planar density: 150 g/m^2)

Principal directions MD and CD are defined on the fabric plane (Figure 5.16) with respect to the direction of fibre flow on the conveyor during production. In addition to these principal directions, the thickness direction (TD) is introduced to complete a 3D principal coordinate system for a nonwoven fabric. As seen in Figure 5.19, TD refers to a principal axis normal to the fabric plane. Mechanical properties of nonwoven fabrics will be calculated based on these three principal directions in Chapter 6.

As a result of examinations performed with SEM and X-ray micro CT techniques, it is concluded that thermally bonded nonwoven fabrics are composed of two distinct regions having different microstructures, which are the source of

different deformation behaviours of constituents. The fibre matrix does not have compressive strength due to a low threshold for buckling of individual fibres under compression. This region has also negligible bending stiffness that causes the fabric to behave like a membrane. On the other hand, bond points are similar to reinforced composite materials having randomly distributed fibres of core material. Bond points are solid and continuous regions of nonwoven fabrics. Hence, the bond pattern and shape will affect the mechanical performance of fabric significantly. As a result of differences in the microstructures of these regions, they will be handled separately in numerical modelling.

Another important point about the microstructure of nonwoven fabrics is the random orientation of fibres. Random orientation of fibres could be observed with both examination techniques in 2D as well as in 3D. As explained in Chapter 3, due to this randomness, the deformation behaviour of nonwoven fabrics depends on the direction of applied load. Therefore, results of tensile tests applied on fabric samples in different loading directions will differ. This behaviour could be observed in mechanical test results given in the next section, which is about mechanical performance of thermally bonded nonwovens.

5.3. Mechanical Behaviour of Thermally Bonded Bicomponent Fibre Nonwovens

Mechanical performance of thermally bonded nonwoven fabrics should be exposed via mechanical experiments in order to understand and represent their behaviour in numerical modelling. An adequate numerical model should include deformation characteristics obtained in this section. Furthermore, experimental results of this section will be used to improve and verify the numerical model introduced in this study. Experimental results introduced in this section will be considered from the computational mechanics point of view rather than textile engineering one.

Tensile testing is the first step of mechanical experiments in order to have an initial insight into the deformation behaviour. Bicomponent fibre nonwoven samples

are subjected to tension tests with Hounsfield Benchtop Tester (Figure 5.20) having ± 800 N load cell and pneumatic grips. Samples are loaded in tension along various directions with various loading rates to observe their rate-dependent anisotropic behaviour. Apart from tension tests, nonwoven samples are subjected to compression tests in thickness direction (TD) to observe their behaviour along TD. Finally, cyclic loading tests are performed on nonwoven fabrics to study their elasticity.



Figure 5.20. Hounsfield Benchtop Tester with pneumatic grips

5.3.1. Simple Tension Tests

Thermally bonded bicomponent fibres are subjected to simple tension tests to analyse their deformation behaviour. Physical properties of nonwoven fabrics tested in this stage are given in Table 5.5. In addition to these properties, the bond shape and pattern are important factors affecting mechanical performance of these fabrics (Section 5.2). Bond points of fabrics tested in this section have a diamond shape, and their pattern is given in Figure 5.21. Dimensions of the specimens tested along MD and CD are 30 mm in length and 15 mm in width. These dimensions are large

enough to capture a typical behaviour of thermally bonded nonwovens free of edge effects (Hou, 2010) since they cover a fabric area of approximately 15 x 8 bond points, and are convenient for mechanical testing.

| Fibre Material (Core/Sheath) | Nonwoven Fabric | | | | | | | | |
|--|-----------------|------|------|--------|------|------|--------|-----|------|
| | PP/PE | | | PA6/PE | | | PET/PE | | |
| Fibre Cross-Section Fraction (%) (Core/Sheath) | 75/25 | | | | | | | | |
| Fibre Diameter (μm) | 20 | | | 18 | | | 16 | | |
| Fabric Planar Density (g/m^2) | 50 | 100 | 150 | 50 | 100 | 150 | 50 | 100 | 150 |
| Matrix Thickness (mm) | 0.35 | 0.47 | 0.55 | 0.30 | 0.42 | 0.50 | 0.28 | 0.4 | 0.45 |
| Gauge Length (mm) | 30 | | | | | | | | |
| Width (mm) | 15 | | | | | | | | |

Table 5.5. Physical properties of thermally bonded nonwoven fabrics used in this research.

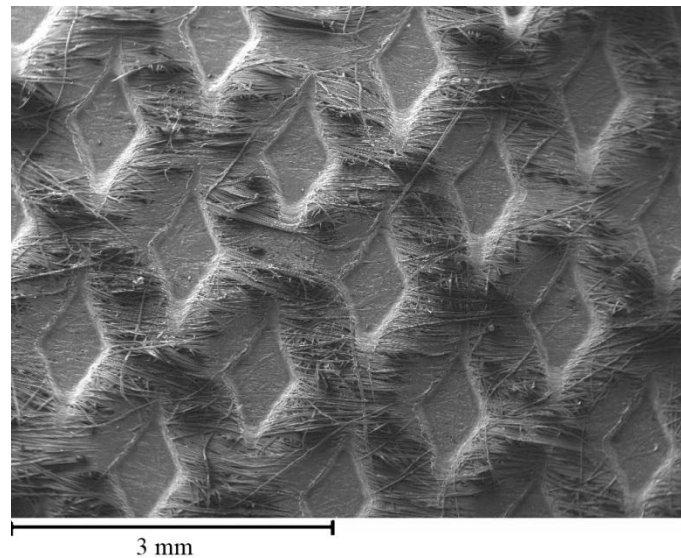


Figure 5.21. Bond pattern of nonwoven fabrics given in Table 5.5 (fibre: PA6/PE, planar density: 150 g/m^2)

As explained in the previous section, nonwoven fabrics are manufactured with fibres having random orientations. Due to the manufacturing technique, these fabrics are expected to possess anisotropic mechanical properties. In order to observe this mechanical anisotropy, fabric samples are tested with respect to their planar principal

directions which are MD and CD. Various deformation rates are applied in tension tests to observe strain-rate sensitivity in their mechanical performance.

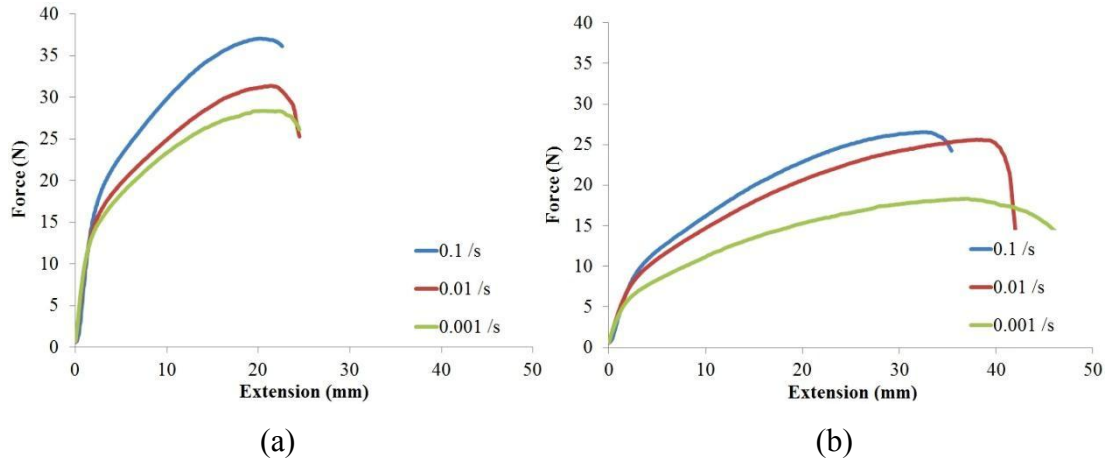


Figure 5.22. Simple tension test results for nonwoven fabric tested in MD (a) and in CD (b) for three deformation rates (fibre: PP/PE, planar density: 50 g/m², specimen dimensions: 30 mm x 15 mm, scatter: ±10%)

Simple tension tests for thermally bonded nonwoven fabrics described in Table 5.5 are performed and curves of 50 g/m² PP/PE thermally bonded nonwoven fabric are shown in Figure 5.22 as typical examples. These curves are given in terms of force vs. extension to compare with their numerical model results. Here, it is obvious that direction of applied load affects the deformation performance of these fabrics. As explained in Section 3.1, a majority of fibres in nonwovens tend to orient along MD rather than CD. This phenomenon could be observed in a typical ODF graph shown in Figure 3.2. As a result of this, strength of nonwoven fabrics in MD is higher than that in CD. Tension curves in Figure 5.22 reflect this anisotropic behaviour.

In addition to mechanical anisotropy, nonwoven fabrics exhibit strain-rate effects. As seen in Figure 5.22, as the strain rate increases, the force required to deform material increases as well. This behaviour originates from time-dependent viscous deformation performance of polymer-based fibres (Section 5.1). Another interesting point is the damage behaviour, which is related to fabric's microstructure.

According to tension test results, rupture strain of fabrics is significantly lower than that of their fibres. The main reason for this is premature failure of fibres at the fibre-bond interface (Michielsen *et al.*, 2006).

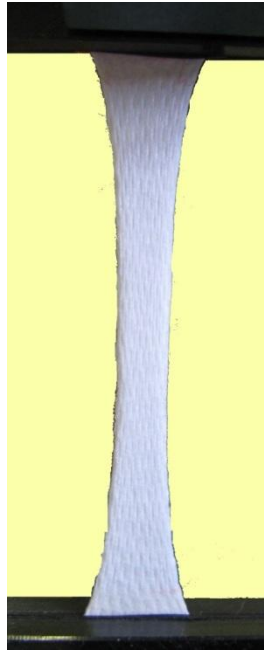


Figure 5.23. Nonwoven fabric under tension (fibre: PA6/PE, planar density: 100 g/m², initial specimen dimensions: 30 mm x 15 mm)

A tangential modulus curve could be plotted based on homogenized stress *vs.* strain curve of fabrics for better understanding of their behaviour. In order to evaluate experimental data regardless of specimen's dimensions, homogenized stress *vs.* strain curve is utilized. During the calculation of homogenized stress, nonwoven fabrics are assumed as homogenous materials, and matrix thickness in Table 5.5 is assumed as fabric thickness for calculating current cross-sectional area at each data point. The tangential modulus is the slope of stress *vs.* strain curve at a specified strain (Figure 5.24). This information is important for predicting stress evolution during deformation; it can inform us about the linearity of deformation behaviour. The tangential modulus (E_t) is calculated as

$$E_t = \frac{d\sigma}{d\varepsilon} \quad (5.1)$$

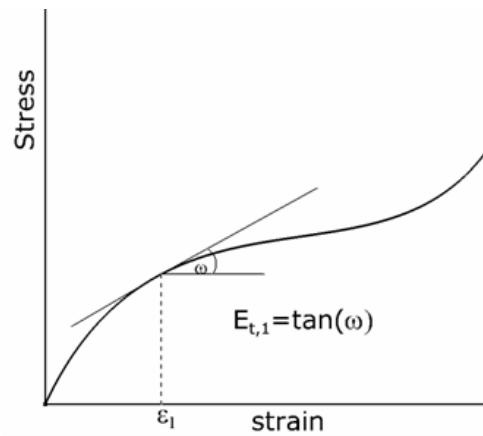


Figure 5.24. Graphical definition of tangential modulus (E_t)

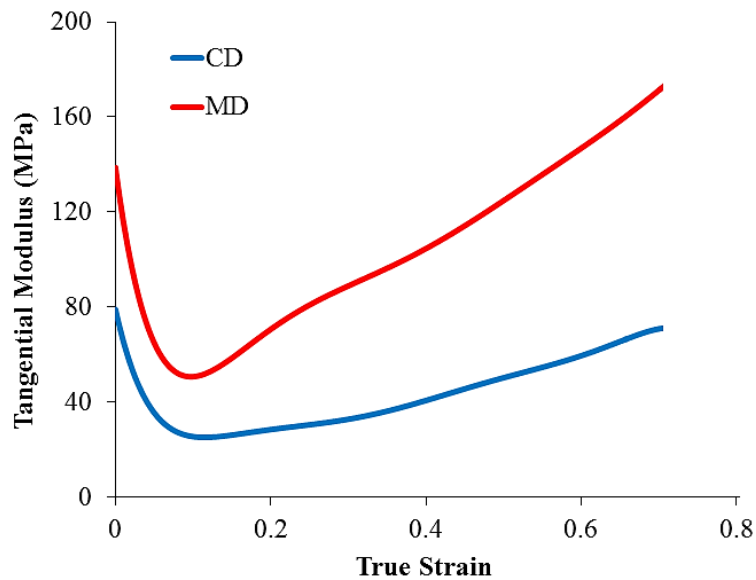


Figure 5.25. Tangential modulus curves of nonwoven fabric in MD and CD (fibre: PA6/PE, planar density: 150 g/m^2)

Apparently, for linear portions of the graphs, such as elastic region of metals, the tangential modulus remains constant. According to Figure 5.25, nonwoven fabrics have a highly nonlinear deformation behaviour similar to that of their fibres. The tangential modulus decreases up to strain of 0.1 and starts to increase thereafter. The expected behaviour of fibres in the fabric during the initial stage of deformation is their reorientation to diminish their angle with respect to the loading direction.

Besides, some curly fibres start to carry load as they get straightened at the beginning of deformation. These expected performances should increase the tangential modulus of material in the loading direction. However, Figure 5.25 demonstrates the opposite trend up to 0.1 strain value. Therefore, nonlinearity of the material cannot be explained by the mentioned deformation mechanisms linked to individual fibres leading to geometric nonlinearity. Therefore, it is concluded that this nonlinearity originates from the behaviour of polymer-based bicomponent fibres. This conclusion will play an important role in developing the methodology for computing the mechanical properties of nonwoven fabrics based on their single-fibre behaviour.

5.3.2. Compression Tests in Thickness Direction

Fabrics are membrane-like structures and they can only carry loads in tensile direction in their plane. The main reason for applying compression along TD is to verify the poor performance of fibre matrix in this direction. Mechanical properties for this direction are also necessary in numerical modelling. In order to compare mechanical performance in TD with that in MD and CD, homogenized stress *vs.* strain data is used. As explained before, the term “homogenized” is used because nonwovens are not homogeneous materials. For the sake of dimensionless comparison, thickness of fibre matrix is assumed to be representative thickness of the homogenized nonwoven material. A cross-sectional area is recalculated for each strain level based on this assumption. Dimensions of specimens subjected to compression tests are 10 mm x 10 mm; thickness of the fabric is used as the gauge length (Table 5.5). Deformation rate is the same as used in tensile tests performed along MD and CD.

As explained in Section 5.2, due to porous and highly compressible structure of the matrix region, strength in TD is negligibly low when compared to that in MD and CD (Figure 5.26). Due to the type of applied displacement in compression test, stress values of TD curve in Figure 5.26 are negative. In the compression test, it is the matrix region that is exposed to compression rather than bond points because thickness of the bond points is approximately 30% of that of the matrix (Figure

5.27). In fact, bond points are solid regions with higher yield strength with respect to matrix region in TD. Therefore, mechanical performance of matrix region up to the compression distance, which is approximately 70% of the matrix thickness, is obtained from compression tests. This distance varies with planar density and fibre diameter.

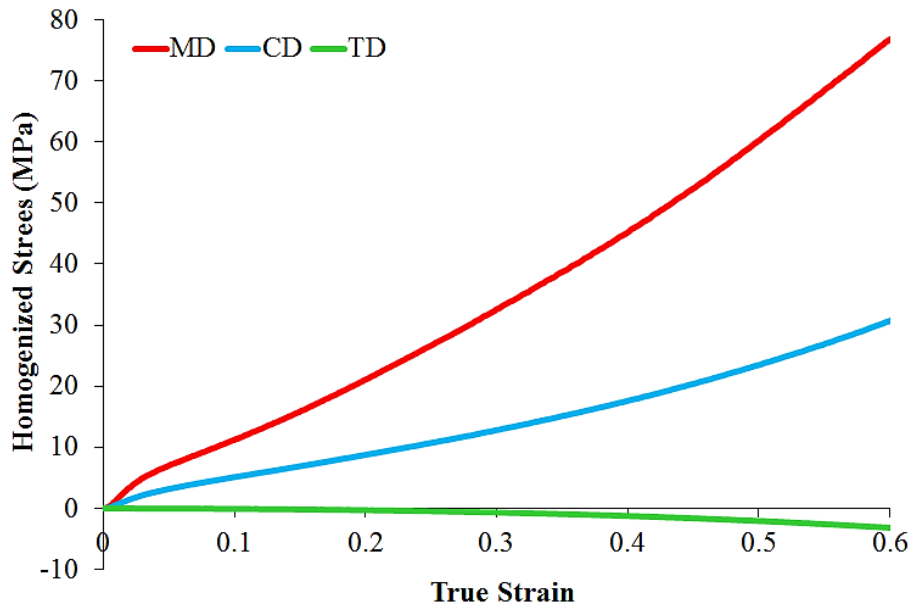


Figure 5.26. Mechanical behaviour of thermally bonded nonwoven fabric in MD and CD and TD (fibre: PA6/PE, planar density: 150 g/m², strain rate: 0.01 s⁻¹, scatter: ±10%) (Absolute magnitude of true strain is used for TD)



Figure 5.27. X-ray micro CT image of through-thickness cross section of thermally bonded nonwoven (fibre: PA6/PE, planar density: 150 g/m²)

5.3.3. Cyclic Loading Tests

The aim of this section is to investigate the elastic behaviour of thermally bonded nonwoven fabrics. Each specimen with dimensions 30 mm x 15 mm is subjected to consecutive loading and unloading cycles with increasing force amplitude in each loading stage. As explained in Section 5.1.2, in such tests spring back reveals pure-elastic deformation characteristics of a material. In order to evaluate experimental data regardless of specimen dimensions, homogenized stress *vs.* strain data is utilized as above.

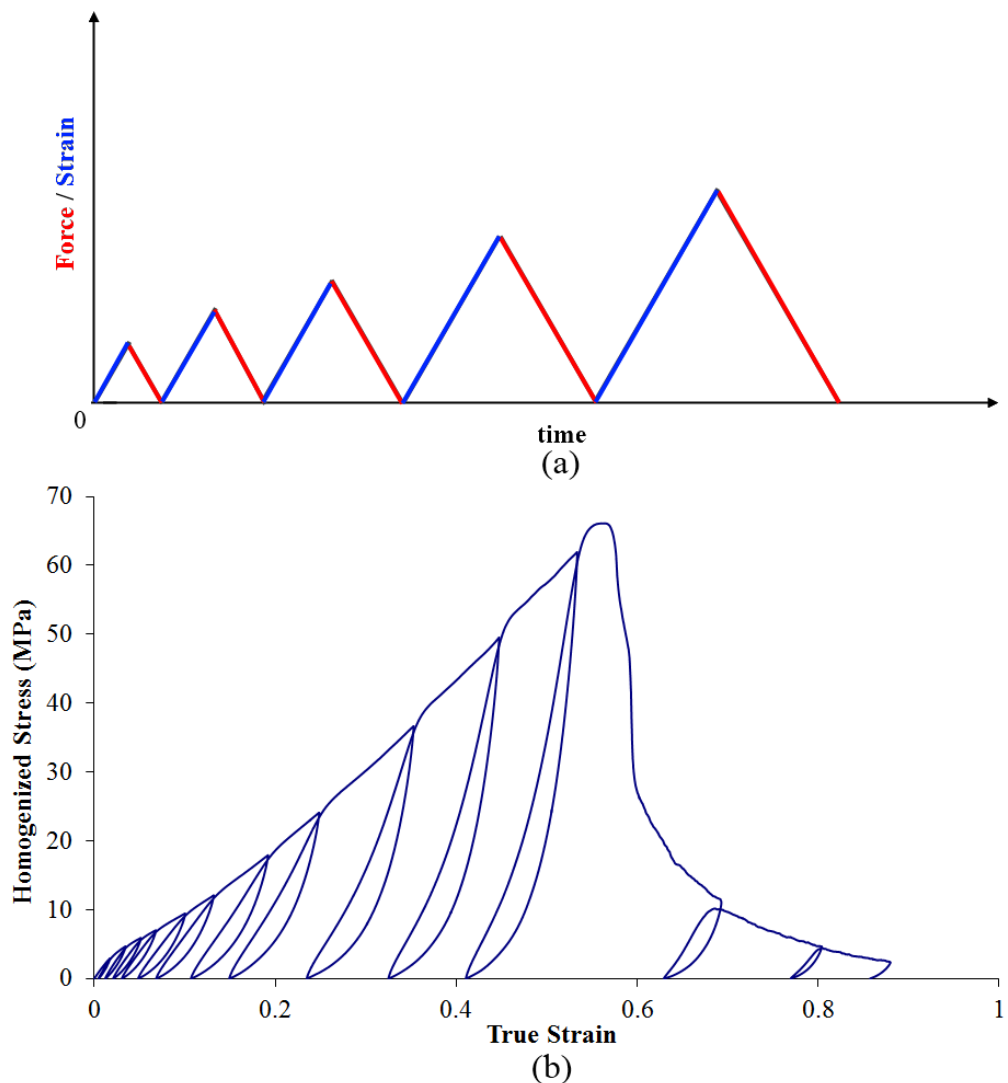


Figure 5.28. Cyclic loading of nonwoven fabric in MD (strain range: 0-1) (fibre: PA6/PE, planar density: 100 g/m²) (b) and corresponding loading-unloading control graph (a)

Cyclic loading tests reveal viscoelastic behaviour of the material, which could be observed during the unloading stage of each cycle (Figure 5.28). Similar to the constituent fibres, nonwovens exhibit time-dependent mechanical properties generating hysteresis loops during each load cycle. Due to these properties, a portion of elastic energy is dissipated by the material. According to the results of relaxation experiments performed with bicomponent fibres, we can conclude that the viscous behaviour of these fabrics is originating from their bicomponent fibres.

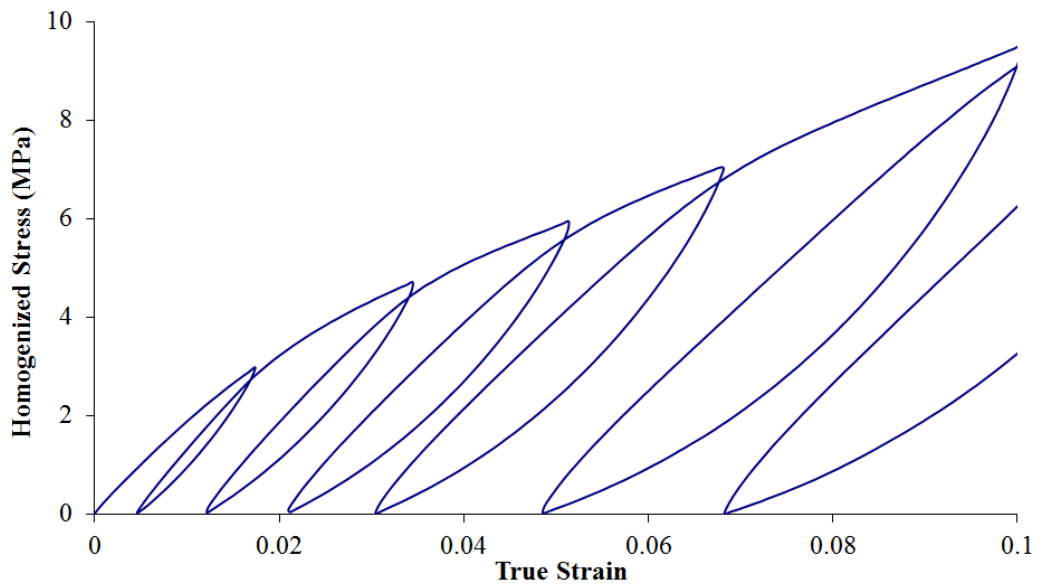


Figure 5.29. Cyclic loading of nonwoven fabric in MD (strain range: 0-0.1) (fibre: PA6/PE, planar density: 100 g/m²)

Figure 5.29 is the magnified version of Figure 5.28 to analyse the yield behaviour at early stages of deformation. The nonwoven fabric deforms plastically, even extended to 0.01 strain level, according to Figure 5.29. Therefore deformation of such fabrics is mainly governed by plasticity. To sum up, deformation characteristics of polymer-based bicomponent fibres is retained for the nonwoven fabrics manufactured with them. As explained in Chapter 2, one of these characteristics is temperature-history-dependent mechanical properties which will be explained in the next section.

5.4. Effect of Calendering Temperature on Mechanical Performance of Nonwovens

Mechanical properties of polymer materials are influenced by the temperature history they are exposed to. Therefore, any temperature change during the hot calendering stage affects the mechanical behaviour of thermally bonded nonwovens by affecting bonding between fibres. In order to investigate this effect, hot and cold calendered nonwoven specimens having identical physical properties are subjected to tension tests.

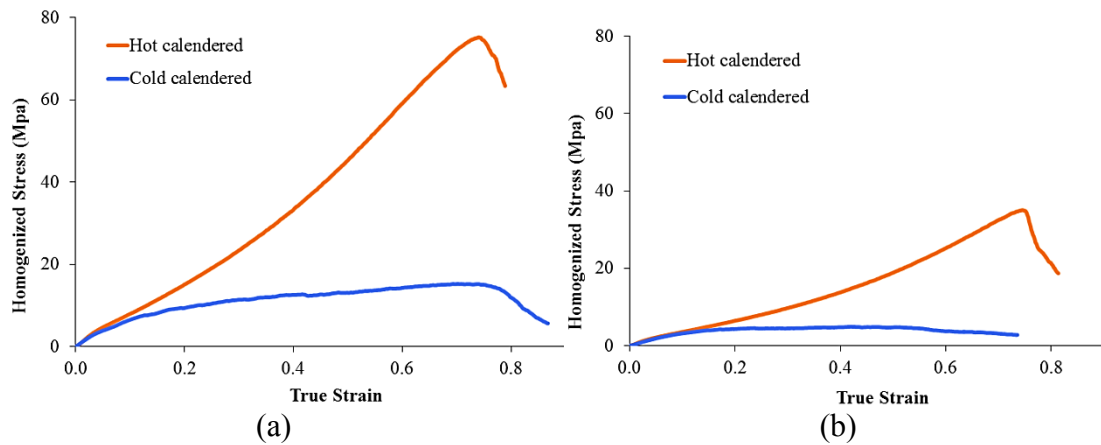


Figure 5.30. Mechanical behaviour of hot and cold calendered nonwoven fabrics in MD (a) and CD (b) (fibre: PA6/PE, planar density: 150 g/m^2 , strain rate: 0.01 s^{-1} , scatter: $\pm 10\%$)

According to Figure 5.30, effect of heat during calendering is very important for bonding of fibres and the resultant mechanical response of the fabric. When fabrics are manufactured with cold calendering, contribution of bond points to the mechanical response of structure decreases significantly. The change in damage behaviour is a result of this decreased contribution. Due to heat generated during hot calendering, the sheath material is melted not only in the bond regions but also in some parts of matrix (Figure 5.15). As described before, this phenomenon increases the material's macroscopic continuity and stiffness of fabric. Figure 5.31 demonstrates how this continuity affects the damage behaviour of nonwoven fabrics.

Apparently, failure of the hot calendered specimen corresponds to premature failure of fibres at the fibre-bond interface, and due to the macroscopic continuity, damage is localised based on stress concentration (Figure 5.31). On the other hand, the cold calendered specimen in Figure 5.31b deforms in an inhomogeneous way as if it has no bond points. Hence, damage is not localised as a result of the stress distributed on individual fibres.

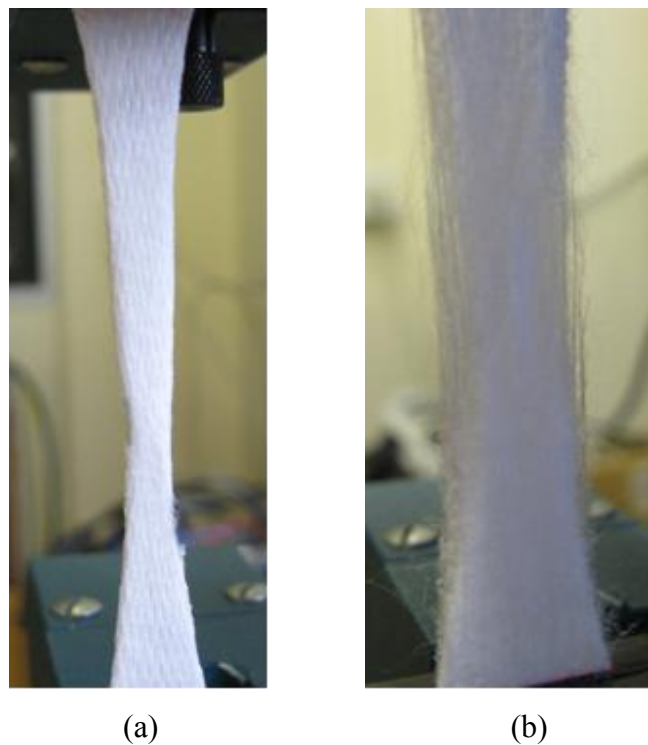


Figure 5.31. Damage behaviour of nonwoven fabrics manufactured with hot calendering (a) and cold calendering (b) (fibre: PA6/PE, planar density: 150 g/m²)

The effect of bonding temperature will be considered in the assessment of the mechanical properties in Chapter 6. In order to do this, the effect of bonding temperature on the mechanical properties of the fabric should be investigated experimentally. For this purpose tensile tests are performed on PP/PE 50 g/m² nonwoven specimens calendered at temperatures of 110°C, 120°C, 130°C and 140°C, the last being the ideal bonding temperature and the experimental results are given in Figure 5.32. Dimensions of the specimens are 30 mm x 15 mm.

According to Figure 5.32, deformation performance of a fabric is correlated to its calendering temperature. Not only flow stress, but also damage behaviour changes with calendering temperature. Ultimate tensile strength decreases dramatically with decreasing calender temperature (140°C is the ideal bonding temperature). Up to a strain level between 0.2 and 0.3 (vertical dashed lines in Figure 5.32), flow stress is directly proportional to the calendering temperature within the studied range. Beyond this strain value proportionality is lost due to gradual damage initiation in samples with lowest bonding temperature, i.e. especially the one calendered at 110°C. Therefore it could be assumed that, as long as damage is not present in the material, there is a correlation between flow curve of a nonwoven and its calendering temperature.

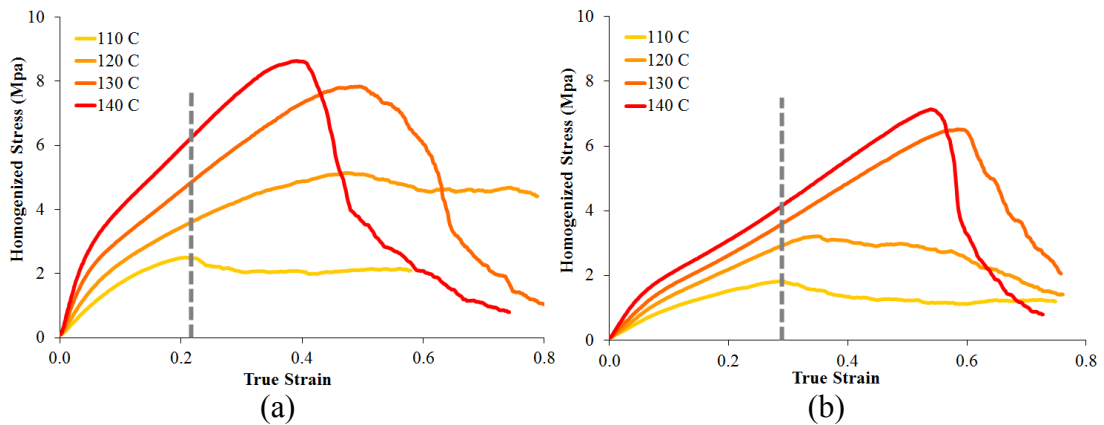


Figure 5.32. Mechanical behaviour of nonwovens manufactured with various calendering temperatures in MD (a) and CD (b) (fibre: PP/PE, planar density: 50 g/m², scatter: ±10%)

For decreasing temperatures below the ideal one, flow curves and elastic moduli of the regions tend to decrease; whereas for higher calender temperatures, flow curves and elastic moduli remain at the levels corresponding to those at the ideal temperature, but fracture strain of the matrix decreases due to premature failure of fibres at the fibre-bond interface (Michielsen *et al.*, 2006). In most cases, thermally bonded nonwovens are calendered at ideal temperature which is approximately 140°C for the fabrics described in Table 5.5. The ideal calender temperature may increase slightly with increasing planar density.

A practical way to determine a correlation between mechanical response of a thermally bonded nonwoven and its calendering temperature is to derive normalized flow stress vs. calendering temperature graph. The normalized flow stress $\bar{\sigma}(T)$ at a specific calendering temperature T could be defined as

$$\bar{\sigma}(T) = \frac{\sigma(T)}{\sigma(T_{\text{ideal}})}, \quad (5.2)$$

where $\sigma(T_{\text{ideal}})$ is the flow stress at ideal calendering temperature T_{ideal} and $\sigma(T)$ is the flow stress at a specific calendering temperature.

A linear relation between the calendering temperature and mechanical response of the material is rebuilt in Figure 5.33. The effect of bonding temperature on the mechanical behaviour of MD and CD differs slightly. This is due to the randomness in the structure. It is assumed that the relationship between calendering temperature and the mechanical behaviour of nonwoven materials is linear (Figure 5.33); this linear empirical correlation will be included into the numerical model used to compute the mechanical properties of nonwoven fabrics in Chapter 6.

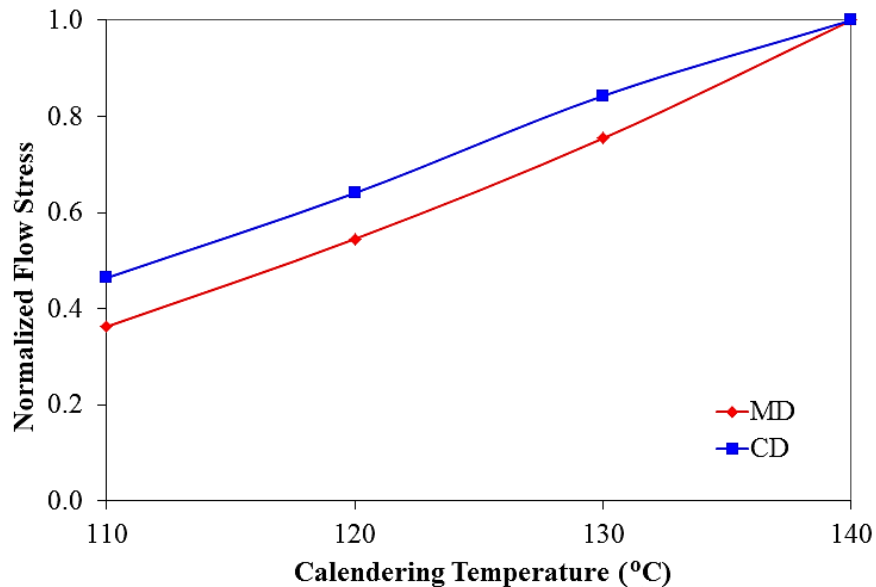


Figure 5.33. Normalized flow stress graph of the flow curves in Figure 5.32 (fibre: PP/PE, planar density: 50 g/m²)

5.5. Conclusions

To sum up, the mechanical behaviour of thermally bonded bicomponent fibre nonwovens is non-trivial and differs from that of conventional structural materials; only a few studies related to a similar behaviour were performed (Makela and Ostlund, 2003; Cox, 1952). The material behaviour could be summarized as anisotropic and nonlinear (elastic-plastic) combined with viscous effects. This type of behaviour is not implemented in the standard FE software packages, e.g. hypoelastic and hyperelastic (isotropic only) material models are used for nonlinear elasticity but they do not support plasticity. Therefore a suitable material model should be implemented in FE environment to reflect the real-life performance of these materials.

According to the experimental results presented in this chapter, it is concluded that thermally bonded nonwoven fabrics have a unique mechanical behaviour. This behaviour is dissimilar to that of composites, polymers, metals and woven textiles, but it is a mixture of them. These fabrics demonstrate mechanical anisotropy like composites, nonlinear elasticity and viscous effects like polymers, and nonlinear large strain plasticity like metals. The most important feature making them unique by means of mechanical performance is that they are composed of two distinct regions (bond points and the fibre matrix) containing randomly oriented fibres. On the other hand, because these fabrics are made of polymer materials their mechanical response depends on the temperature history they are exposed to. Any temperature change during manufacturing process, such as calendaring temperature, affects their mechanical behaviour.

The experimental results obtained in this chapter will be used for the computation of mechanical properties of these fabrics. Anisotropic mechanical properties of fabrics will be assessed based on the mechanical properties of their fibres, which are the sources of characteristic deformation behaviour of fabrics. The next chapter aims to explain the procedure for computing mechanical properties of thermally bonded bicomponent fibre nonwovens based on the deformation characteristics of their fibres, their microstructure and manufacturing parameters.

CHAPTER VI

6. ASSESSMENT OF MECHANICAL PROPERTIES OF THERMALLY BONDED NONWOVENS

A numerical model, which aims to reproduce a real-life deformation behaviour of thermally bonded nonwovens, requires accurate material properties. The structured nonwovens are composed of two regions (bond points and fibre matrix) having distinct mechanical properties. As demonstrated in Section 5.2, the main reason for difference in mechanical properties of bond points and fibre matrix is their microstructures, which are determined by manufacturing parameters. As a consequence of difference in their microstructures, bond points and fibre matrix will be assigned distinct material properties in the numerical model introduced in Chapter 7. Therefore, mechanical properties of these regions should be assessed separately.

This chapter is dedicated to the assessment of mechanical properties of bond points and matrix considering mechanical anisotropy in the microstructure due to randomly oriented fibres. In the first section, mechanical anisotropy of nonwovens will be analysed. An algorithm is developed to compute an orientation distribution of fibres in the material and its anisotropy. Furthermore, the effect of deformation on mechanical anisotropy of nonwoven fabrics is studied. In the second section, assessment of anisotropic viscoelastic-plastic mechanical properties of bond points and a fibre matrix will be explained. A second algorithm based on a single-fibre behaviour and manufacturing parameters of fabric is developed for this assessment.

6.1. Analysis of Anisotropy in Thermally Bonded Nonwoven Fabrics

Mechanical anisotropy is the most prominent feature of nonwoven materials, and it should be included in their numerical models. This phenomenon is related to random orientation of fibres constituting complex microstructures of nonwovens. Nonuniform orientation distribution of fibres in the microstructure leads to a direction-dependent mechanical response, which could be observed in the tensile test results of nonwovens shown in Section 5.3.

A novel approach to study the relation between mechanical anisotropy of thermally bonded nonwovens and their random structure is developed in this section. The procedure to derive this relation starts with obtaining orientation distribution function (ODF) that quantifies randomness in the microstructure. Then, anisotropic parameters are computed based on the ODF of fibres. Determination of these parameters is vital for assessing material properties required for the numerical model. Finally, the effect of deformation on the anisotropic parameters is considered based on several experimental case studies, to check the validity of these parameters for large deformations.

6.1.1. Orientation Distribution Function

As explained in Section 3.1, the character of orientation distribution of fibres is represented by ODF in the literature. The ODF of a nonwoven can be computed using micro-scale images of its fibre matrix employing digital image processing techniques. There are two main methods used in image processing to determine ODF: the Fast Fourier Transform (FFT) (Kim and Pourdeyhimi, 2001) and the Hough Transform (HT) (Xu and Yu, 1997; Ghassemieh *et al*, 2002a). As explained in Section 3.1, HT gives robust and faster results for dense structures.

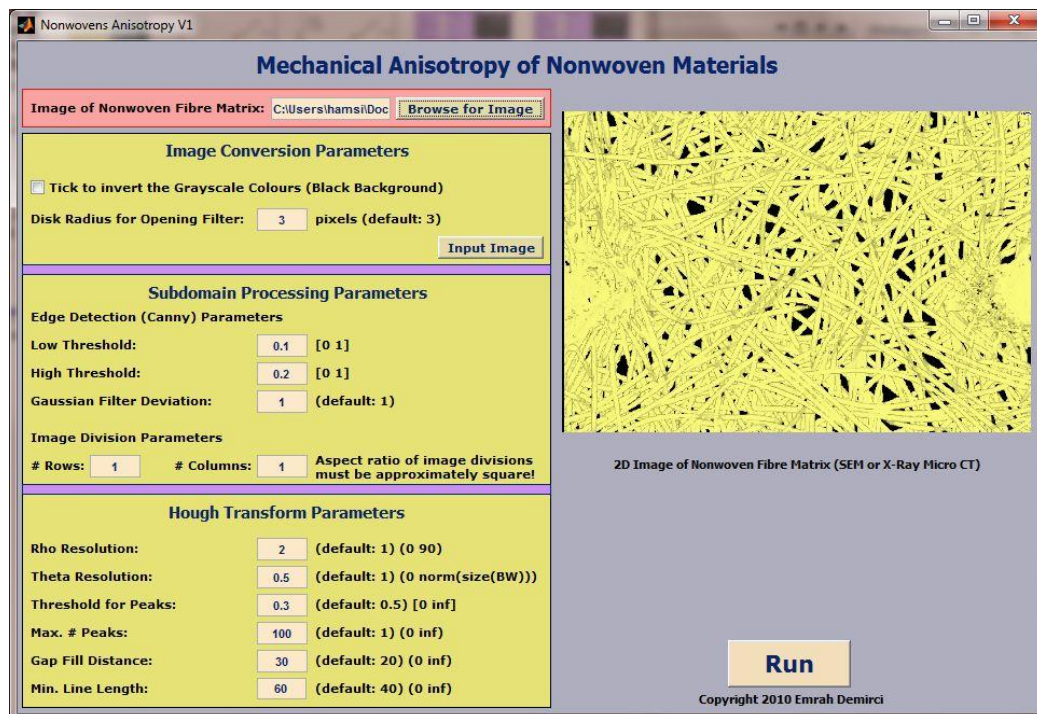


Figure 6.1. GUI of Nonwovens Anisotropy V1 for computing ODF and mechanical anisotropy of fibrous materials

Shorter computation times and robustness with regard to image noise lead to the introduction of a new code based on HT method to analyse the ODF of nonwoven fibrous materials in this study. The new code – Nonwovens Anisotropy V1 – is generated in MATLAB[®] software because of its broad function library for digital image processing. The code has a user-friendly graphical user interface (GUI)

and could be used as a stand-alone application in Microsoft® Windows®-based systems (Figure 6.1).

Nonwovens Anisotropy V1 can compute the ODF of a fibre matrix from its micro-scale image obtained with SEM or X-ray micro CT techniques. The code acquires the image and transforms it into a 3D matrix containing 8 bits of red (R), green (G) and blue (B) colour channels for image processing. Initially, the acquired image in RGB (colour scale) format is converted to a 2D grey scale image and filtered for several noise conditions, such as *salt & pepper* (Gonzalez and Woods, 2002). Then edges of the objects (fibres) in the grey scale image are detected and value 1 is assigned to them; 0 is assigned to the rest of the image by the algorithm. As a result of this process, a 2D image matrix containing binary values is generated for the HT. Finally, pixel coordinates of edge points are converted into a Hough domain in order to calculate the connectivity and continuity of fibre lines. The image processing steps followed for detecting fibres and their orientations in a fibre matrix from its micro-scale image are illustrated as blocks in Figure 6.2.

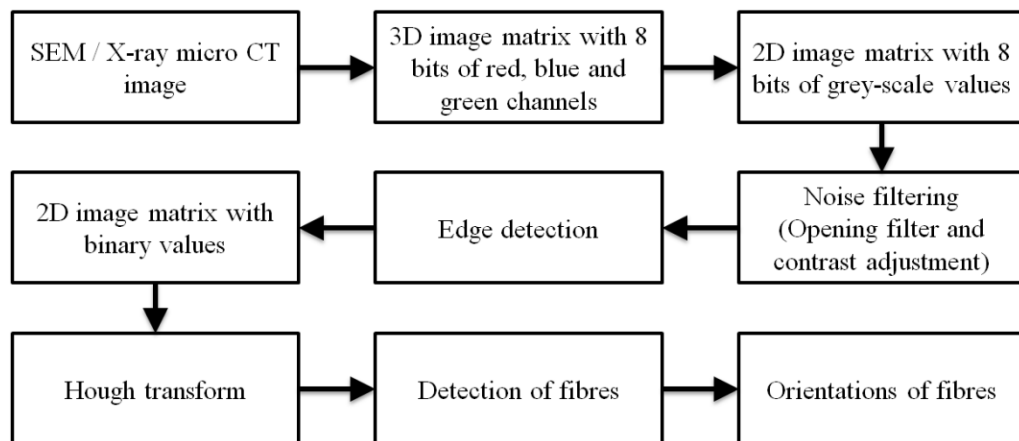


Figure 6.2. Image processing steps followed in Nonwovens Anisotropy V1 algorithm

When a line is detected in the algorithm, a red line is drawn on it to verify its detection (Figure 6.3a). Once the line is detected, its orientation is calculated based on its start and end points. Curvature on the lines is tolerated up to a threshold value, which could be changed depending on the microstructure. This code could detect the

ODF of fibres in any type of fibrous material with distinguishable fibres, e.g. fibrous metal networks, fibre-reinforced composites. MATLAB[®] digital image processing functions used in the algorithm are robust in a way that critical parameters, such as thresholds, are automatically determined by the program and the process is not entirely dependent on the user's specific choices. The parameters in the GUI (Figure 6.1) either define limits for functions or enhance configurability. Following four images with different characteristics are analysed in this section with the same GUI parameters except for image division ones to justify the robustness of the developed software.

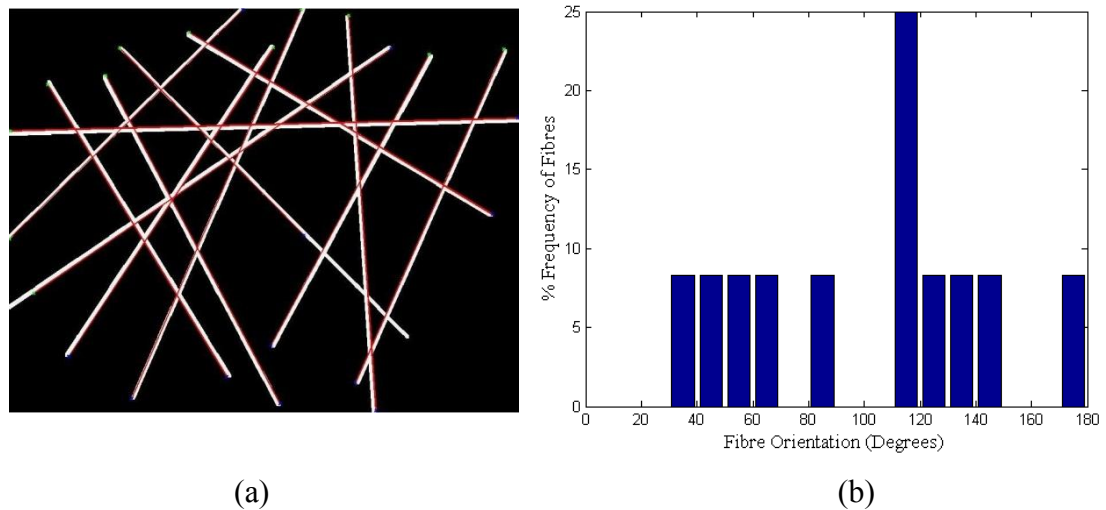


Figure 6.3. Binary image containing randomly oriented twelve lines (a) and their ODF computed with Nonwovens Anisotropy V1 (b)

An image containing twelve artificial white lines with random orientations is used to demonstrate the algorithm (Figure 6.3a). In the image are there red lines drawn on the white ones by the code indicating their detection. In this way, a user can calibrate the digital image processing parameters of the code regarding light and noise conditions, and a size of fibres. The ODF of lines in Figure 6.3a is given in Figure 6.3b in the form of frequency of fibres (%) vs. fibre orientation (degrees) graph. The frequency of fibres for an angle refers to the ratio of number of fibres aligned along the direction with an angle from the respective range to the total amount of fibres: hence the sum of the frequency values in an ODF graph yields

100%. In this study, the angle range $[0^\circ, 180^\circ]$ is used for the axes of abscissas for ODF graphs, with 90° corresponding to the MD of nonwoven fabric. Therefore, vertical and horizontal directions of the image, which will be processed by the code, should coincide with MD and CD of fabric, respectively.

Nonwovens Anisotropy V1 is tested with two fibre matrix images (Figures 6.4a and 6.5a) having distinct ODF characteristics. In the first case, a micro-scale image of a nonwoven's matrix region – Figure 6.4a – containing fibres parallel to MD is processed with the code. According to its ODF graph (Figure 6.4b), the majority of fibres are oriented along angles close to 90° , as can be observed in the image of fibre matrix (Figure 6.4a). In the second case, orientation of fibres in the image (Figure 6.5a) is nearly random. Randomness in the microstructure is reflected in its ODF graph (Figure 6.5b) determined by the code. The character of ODF is confirmed by the micro-scale image shown in Figure 6.5a. Thus, Figures 6.4 and 6.5, showing fibre matrix images and their ODF graphs, demonstrate effectiveness of the developed code.

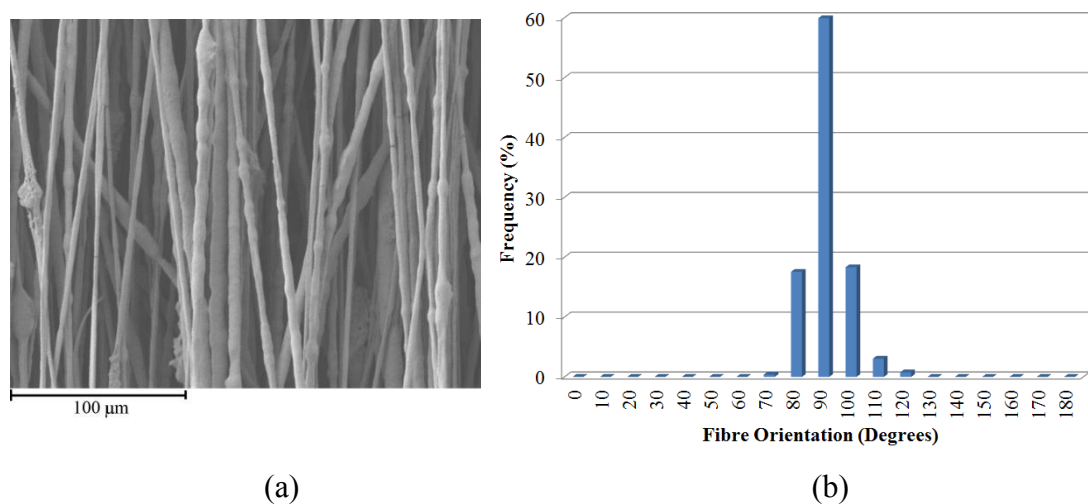


Figure 6.4. SEM image of nonwoven fabric (a) and its ODF computed with Nonwovens Anisotropy V1 (b)

Another feature of the code is subdomain processing, which improves the results by dividing the image into a user-defined number of subdomains for

processing. In this technique, the ODF of each subdomain is computed separately considering its own noise and light conditions. A weighted mean of subdomain ODFs is employed as the resultant ODF of the complete image. This homogenized approach yields a more adequate ODF for the nonwoven fabric, since it considers local deviations in orientation. The most important rule to use this feature is to keep aspect the ratio of image subdomains approximately square. This feature is useful not only for dense materials, but also for several issues originating in imaging conditions, such as local brightness in SEM images or *salt & pepper* noise in X-ray micro CT images.

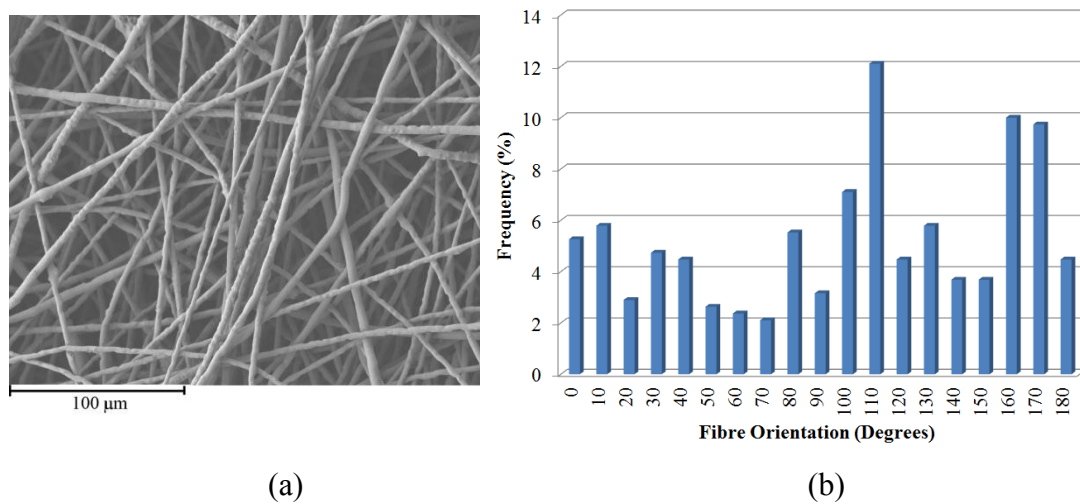


Figure 6.5. SEM image of nonwoven fabric (a) and its ODF computed with Nonwovens Anisotropy V1 (b)

The subdomain processing feature of the code is tested using an X-ray micro CT image of the PP/PE nonwoven fabric having a dense fibrous structure shown in Figure 6.6. It is obvious that fibres in Figure 6.6 are less distinguishable than the ones in Figures 6.4a and 6.5a due to the image scale and high fibre density. In order to increase distinguishability of individual fibres, the image is divided into six sub-images having aspect ratios closed to that of a square. The code generates these sub-images (Figure 6.7) each showing a specific region of the main image (Figure 6.6). Detected fibres in each subdomain are designated with red lines drawn on top of

them (Figure 6.7). Red lines indicating orientations of fibres help a user to optimize the outcome with respect to microstructure and imaging conditions.

An interesting point is that two of the sub-images in Figure 6.7 are brighter than the others because each one is processed based on its own brightness and noise conditions. In other words, pixel values change as a result of histogram equalization applied to the binary form of sub-images for making fibre boundaries more distinguishable. In this case, the light source, which increases brightness of nearby regions, is located at the right bottom corner of the image in Figure 6.6.

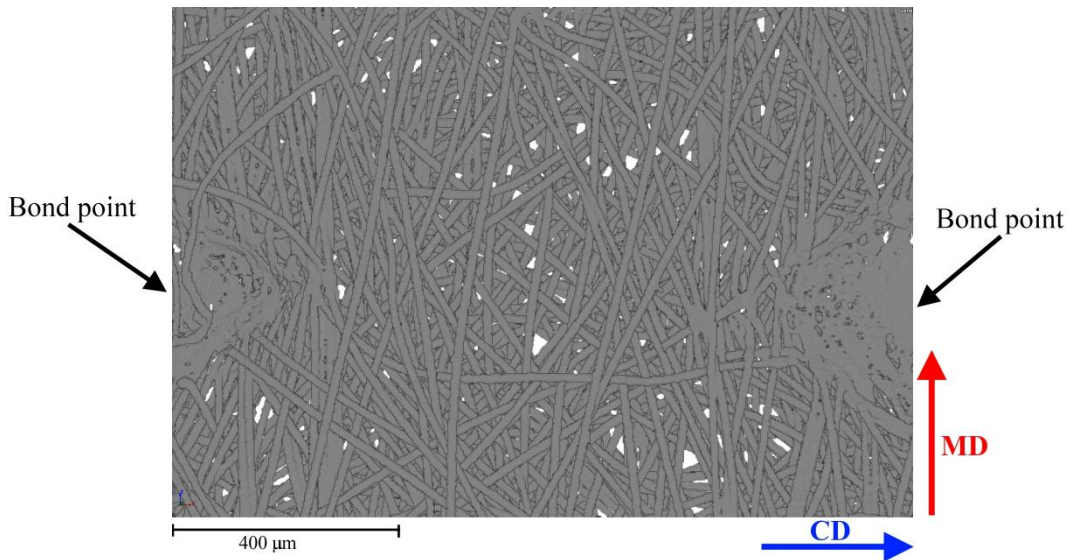


Figure 6.6. X-ray micro CT image of nonwoven fibre matrix region (fibre: PP/PE, planar density: 50 g/m²)

The ODF of each subdomain in Figure 6.7 is computed separately by the code and given in Figure 6.8. It is obvious that ODF characteristics of each region are different, due to randomness in the microstructure. At this point, it should be emphasized that position and size of the input image area of the nonwoven material play an important role in determining a representative ODF. The X-ray micro CT image in Figure 6.6 covers an area between neighbouring bond points along CD and MD that form a periodic bond pattern. Two horizontal boundary bond points along CD, which are excluded from ODF computation due to lack of fibre boundaries,

could be seen partially at the right and left edges of fibre matrix in Figure 6.6. Computation efficiency of the code could be improved by increasing the resolution and sharpness of input image. The fibre-detection possibility increases with increased sharpness and resolution at pixels located on fibre boundary regions. Additionally, the number of image divisions could be increased together with image resolution and sharpness to obtain a more adequate ODF for nonwoven material.

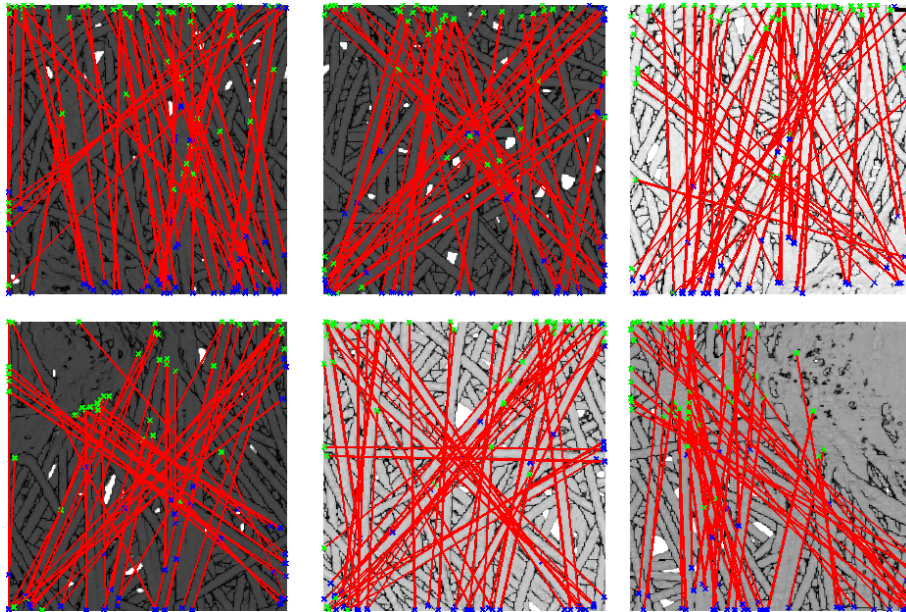


Figure 6.7. Subdomains of fibre matrix image (Figure 6.6) processed with Nonwovens Anisotropy V1

The resultant ODF of the PP/PE nonwoven fibre matrix shown in Figure 6.6, computed based on ODFs obtained for each subdomain (Figure 6.8), is given in Figure 6.9. Based on the number and orientations of fibres computed in each sub-image, a resultant ODF graph for the complete image is generated by the code. This ODF graph reflects the orientation distribution of the overall fibrous network based on particular regions. The resultant ODF computed by the code will be used to characterize the randomness of the fabric's microstructure.

To sum up, a practical user-friendly code for computing the ODF of fibrous materials is introduced in this section. Using the subdomain processing feature with a

larger number of image divisions will improve ODF results. Additionally, increased image resolution and sharpness contribute to fibre detection capability of the code, which improves the computed resultant ODF. This ODF graph will be used to determine anisotropic parameters, which are necessary for assessing anisotropic mechanical properties of nonwoven materials. The derivation of these parameters from the ODF graph will be explained in the next section.

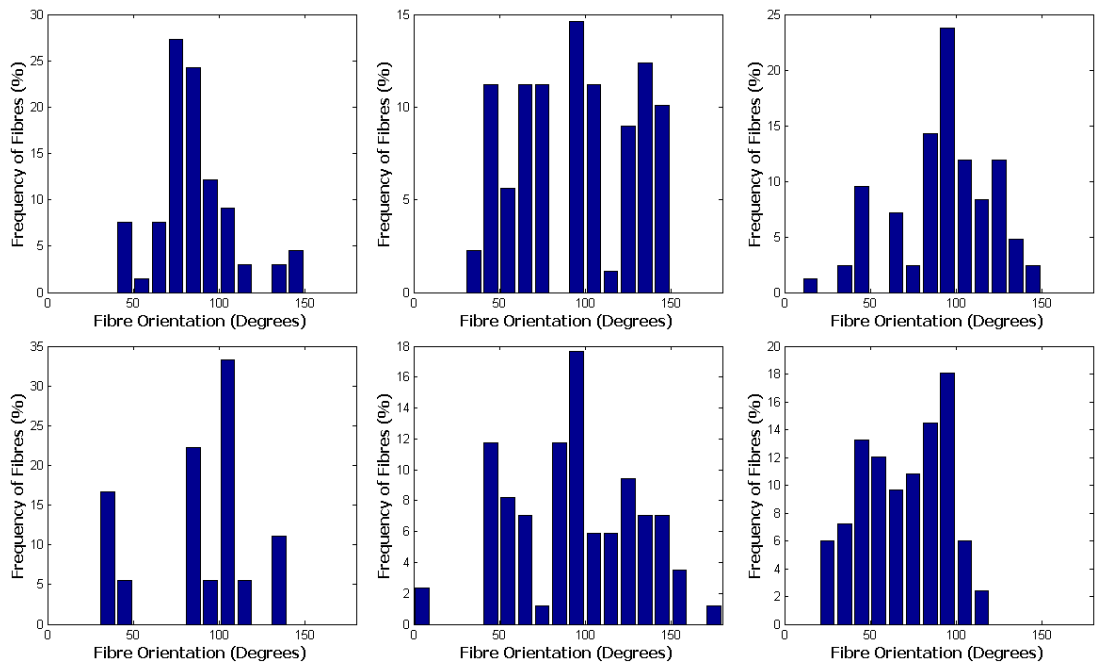


Figure 6.8. ODF of each subdomain in Figure 6.7

6.1.2. Anisotropic Parameters

Anisotropy is an unavoidable phenomenon in nonwovens; therefore it should be taken into account during the computation of their mechanical properties. The level of direction-dependency of the mechanical response is very important for results of simulations. As the number of material symmetry planes decreases, the amount of parameters defining the direction-dependant behaviour increases significantly, hence increasing the complexity of material definition as well as the computation time. Orthogonal anisotropy (orthotropy), having three symmetry planes, can sufficiently define the level of anisotropy for thermally bonded nonwovens. The principal

directions of orthotropy in nonwovens can be assumed as coincident with their principal directions – MD, CD and TD – for definition of their viscoelastic-plastic parameters.

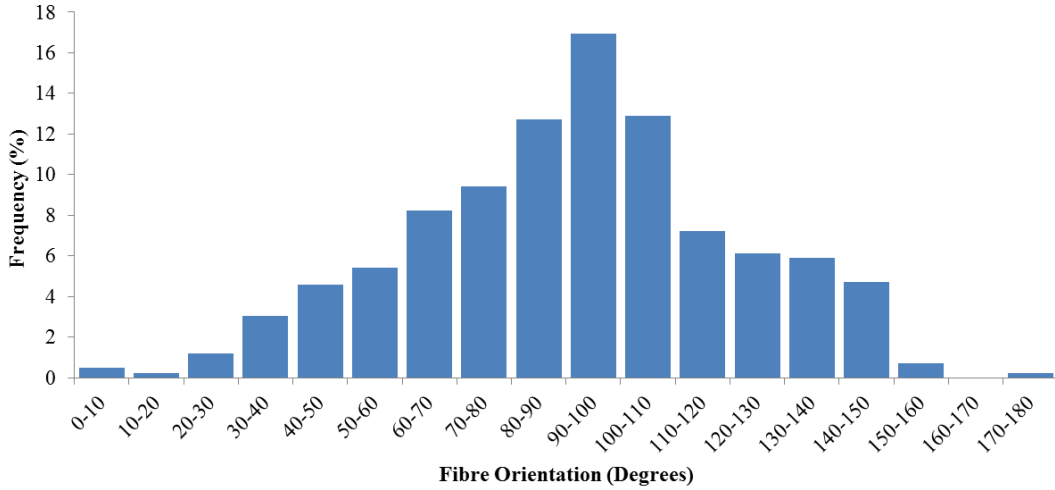


Figure 6.9. Resultant ODF obtained from subdomain ODFs in Figure 6.8

The main source of anisotropy is the nonuniform orientational distribution of fibres causing a direction-dependent response. The nonuniformity can be quantified with the use of the ODF, which will be used to calculate of orthotropic parameters. Due to the nature of orthotropy, these parameters are assumed to be symmetric with respect to MD and CD on fabric plane. The parameters defining the level of orthotropy are calculated from the ODF in Nonwovens Anisotropy V1, according to the following equations;

$$C_{MD} = \frac{\sum_{i=1}^N |\sin \alpha_i|}{\sum_{i=1}^N |\sin \alpha_i| + \sum_{i=1}^N |\cos \alpha_i|}, \quad (6.1)$$

$$C_{CD} = \frac{\sum_{i=1}^N |\cos \alpha_i|}{\sum_{i=1}^N |\sin \alpha_i| + \sum_{i=1}^N |\cos \alpha_i|},$$

where C_{MD} and C_{CD} are the parameters defining the level of orthotropy in MD and CD (obviously, $C_{MD} + C_{CD} = 1$) that are used to calculate the stress-strain curves of the nonwoven material for MD and CD; α_i is the angle between the axis of the i^{th} fibre and CD; N is the total number of fibres accounted by the ODF algorithm.

Orthotropy of a nonwoven material could be determined with two possible approaches: (i) using parameters obtained from the ODF (Equation 6.1) and (ii) using the stress-strain results of tensile tests performed along MD and CD. In order to compare these approaches quantitatively, two orthotropic ratios – experimental (R_E) and theoretical (R_T) – are introduced to define the level of direction-dependent mechanical behaviour on fabric plane. R_E is defined as

$$R_E = \frac{\sigma_{MD}}{\sigma_{CD}}, \quad (6.2)$$

where σ_{MD} and σ_{CD} are the stresses along MD and CD obtained from the tensile test results. On the other hand, to obtain the level of orthotropy from the constants C_{MD} and C_{CD} , which are computed with Nonwovens Anisotropy V1 using the ODF of nonwoven fabric, R_T is introduced as follows

$$R_T = \frac{C_{MD}}{C_{CD}}. \quad (6.3)$$

Values of R_E and R_T of the PP/PE nonwoven fabric shown in Figure 6.6 are compared using the ODF of the fabric given in Figure 6.9. Here, R_T is found using Equation 6.3, which requires C_{MD} and C_{CD} parameters. According to Equation 6.1, C_{MD} and C_{CD} of the PP/PE nonwoven fabric are 0.65 and 0.35, respectively, which in turn yield a R_T value of 1.86. On the other hand, tensile test results of the fabric in Section 5.3 are used to draw the R_E curve using Equation 6.2. According to Figure 6.10, orthotropy of the nonwoven varies with deformation due to reorientation of

fibres. The mean value of R_E curve – $1.77 \pm 22\%$ – is also given in Figure 6.10. For an isotropic material, R_E is always 1 due to an infinite number of symmetry planes causing direction-independent stress-strain curve.

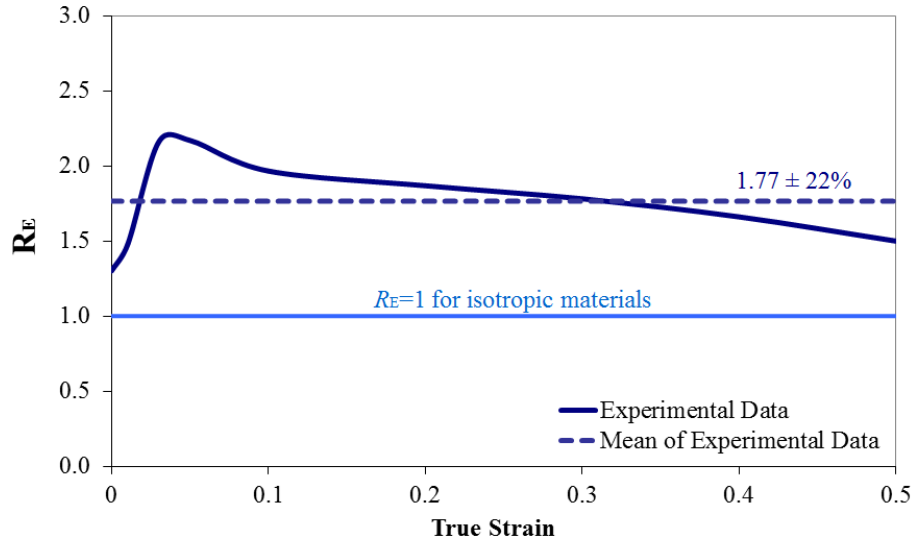


Figure 6.10. Experimental orthotropic ratio of nonwoven fabric (fibre: PP/PE, planar density: 50 g/m^2)

According to Table 6.1, which contains the mean value of R_E curve and R_T for various nonwoven fabrics, their orthotropic ratios calculated from the ODF are close to those determined with tensile test results. Apparently, R_T values are well within the variability range of R_E curves. So according to the results in Table 6.1, accuracy of Nonwovens Anisotropy V1 in predicting the level of mechanical orthotropy using microstructural images of a nonwoven fabric is promising. As a consequence of this agreement, C_{MD} and C_{CD} parameters computed by the code will be used to assess orthotropic mechanical properties of nonwoven fabrics.

To sum up, anisotropy of nonwoven materials is analysed in this section by means of quantification of their random fibrous microstructure. The developed code – Nonwovens Anisotropy V1 – is used to perform this analysis using micro-scale images of fibre matrix obtained with SEM or X-ray micro CT techniques. Randomness in the fabric microstructure is quantified with the ODF, which is

computed with the developed code from the microstructural image of nonwovens. A relation between the ODF and mechanical anisotropy is suggested introducing orthotropic parameters representing a direction-dependent mechanical response of nonwovens. These parameters will be a part of the procedure for computing the orthotropic mechanical properties of thermally bonded nonwoven materials.

| | PP/PE 50 g/m ² | PA6/PE 100 g/m ² | PA6/PE 150 g/m ² |
|-------|---------------------------|-----------------------------|-----------------------------|
| R_E | 1.77±22% | 2.55±12% | 2.30±7% |
| R_T | 1.86 | 2.64 | 2.59 |

Table 6.1. Experimental and theoretical orthotropic ratios of several nonwoven fabrics

6.2. Analysis of Orthotropic Mechanical Properties

Nonwoven materials are composed of two regions – bond points and fibre matrix – having distinct mechanical properties. As explained in Section 5.2, the main reason of this distinction is the difference in their microstructures; with bond points being solid and continuous structures whereas the fibre matrix is porous and compressible. Besides, due to random orientation of fibres, the mechanical behaviour of these regions is anisotropic. Therefore, direction-dependent mechanical properties of these regions should be treated separately.

This section aims to analyse mechanical properties of bond points and fibre matrix using several parameters related to (i) manufacturing processes, (ii) bicomponent fibre performance and (iii) constituent polymer materials. Mechanical properties will be determined based on orthotropic symmetry conditions, which can sufficiently define the level of anisotropy for thermally bonded nonwovens. Orthogonal directions of nonwovens – MD, CD and TD – will be used as principal directions of orthotropy.

Analysis of orthotropic mechanical properties of nonwoven materials is performed with a specially developed algorithm. Similar to the previous one, introduced for anisotropy analysis in the previous section, this algorithm is also written in MATLAB[®] software. Having a GUI shown in Figure 6.11, the code could

be used as a stand-alone application in Microsoft® Windows®-based systems. The code – Nonwovens V4 – was introduced and improved throughout the research period for determining the orthotropic viscoelastic-plastic mechanical properties of bond points and fibre matrix regions of nonwoven materials. In order to submit the analysis results, this code generates two Excel® files; the first one containing all the inputs and outputs of the algorithm including orthotropic viscoelastic-plastic properties of nonwoven regions, and the second one containing specific input data for MSC.Marc® FE software package.

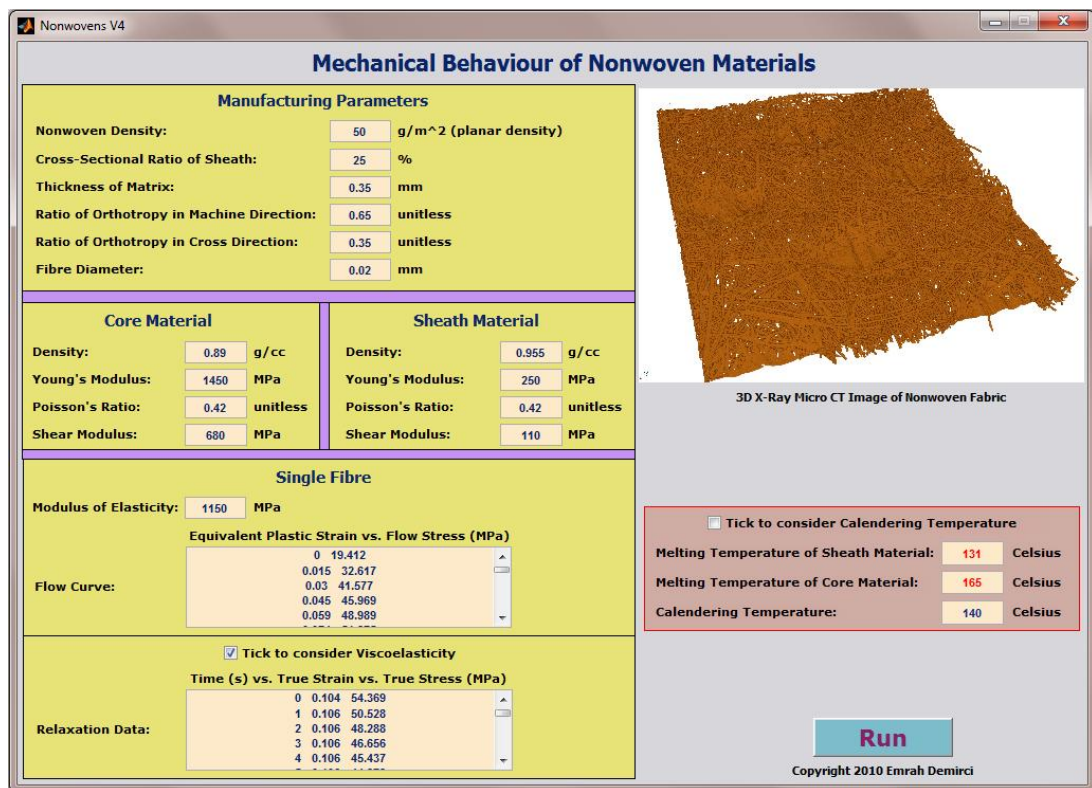


Figure 6.11. GUI of Nonwovens V4 for analysing orthotropic viscoelastic-plastic mechanical properties of thermally bonded bicomponent fibre nonwoven materials

The input parameters required to assess mechanical properties of thermally bonded bicomponent fibre nonwovens using Nonwovens V4 are based on several types of data such as manufacturing parameters, properties of constituent fibres and polymer constituents. Table 6.2 classifies the required input parameters for the GUI of the code regarding to their types. The parameters related to manufacturing are set

during the production stages of nonwovens (Section 2.2), such as C_{MD} and C_{CD} are computed based on the ODF which stems from the web-manipulation stage of manufacturing. Basically, these are the design parameters of a nonwoven fabric according to its application area. On the other hand, the second type of parameters is related to a raw form of the polymer materials used for core and sheath parts of bicomponent fibres. The last type of parameter is based on mechanical behaviour of a single bicomponent fibre, which could be obtained with tensile and relaxation tests explained in Section 5.1.

| Manufacturing Parameters | Properties of Core and Sheath Materials | Properties of Single Fibre |
|------------------------------|---|----------------------------|
| Nonwoven planar density | Density | Young's modulus |
| Sheath cross-sectional ratio | Young's modulus | Flow curve |
| Thickness of fibre matrix | Poisson's ratio | Relaxation curve |
| C_{MD} and C_{CD} | Shear modulus | |
| Fibre diameter | Melting temperature | |
| Calendering temperature | | |

Table 6.2. Input parameters for Nonwovens V4

The parameters listed in Table 6.2 are facilitated in various stages of the Nonwovens V4 algorithm. After acquiring these parameters, the algorithm starts with calculating the number of fibres per 1 mm^2 fabric area using the orthotropic parameters and nonwoven planar density. Since fibres act as trusses, and C_{MD} and C_{CD} represent the mechanical orthotropy on fabric plane, randomly oriented fibres could be represented with truss elements oriented along MD and CD with the ratio induced by orthotropy (Figure 6.12). With this approach, orthotropy in the material is provided by the ratio of the number of truss elements oriented along MD to that along CD. This approximation simplifies the problem with regard to the number of variables required to define the mechanical behaviour and computation time. Based on this approximation, orthotropic mechanical properties of bond points and the fibre matrix are computed with homogenizing the mechanical behaviour of fibre elements

in these regions based on their volumes. Equations, which are mainly developed for composite materials, will be employed for this homogenization due to their structural similarity to thermally bonded nonwoven materials.

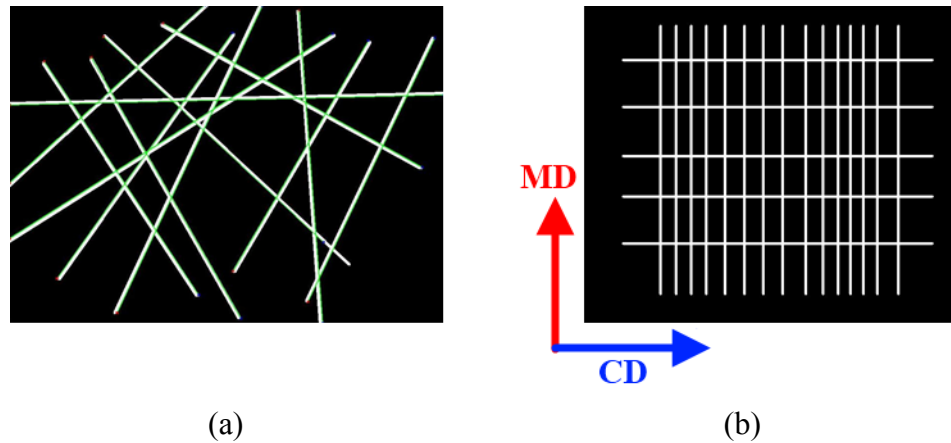


Figure 6.12. Truss elements oriented along principal directions (b) representing orthotropic behaviour of randomly oriented ones (a)

Assessment of mechanical properties of bond points and the fibre matrix is described here for a case study on PP/PE 50 g/m² nonwoven fabric. Input parameters of this fabric for Nonwovens V4 are present on the GUI image in Figure 6.11. Additionally, all the required data for the algorithm including the flow and relaxation curves of bicomponent fibres could be found in Chapter 5. The procedure for analysing mechanical properties of bond points and fibre matrix in the algorithm will be explained for three types of behaviour: elastic, plastic and viscous.

6.2.1. Elastic Properties

Elastic properties of bond points and fibre matrix are handled separately due to difference in their microstructures causing variations in their mechanical behaviour. The algorithm treats the bond points as a composite material and calculates the elastic properties using the Rule of Mixtures (RoM) (Roesler *et al.*, 2007) based on the properties and volume (area) fraction of the core and sheath materials. RoM is not employed in determining the single fibre behaviour due to availability of tensile test results, but mechanical tests of bond points are cumbersome due to their small

dimensions and random microstructure. A theoretical approach, such as RoM, for computing the mechanical properties of bond points could be used. Elastic moduli and Poisson's ratios in MD and CD are calculated based on the RoM (Roesler *et al.*, 2007) as

$$E = E^A V^A + E^B V^B, \quad (6.4)$$

$$\nu = \nu^A V^A + \nu^B V^B, \quad (6.5)$$

where E and ν are the resultant modulus of elasticity and resultant Poisson's ratio; $E^{A,B}$ and $\nu^{A,B}$ are the elastic moduli and Poisson's ratios, and $V^{A,B}$ are volumetric fractions of materials A and B, respectively. For bond points, materials A and B correspond to core and sheath materials. On the other hand, the parameters in TD, which is the transverse direction, are calculated based on Halpin-Tsai equations (Chou, 1992) used for composites as follows:

$$\frac{E_T}{E_B} = \frac{1 + 2\eta V_A}{1 - \eta V_A}, \quad (6.6)$$

$$\eta = \frac{(E_A / E_B) - 1}{(E_A / E_B) + 2},$$

where E_T is the modulus of elasticity in the transverse direction (TD) and V_f is the volumetric fraction of the fibres in a composite material, which in our case correspond to that of the core material of the bicomponent fibres. In-plane shear modulus of bond points G_{LT} is also calculated with Halpin-Tsai equations (Chou, 1992) as

$$\frac{G_{LT}}{E_B} = \frac{1 + \eta V_A}{1 - \eta V_A}, \quad (6.7)$$

$$\eta = \frac{(G_A / G_B) - 1}{(G_A / G_B) + 1}.$$

On the other hand, the matrix region behaves as a membrane having negligible bending stiffness due to low flexural stiffness of individual fibres. Elastic moduli of the matrix in MD and CD are computed with the RoM as in bond points (Equation 6.4), whereas it is considered negligibly small in TD (depending on convergence conditions, it could be assumed zero). The Poisson’s ratio in the fabric’s plane is also computed with RoM according to Equation 6.5, but due to compressible structure of fibre matrix, other Poisson’s ratios are assumed to be equal to zero. Shear moduli of the fibre matrix are derived from its elastic moduli and Poisson’s ratios, accordingly.

| | Bond Point | Fibre Matrix |
|------------------------------------|--------------------------|--------------------------|
| E_{MD} (MPa) | 604.9 | 95.3 |
| E_{CD} (MPa) | 325.7 | 51.3 |
| E_{TD} (MPa) | 892.8 | 0.8 |
| $\nu_{MD,CD}$ | 0.42 | 0.42 |
| $\nu_{CD,TD}$ | 0.42 | 0 |
| $\nu_{TD,MD}$ | 0.42 | 0 |
| $G_{MD,CD}$ (MPa) | 369.4 | 58.2 |
| $G_{CD,TD}$ (MPa) | 198.9 | 31.4 |
| $G_{TD,MD}$ (MPa) | 545.3 | 0.5 |
| Density (Mg/mm³) | 9.0625×10^{-10} | 1.4285×10^{-10} |

Table 6.3. Elastic properties of PP/PE 50 g/m² nonwoven regions analysed with Nonwovens V4

Finally, thickness of bond points is derived using the fabric’s planar density assuming that these regions are nonporous. Homogenized volumetric densities are assessed based on the thicknesses of two regions having the same planar density. The orthotropic elastic mechanical properties of the PP/PE 50 g/m² nonwoven fabric are analysed using its input parameters shown in Figure 6.11. The outcome of the analysis is given in Table 6.3.

6.2.2. Plastic Properties

Plastic properties define the irreversible deformation behaviour when yield stress of the material is exceeded. According to the tensile test results in Section 5.3, a large-strain deformation behaviour of nonwovens is characterized by the direction of applied load. In order to model their anisotropic mechanical behaviour in plasticity, the Hill's anisotropic flow theory is employed in numerical modelling (Hill, 1950). This model requires flow curves (equivalent plastic strain vs. true stress) for principal directions of the material (MSC.Marc[®], 2008r1). The flow curves of bond points and fibre matrix are obtained by normalization of the fibre flow curve using the orthotropic ratios obtained from the ODF as normalization factors. According to the normalization, the flow curve (σ_i) for MD and CD is calculated as follows:

$$\sigma_i = \sigma_f \left(\frac{C_i n A_f}{t} \right), \quad (6.8)$$

where σ_f and A_f are the flow curve and cross-sectional area of the fibre; n is the number of fibres per 1 mm² fabric area; C_i is the orthotropic ratio related to the principal direction of the flow curve denoted by i , and t is thickness of the region.

In the suggested computation algorithm the plastic behaviour of the fibre matrix in TD is implemented employing a flow curve with very small non-zero values. Finally, the flow curve of bond points in TD is assumed proportional to that in MD according to

$$\sigma_{b,TD} = \sigma_{b,MD} \left(\frac{E_{b,TD}}{E_{b,MD}} \right), \quad (6.9)$$

where $\sigma_{b,TD}$ and $\sigma_{b,MD}$ are the flow curves, and $E_{b,TD}$ and $E_{b,MD}$ are the elastic moduli of bond points in TD and MD, respectively. $E_{b,TD}/E_{b,MD}$ represents the ratio of tensile performance in TD to that in MD. Flow curves of bond points and the fibre

matrix of the PP/PE 50 g/m² nonwoven fabric assessed with the developed algorithm, which uses correlations and assumptions given in this section, are shown in Figure 6.13.

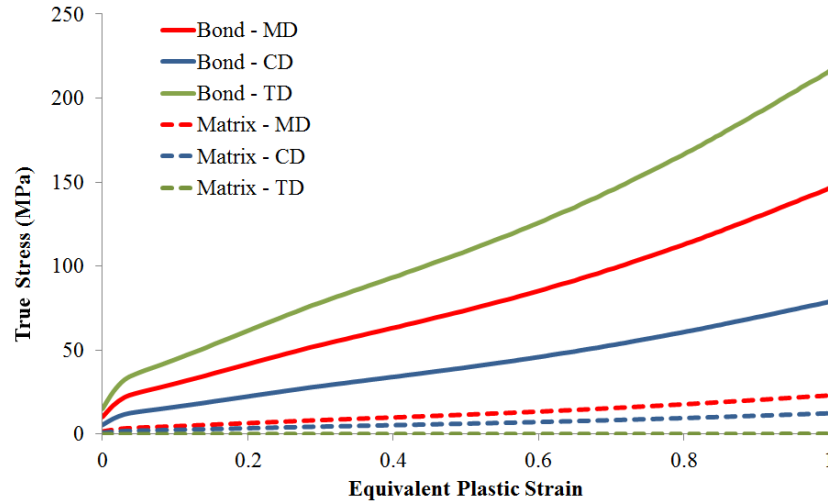


Figure 6.13. Assessment of flow curves of bond points and fibre matrix of PP/PE 50 g/m² nonwoven

Figure 6.13 shows the flow curves of the constituent regions of the PP/PE 50 g/m² nonwoven computed with the algorithm up to the strain level of 1, which is the maximum rupture strain of the material. As explained in Section 5.3, the deformation behaviour of thermally bonded nonwoven fabrics used for this study is mainly governed by plasticity rather than elasticity, so the flow curves generated by the algorithm have a plastic strain range up to 1 in Figure 6.13. Obviously, the plastic behaviour of thermally bonded bicomponent fibre nonwovens may vary according to the type of their core and sheath materials and manufacturing parameters. The developed fully-parametric algorithm accounts for this. Besides, a difference in real-life mechanical performance of bond points and matrix is reflected in the analysed ones according to Figure 6.13. Poor mechanical performance of the fibre matrix in TD is represented with very small non-zero values, which are negligibly small with respect to other curves. These curves can be used to define the plastic deformation behaviour of the regions in any numerical scheme using the Hill's anisotropic flow theory.

6.2.3. Viscous Properties

Viscous properties are necessary to define the time-dependent behaviour of materials. The relaxation test results in Section 5.1 reveal the viscous behaviour of bicomponent fibres, which characterizes the time-dependent mechanical response of thermally bonded nonwovens. This is the reason to analyse viscous properties of bond points and the fibre matrix based on the relaxation behaviour of bicomponent fibres.

Relaxation curve (time *vs.* true strain *vs.* true stress) of a single fibre is required for obtaining the orthotropic viscous properties of bond points and the fibre matrix. Tensile and shear relaxation moduli of the fibre with respect to time ($E_f(t)$ and $G_f(t)$), which represent its time-dependent mechanical behaviour, are defined as (Ward and Sweeney, 2004)

$$E_f(t) = \frac{\sigma_f(t)}{\varepsilon_0}, \quad (6.10)$$

and

$$G_f(t) = \frac{E_f(t)}{2(1+\nu_f)}, \quad (6.11)$$

where ε_0 is the constant strain level in the relaxation test; $\sigma_f(t)$ is the fibre relaxation curve (stress *vs.* time) and ν_f is the Poisson's ratio of the fibre. Similar to elastic and plastic properties defined above, viscous ones are orthotropic as well. In order to define orthotropic viscosity in the numerical model, tensile and shear relaxation moduli and Poisson's ratio during relaxation in MD, CD and TD are required.

Similar to the normalization approach pursued in the previous part for analysing plastic properties, viscous properties of bond points and fibre matrix are obtained by normalization of tensile and shear relaxation moduli of fibre with

normalization factors composed of elastic and shear moduli of regions and the fibre. Equations suggested for the normalization are

$$E_i(t) = E_f(t) \left(\frac{E_i}{E_f} \right), \quad (6.12)$$

and

$$G_i(t) = G_f(t) \left(\frac{G_i}{G_f} \right), \quad (6.13)$$

where $E_i(t)$ and $G_i(t)$ are the tensile and shear relaxation moduli with respect to time; E_i and G_i are the elastic and shear moduli of the region, and E_f and G_f are the elastic and shear moduli of the fibre, respectively, i denoting the principal directions (MD, CD and TD). It is assumed that the ratio of the elastic modulus of a region to that of the fibre is retained for respective relaxation moduli. On the other hand, the Poisson's ratios of the regions are assumed constant and equal to their initial values assessed in the elastic properties. According to Equations 6.12 and 6.13, tensile and shear relaxation moduli curves of bond points and fibre matrix of the PP/PE 50 g/m² nonwoven fabric determined with Nonwovens V4 are given in Figure 6.14.

Since the relaxation behaviour of regions are obtained from that of the fibre using normalization, curves in Figure 6.14 are proportional to the relaxation curve of the fibre. According to their microstructure, which plays an important role in energy dissipation capacity, bond points attenuate more energy per unit volume than the fibre matrix. This phenomenon is reflected in the relaxation moduli results obtained with the algorithm. Viscous effects are analysed up to 60000 s (more than 16 hr), which is sufficient for observing zero relaxation rate which refers to zero slope in the relaxation moduli curves. These curves could be used in any numerical modelling software to define the orthotropic viscous properties of thermally bonded

nonwovens. The viscous behaviour will be implemented as a part of viscoelasticity in the numerical model of thermally bonded nonwovens in the next chapter.

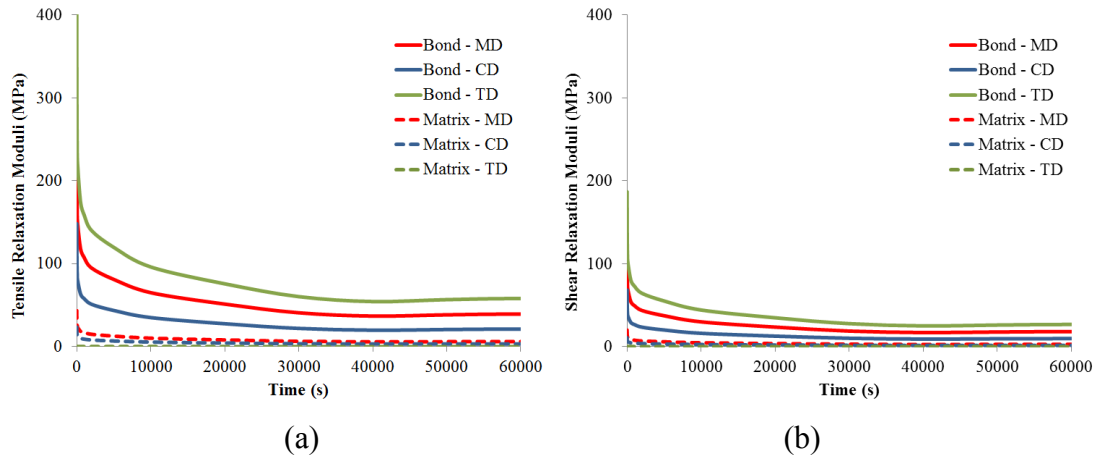


Figure 6.14. Tensile (a) and shear (b) relaxation moduli curves of bond points and fibre matrix of PP/PE 50 g/m² nonwoven

Assessment of viscous properties is the last part for defining the mechanical behaviour of thermally bonded nonwovens composed of bond points and fibre matrix regions. A complete analysis of orthotropic time-dependent mechanical properties of the nonwoven regions is explained in this section. Equations and the assumptions introduced in this section are implemented in the developed. Several assumptions are made in this section to assess particular mechanical properties since mechanical tests of bond points are cumbersome due to their small dimensions and random microstructure. Mechanical properties of bond points and fibre matrix analysed in this section will be used in the numerical models introduced in the next chapter. Accuracy of the analysis discussed here will be assessed based on comparison of results of the numerical simulations with the respective experimental data in the next chapter.

6.3. Conclusions

A practical way to determine the viscoelastic-plastic mechanical properties of thermally bonded nonwoven materials is presented in this chapter. The procedure

starts with analysis of the anisotropy induced by randomly oriented fibres using their ODF. A numerical relation between ODF and mechanical anisotropy of nonwoven material is introduced and verified experimentally. A code – Nonwovens Anisotropy V1 – based on the Hough transform technique is developed in MATLAB[®] to analyse the orientation distribution of fibres and the mechanical anisotropy of the fabric. Another code – Nonwovens V4 – is introduced to assess the orthotropic elastic, plastic and viscous mechanical properties of bond points and fibre matrix using the manufacturing parameters of the nonwoven fabric and the mechanical properties of a constituting single fibre. In order to calculate these properties, this code uses several schemes, such as Halpin-Tsai and RoM, developed for composite materials which are partially similar to thermally bonded nonwoven materials. Two codes introduced in this chapter may serve industry and research as useful tools for product development and optimization as well as numerical modelling. They are based on experimentally-acquired input parameters, and their GUIs do not require a deep knowledge of computational mechanics. The developed algorithms are fully parametric and independent of the bond pattern and shape. In the next chapter, results of these codes will be used to generate a parametric FE model of thermally bonded nonwoven materials in order to predict their deformation performance.

CHAPTER VII

7. FINITE ELEMENT SIMULATIONS OF THERMALLY BONDED BICOMPONENT FIBRE NONWOVENS

Numerical simulations of microstructured materials are necessary for predicting their behaviour during service since analytical solutions for them are hardly possible. The main goal of simulations is to eliminate/reduce the trial-and-error stage of product design and development. As Section 4.5 explains, very few studies could be found in the literature concerning numerical modelling of nonwovens and these studies offer only partial 2D solutions for prediction of a complex mechanical response of nonwovens to loading. Therefore, generating a realistic 3D numerical model will be a novel contribution to the design and manufacturing of nonwoven materials.

Finite element (FE) modelling is the most suitable computational tool to simulate the deformational behaviour of nonwovens under service loadings. Having distinct anisotropic mechanical properties for two regions analysed in the previous stage of this study, the fabric will be modelled in the FE software – MSC.Marc[®] – using 3D shell elements with thicknesses identical to those of the bond points and fibre matrix. Unlike the existing numerical models in the literature (Section 4.5), this model will be in 3D and capable of simulating a buckling phenomenon.

This chapter aims to explain the last stage of the research methodology linked to introducing the FE model for simulation of thermally bonded bicomponent fibre nonwovens. In this chapter, FE simulations of the deformation behaviour of such nonwovens will be described using four sample models for various fabrics and loading conditions. Each model will simulate a different case, which will be carried out experimentally as well. Initially, the modelling strategy for four cases will be explained. Then microstructure and manufacturing parameters of the nonwoven fabric in each case will be provided. Additionally, anisotropic viscoelastic-plastic mechanical properties of the fabric regions computed with the algorithms, which are introduced in Chapter 6, will be given. Boundary conditions applied in each FE model will be explained as well. Finally, results of the FE simulations and respective experiments will be compared accordingly to evaluate efficiency of the proposed numerical modelling approach.

7.1. Models

A numerical modelling strategy for thermally bonded nonwoven materials is illustrated using four case studies in this chapter. Each case represents a different scenario in terms of either loading condition or the type of fabric used. Four cases are simulated with four corresponding FE models to reproduce the behaviour of nonwovens in the numerical environment. Types of fabrics and loading conditions utilized in these cases and notation for their corresponding simulation models are illustrated in Table 7.1.

| | Fabric Type | Loading Condition | Experimental Case |
|----------------|-----------------------------------|--------------------------|---|
| Model A | 50 g/m ² PP/PE 75/25 | Quasi-static | Tensile testing (0.01 s ⁻¹) |
| Model B | 150 g/m ² PA6/PE 75/25 | Quasi-static | Tensile testing (0.01 s ⁻¹) |
| Model C | 35 g/m ² PP/PE 50/50 | Quasi-static | Tensile testing (0.01 s ⁻¹) |
| Model D | 50 g/m ² PP/PE 75/25 | Dynamic | Drop-weight testing |

Table 7.1. Distinctive features of four models developed in this research

The proposed numerical modelling approach in this research is implemented with the four models (Models A, B, C and D) shown in Table 7.1. Validity of the modelling strategy is tested via comparing the FE simulation results of these models with the corresponding experiments. Multi-variable and significant changes are performed between each model to justify the efficiency of the modelling approach with reasonable number of models. FE models are generated in the MSC.Marc[®] commercial FE software package due to its broad material behaviour library and large-strain simulation capability with orthotropic yield criterion, which are crucial for this study. Each model is built to incorporate two regions – bond points and fibre matrix – having distinct mechanical properties assessed with the algorithms introduced in Chapter 6.

Proper implementation of orthotropic viscoelastic-plastic mechanical properties of the fabric regions in the FE software requires a suitable element type which can handle their complex deformation behaviour. The element type preferred in the FE software is Element 139 which is sketched in Figure 7.1. This is a four-node, thin-shell element with global displacements and rotations as degrees of freedom. Bilinear interpolation is used for the coordinates, displacements and the rotations. The membrane strains are obtained from the displacement field, the curvatures from the rotation field. The element can be used in analysis of curved shell as well as of complicated plate structures. Due to its simple formulation – when compared to standard higher-order shell elements – it is computationally less expensive and, therefore, very attractive in nonlinear analysis. Besides, the element is not very sensitive to distortion, and an updated Lagrange formulation enables this element

type to simulate large-strain plasticity, which is observed in nonwovens. All constitutive relations can be used with this element including viscoelasticity. Due to these critical capabilities, Element 139 seems an appropriate shell element for building FE models of nonwovens studied in this research.

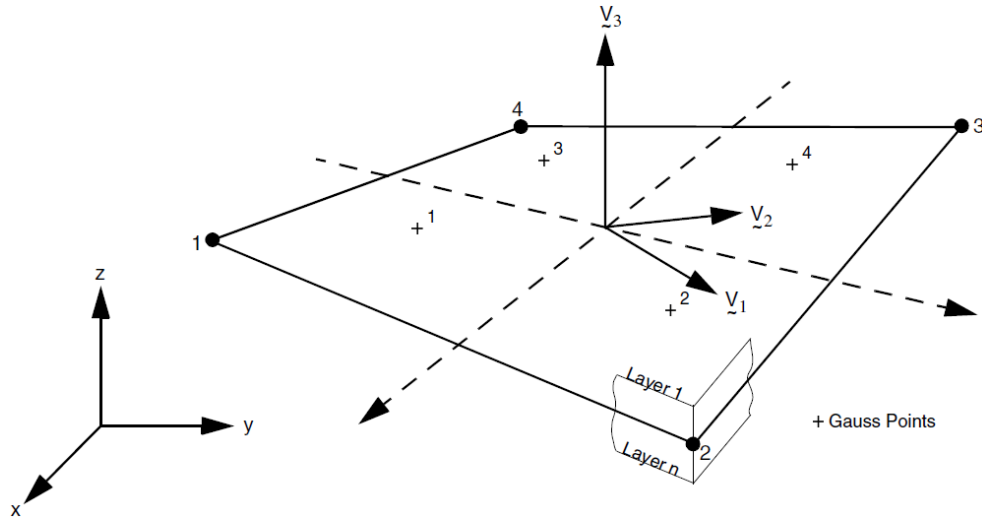


Figure 7.1. Form of shell element used in FE modelling of nonwovens
(MSC.Marc[®], 2008r1)

Four FE models are built in MSC.Marc[®] software using four-node shell elements (Element 139) to represent mechanical performance of bond points and fibre matrix regions constituting the nonwoven sample. Depending on the bond pattern and size of the specimen, mesh structure of the FE models vary slightly. Detailed information about mesh structure and dimensions of the four FE models is given below to illustrate differences in their structure.

7.1.1. Models A and B

Models A and B simulate tensile testing of 50 g/m² PP/PE 75/25 and 150 g/m² PA6/PE 75/25 nonwoven fabrics, respectively. These FE models aim to reproduce effects of variations in the fabric planar density and bicomponent fibre type on the mechanical performance of thermally bonded nonwovens in the numerical scheme. Simulating simple tensions tests is the most convenient way to observe these effects

with the proposed FE models. In order to simulate real-life behaviour of thermally bonded bicomponent fibre nonwovens, their FE models are built accounting for two distinct regions (Figure 7.2) – bond points and fibre matrix – since they exhibit distinct deformation characteristics. Models A and B are introduced together because they have identical bond patterns formed during hot calendering stage. Dimensions of the periodic diamond-shape bond pattern in the FE models are identical to those in the fabric samples used in experiments (Figure 7.2). FE meshes in Models A and B are generated using the geometry of the bond pattern, obtained from the SEM image of the fabric shown in Figure 7.3a. Meshing the fibre matrix region takes place after that of the bond pattern. Assigning mechanical properties and thickness values of the two regions becomes more practical with meshing them separately. As a result of this meshing approach, geometry and pattern of the bond points and those of their representative numerical elements are identical (see Figures 7.2 and 7.3).

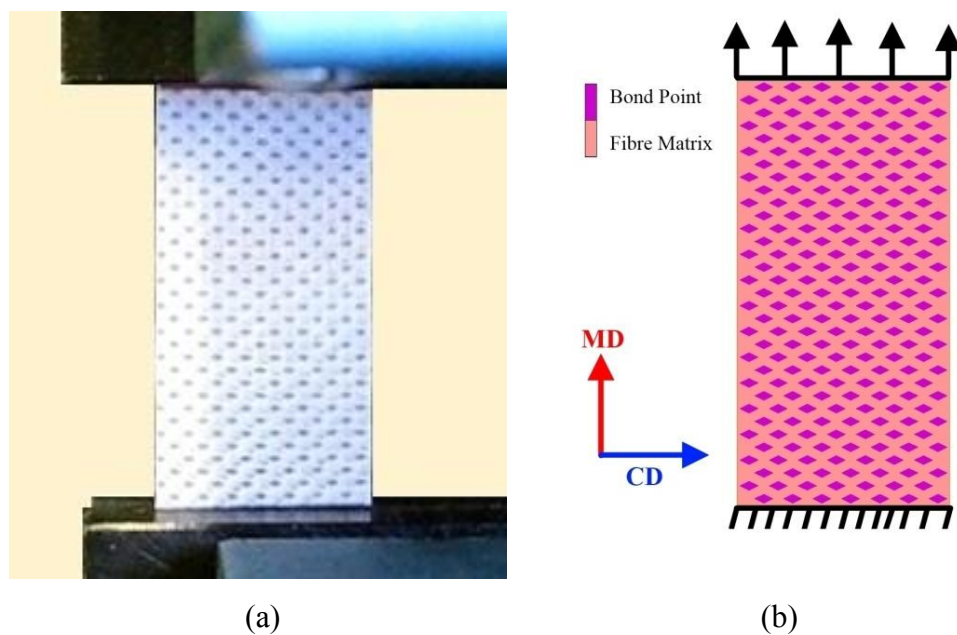


Figure 7.2. Nonwoven tensile test sample (a) and corresponding FE model (Models A and B) (b)

Nonwoven specimens with dimensions 30 mm x 15 mm are simulated with Models A and B having identical bond pattern shown in Figure 7.2. Since these models simulate tensile tests in MD and CD, orientation of bond pattern with regard

to the principal directions of the fabric is arranged depending on the direction of applied extension in the tests. Regions of bond points and the fibre matrix in Models A and B are composed of the four-node shell elements (Element 139), which mesh the bond pattern geometry accurately (Figure 7.3). Each model consists of 15000 shell elements (16 elements per bond point) having three integration points through thickness. The FE mesh structure of Models A and B is shown in Figure 7.3, which is the magnified version of the complete fabric model in Figure 7.2. An average element's edge length in both regions is 0.188 mm. Thickness parameters of shell elements modelling the bond point and the fibre matrix regions match the real thickness values of these regions measured from X-ray micro CT images. These parameters for the regions will be provided in the next section; they are defined by the manufacturing process.

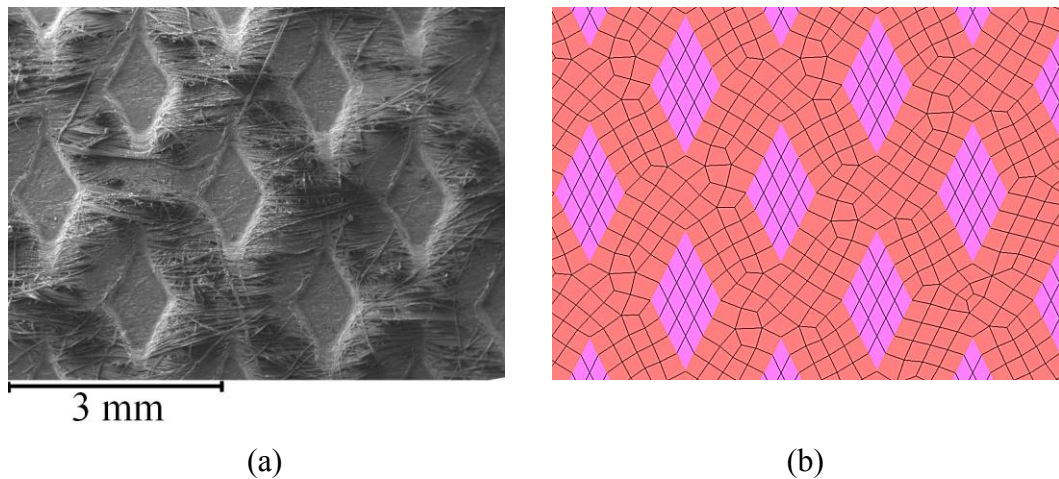


Figure 7.3. SEM image of thermally bonded bicomponent fibre nonwoven (a) and corresponding FE model (Models A and B) (b)

7.1.2. Model C

Model C is developed to simulate deformation behaviour of a 35 g/m² PP/PE 50/50 thermally bonded nonwoven fabric under simple tension tests in MD and CD. This fabric and its bicomponent fibres are different from those introduced in Chapter 5. Unlike the bicomponent fibres introduced in Section 5.1, cross-sectional core/sheath ratio of the fibres of this fabric is 50/50. Besides, the nonwoven web is calendered

out with a rectangular periodic bond pattern. On the other hand, although this research deals with thermally bonded nonwovens with planar fabric densities more than 50 g/m^2 , behaviour of the fabric with 35 g/m^2 planar density is simulated to expand the limits of the proposed numerical modelling approach in this study. Efficiency of continuous elements (shell elements) in modelling the fibre matrix region depends on homogeneity of fibre distribution in this region. Below 50 g/m^2 , it starts to deteriorate with decreasing planar density. Modelling the fibre matrix region of low-density nonwovens with discontinuous elements (truss elements) gives more accurate results (Hou *et al.*, 2009). As a result of this fact, Model C is introduced to examine the limits of the proposed FE modelling approach in terms of planar web density, which affects homogeneity of the fibrous microstructure.

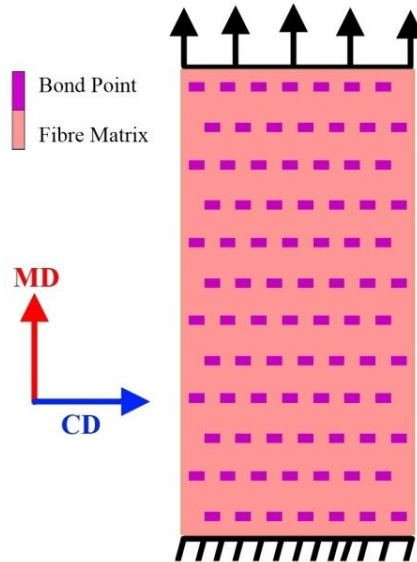


Figure 7.4. FE model of nonwoven tensile test sample (Model C)

Nonwoven specimens with the same dimensions – $30 \text{ mm} \times 15 \text{ mm}$ – are simulated with Model C having the rectangular bond pattern shown in Figure 7.4. The principal axes of the fabric model in Figure 7.4 could be figured out from the orientation of the bond points and pattern. Model C consists of 2926 four-node thin-shell elements (4 elements per bond point) having three integration points through thickness (Figure 7.5). Similar to Models A and B, FE mesh is based on the bond-

pattern geometry obtained from the SEM image of the nonwoven material shown in Figure 7.5. An average element's edge length for the complete model is 0.5 mm. Thicknesses of the fabric regions and that of their corresponding elements are identical; their magnitudes will be provided in the next section.

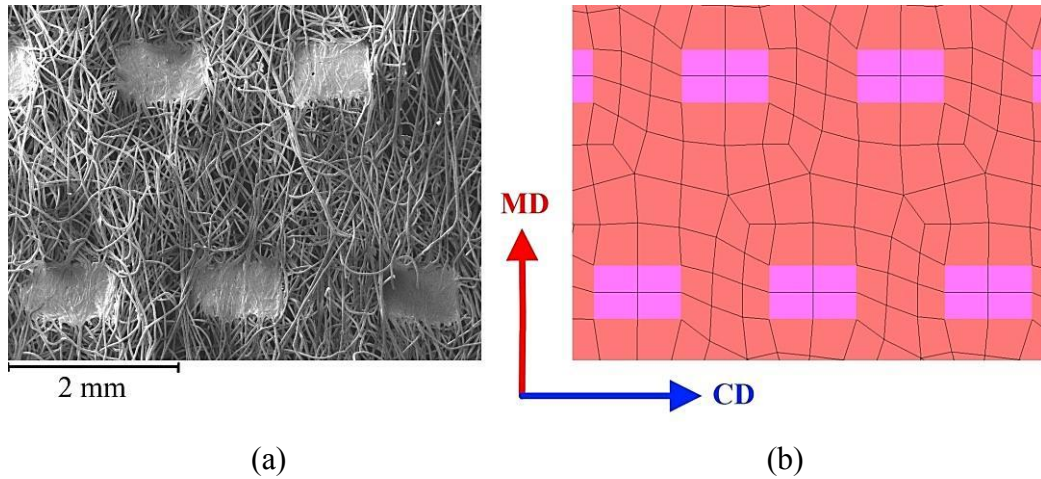


Figure 7.5. SEM image of 35 g/m² PP/PE 50/50 thermally bonded nonwoven (a) and corresponding FE model (Model C) (b)

7.1.3. Model D

Model D simulates dynamical behaviour of 50 g/m² PP/PE 75/25 thermally bonded nonwoven in drop-weight testing. Although a mechanical response of this fabric to 2D loading conditions on the fabric plane is simulated with Model A, a more challenging model with out-of-plane loading conditions is necessary to highlight 3D simulation capability of the modelling approach proposed in this research. In addition to handling 3D loading conditions, Model D reproduces energy dissipation characteristics of the nonwoven material explicitly. In order to build such a model and to verify it experimentally, a free-falling metal sphere, bouncing on the nonwoven material, is simulated.

The metal sphere is released to fall free onto the fabric, and it consecutively bounces back several times with a gradually decreasing bouncing height after each impact due to energy-dissipation mechanisms related to viscoelasticity in the

nonwoven material. Model D can replicate dissipation of elastic energy in each spring back cycle, which causes a gradual decrease of bouncing heights in the real-life experiment. On the other hand, as a result of out-plane-loading due to impact of the sphere normal to the fabric plane, the material is exposed to complex loading conditions including time-dependent variable contact. Obviously, Model D is more advanced than Models A, B and C, simulating unidirectional loading of nonwoven samples in tensile tests. With these complex 3D loading conditions, Model D aims to completely reveal the capabilities of the developed numerical modelling approach.

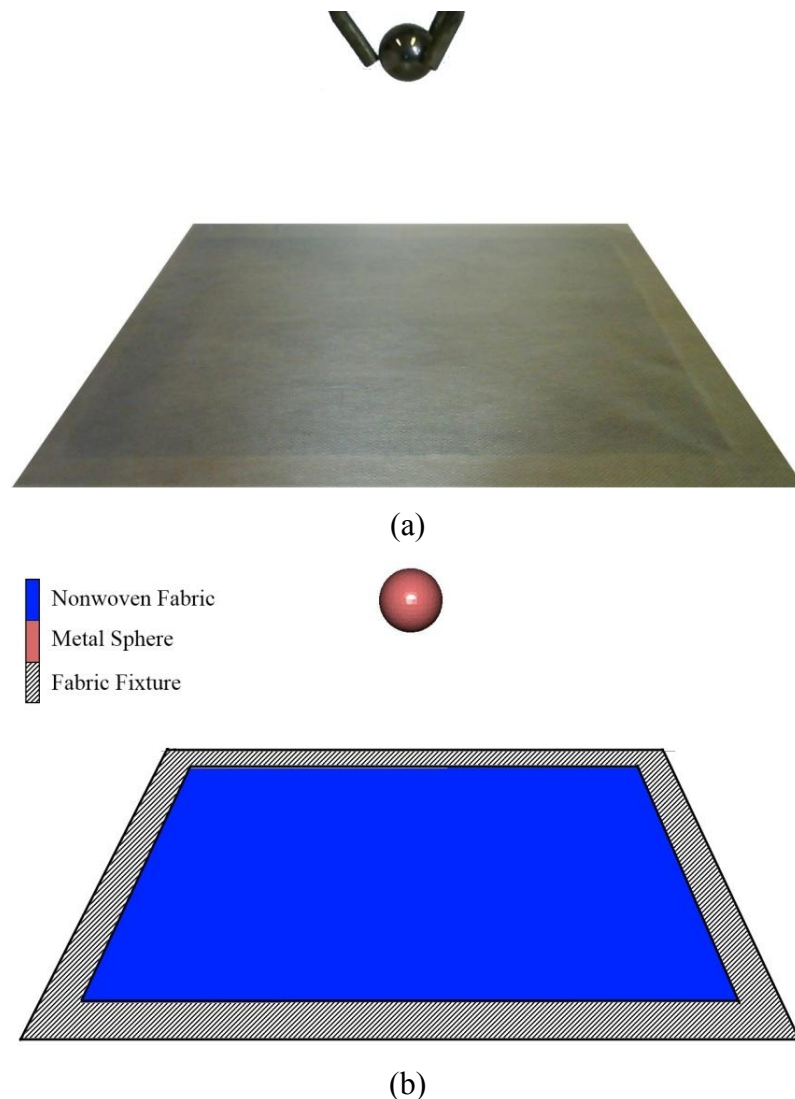


Figure 7.6. Test setup of Model D (a) and corresponding FE model (b)

A metal sphere with a mass of 43.4 g and a diameter of 22 mm is positioned 100 mm above the nonwoven material with dimensions 200 mm x 200 mm (Figure 7.6). Except for the average element edge length, Model D is generated using the same FE modelling strategy practiced for Model A, e.g. the type of shell elements, bond geometry and pattern, since both models simulate the same nonwoven material. Due to a large size of the nonwoven material in Model D, the average element's edge length for the complete model is increased to 0.75 mm (1 element per bond point) in order to decrease the computational power required for simulation, since the average element's length of 0.188 mm corresponds to 1,300,000 elements for Model D. As a result of this modification, the total number elements in the model decreases to 88500. The metal sphere is modelled as a rigid body with weight, since its stiffness is much higher than that of the studied nonwoven material. Finally, a contact condition between the metal sphere and the nonwoven is provided with "Touching" option of the FE software, which guarantees separation of bodies in the absence of combining forces when the sphere bounces upwards. Decreasing computation time for Model D is crucial since the model incorporates three types of nonlinearity (material, contact and geometric) with a highly complicated material behaviour including anisotropy and viscosity. This is the main reason to use a bond-point-size shell element and modelling the sphere as a rigid body.

Model D provides a broad view of capabilities of the proposed FE modelling approach to simulate complex mechanical behaviours of thermally bonded nonwoven materials whereas Models A, B and C concentrate on the mechanical response of nonwoven fabrics manufactured with various fibre types, bond shapes, patterns and planar densities. Each model has a specific aim for reproducing the effects of these particular manufacturing parameters in the numerical scheme. The next section provides manufacturing parameters of the fabrics simulated with the developed models.

7.2. Microstructure and Manufacturing Parameters

The FE models presented in the previous section requires assignment of mechanical properties for regions of bond points and the fibre matrix to the elements modelling them. These mechanical properties can be assessed from the manufacturing parameters and microstructure of the nonwoven with the algorithms developed in Chapter 6. This section provides necessary input data for the assessment of orthotropic viscoelastic-plastic mechanical properties for two modelled regions with the introduced algorithms. Initially, mechanical anisotropy in the material should be determined with the Mechanical Anisotropy V1 algorithm, which requires either SEM or X-ray micro CT image of the fibre matrix region. Secondly, orthotropic viscoelastic-plastic mechanical properties of the bond points and the fibre matrix regions are analysed with the Nonwovens V4 algorithm. The latter requires several parameters related to manufacturing parameters of the nonwoven fabric and mechanical properties of its bicomponent fibres and core/sheath materials. These input parameters and SEM images of fibre matrix regions required for assessing mechanical properties of the nonwoven regions for each model are given below.

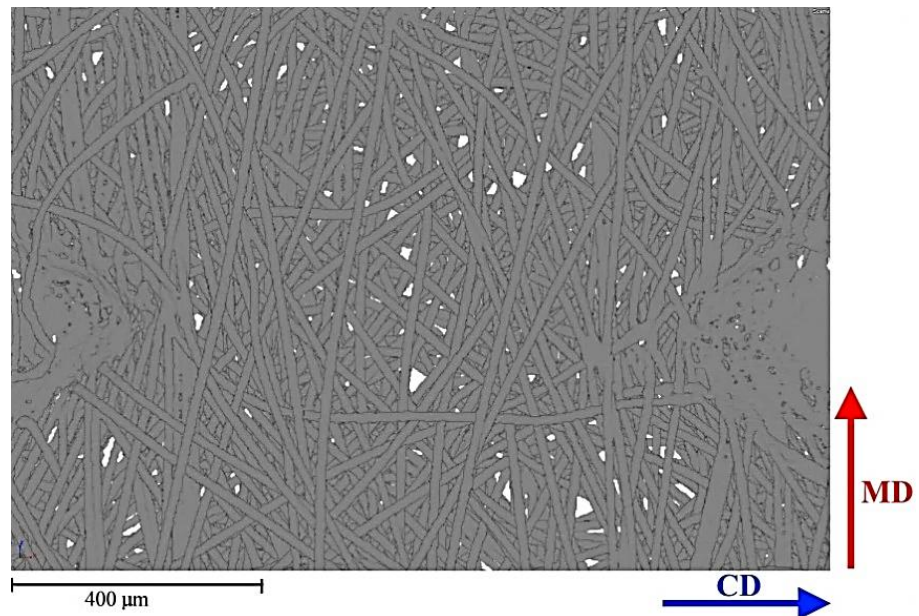


Figure 7.7. X-ray micro CT image of fibre matrix region of 50 g/m² PP/PE 75/25 thermally bonded nonwoven simulated with Models A and D

7.2.1. Models A and D

Models A and D simulate the mechanical behaviour of 50 g/m² PP/PE 75/25 thermally bonded nonwoven material. The material is calendered out with a diamond-shape periodic bond pattern shown in Figure 7.3. Assessment of mechanical properties of the nonwoven regions starts with analysing anisotropic parameters (C_{MD} and C_{CD}) using the Nonwovens Anisotropy V1 algorithm. An X-ray micro CT image of the fibre matrix region of 50 g/m² PP/PE 75/25 thermally bonded nonwoven, which could be used for the analysis, is provided in Figure 7.7.

Assessment of mechanical properties of regions of bond points and the fibre matrix can be carried out after obtaining anisotropic parameters with the image analysis. The manufacturing parameters of 50 g/m² PP/PE 75/25 thermally bonded nonwoven, which are processed by the algorithm, are given in Table 7.2.

| Manufacturing Parameters | Models A and D |
|---|-----------------------|
| Nonwoven Planar Density (g/m ²) | 50 |
| Cross-Sectional Ratio of Sheath (%) | 25 |
| Thickness of Fibre Matrix (mm) | 0.35 |
| C_{MD} and C_{CD} | 0.65 and 0.35 |
| Fibre Diameter (mm) | 0.02 |
| Calendering Temperature (°C) | 140 |

Table 7.2. Manufacturing parameters of 50 g/m² PP/PE 75/25 thermally bonded nonwoven simulated with Models A and D

In addition to manufacturing parameters, several mechanical and physical properties of the polymer materials, which are used in core and sheath parts of bicomponent fibres, are necessary for the analysis with the algorithm. These properties could be obtained from the manufacturer’s datasheet for the raw forms of the polymers which are used as supply materials for nonwoven manufacturing. Table 7.3 provides the properties of core and sheath polymers used in the manufacturing of the nonwoven fabric simulated with Models A and D.

| | Core | Sheath |
|-----------------------------------|------|--------|
| Material | PP | PE |
| Density (g/cm³) | 0.89 | 0.955 |
| Young's Modulus (MPa) | 1450 | 250 |
| Poisson's Ratio (mm) | 0.42 | 0.42 |
| Shear Modulus (MPa) | 680 | 110 |
| Melting Temperature (°C) | 165 | 131 |

Table 7.3. Properties of core and sheath materials for manufacturing 50 g/m² PP/PE 75/25 thermally bonded nonwoven simulated with Models A and D

The last input data for the analysis of mechanical properties of nonwoven regions is the mechanical behaviour of PP/PE 75/25 fibres obtained with simple tension and relaxation tests (Figure 7.8). Flow (equivalent plastic strain vs. true stress) and relaxation (time vs. true strain vs. true stress) curves defining the time-dependent mechanical performance of bicomponent fibres that constitute the nonwoven material should be present to finalize the complete set of data used for assessing orthotropic viscoelastic-plastic mechanical properties of two modelled regions.

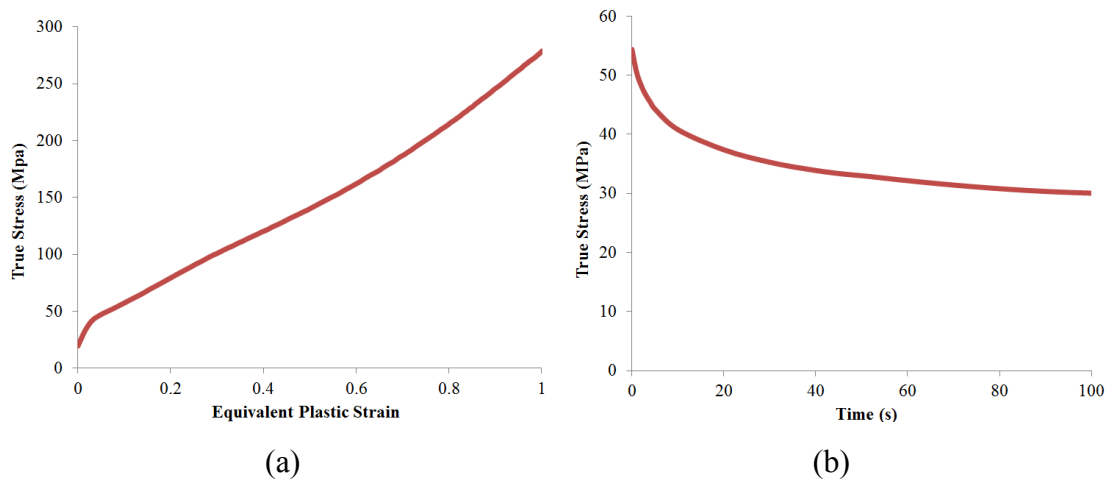


Figure 7.8. Experimental flow (strain rate: 0.01 s⁻¹) (a) and relaxation (constant strain: 0.1) (b) curves of PP/PE 75/25 fibre

The procedures of extracting a sample fibre and making experiments to determine its mechanical performance are explained in Section 5.1. The flow curve of the PP/PE fibre shown in Figure 7.8 is obtained via a simple tension test performed with deformation rate of 0.01 s^{-1} . The flow curve is provided up to the equivalent plastic strain value of 1 because the fabric, which is simulated with the assessed mechanical properties based on this curve, ruptures approximately at this point when extended in CD. According to tensile test graphs of 50 g/m^2 PP/PE 75/25 nonwoven fabrics in Section 5.3, rupture strain in MD is less than that in CD. As a result of this fact, maximum rupture strain, corresponding to that in CD, is taken into account for the determination of strain range in the flow curve of the fibres used in the analysis. On the other hand, the relaxation curve of the fibre shown in Figure 7.8 is obtained at constant strain level of 0.1. The relaxation behaviour is provided up to 100 s which is the time scale of a tension test up to the strain value of 1 with 0.01 s^{-1} deformation rate. Model D simulates a time-scale of 1 s that is well within the range of the supplied relaxation curve. The strain range of the flow curve and time scale of the relaxation curve, which are used for the analysis, can vary according to the rupture strain of the material and duration of loading conditions in the simulation.

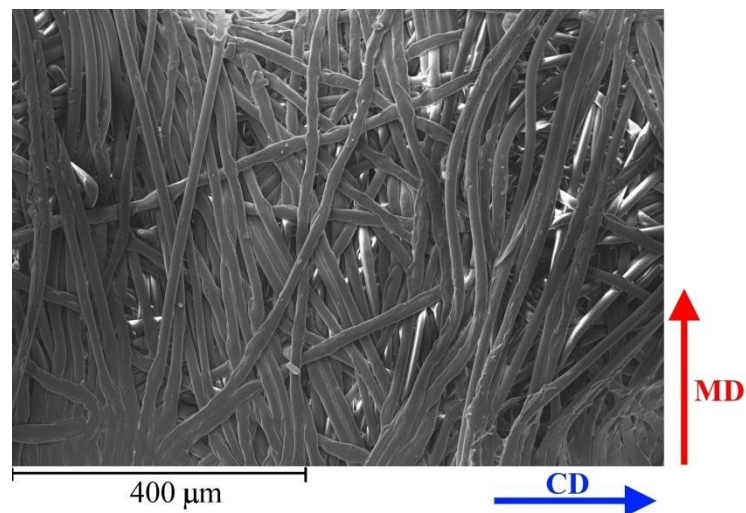


Figure 7.9. SEM image of fibre matrix region of 150 g/m^2 PA6/PE 75/25 thermally bonded nonwoven simulated with Model B

7.2.2. Model B

Model B simulates the mechanical behaviour of 150 g/m² PA6/PE 75/25 thermally bonded nonwoven material. The material is calendered out with a diamond-shape periodic bond pattern shown in Figure 7.3. Assessment of mechanical properties of the nonwoven regions takes place after analysing anisotropic parameters with the Nonwovens Anisotropy V1 algorithm. C_{MD} and C_{CD} in Table 7.4 are determined using the SEM image of the fibre matrix region of the nonwoven in Figure 7.9.

In addition to the anisotropic, the algorithm needs parameters linked to manufacturing of the nonwoven fabric. The manufacturing parameters of 150 g/m² PA6/PE 75/25 thermally bonded nonwoven processed by the algorithm are given in Table 7.4.

| Manufacturing Parameters | Model B |
|---|----------------|
| Nonwoven Planar Density (g/m ²) | 150 |
| Cross-Sectional Ratio of Sheath (%) | 25 |
| Thickness of Fibre Matrix (mm) | 0.5 |
| C_{MD} and C_{CD} | 0.72 and 0.28 |
| Fibre Diameter (mm) | 0.018 |
| Calendering Temperature (°C) | 150 |

Table 7.4. Manufacturing parameters of 150 g/m² PA6/PE 75/25 thermally bonded nonwoven simulated with Model B

Properties of polymer materials, which are utilized as core and sheath parts of bicomponent fibres, are also necessary for the analysis of the mechanical properties of fabric regions with the algorithm. Table 7.5 provides the properties of core and sheath polymers used in the manufacturing of the nonwoven fabric simulated with Model B.

| | Core | Sheath |
|-----------------------------------|------|--------|
| Material | PA6 | PE |
| Density (g/cm³) | 1.13 | 0.955 |
| Young's Modulus (MPa) | 3000 | 250 |
| Poisson's Ratio (mm) | 0.42 | 0.42 |
| Shear Modulus (MPa) | 760 | 110 |
| Melting Temperature (°C) | 220 | 131 |

Table 7.5. Properties of core and sheath materials for manufacturing 150 g/m² PA6/PE 75/25 thermally bonded nonwoven simulated with Model B

Plastic and viscous behaviours of nonwoven regions are analysed based on the results of simple tension and relaxation tests of PA6/PE 75/25 fibres (Figure 7.10). Flow and relaxation curves of the fibre defining its time-dependent large-strain mechanical behaviour are provided in Figure 7.10.

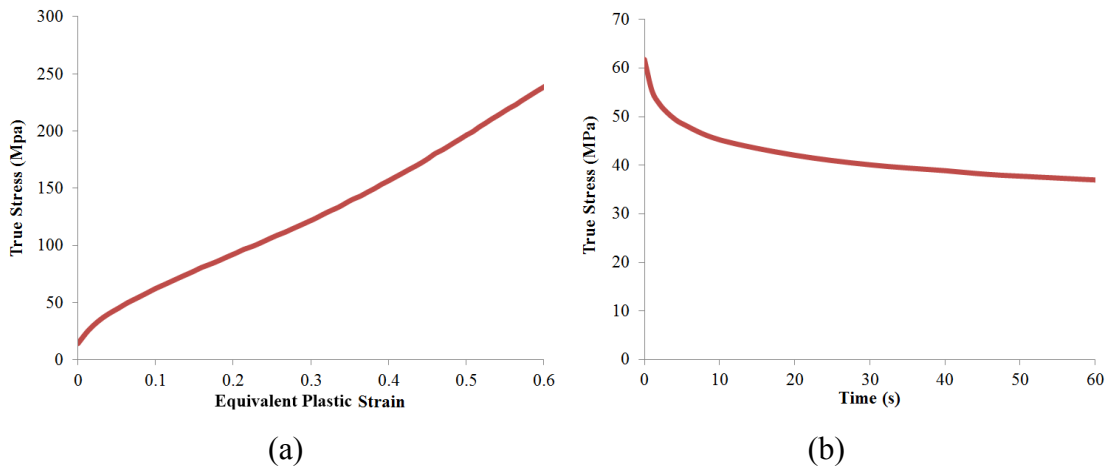


Figure 7.10. Experimental flow (strain rate: 0.01 s⁻¹) (a) and relaxation (constant strain: 0.1) (b) curves of PA6/PE 75/25 fibre

The fibre's flow curve shown in Figure 7.10 is obtained via a simple tension test performed with a deformation rate of 0.01 s⁻¹. The flow curve is provided up to the equivalent plastic strain value of 0.6 because the fabric simulated with Model B ruptures approximately at this point. The relaxation test of the fibre is performed at a constant strain level of 0.1; the respective curve in Figure 7.10 is given for first 60 s,

which is the time scale of the tensile test simulation with Model B up to the strain value of 0.6 with the modelled extension rate.

7.2.3. Model C

Model C simulates the mechanical behaviour of 35 g/m² PP/PE 50/50 thermally bonded nonwoven material. Unlike the nonwovens simulated with the other models, this nonwoven is manufactured with short and crimped fibres bonded together with a rectangular periodic bond pattern shown in Figure 7.5. In order to determine anisotropic parameters in Table 7.6, a SEM image of the fibre matrix region of the nonwoven in Figure 7.11 is analysed with the Nonwovens Anisotropy V1 algorithm.

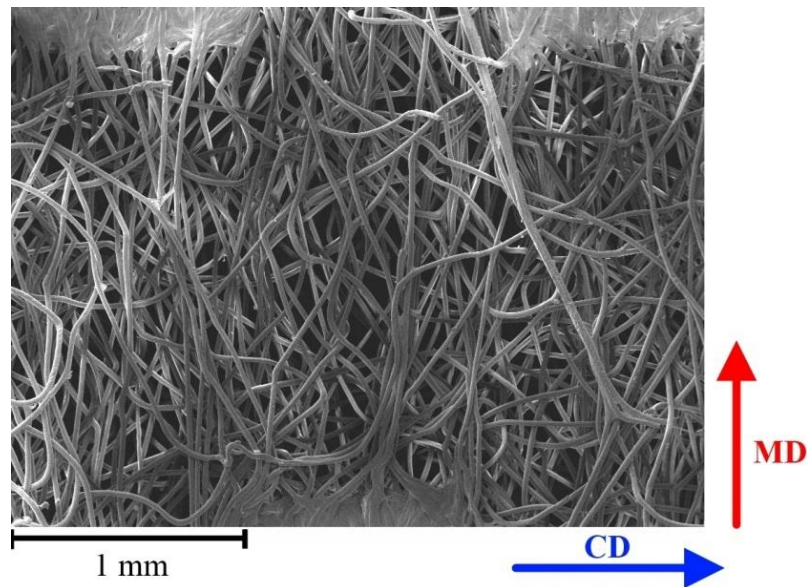


Figure 7.11. SEM image of fibre matrix region of 35 g/m² PP/PE 50/50 thermally bonded nonwoven simulated with Model C

Apart from anisotropic parameters based on the microstructural randomness caused by the web manipulation stage, there are several parameters linked to other manufacturing stages of the nonwoven; these parameters are provided in Table 7.6. Several properties of the core and sheath materials given in Table 7.7 are also required to analyse mechanical properties of fabric regions with the Nonwovens V4

algorithm. These properties are available in the datasheet of the corresponding polymer's supplier company.

| Manufacturing Parameters | Model C |
|--|----------------|
| Nonwoven Planar Density (g/m^2) | 35 |
| Cross-Sectional Ratio of Sheath (%) | 50 |
| Thickness of Fibre Matrix (mm) | 0.4 |
| C_{MD} and C_{CD} | 0.84 and 0.16 |
| Fibre Diameter (mm) | 0.023 |
| Calendering Temperature ($^{\circ}\text{C}$) | 140 |

Table 7.6. Manufacturing parameters of 35 g/m^2 PP/PE 50/50 thermally bonded nonwoven simulated with Model C

| | Core | Sheath |
|--|-------------|---------------|
| Material | PP | PE |
| Density (g/cm^3) | 0.89 | 0.955 |
| Young's Modulus (MPa) | 1450 | 250 |
| Poisson's Ratio (mm) | 0.42 | 0.42 |
| Shear Modulus (MPa) | 680 | 110 |
| Melting Temperature ($^{\circ}\text{C}$) | 165 | 131 |

Table 7.7. Properties of core and sheath materials for manufacturing 35 g/m^2 PP/PE 50/50 thermally bonded nonwoven simulated with Model C

Results of simple tension and relaxation tests for PP/PE 50/50 fibre provide the last data set for defining the viscoelastic-plastic behaviour of the fabric regions. Figure 7.12 shows the flow and relaxation curves obtained with these tests. The flow curve of PA6/PE fibre is obtained via a simple tension test performed with the same strain rate of 0.01 s^{-1} . The flow curve is provided up to the equivalent plastic strain value of 0.25 since this is the rupture point of the fabric simulated with Model C. During the relaxation test, fibre is kept at strain level of 0.1 constantly. The relaxation curve in Figure 7.12 is provided up to 25 s, which is the time scale of the

tensile test simulation with Model C up to the strain value of 0.25 with a strain rate of 0.01 s^{-1} .

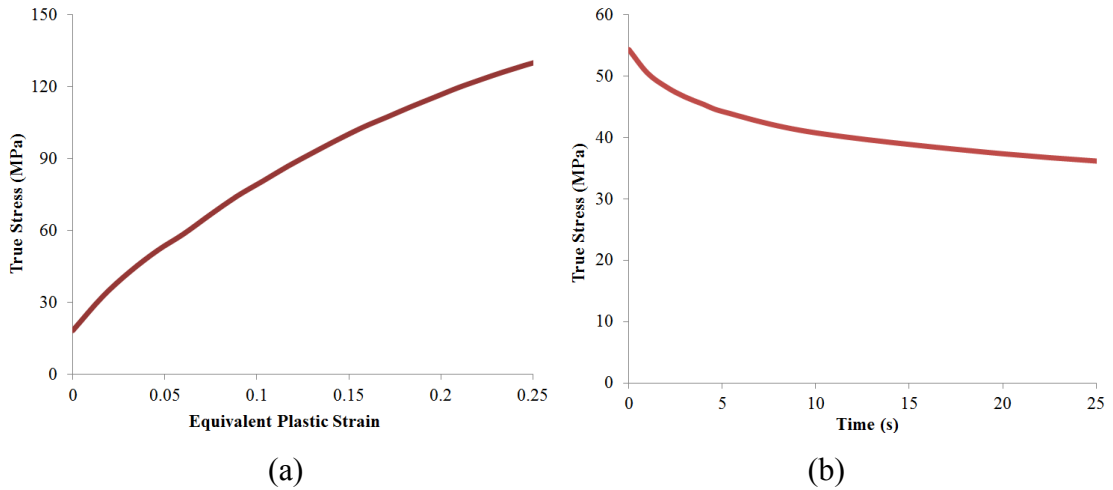


Figure 7.12. Experimental flow (strain rate: 0.01 s^{-1}) (a) and relaxation (constant strain: 0.1) (b) curves of PP/PE 50/50 fibre

The necessary input parameters for analysing orthotropic viscoelastic-plastic mechanical properties of regions of bond points and the fibre matrix of the nonwovens simulated with the four models are supplied in this section. These properties are determined in the next section based on the procedures explained in Chapter 6 using the Nonwovens V4 algorithm and the input parameters provided.

7.3. Assessment of Mechanical Properties

Based on the input parameters related to the nonwovens simulated with the models, mechanical properties of bond point and fibre matrix regions of each model are assessed in this section. Properties of each model are assigned based on the orthotropic symmetry formulation in the FE software. These properties are classified as elastic, plastic and viscous, representing various characteristics of deformation. The assessed mechanical properties are assigned to the elements generated in

MSC.Marc[®] software, but they could be used with other FE software packages as well.

In this section, computed elastic properties – modulus of elasticity (E), Poisson’s ratio (ν) and shear modulus (G) – are denoted with MD, CD and TD indices referring to the principal directions of orthotropy in nonwovens. The plastic and viscous behaviours will be delivered in the form of curves defining their strain-dependent nonlinear characteristics throughout the deformation history. Orthotropic viscoelastic-plastic mechanical properties of nonwoven regions analysed with the Nonwovens V4 algorithm for each model are provided below.

7.3.1. Models A and D

Orthotropic viscoelastic-plastic properties of the bond point and fibre matrix regions of Models A and D, which simulate deformation behaviour of the 50 g/m² PP/PE 75/25 thermally bonded nonwoven material, are delivered in this part. Parameters defining the elastic behaviour of regions in these models are given in Table 7.8.

| | Bond Point | Fibre Matrix |
|------------------------------------|--------------------------|--------------------------|
| E_{MD} (MPa) | 604.9 | 95.3 |
| E_{CD} (MPa) | 325.7 | 51.3 |
| E_{TD} (MPa) | 892.8 | 0.8 |
| $\nu_{MD,CD}$ | 0.42 | 0.42 |
| $\nu_{CD,TD}$ | 0.42 | 0 |
| $\nu_{TD,MD}$ | 0.42 | 0 |
| $G_{MD,CD}$ (MPa) | 369.4 | 58.2 |
| $G_{CD,TD}$ (MPa) | 198.9 | 31.4 |
| $G_{TD,MD}$ (MPa) | 545.3 | 0.5 |
| Thickness (mm) | 0.055 | 0.35 |
| Density (Mg/mm³) | 9.0625×10^{-10} | 1.4285×10^{-10} |

Table 7.8. Orthotropic elastic properties of 50 g/m² PP/PE 75/25 nonwoven regions used in Models A and D

Flow curves (equivalent plastic strain vs. true stress), which define the Hill's anisotropic yield criterion (Hill, 1950) for the two nonwoven regions, are shown in Figure 7.13. These curves could be used with any FE software supporting anisotropic yield phenomenon.

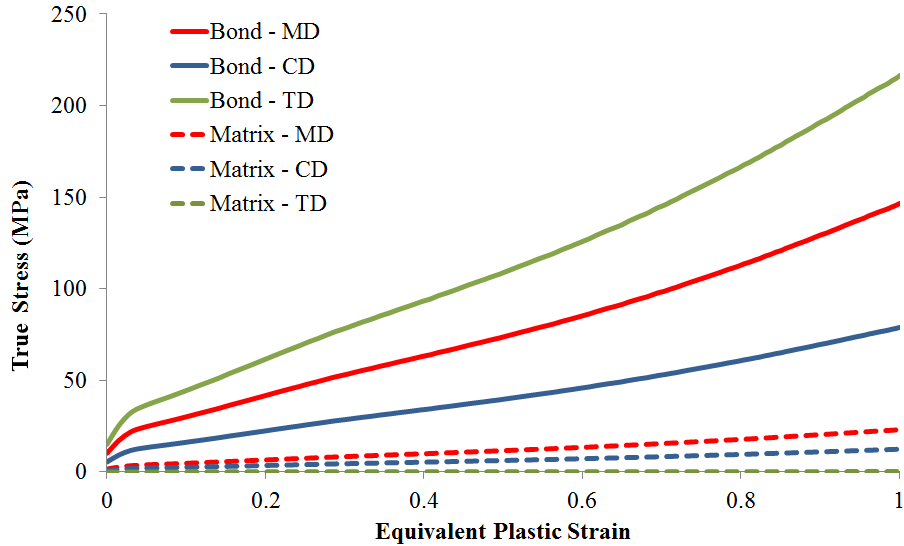


Figure 7.13. Flow curves of 50 g/m² PP/PE 75/25 nonwoven regions used in Models A and D

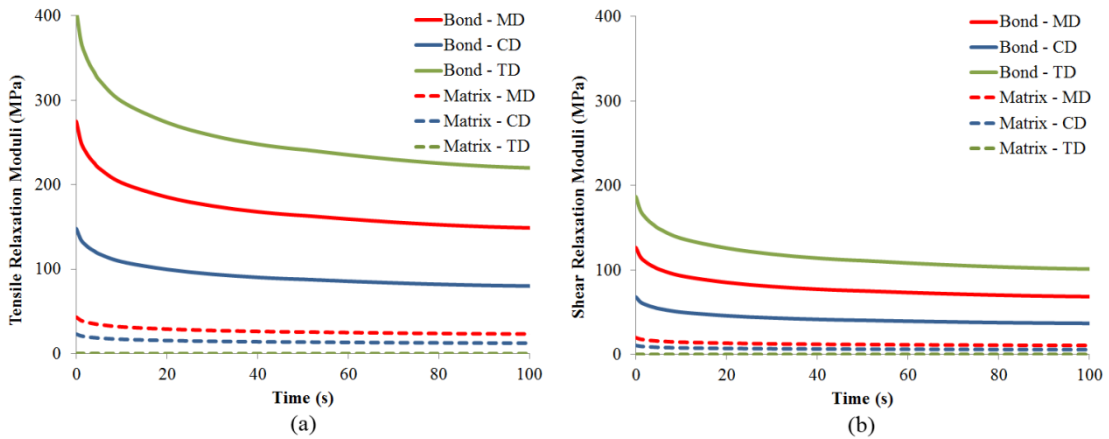


Figure 7.14. Orthotropic tensile (a) and shear (b) relaxation moduli of 50 g/m² PP/PE 75/25 nonwoven regions used in Models A and D

Time-dependent mechanical performance of elements of bond points and fibre matrix are introduced with viscous effects, observed in relaxation tests. FE models of

nonwovens in this research require curves of orthotropic tensile and shear relaxation moduli of the nonwoven regions to simulate their time-dependent deformation performance. Tensile and shear relaxation curves shown in Figure 7.14 could be used with any numerical scheme supporting orthotropic viscoelasticity.

7.3.2. Model B

Orthotropic viscoelastic-plastic properties of the bond point and fibre matrix regions of Model B, which simulates the deformation behaviour of the 150 g/m² PA6/PE 75/25 thermally bonded nonwoven material, are provided below starting with the elastic ones shown in Table 7.9.

| | Bond Point | Fibre Matrix |
|------------------------------------|----------------------------|-------------------------|
| E_{MD} (MPa) | 1411.8 | 389.9 |
| E_{CD} (MPa) | 549.1 | 151.6 |
| E_{TD} (MPa) | 1326.1 | 3.2 |
| $\nu_{MD,CD}$ | 0.42 | 0.42 |
| $\nu_{CD,TD}$ | 0.42 | 0 |
| $\nu_{TD,MD}$ | 0.42 | 0 |
| $G_{MD,CD}$ (MPa) | 390.4 | 107.8 |
| $G_{CD,TD}$ (MPa) | 151.8 | 41.9 |
| $G_{TD,MD}$ (MPa) | 366.7 | 0.9 |
| Thickness (mm) | 0.138 | 0.5 |
| Density (Mg/mm³) | 10.862 x 10 ⁻¹⁰ | 3.0 x 10 ⁻¹⁰ |

Table 7.9. Orthotropic elastic properties of 150 g/m² PA6/PE 75/25 nonwoven regions used in Model B

Six flow curves, which define the anisotropic plastic behaviour of two nonwoven regions, are given in Figure 7.15. These curves are supplied up to 0.6 strain level, which is the limit of tensile test simulation with Model B due to failure of the fabric.

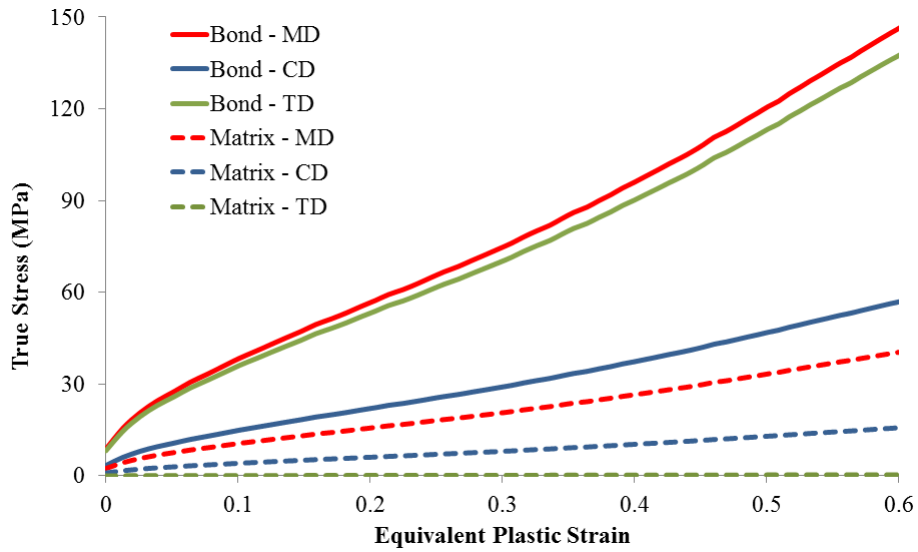


Figure 7.15. Flow curves of 150 g/m² PA6/PE 75/25 nonwoven regions used in Model B

Tensile and shear relaxation curves shown in Figure 7.16 are used in Model B to reproduce the fabric’s time-dependent behaviour. Stress attenuation during the tensile test is implemented in simulations with these curves via the viscoelasticity option.

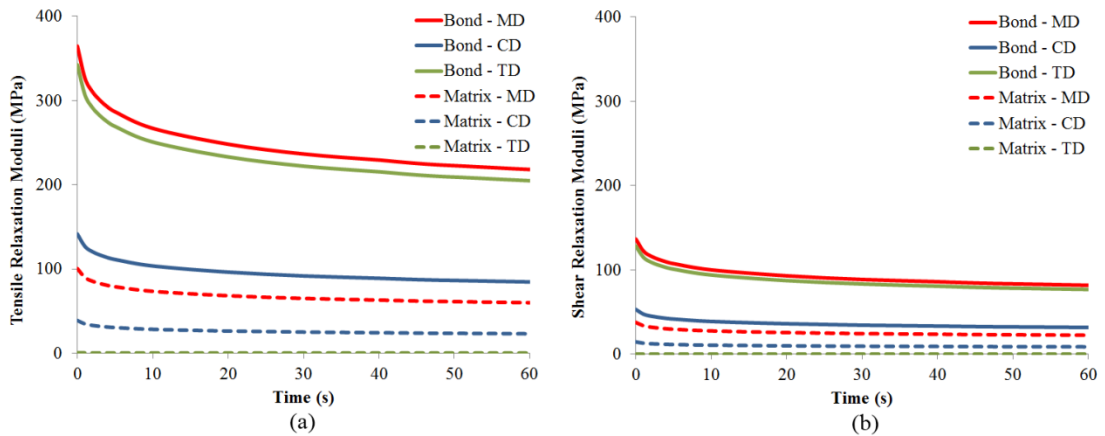


Figure 7.16. Orthotropic tensile (a) and shear (b) relaxation moduli of 150 g/m² PA6/PE 75/25 nonwoven regions used in Model B

7.3.3. Model C

Orthotropic viscoelastic-plastic properties of the regions of bond points and the fibre matrix of Model C, which simulates tensile testing of the 35 g/m² PP/PE 50/50 thermally bonded nonwoven material, are computed in this part. The elastic properties of the fabric regions calculated with the Nonwovens V4 algorithm are shown in Table 7.10.

| | Bond Point | Fibre Matrix |
|-------------------------------------|-------------------------|-------------------------|
| E_{MD} (MPa) | 683.7 | 64.9 |
| E_{CD} (MPa) | 130.2 | 12.4 |
| E_{TD} (MPa) | 583.3 | 0.5 |
| $\nu_{MD,CD}$ | 0.42 | 0.42 |
| $\nu_{CD,TD}$ | 0.42 | 0 |
| $\nu_{TD,MD}$ | 0.42 | 0 |
| $G_{MD,CD}$ (MPa) | 234.2 | 22.2 |
| $G_{CD,TD}$ (MPa) | 44.6 | 4.2 |
| $G_{TD,MD}$ (MPa) | 199.8 | 0.2 |
| Thickness (mm) | 0.0379 | 0.4 |
| Density (Mg/mm³) | 9.225×10^{-10} | 0.875×10^{-10} |

Table 7.10. Orthotropic elastic properties of 35 g/m² PP/PE 50/50 nonwoven regions used in Model C

Following the elastic behaviour, the plastic one is provided by means of six flow curves in Figure 7.17 defining the anisotropic irreversible deformation performance of two nonwoven regions constituting Model C. Since the fabric starts to fail at strain level of 0.25, flow curves are provided up to this point. In addition to plasticity, the viscous behaviour of the fabric is also considered in Model C. Tensile and shear relaxation curves shown in Figure 7.18 are used in the material definition used to reproduce the fabric's time-dependent behaviour. Energy dissipation due to viscous effects during the tensile test is accounted for with these curves via the viscoelasticity option in the FE software.

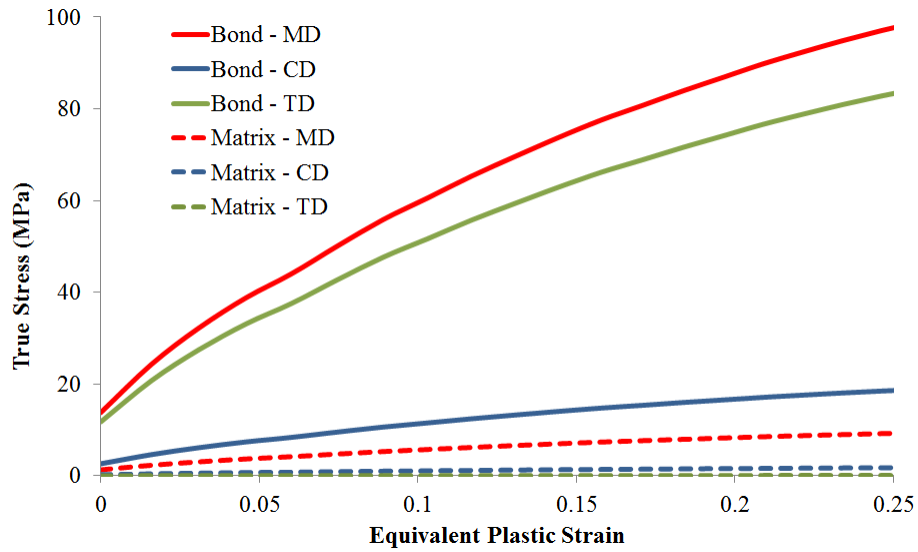


Figure 7.17. Flow curves of 35 g/m² PP/PE 50/50 nonwoven regions used in Model C

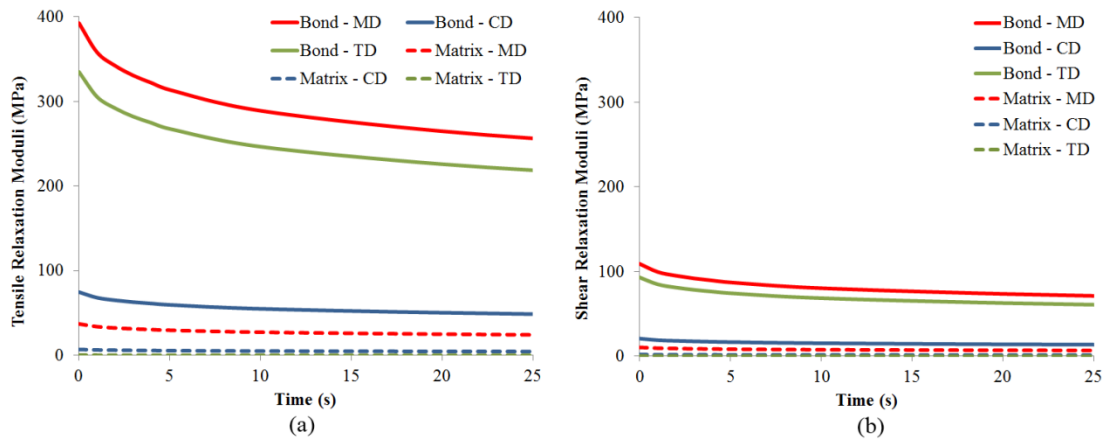


Figure 7.18. Orthotropic tensile (a) and shear (b) relaxation moduli of 35 g/m² PP/PE 50/50 nonwoven regions used in Model C

The computed mechanical properties of the regions of bond points and the fibre matrix provided in this section are assigned to the elements representing respective regions in the models. These properties can define large-strain orthotropic viscoelastic-plastic deformation behaviour of nonwovens modelled in any FE software package. The structure of FE models and the mechanical properties assigned to their elements were explained above. Apart from these, the FE models require appropriate boundary conditions to simulate real-life loading cases.

7.4. Boundary Conditions

Boundary conditions in FE analysis can be defined as the set of loading parameters required to accomplish a specific numerical solution. In FE modelling, boundary conditions are direct links between the simulation and respective real-life problem since they represent the applied loads and constraints in the real-life case. There are three types of boundary conditions applied in the FE models introduced in this chapter: fixed displacement, rate-controlled displacement and constant acceleration. The choice of boundary conditions depends on the problems simulated with the models. In this study, the FE models can be classified into two groups according to their boundary conditions.

7.4.1. Models A, B and C

Models A, B and C simulate the deformation behaviour of nonwoven specimens with dimensions 30 mm x 15 mm exposed to tensile testing at a specific deformation rate. Boundary conditions in these models should reflect loading conditions on nonwoven specimens in a tensile testing machine. Tensile test parameters of the nonwoven specimens, which are simulated with these models, are identical, so are their boundary conditions.

The boundary conditions in Models A, B and C are applied to the edges A-B and C-D of the model shown in Figure 7.19. Except for the degree of freedom, which corresponds to the tensile loading direction, along edge C-D, the fixed displacement condition is applied to the translational degrees of freedom on the nodes along both edges of the model. As a boundary condition in the model, the constant deformation rate, which is identical to the one in tensile tests, is applied to the nodes along edge C-D in the tensile loading direction. Its magnitude of 0.01 s^{-1} corresponds to the grip speed of 0.3 mm/s for the gauge length of 30 mm in the tensile tests. This deformation rate is suitable to minimize the rate effects in the nonwoven materials studied in this research. Slower or faster deformation rates in a tensile test may amplify particular effects of the viscous behaviour, e.g. the creep behaviour can be

observed at very low deformation rates. In order to concentrate on the efficiency of FE models in reproducing the elastic-plastic behaviour of the nonwovens, the chosen deformation rate is preferred. Model D concentrates on the viscous behaviour of thermally bonded nonwoven fabrics in terms of energy dissipation during spring back behaviour.

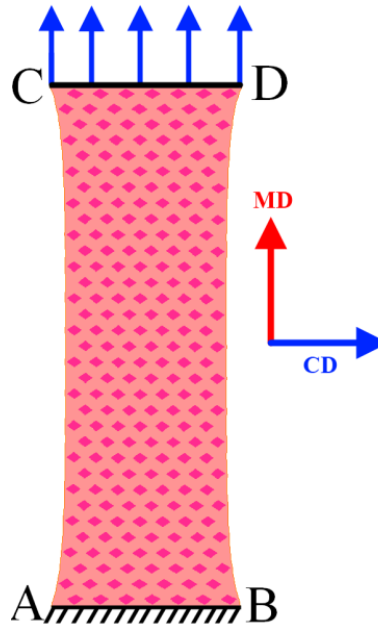


Figure 7.19. FE model of tensile-test specimen with boundary conditions

7.4.2. Model D

Model D simulates a free-falling metal sphere released still above the nonwoven fabric to attain consecutive bounces with a gradually decreasing height in each bounce due to energy dissipation mechanisms related to viscoelasticity in the nonwoven material. Due to inertial effects induced by gravity, Model D uses a dynamic formulation of the FE software. The total time of the simulation is 1 s. There are two sets of boundary conditions in this model: fixed displacement and constant acceleration. Translational degrees of freedom on the nodes along four edges (A-B, B-C, C-D and A-D) of the square-shaped fabric in Model D are assigned with the fixed displacement condition (Figure 7.20). A constant gravitational acceleration of 9.812 m/s^2 is applied to the rigid body of the metal sphere with a

mass of 43.4 g to simulate its free fall in the direction of gravitational force illustrated in Figure 7.20. Finally, the initial velocity of the sphere is given as 0, since the sphere is released from its steady-state position located 100 mm above the fabric plane.

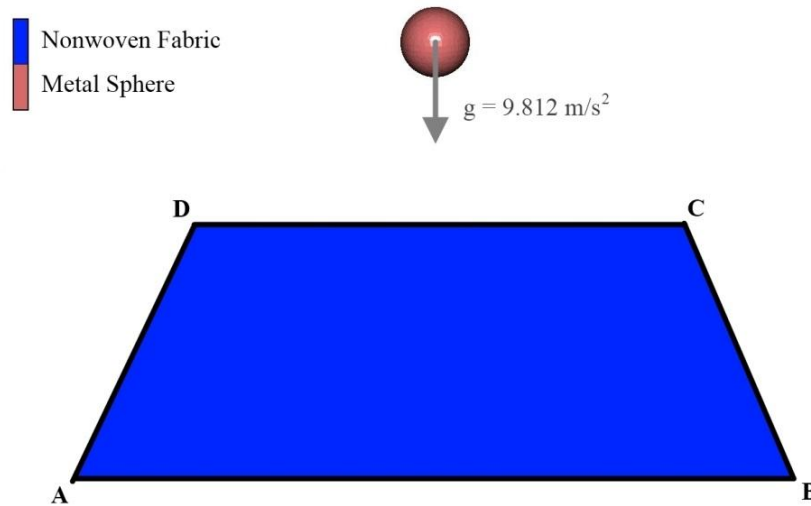


Figure 7.20. Components of Model D with boundary conditions

The boundary conditions applied to the models are independent of the element size, since they are applied to the specimen edges, related to their geometry rather than their FE mesh. Besides, these boundary conditions are the most commonly used ones in FE software packages and their application is straight-forward. The procedure for generating the FE models for simulating time-dependent mechanical behaviour of thermally bonded bicomponent fibre nonwovens is finalized with the illustration of respective boundary conditions. This procedure could be accomplished in any commercial FE software package with a material library capable of implementing large-strain orthotropic viscoelastic-plastic material behaviour.

In order to evaluate the success of numerical modelling approach proposed in this research, four sample models introduced in this chapter should be verified with appropriate experiments. Results of the FE models and their experimental verifications are available in the next part.

7.5. Results and Experimental Verification

With the FE models introduced in this chapter, deformation performance of thermally bonded nonwovens with various manufacturing parameters and boundary conditions is simulated. As explained in Section 7.1, each model focuses on a different material or loading condition in order to observe the capabilities of the proposed numerical modelling procedure. The process of developing the FE models was illustrated in detail above starting with meshing based on the fabric's bond pattern and ending with the application of boundary conditions related to modelled cases. During this process, the algorithms introduced in Chapter 6 significantly reduce the required time for computing mechanical anisotropy and assessing the orthotropic mechanical properties of nonwoven regions.

A novel numerical modelling technique should be verified experimentally for further academic and industrial applications. This section provides results of the simulations performed with the developed FE models and their experimental verifications. The quality of the proposed modelling approach is evaluated by means of comparing the material's real-life behaviour with the simulated one. For this purpose, each FE model is compared with the respective experiment using a quantitative result which could be obtained both experimentally and numerically, for instance, the force-displacement curve for Models A, B and C simulating tensile tests and the bounce height of the sphere for Model D simulating a bouncing metal sphere.

7.5.1. Model A

Tensile testing of the 50 g/m² PP/PE 75/25 thermally bonded nonwovens with a diamond-shape bond pattern is simulated with Model A to analyse their mechanical performance. Nonwoven specimens with a gauge length of 30 mm and width of 15 mm are extended with a strain rate of 0.01 s⁻¹. Equivalent von Mises stress distribution in the models simulating the tension tests in MD and CD are given in Figures 7.21 and 7.22, respectively. Due to stiffer structure of bond points, stresses are more concentrated in these regions (Figures 7.21b and 7.22b). On the other hand,

deformation of bond points is less than that of matrix reflecting the real-life response leading to failure of matrix before failure of bond points in tension.

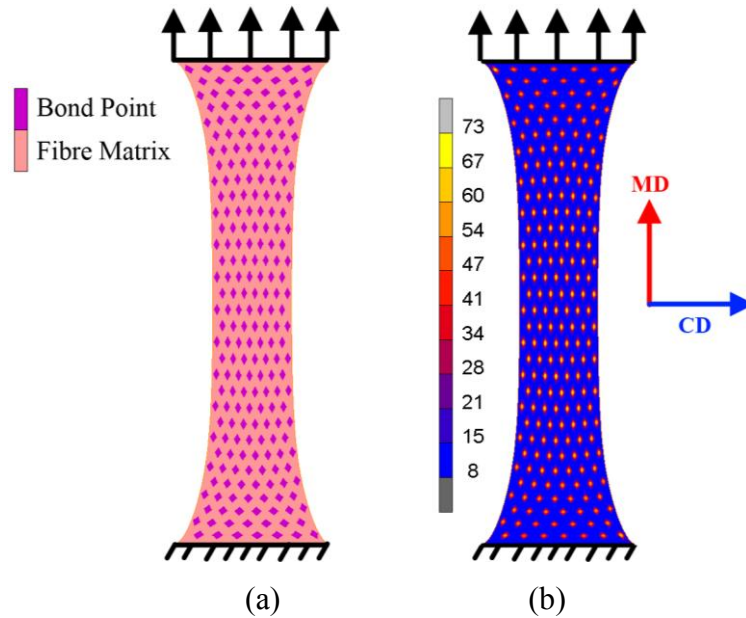


Figure 7.21. FE results for deformed nonwoven in Model A after 60% extension in MD: (a) regions in deformed model; (b) equivalent von Mises stresses (MPa)

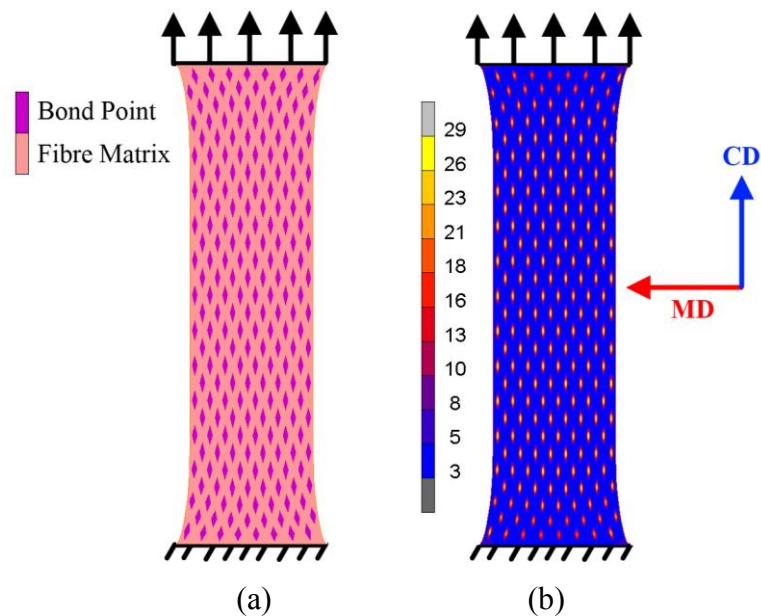


Figure 7.22. FE results for deformed nonwoven in Model A after 60% extension in CD: (a) regions in deformed model; (b) equivalent von Mises stresses (MPa)

The anisotropic mechanical behaviour of nonwovens is also reproduced with the proposed numerical model when the FE results in Figures 7.21 and 7.22 are compared. Stress values obtained in simulation of the tension test in MD are higher than those in CD reflecting the real-life direction-dependant mechanical response of nonwovens. Besides, the difference in geometry of the deformed models reflects the anisotropic deformation behaviour of nonwovens subjected to tensile tests. For comparability, the FE results in Figures 7.21 and 7.22 are illustrated for 60% extension where the 50 g/m² PP/PE 75/25 thermally bonded nonwoven starts to fail in the tensile test performed in MD.

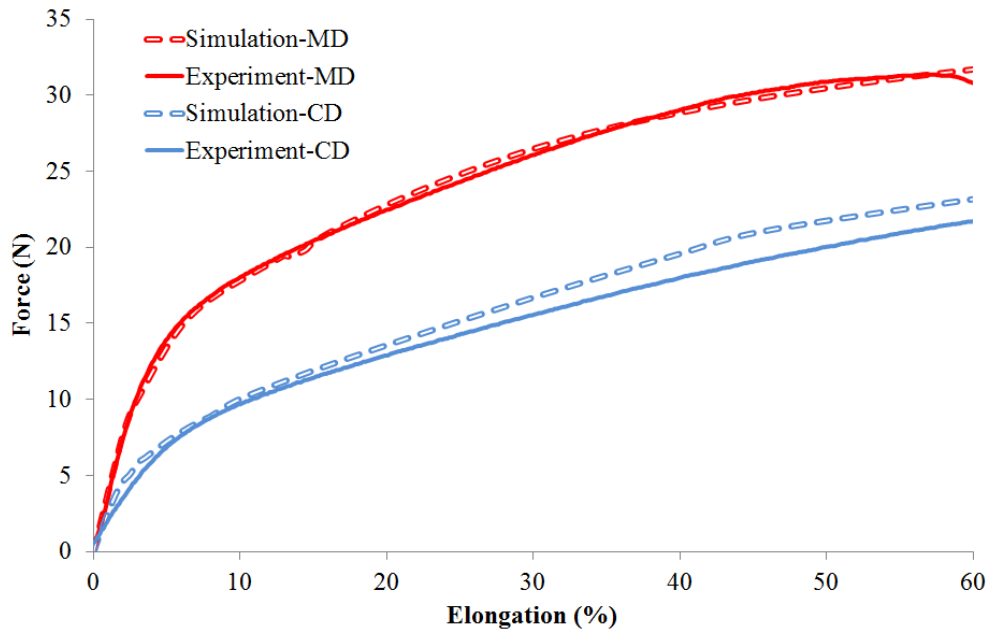


Figure 7.23. Force-extension curves from tensile tests and FE simulations in MD and CD for 50 g/m² PP/PE 75/25 thermally bonded bicomponent fibre nonwovens

To compare the obtained FE results with respective experiments, the force-displacement curve, acquired in real-life tests, is calculated in the FE software based on computed stresses (Figure 7.23). As obvious from Figure 7.23, the FE simulation results and the experimental data are in good agreement. The slight deviation of the numerical results from experimental ones can be explained by the effect of several secondary factors not accounted for in the model. Among them are the curliness of

fibres, inter-fibre friction in the matrix region, etc. Furthermore, some of the surface parts of the matrix region are molten due to heat generated during the calendering stage. Apparently, the input data such as the flow curve of a single fibre is crucial for providing a representative mechanical performance for the fibres composing the nonwoven fabric. Despite some possible sources of deviation, the FE model successfully reproduces the response of the nonwoven specimens to tensional load.

7.5.2. Model B

Mechanical performance of the 150 g/m² PA6/PE 75/25 thermally bonded nonwovens is analysed with Model B in the FE environment. The nonwoven specimen simulated with this model has identical dimensions, bond shape and pattern with those of Model A. Simulations of tensile tests performed in MD and CD are carried out with Model B, and the resulting distribution of equivalent von Mises stresses in the models are shown in Figures 7.24 and 7.25. Stress concentration in regions of thin bond points, observed in the FE results of Model B, is similar to the case in Model A.

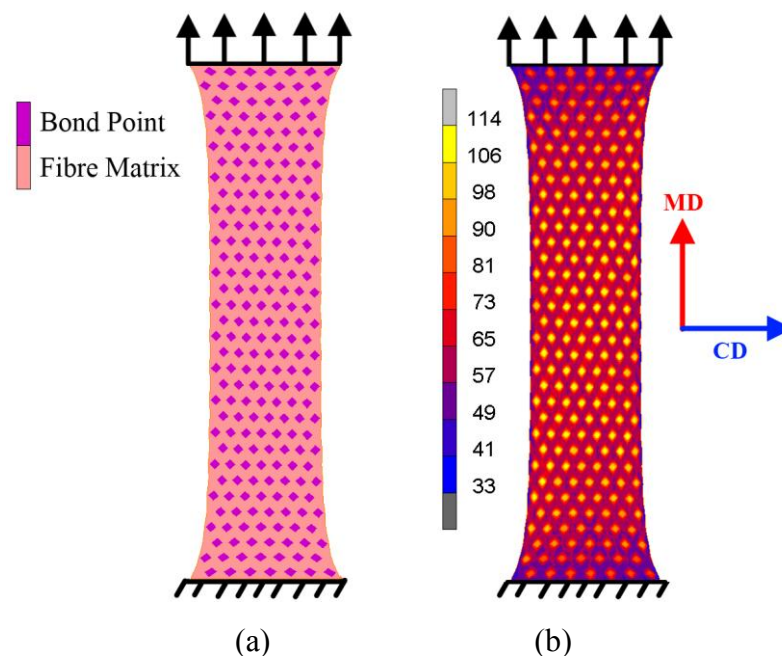


Figure 7.24. FE results for deformed nonwoven in Model B after 70% extension in MD: (a) regions in deformed model; (b) equivalent von Mises stresses (MPa)

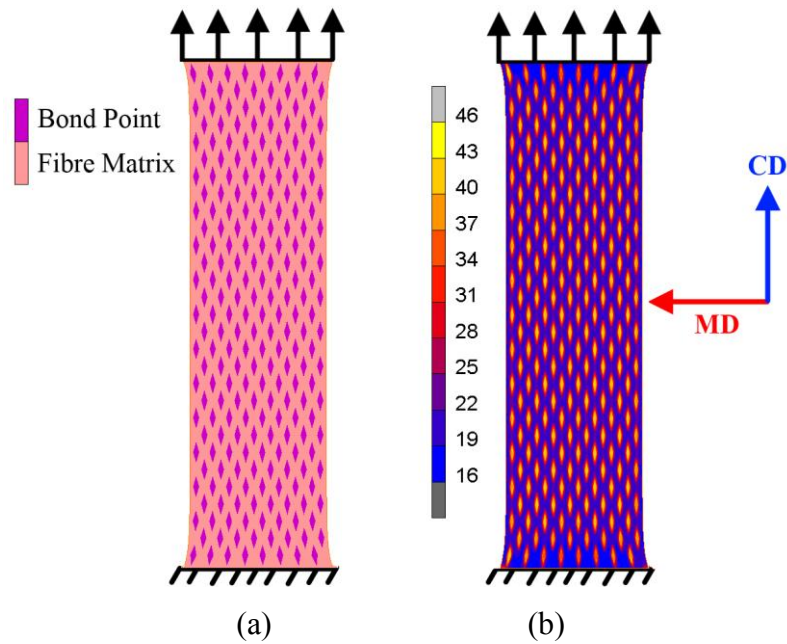


Figure 7.25. FE results for deformed nonwoven in Model B after 70% extension in CD: (a) regions in deformed model; (b) equivalent von Mises stresses (MPa)

According to the computed mechanical properties of the regions of bond points and the fibre matrix of models in Section 7.3, mechanical performances of the regions in Model B are higher than those in Model A due to a three-times-larger planar density of fabric and superior fibre strength. As a result of this difference, stress values observed in the FE results of Model B are significantly higher than those of Model A despite the contribution of 10% increased tensile extension. Obviously, the proposed numerical model can reproduce the effects of variation in fabric's planar density and the type of bicomponent fibre on the overall deformation response of thermally bonded nonwovens. Direction-dependent deformation behaviour is also captured with Model B which results in distinct geometries shown in Figures 7.24a and 7.25a at 70% extension in MD and CD, accordingly. Besides, due to increased stress in the neck region as a result of nonuniform cross-section, deformation of bond points in this region are higher than that of bond points located near the grip regions. The FE results in Figures 7.24 and 7.25 are shown for 70% extension, i.e. the moment, at which damage initiates in the tensile tests of 150 g/m^2 PA6/PE 75/25 thermally bonded nonwovens.

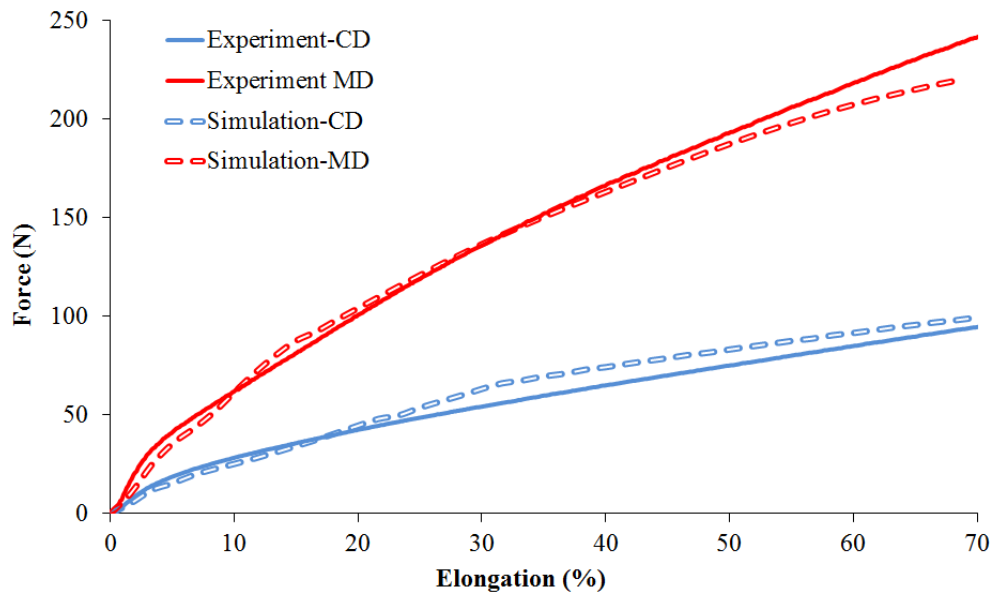


Figure 7.26. Force-extension curves from tensile tests and FE simulations in MD and CD for 150 g/m² PA6/PE 75/25 thermally bonded bicomponent fibre nonwovens

The force-displacement curves obtained with the tensile tests are compared with those obtained with Model B in Figure 7.26. Apparently, tensile test results in MD and CD confirm the suitability of the proposed numerical model. As a result of the increased fabric planar density and different fibre type constituting the nonwoven, the level of load required to deform the nonwoven in Model B is at least three times the one in Model A. The numerical model introduced in this study analyses these differences successfully due its parametric scheme. As explained above, there is a slight deviation of the numerical results from experimental ones that can be explained by the effect of several secondary factors not accounted for in the model, e.g. curliness of fibres, deviation of manufacturing parameters, etc. Despite the slight deviation, results of the numerical model and tensile tests in Figure 7.26 are in good agreement, proving the efficiency of the FE models developed in the research.

7.5.3. Model C

Model C simulates the 35 g/m² PP/PE 50/50 thermally bonded nonwovens with a rectangular bond pattern. As explained in Section 7.1, this model is introduced to test

the limits of applicability of the developed modelling approach since the nonwoven simulated with Model C has a critically low planar density, and its fibres are short and crimped unlike the ones explained in Section 5.1. The FE models developed in this research represent the bond point and fibre matrix regions with shell elements. Efficiency of these elements in representing the anisotropic behaviour of these regions depends on homogeneity in the volumetric distribution of fibres on the fabric plane. As observed in the FE results of Models A and B, shell elements are successful in representing the structure of regions of bond points and a fibre matrix since planar densities of the fabrics are at least 50 g/m^2 , which could be assumed as volumetrically homogeneous. Efficiency of the numerical modelling approach for a low planar density is evaluated considering the simulations of the tensile tests performed with Model C. A stress distribution in the FE model simulating the tension test of 35 g/m^2 PP/PE 50/50 thermally bonded nonwoven in MD is given in Figure 7.27.

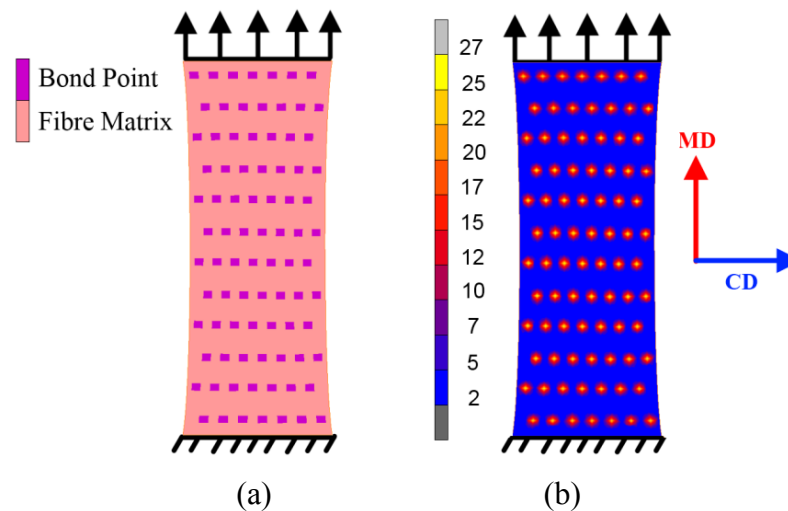


Figure 7.27. FE results for deformed nonwoven in Model C after 25% extension in MD: (a) regions in deformed model; (b) equivalent von Mises stresses (MPa)

The FE results of Model C in Figure 7.27 demonstrate the capability of the introduced numerical model to reproduce the deformation behaviour of a nonwoven, calendered with various bond shapes and patterns. Having a considerably lower planar density and being manufactured with short and crimped fibres, the damage

point of the nonwoven simulated with Model C corresponds to approximately 25% extension. Stress values shown in Figure 7.27 are significantly lower than those observed in Models A and B due to the level of applied extension. Additionally, poor mechanical properties of the fabric regions due to low planar density contribute to the reduction of stresses observed in Figure 7.27.

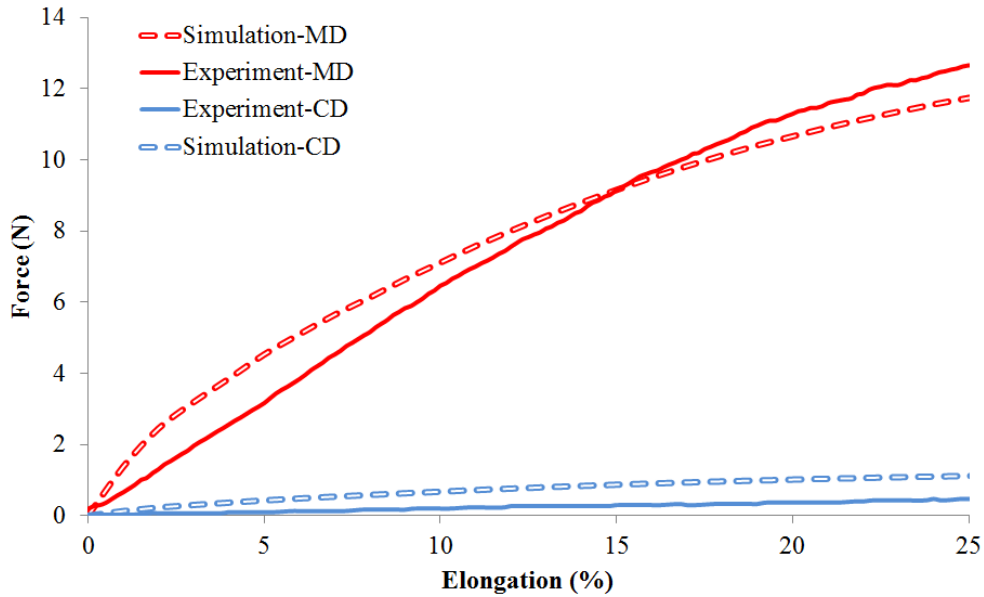


Figure 7.28. Force-extension curves from tensile tests and FE simulations in MD and CD for 35 g/m² PP/PE 50/50 thermally bonded bicomponent fibre nonwovens

To compare the FE results of Model C with respective experiments, the force-extension curves obtained from the tensile tests and assessed in the FE software, based on the computed stresses, are illustrated in Figure 7.28. Despite the fact that the nonwoven is beyond the limit of simulatability with the introduced modelling approach due to its low planar density, results of the FE simulations are still in relatively good agreement with the experimental data. Obviously, deviation of the numerical results in Figure 7.28 is more than that in Figure 7.23 (Model A) and Figure 7.26 (Model B). The main sources of this difference are short and crimped fibres constituting the nonwoven simulated with Model C, e.g. in Figure 7.28 up to 15% extension the numerical results are higher than the experimental ones since a significant portion of fibres do not contribute to the stiffness of the fabric until they

are straightened in the tensile test. As a result, simulating a nonwoven with a planar density lower than 35 g/m^2 may amplify the deviation of numerical results. Although the fibre type, bond pattern and planar density of 35 g/m^2 PP/PE 50/50 nonwoven are rather different from those of the nonwovens simulated with Models A and B, the FE model successfully reproduces the mechanical response of the nonwoven specimens simulated with Model C to tensional load.

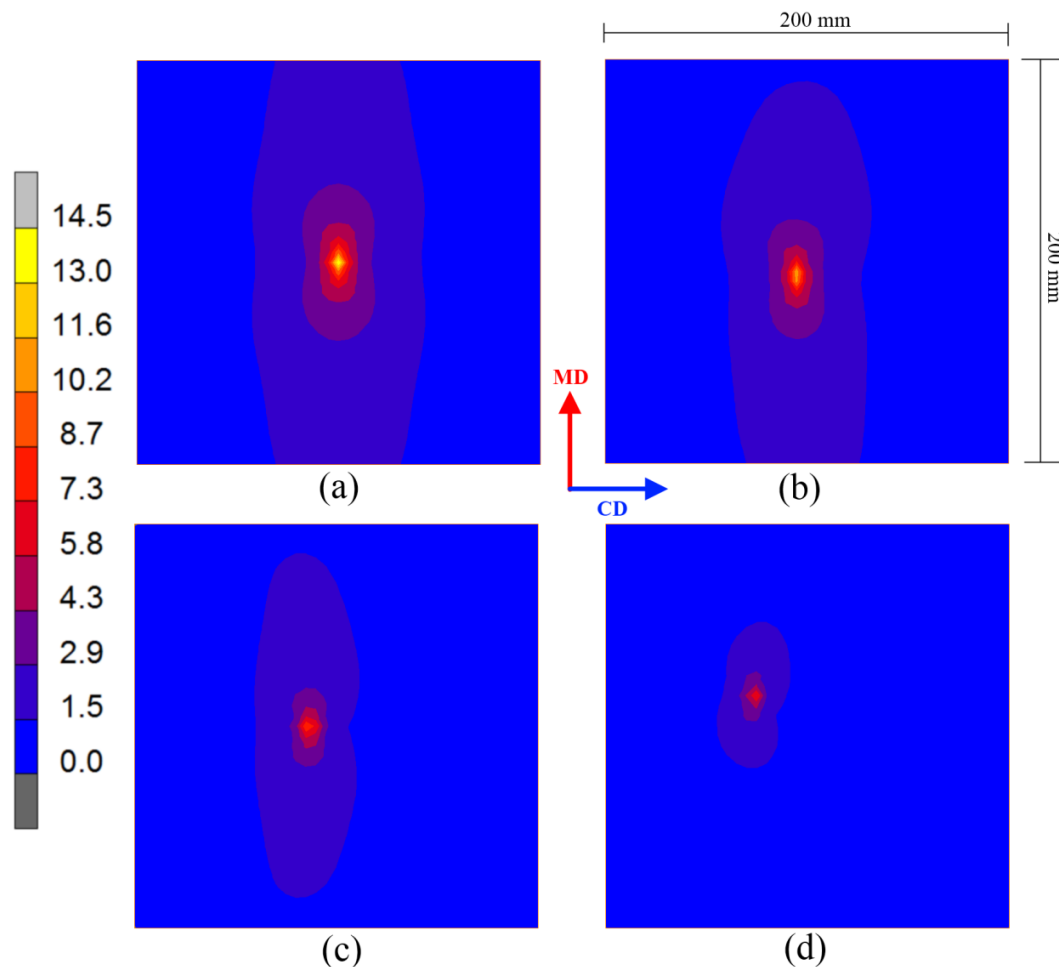


Figure 7.29. Equivalent von Mises stress distribution (MPa) of deformed nonwoven in Model D at first (a), second (b), third (c) and fourth (d) impacts

7.5.4. Model D

Model D simulates the time-dependent mechanical behaviour of 50 g/m^2 PP/PE 75/25 thermally bonded nonwoven under drop weight testing. This model focuses on

reproducing the viscous deformation characteristics of nonwovens explicitly with an out-of-plane loading condition, which is commonly observed in various ballistics and sports applications. As explained in Section 7.1, in order to simulate an out-of-plane loading with a practical application, a steel sphere located 100 mm above the fabric plane is released from its steady-state position to attain a consecutive bouncing motion for a period of 1 s on the nonwoven plane, which is fixed at all edges.

Stress distribution in the nonwoven model as a result of four consecutive sphere impacts are given in Figure 7.29. These stresses are obtained for the states when the nonwoven starts to spring back and throw the sphere upwards against gravity. Each of these states corresponds to maximum deformation of the nonwoven in each bounce cycle. As observed in Figure 7.29, the stress level decreases in each impact due to a decreased height of each bounce. As a result of viscous effects implemented in the model, a significant portion of system's energy is dissipated at each spring back taking place at loading-unloading cycles. As the energy is absorbed by the nonwoven in each bounce, the maximum height, that the sphere reaches, decreases. This behaviour is observed in the real-life deformation response of thermally bonded nonwovens illustrated in Figure 7.30 and in the FE results of Model D.

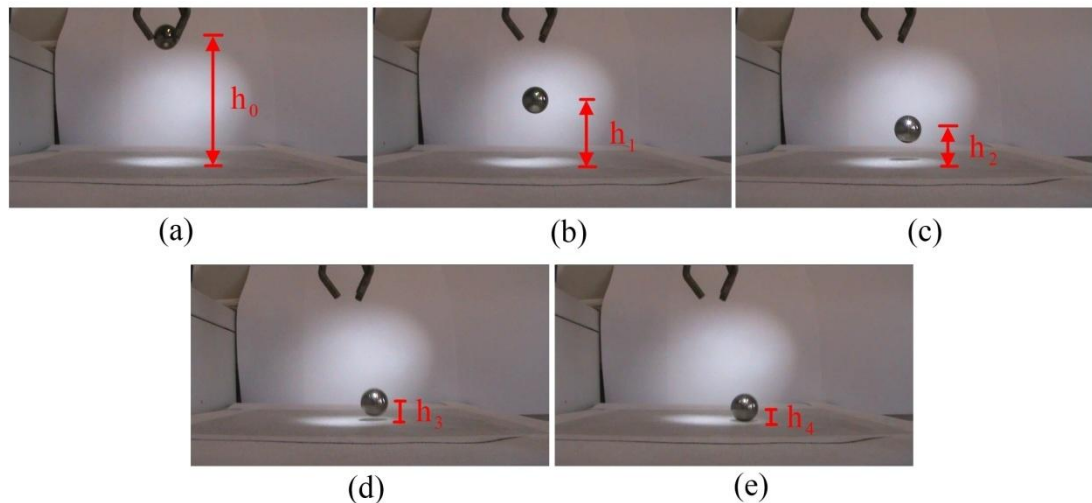


Figure 7.30. Metal sphere at initial height (h_0) (a), and its maximum heights at first (b), second (c), third (d) and fourth (e) bounces (h_i : height of the sphere at i^{th} bounce)

The sphere's position at each impact in Figure 7.29 is obvious due to stress concentration observed at the contact region between the sphere and the nonwoven. Except for the first impact (Figure 7.29a), in which the sphere drops naturally to the centre of the fabric, the sphere hits the fabric at different locations rather than the centre in the subsequent impacts. Additionally, due to anisotropic mechanical properties of the nonwoven, stress evolution in MD is more than that in CD due to stiffer behaviour in MD (Figure 7.29). On the other hand, the fabric model is inhomogeneous since it is composed of two distinct regions with distinct mechanical properties. As a result of these facts, different impact locations are observed in the FE results of Model D, which is consistent with our experimental observations.

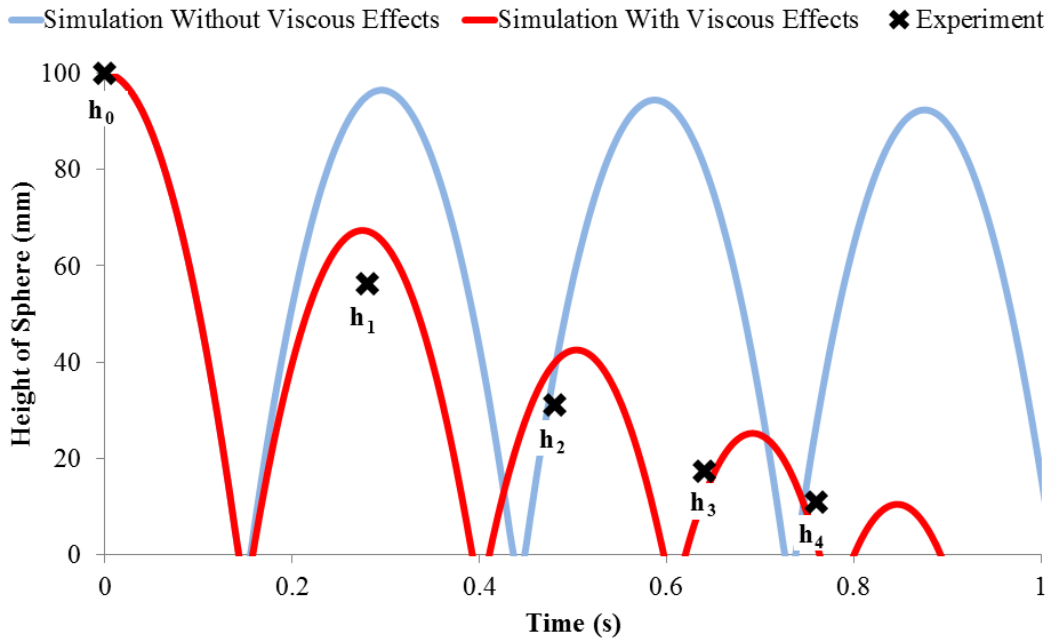


Figure 7.31. Height of sphere in experiment and FE simulations performed with Model D

To compare the FE results of Model D with the experiment, evolution of the height of sphere obtained in the simulation and the maximum height of the sphere, recorded at each bounce in the experiment, are given in Figure 7.31. The height in the experiment and simulations corresponds to the distance between the fabric plane and the centre of the metal sphere. The maximum height of the sphere at each bounce in the experiment shown in Figure 7.30 are recorded with a camera and displayed in

Figure 7.31. Besides, in order to illustrate the importance of viscous effects in modelling the mechanical behaviour of thermally bonded nonwoven materials, simulations with Model D are implemented with and without introduction of the viscous parameters defining the material properties of nonwoven regions in the FE software. As obvious from Figure 7.31, if viscous effects are switched off in the FE simulation, the sphere will bounce endlessly, attaining the initial height in each bounce, due to absence of energy dissipation related to viscous effects. In the real case, where viscous effects take place, FE results of Model D are consistent with the experimental ones confirming the success of the proposed numerical modelling approach for simulating the mechanical behaviour of thermally bonded nonwovens. The slight deviation of the numerical results from experimental ones is due to unaccounted factors, which also contribute to damping mechanism of the material, such as inter-fibre friction. In spite of the slight deviation, the FE model reproduces the viscous deformation behaviour of nonwoven specimen, which is characterized by the changing bouncing height of the metal sphere, successfully.

7.6. Conclusions

Detailed explanation of the numerical modelling of thermally bonded bicomponent fibre nonwovens is made in this chapter by illustrating the development stages of four FE models that simulate various types of fabrics and loading conditions. Due to their unique microstructure and polymer-based constituents leading to complex deformation mechanisms, the nonwoven fabrics are modelled employing two distinct regions with different mechanical properties. These properties are calculated with the developed code – Nonwovens V4 – accounting for the manufacturing parameters and properties of single bicomponent fibres that provides the data independent of the bond shape and pattern (Section 6.2). On the other hand, anisotropy of the material is computed with another developed algorithm – Nonwovens Anisotropy V1 – using a SEM or X-ray micro CT image of the microstructure of its fibre matrix region (Section 6.1). With the FE models composed of regions of bond points and the fibre matrix with different anisotropic viscoelastic-plastic material properties, the time-

dependent 3D deformation response of various nonwovens is simulated in the FE software. The procedure followed in this chapter to simulate the complex deformation behaviour of thermally bonded bicomponent fibre nonwovens is described in the flow chart shown in Figure 7.32.

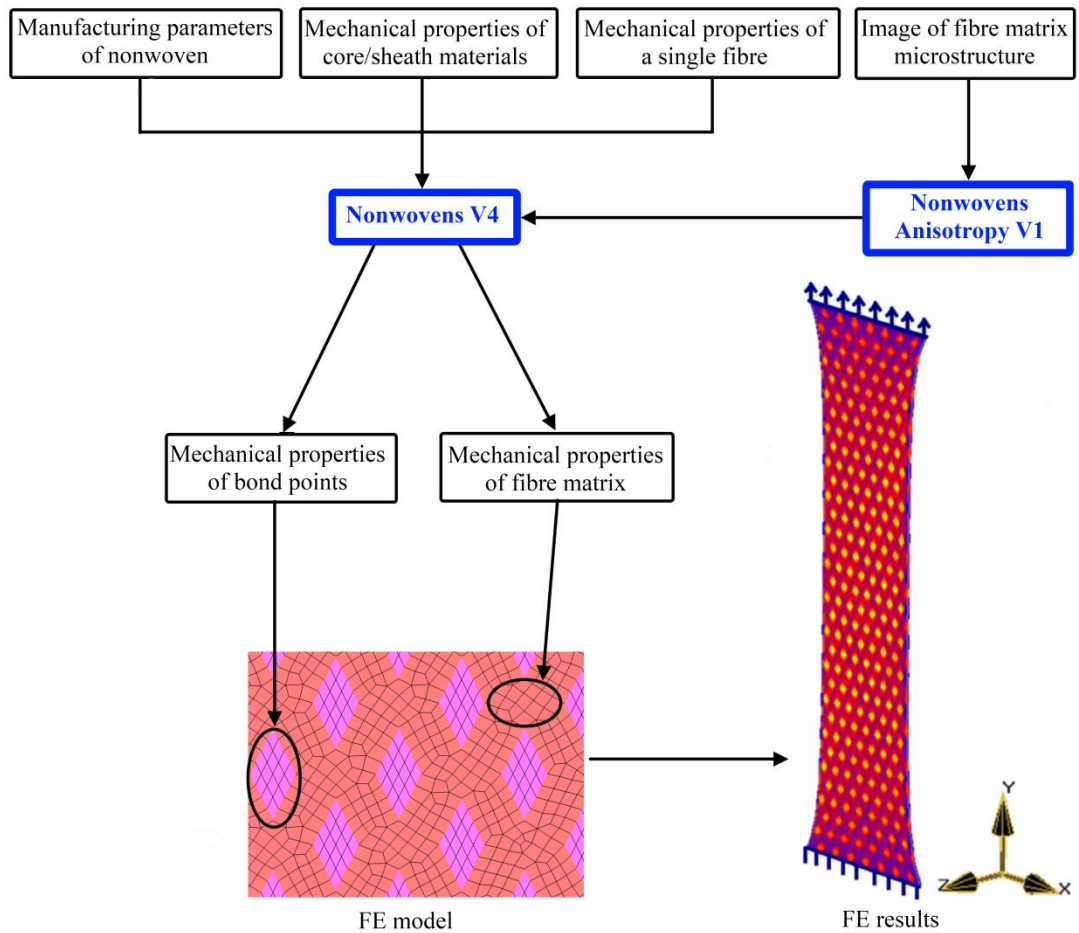


Figure 7.32. Procedure of FE simulation of thermally bonded bicomponent fibre nonwovens in the research

In order to simplify the numerical modelling scheme, several assumptions are made in the procedure for simulating the mechanical behaviour of thermally bonded bicomponent fibre nonwovens. The numerical modelling scheme assumes that:

- Nonwoven fabric is bonded with the ideal bonding pressure that yields nonporous bond points,

- Length of raw unbonded fibres is significantly more than the largest interval between two adjacent bond points,
- Bicomponent fibres are not damaged at fibre matrix region causing strength loss in the fabric,
- Variation of the thickness at bond points and fibre matrix is negligible,
- Mechanical properties of a single fibre used in the numerical scheme are typical to that of fibres used to manufacture the nonwoven fabric,
- ODF and mechanical anisotropy are characteristic for the entire fabric,
- Regions of bond points and fibre matrix possess orthotropic symmetry,
- Structure of the nonwoven fabric is homogeneous and continuous which are generally achieved with a fabric planar density of at least 50 g/m².

The novel approach followed in this research to predict the time-dependent mechanical performance of thermally bonded nonwovens is promising since results of the introduced FE models are in good agreement with the experimental data. The numerical model proposed in this study is effective in predicting the real-life deformation characteristics of thermally bonded nonwovens, verified with experiments and ready to use for several applications, such as ballistics and sports applications. It can be built into any commercial FE software package, capable of implementing orthotropic viscoelasticity and plasticity procedures such as the Hill's orthotropic yield criterion, in order to predict response of various nonwoven materials under arbitrary loading conditions.

CHAPTER VIII

8. CONCLUSIONS

A novel approach for predicting the complex mechanical behaviour of thermally bonded bicomponent fibre nonwovens under 3D time-dependent loading conditions is introduced in the thesis. Development of the approach for predicting the real-life deformation behaviour of these materials started with a thorough literature review about general characteristics of nonwoven materials including manufacturing methods, application areas and physical properties. Background information about nonwovens is vital for understanding their mechanical behaviour, which is necessary for development of their numerical models. Secondly, general mechanical characteristics of nonwoven fabrics were analysed in order to have a better understanding of the features affecting their mechanical behaviour. Then, theoretical foundation of modelling the mechanical behaviour of materials was given for elastic, plastic and viscous behaviours that are observed in nonwoven materials. Additionally, a review of the finite element method was provided since it was used as a numerical modelling tool in the study; existing numerical models of nonwoven

materials were studied as well. After providing general background information about the material and respective numerical modelling tools, experimental studies related to the thermally bonded bicomponent fibre nonwovens were discussed. Not only the fabrics but also their constituent fibres were subjected to tensile, cyclic loading and relaxation tests. The mechanical behaviour of nonwovens and of their fibres were investigated, since results of the experiments played an important part in development and verification of the numerical model. Microstructure of several thermally bonded bicomponent fibre nonwovens were examined with SEM and X-ray micro CT techniques. A stand-alone application code – Nonwovens Anisotropy V1 – was written in MATLAB[®] software to analyse the ODF and mechanical anisotropy of the nonwovens based on the images of their random fibrous microstructure using the Hough transform technique. Then another stand-alone code – Nonwovens V4 – was introduced to determine the orthotropic viscoelastic-plastic mechanical properties of regions of bond points and fibre matrix in nonwoven materials based on properties of fibres and manufacturing parameters such as the planar density, core/sheath ratio, fibre diameter etc. Finally, the nonwovens, having distinct anisotropic mechanical properties for two regions, were modelled in the FE software – MSC.Marc[®] – with shell elements having thicknesses identical to those of bond points and the fibre matrix. FE simulations and respective experimental results were compared to evaluate efficiency of the proposed numerical modelling approach.

As a result of the experimental and numerical studies carried out in this research, it can be concluded that:

- Polymer-based fibres used to manufacture nonwovens exhibit large-strain nonlinear viscoelastic-plastic deformation behaviour.
- Having randomly distributed polymer-based fibres and being composed of two discrete regions – bond points and matrix – nonwovens have a unique mechanical behaviour that is partially similar to, but still differs from, that of composites, polymers and woven fabrics.
- The mechanical behaviour of thermally bonded bicomponent fibre nonwovens is linked to that of their constituent fibres.

- The deformation behaviour of these materials is time-dependent and mainly governed by plasticity.
- The mechanical behaviour of the fibre matrix and that of bond points are dissimilar due to their distinct microstructure.
- Calendering temperature affects the deformation characteristics of thermally bonded nonwovens significantly.
- Random orientation of fibres is the main source of direction-dependent mechanical response of nonwovens.
- Mechanical anisotropy of the structure could be analysed based on the orientation distribution fibres.
- Anisotropic mechanical properties of bond points and fibre matrix of nonwoven materials could be assessed based on properties of their constituent fibres and manufacturing parameters such as the planar density, core/sheath ratio, fibre diameter etc.
- Regarding the four case studies introduced in Chapter 7, the proposed numerical modelling approach for simulating 3D time-dependent mechanical performance of thermally bonded nonwovens is promising since results of the introduced FE models are in good agreement with the obtained experimental data.
- Shell elements are effective in modelling of nonwoven regions in the FE environment.

8.1. Outcomes

Main outcomes of the research are:

1. A better understanding of the deformation behaviours of thermally bonded nonwovens and their bicomponent fibres are gained with this research. Specific features of mechanical responses of thermally bonded nonwovens and their polymer-based fibres are clarified from the computational mechanics point of view enabling designers and manufacturers to consider

nonlinear large-strain viscoelastic-plastic behaviour of nonwovens in their design, manufacturing and usage.

2. A tool capable to predict the effects of microstructure on the overall mechanical properties of thermally bonded nonwoven materials is introduced in the study. Nonwoven manufacturers can utilize Nonwovens Anisotropy V1 code to design and optimize the microstructure of their products.
3. Accurate prediction of the mechanical properties of thermally bonded nonwovens with a new code – Nonwovens V4 – is developed during the research through a few assumptions. It can serve industry in design and optimization of nonwovens with respect to their manufacturing parameters and structural features.
4. Based on the assumptions stated in Section 7.6, a parametric 3D finite element model is developed in the research to simulate the real-life performance of thermally bonded nonwovens. Unlike the existing numerical models in the literature (see Section 4.5), the model developed in the thesis is capable of simulating 3D loading conditions of thermally bonded nonwovens as well as their time-dependent anisotropic behaviour. The numerical model introduced in this research is a novel contribution to scientific knowledge.

8.2. Future Work

The FE model developed in this study is a potential tool for product development and optimization. Manufacturers and designers can facilitate the introduced model for predicting the real-life deformation behaviour of thermally bonded nonwovens, and design and optimize the material accordingly, for instance, design of sports products containing nonwoven fabrics could be a field for using the FE model and codes developed in the thesis. On the other hand, the model is recently developed and therefore its functionality should be tested with further experiments using various types of nonwoven fabrics. Besides, the scope of the modelling should be improved with additional deformation characteristics of nonwovens, such as damage behaviour.

Damage is an unavoidable phenomenon when a material is exposed to excessive loads or deformations, or a combination of them depending on the loading conditions and material's deformation characteristics. The next step in modelling the mechanical behaviour of the material is the damage behaviour. Characterisation of damage behaviour and its effect on the material performance enables us to simulate the material's failure mechanisms under various loading conditions. To achieve this, different relationships known as *damage criteria*, should be determined based on material's properties, such as toughness, damage strain, etc.

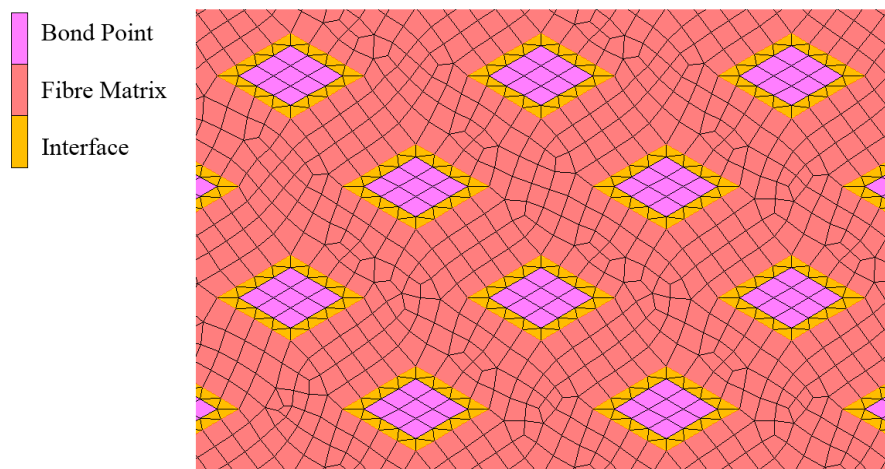


Figure 8.1. FE model of thermally bonded nonwovens with interface region for simulating damage behaviour

The numerical model introduced in this research offers a practical tool for simulation of thermally bonded bicomponent fibre nonwovens covering reversible and irreversible deformation types with viscous effects. In order to extend the capabilities of the numerical model, the damage behaviour could be implemented as one of mechanical properties of nonwovens. This implementation requires nonwovens-specific damage criteria, accounting for their manufacturing parameters, fibre properties, etc. In order to predict the limits of deformation due to damage in real-life applications, criteria of damage initiation and evolution of damage in nonwovens should be studied, both experimentally and numerically.

Damage initiation in nonwovens corresponds to premature failure of fibres at the fibre-bond interface (Michielsen *et al.*, 2006). Hence, damage criteria for the thermally bonded nonwoven fabrics could be implemented in the developed numerical model with introducing a third nonwoven region – interface region – where damage initiates (Figure 8.1). As shown in Figure 8.1, the interface region is currently modelled with one layer of elements acting as a transition between bond point and fibre matrix regions. With the improved numerical model proposed for future studies, failure of the fabric commences at the interface region elements fulfilling the damage criteria developed for the fabric, and then propagates to other regions. On the other hand, various experiments should be performed to develop parametric damage criteria for the nonwovens and verify results of numerical modelling related to the damage behaviour. The future work illustrated here will improve capabilities of the numerical modelling approach to simulate the mechanical behaviour of thermally bonded bicomponent fibre nonwovens explained in the thesis.

REFERENCES

Adanur, S. and Liao, T. (1999), 'Fiber Arrangement Characteristics and Their Effects on Nonwoven Tensile Behavior', *Textile Research Journal* **69**(11), 816-824.

Albrecht, W., Fuchs, H. and Kittelmann, W. (2003), *Nonwoven Fabrics: Raw Materials, Manufacture, Applications, Characteristics, Testing Processes*, WILEY-VCH, Weinheim, Germany.

Asaro, R. J. and Lubarda, V. A. (2006), *Mechanics of Solids and Materials*, Cambridge University Press, Cambridge, UK.

Backer, S. and Petterson, D. (1960), 'Some Principles of Nonwoven Fabrics 1', *Textile Research Journal* **30**(9), 704-711.

Barakat, N. (1971), 'Interferometric studies on fibers. Part I. Theory of interferometric determination of indices of fibers', *Textile Research Journal* **41**(2), 167-170.

Barauskas, R. and Abraitene, A. (2007), 'Computational Analysis of Impact of a Bullet Against the Multilayer Fabrics in LS-DYNA', *International Journal of Impact Engineering* **34**(7), 1286-1305.

Batra, S. K. (1998), *Basics of Nonwoven Fabrics and Technology*, NCRC, NC State University, Raleigh, USA.

Belytschko, T., Liu, W. K. and Moran, B. (2000), *Nonlinear Finite Elements for Continua and Structures*, Wiley, New York, USA.

Bhat, G. S., Jangala, P. K. and Spruiell, J. E. (2004), 'Thermal Bonding of Polypropylene Nonwovens: Effect of Bonding Variables on the Structure and Properties of the Fabrics', *Journal of Applied Polymer Science* **92**(6), 3593-3600.

Bhat, G. S., Nanjundappa, R. and Kotra, R. (2002), 'Development of Structure and Properties During Spunbonding of Propylene Polymers', *Thermochimica Acta* **392-393**, 323-328.

Brinson, H. F. and Brinson, L. C. (2008), *Polymer Engineering Science and Viscoelasticity*, Springer, New York, USA.

Britton, P. N., Sampson, A. J., Elliott, C. F., Graben, H. W. and Gettys, W. E. (1983), 'Computer Simulation of the Mechanical Properties of nonwoven Fabrics. Part I: The Method', *Textile Research Journal* **53**(6), 363-368.

Britton, P. N., Sampson, A. J. and Gettys, W. E. (1984), 'Computer Simulation of the Mechanical Properties of nonwoven Fabrics. Part II: Bond Breaking', *Textile Research Journal* **54**(1), 1-5.

Britton, P. N., Sampson, A. J. and Gettys, W. E. (1984), 'Computer Simulation of the Mechanical Properties of nonwoven Fabrics. Part III: Fabric Failure', *Textile Research Journal* **54**(7), 425-428.

Callister, W. (2003), *Materials Science and Engineering, An Introduction*, John Wiley and Sons, Utah, USA.

Chakrabarty, J. (2006), *Theory of Plasticity*, Elsevier Butterworth-Heinemann, Oxford, UK.

Chidambaram, A., Davis, H. and Batra, S. K., ed., (2000), *Strength Loss In Thermally Bonded Polypropylene Fibers*, INTC 2000 Conference, Dallas, USA.

Chou, T.-W. (1992), *Microstructural Design of Fiber Composites*, Cambridge University Press, Cambridge, UK.

Cook, R. D. (1995), *Finite Element Modeling for Stress Analysis*, John Wiley and Sons, New York, USA.

Cox, H. L. (1952), 'The Elasticity and Strength of Paper and Other Fibrous Materials', *British Journal of Applied Physics* **3**, 72-79.

Datla, V. M. (2002), 'The Influence of Fiber Properties and Processing Conditions on the Characteristics of Needled Fabrics', Master's thesis, North Carolina State University.

Dharmadhikary, R. K., Gilmore, T. F., Davis, H. A. and Batra, S. K. (1995), 'Thermal Bonding of Nonwoven Fabrics', *Textile Progress* **26**, 20-21.

EDANA (2010), 'The European Nonwovens Industry in a Global Context', [Online] <http://www.edana.org/content/default.asp?PageID=143> [02/07/2010].

- EDANA (2009a), 'What are Nonwovens', [Online]
<http://www.edana.org/content/default.asp?PageID=33> [09/06/2009].
- EDANA (2009b), 'Applications', [Online]
<http://www.edana.org/Content/Default.asp?PageID=37> [09/06/2009].
- Fedorova, N. (2006), 'Investigation of the Utility of Islands-in-the-Sea Bicomponent Fiber Technology in the Spunbond Process', PhD thesis, North Carolina State University.
- Ferry, J. D. (1980), *Viscoelastic Properties of Polymers*, John Wiley and Sons, USA.
- Fibertex A/S (2009), 'Automotive/Superior nonwovens inside', [Online]
<http://www.fibertex.com/en-GB/business-areas/Automotive/Applications/Pages/default.aspx> [09/06/2009].
- Gao, X. and Huang, H. Y. (2004), 'Thermal Bonding of Nonwoven Fabrics', [Online]
<http://www.engr.utk.edu/mse/pages/Textiles/Thermal Bonding.htm> [09/06/2009].
- Ghassemieh, E., Acar, M. and Versteeg, H. (2002), 'Microstructural Analysis of Non-woven Fabrics Using Scanning Electron Microscopy and Image Processing. Part 1: Development and Verification of the Methods', *Proc. Instn. Mech. Engrs., Part L: J. Materials: Design and Applications* **216**, 199-207.
- Ghassemieh, E., Acar, M. and Versteeg, H. (2002), 'Microstructural Analysis of Non-woven Fabrics Using Scanning Electron Microscopy and Image Processing. Part 2: Application to Hydroentangled Fabrics', *Proc. Instn. Mech. Engrs., Part L: J. Materials: Design and Applications* **216**, 211-218.

Ghassemieh, E., Versteeg, H. and Acar, M. (2001), 'Microstructural Analysis of Fiber Segments in Nonwoven Fabrics Using SEM and Image Processing', *International Nonwovens Journal* **10**(2), 26-31.

Giroud, J. P. (2004), 'Poisson's Ratio of Unreinforced Geomembranes and Nonwoven Geotextiles Subjected to Large Strains', *Geotextiles and Geomembranes* **22**(4), 297-305.

Gitman, I. M., Askes, H. and Sluys, L. J. (2007), 'Representative Volume: Existence and Size Determination', *Engineering Fracture Mechanics* **74**(16), 2518-2534.

Gonzalez, R. C. and Woods, R. E. (2002), *Digital Image Processing*, Prentice Hall, New Jersey, USA.

Gusick, G. E., Hearle, J. W. S., Michie, R. I. C. and Peters, R. H. (1963), 'The Physical Properties of Nonwoven Fabrics', *Journal of the Textile Institute* **54**, 52-74.

Hamza, A. A., Fouda, I. M. and Ei-Farahaty, K. A. (1986), 'Interferometric Determination of Optical Properties of Bicomponent Fibers', *International Journal of Polymeric Materials* **11**(3), 169-184.

Hearle, J. W. S. and Ozsanlav, V. (1979), 'Studies of Adhesive-Bonded Non-woven Fabrics Part III: The Determination of Fiber Orientation and Curl', *Journal of the Textile Institute* **70**(11), 487-498.

Hietel, D. (2006), *Simulation of Fiber Dynamics*, in , Fraunhofer Institut Techno- und Wirtschaftsmathematik, Kaiserslautern, Germany.

Hill, R. (1950), *The Mathematical Theory of Plasticity*, Oxford University Press, New York, USA.

Hosford, W. F. (2005), *Mechanical Behavior of Materials*, Cambridge University Press, Cambridge, UK.

Hou, X., Acar, M. and Silberschmidt, V. V. (2009), '2D finite element analysis of thermally bonded nonwoven materials: Continuous and discontinuous models', *Computational Materials Science* **46**, 700-707.

Hou, X. (2010), 'Experimental and Numerical Analysis of Deformation of Low-Density Thermally Bonded Nonwovens', PhD thesis, Loughborough University.

Hoyle, A. G. (1990), 'Thermal Bonding of Nonwoven Fabrics', *Tappi Journal* **7**, 85-88.

Ikegami, K., Lemaitre, J., ed., (2001), *Handbook of Materials Behavior Models, Volume 1: Deformations of Materials*, Academic Press, California, USA, Chapter: Background on Viscoelasticity, 95-106.

INDA (2009), 'About Nonwovens', [Online]
http://www.inda.org/category/nwn_index.html [09/06/2009].

Kachanov, L. M., Lauwerier, H. A. and Koiter, W. T., ed. (1971), *Foundations of the Theory of Plasticity*, Vol. 12, North Holland Publishing, Amsterdam, NETHERLANDS.

Kaliske, M., Schmidt, M., Lin, G. and Bhashyam, G. (2005), 'Implementation of Nonlinear Anisotropic Elasticity at Finite Strains into ANSYS Including Viscoelasticity and Damage' International Congress on FEM Technology with ANSYS CFX and ICEM CFD Conference', Canonsburg, USA.

- Kim, H. S. (2004a), 'Orthotropic Theory for the Prediction of Mechanical Performance in Thermally Point-Bonded Nonwovens', *Fibers and Polymers* **5**(2), 139-144.
- Kim, H. S. (2004b), 'Relationship between Fiber Orientation Distribution Function and Mechanical Anisotropy of Thermally Point-Bonded Nonwovens', *Fiber and Polymers* **5**(3), 177-181.
- Kim, H. S. and Pourdeyhimi, B. (2001), 'Computational Modeling of Mechanical Performance in Thermally Point Bonded Nonwovens', *Journal of Textile and Apparel, Technology and Management* **1**(4), 1-7.
- Kim, H. S., Pourdeyhimi, B., Abhiraman, A. and Desai, P. (2002), 'Effect of Bonding Temperature on Load-Deformation Structural Changes in Point-Bonded Nonwoven Fabrics', *Textile Research Journal* **72**(7), 645-653.
- Kim, H. S., Pourdeyhimi, B., Abhiraman, A. and Desai, P. (2000), 'Characterization of Structural Changes in Nonwoven Fabrics During Load-Deformation Experiments', *Journal of Textile and Apparel, Technology and Management* **1**(1), 1-6.
- Krcma, R. (1962), *Nonwoven Textiles*, SNTL.
- Krucinska, I., Jalmuzna, I. and Zurek, W. (2004), 'Modified Rheological Model for Analysis of Analysis of Compression of Nonwoven Fabrics', *Textile Research Journal* **74**(2), 127-133.
- Limem, S. and Warner, S. B. (2005), 'Adhesive Point-Bonded Spunbond Fabrics', *Textile Research Journal* **75**(1), 63-72.

Lin, J. H., Xu, Z. H., Lei, C. H. and Lou, C. W. (73), 'Effect of Fiber Arrangement on the Mechanical Properties of Thermally Bonded Nonwoven Fabrics', 2003 **10**(917), 920.

Makela, P. and Ostlund, S. (2003), 'Orthotropic Elastic-Plastic Material Model for Paper Materials', *International Journal of Solids and Structures* **40**(21), 5599-5620.

Marc (2008r1), 'MSC.Marc - User Guide A: Theory and User Information', MSC Software.

Mendelson, A. (1968), *Plasticity, Theory and Application*, Collier-Macmillan, New York, USA.

Michielsen, S., Pourdeyhimi, B. and Desai, P. (2006), 'Review of Thermally Point-Bonded Nonwovens: Materials, Processes, and Properties', *Journal of Applied Polymer Science* **99**(5), 2489-2496.

Miehe, C., Schroder, J. and Schotte, J. (1999), 'Computational Homogenization Analysis in Finite Plasticity, Simulation of Texture Development in Polycrystalline Materials', *Computer Methods in Applied Mechanics and Engineering* **171**(3-4), 387-418.

Mishakov, V. Y., Slutsker, G. Y. and Stalevich, A. M. (2006), 'Modeling the Viscoelasticity of Nonwoven Material with Consideration of the Irreversible Strain Component', *Fibre Chemistry* **38**(1), 50-54.

Mueller, D. H. and Kochmann, M. (2004), 'Numerical Modeling of Thermobonded Nonwovens', *International Nonwovens Journal* **13**(1), 56-62.

Newnham, R. (2005), *Properties of materials : anisotropy, symmetry, structure*, Oxford University Press, Pennsylvania, USA.

Pourdeyhimi, B., Dent, R. and Davis, H. (1997), 'Measuring Fiber Orientation in Nonwovens: Part III: Fourier Transform', *Textile Research Journal* **67**(2), 143-151.

Pourdeyhimi, B., Dent, R., Jerbi, A., Tanaka, S. and Deshpande, A. (1999), 'Measuring Fiber Orientation in Nonwovens: Part V: Real Webs', *Textile Research Journal* **69**(3), 185-192.

Pourdeyhimi, B. and Kim, H. S. (2002), 'Measuring Fiber Orientation in Nonwovens: The Hough Transform', *Textile Research Journal* **72**(9), 803-809.

Pourdeyhimi, B. and Ramanathan, R. (1997), 'Measuring Fiber Orientation in Nonwovens: Part IV: Flow Field Analysis', *Textile Research Journal* **67**(3), 181-187.

Pourdeyhimi, B., Ramanathan, R. and Dent, R. (1996), 'Measuring Fiber Orientation in Nonwovens: Part I: Simulation', *Textile Research Journal* **66**(11), 713-722.

Pourdeyhimi, B., Ramanathan, R. and Dent, R. (1996), 'Measuring Fibre Orientation in Nonwovens: Part II: Direct Tracking', *Textile Research Journal* **66**(12), 747-753.

Price, D. C., Jones, R. and Harland, A. R. (2006), 'Soccer Ball Anisotropy Modelling', *Materials Science and Engineering A* **420**, 100-108.

Purdy, A. T. (1983), *Developments in Non-woven Fabrics*, Vol. 12, The Textile Institute, Manchester, UK.

Ramasubramanian, M. K. and Wang, Y. (2007), 'A Computational Micromechanics Constitutive Model for the Unloading Behavior of Paper', *International Journal of Solids and Structures* **44**(22-23), 7615-7632.

Rawal, A. (2006), 'A Modified Micromechanical Model for the Prediction of Tensile Behavior of Nonwoven Structures', *Journal of Industrial Textiles* **36**(2), 133-149.

Rawal, A., Anand, S. and Shah, T. (2008), 'Optimization of Parameters for the Production of Needlepunched Nonwoven Geotextiles', *Journal of Industrial Textiles* **37**(4), 341-356.

Roesler, J., Harders, H. and Baeker, M. (2007), *Mechanical Behaviour of Engineering Materials - Metals, Ceramics, Polymers and Composites*, Springer, GERMANY.

Russell, S. J. (2007), *Handbook of Nonwovens*, Woodhead Publishing Ltd., Cambridge, UK.

Saville, B. P. (1999), *Physical Testing of Textiles*, Woodhead Publishing Ltd. and The Textile Institute, Cambridge, UK.

Schaff, A. J. and Ogale, A. A. (1991), 'Tensile Viscoelastic Properties of Spunbonded Nonwoven Polypropylene Backing', *Textile Research Journal* **61**(7), 386-392.

Shaw, M. T. and MacKnight, W. J. (2005), *Introduction to Polymer Viscoelasticity*, Wiley-Interscience Publication, New Jersey, USA.

Smith, W. S. (2004), 'Nonwovens in Automotives - More Than Just a Pretty Face', *International Nonwovens Journal* **13**(3), 60-63.

Tekkaya, A. E. (2003), *Finite Element Analysis in Solid Mechanics*, ME 581 Lecture Notes, Ankara, TURKEY.

Tekkaya, A. E. (2002), *Introduction to Finite Element Analysis*, ME 413 Lecture Notes, Ankara, TURKEY.

Ting, T. C. T. (1996), Anisotropic elasticity : theory and applications, Oxford University Press, Illinois, USA.

Wang, X. Y. and Gong, R. H. (2006), 'Thermally Bonded Nonwoven Filters Composed of Bicomponent Polypropylene/Polyester Fiber. I. Statistical Approach for Minimizing the Pore Size', Journal of Applied Polymer Science **101**(4), 2689-2699.

Wang, X. Y., Gong, R. H., Dong, Z. and Porat, I. (2006), 'Abrasion Resistance of Thermally Bonded 3D Nonwoven Fabrics', Wear **262**(2007), 424-431.

Ward, I. M. and Sweeney, J. (2004), An Introduction to the Mechanical Properties of Solid Polymers, John Wiley and Sons, Chichester, UK.

Wei, Q., Wang, X. and Huang, F. (2007), 'Dynamic studies of polypropylene nonwovens in environmental scanning electron microscope', Polymer Testing **26**(1), 2-8.

Weia, Q., Xiaoa, X., Houb, D., Yea, H. and Huang, F. (2008), 'Characterization of Nonwoven Material Functionalized by Sputter Coating of Copper', Surface and Coatings Technology **202**(12), 2535-2539.

Wood, E. J. (1990), 'Applying Fourier and Associated Transforms to Pattern Characterization in Textiles', Textile Research Journal **60**(4), 212-220.

Xina, Y., Huang, Z., Lia, W., Jianga, Z., Tonga, Y. and Wang, C. (2008), 'Core-Sheath Functional Polymer Nanofibers Prepared by Co-electrospinning', European Polymer Journal **44**(4), 1040-1045.

Xu, B. (1996), 'Identifying Fabric Structures with Fast Fourier Transform Techniques', Textile Research Journal **66**(8), 496-506.

Xu, B. and Ting, Y. (1995), 'Measuring Structural Characteristics of Fiber Segments in nonwoven Fabrics', *Textile Research Journal* **65**(1), 41-48.

Xu, B. and Yu, L. (1997), 'Determining Fiber Orientation Distribution in Nonwovens with Hough Transform Techniques', *Textile Research Journal* **67**(08), 563-571.

Zhao, R., Wadsworth, L. C., Sun, C. and Zhang, D. (2003), 'Properties of PP/PET bicomponent melt blown microfiber nonwovens after heat-treatment', *Polymer International* **52**(1), 133-137.